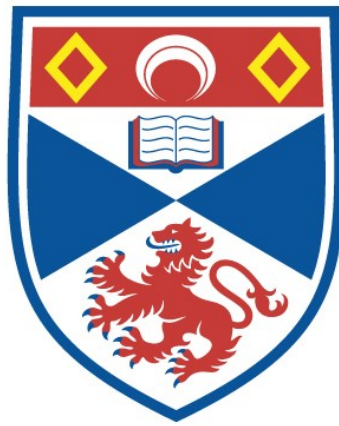


A PETROGENETIC STUDY OF HARRISITE IN THE
ISLE OF RHUM PLUTON, SCOTLAND

Colin H. Donaldson

A Thesis Submitted for the Degree of PhD
at the
University of St Andrews



1975

Full metadata for this item is available in
St Andrews Research Repository
at:

<http://research-repository.st-andrews.ac.uk/>

Please use this identifier to cite or link to this item:

<http://hdl.handle.net/10023/15572>

This item is protected by original copyright

A PETROGENETIC STUDY OF HARRISITE IN THE ISLE OF RHUM PLUTON, SCOTLAND

by

Colin H. Donaldson



Ph.D. thesis

Department of Geology

St. Andrews University

March, 1975

ProQuest Number: 10171174

All rights reserved

INFORMATION TO ALL USERS

The quality of this reproduction is dependent upon the quality of the copy submitted.

In the unlikely event that the author did not send a complete manuscript and there are missing pages, these will be noted. Also, if material had to be removed, a note will indicate the deletion.



ProQuest 10171174

Published by ProQuest LLC (2017). Copyright of the Dissertation is held by the Author.

All rights reserved.

This work is protected against unauthorized copying under Title 17, United States Code
Microform Edition © ProQuest LLC.

ProQuest LLC.
789 East Eisenhower Parkway
P.O. Box 1346
Ann Arbor, MI 48106 – 1346

Th 8401.

Academic Career

I graduated B.Sc. (Hons.) from St. Andrew's University in July 1972. Fieldwork for the present degree was conducted on the Isles of Rhum and Skye during July and August, 1972. In September 1972, I attended the Geology Department of the University of Durham for instruction in reflected light and ore microscopy from Dr. R. Phillips. In October, I received instruction in experimental petrology from Dr. D.L. Hamilton, Geology Department, Manchester University. From January 1973 until the present, I have been at the Johnson Space Center in Texas, being instructed in experimental petrology, electron probe microanalysis, X-ray fluorescence analysis, lunar and terrestrial petrology, computer programming and the theory of crystal growth and chemical diffusion. I have attended the fourth, fifth and sixth Lunar Science Conferences and presented papers at the 1974 Annual Meetings of the American Geophysical Union and the Geological Society of America.

Supervisor's Certificate

I certify that Colin Henry Donaldson has pursued a course of research under our supervision and has fulfilled the requirements of Ordinance 16 (University of St. Andrews). He is qualified to submit this thesis in application for the degree of Doctor of Philosophy.

Signed

Certificate of Originality

I certify that this thesis is my own composition and is based on research carried out by me in the Department of Geology, St. Andrew's University in July-December, 1972 and between 1973 and 1975 in the Planetary and Earth Sciences Division of the Johnson Space Center, and the Lunar Science Institute, Houston, Texas.

Where I am the senior author in the joint papers resulting from this study (Appendix III), my contribution exceeded fifty percent of the required research time and I was responsible for preparation and submission of the manuscript; in the remaining joint papers, the contribution decreases in the order of authors listed, but was never less than fifteen percent.

This thesis has not been submitted to another University.

Signed

CONTENTS

	page
PREFACE	v
ABSTRACT	vi
CHAPTER I GENERAL INTRODUCTION	1
CHAPTER II INTRODUCTION TO HARRISITE AND COMB-LAYERED ROCKS	4
The Rhum lavas, ultrabasic complex and harrisite: previous work	4
Other rocks containing skeletal and dendritic crystals	5
Terminology of layered rocks containing skeletal and branching crystals	6
Harrisite rock types and associated feldspathic veins and pegmatites	8
A definition of harrisite	9
Terminology of non-harrisitic rocks in Rhum	10
CHAPTER III FIELD RELATIONS OF HARRISITE LAYERS	12
Distribution	12
Layer thickness and the proportion of harrisite in the pluton	12
Dip and strike	13
Conformity and lateral continuity of layers	13
Interpretation and evidence for intrusion of crystal-mush magmas	16
CHAPTER IV OLIVINE CRYSTAL SHAPES IN IGNEOUS ROCKS	18
1. Classification of olivine textures and morphologies	18
2. Conclusions concerning harrisite olivine morphology	28
CHAPTER V ORIENTATION AND DISTRIBUTION OF OLIVINE CRYSTALS IN HARRISITE LAYERS: RELEVANCE TO THE CRESCUMULUS	
HYPOTHESIS	30
1. Growth direction of olivine	30

	2. Changes in olivine shapes within harrisite layers and across layer boundaries- 'anatomy' of a harrisite layer	32
	3. The crescumulus hypothesis	33
	4. Relationship of the crescumulus hypothesis to olivine crystals in harrisite	35
CHAPTER VI	RHYTHMICITY AND CYCLICITY IN THE THICKNESS OF HARRISITE LAYERING	38
CHAPTER VII	PETROGRAPHY OF HARRISITE	41
	A. Mineral proportions	41
	B. Crystal abundance and grain size variation	43
	C. Textures of harrisite and associated rocks	45
CHAPTER VIII	MINERAL CHEMISTRY OF HARRISITE AND ADJACENT CUMULATE ROCKS AND PEGMATITES	53
	Olivine	53
	Pyroxenes	55
	Plagioclase	57
	Kaersutite	59
	Phlogopite	61
	Opaque minerals (1) Spinel	61
	(2) Ilmenite	63
	Accessory minerals	65
	Conclusions	65
CHAPTER IX	CRYSTAL GROWTH THEORY AND THE ORIGIN OF OLIVINE SHAPES	67
	Nucleation	67
	Crystal growth rate and nucleation rate as functions of supercooling, number of crystals and melt composition- relation to harrisite origin	68
	Crystallization on the molecular scale- crystal growth rate control of morphology	70
	Thermal and chemical behaviour at the crystal- melt interface- the origin of dendrites and skeletons	72

	Linked parallel-unit branching olivine and the origin of comb-layered harrisite	75
	Summary	77
CHAPTER X	EXPERIMENTAL CRYSTALLIZATION OF OLIVINE	78
	(i) Previous work and introduction	78
	(ii) Aims	79
	(iii) Anhydrous experiments	80
	(iv) Crystallization of hydrous eucrite and peridotite melts	84
	(v) Effect of superheat on olivine shapes	95
	(vi) Comparison of the olivine shapes in anhydrous and hydrous experiments	96
	(vii) Summary and relevance to harrisite	97
CHAPTER XI	HARRISITE PETROGENESIS	102
	I Origins unrelated to the crescumulus hypothesis	102
	II Modification of the crescumulus hypothesis	103
	A. Constraints and some introductory comments ..	104
	B. Mechanisms of supersaturation induction	106
	C. Summary of the conditions during formation of harrisite layers	116
	D. Absence of harrisite in other plutons	118
	III Origin of vectorial crystallization in comb-layered rocks	119
CHAPTER XII	COMPOSITION OF THE RHUM MAGMA AND ITS REGIONAL SIGNIFICANCE	124
CHAPTER XIII	IMPORTANCE OF METASTABLE CRYSTALLIZATION IN PLUTONS AND FUTURE USE OF NON-EQUILIBRIUM EXPERIMENTAL PETROLOGY	130
	1. Comb layers and metastable fractional crystallization	130
	2. Questions concerning the crystallization of large bodies of magma	131

3. Application of non-equilibrium experiments	132
4. Further types of non-equilibrium experimentation	132
ACKNOWLEDGMENTS	134
REFERENCES	135
APPENDIX I PETROGRAPHY OF ROCKS INVESTIGATED BY ELECTRON MICROPROBE	A1
APPENDIX II EXPERIMENTAL TECHNIQUES AND EXPERIMENTAL PETROLOGY STUDY OF SIX RHUM ULTRABASIC ROCKS	A8
APPENDIX III PUBLISHED AND <u>IN PRESS</u> PAPERS RESULTING FROM THIS STUDY	A11

PREFACE

Results embodied in this thesis represent a part of the work performed during tenure of a Natural Environment Research Council NATO Overseas Studentship (September 1972 to August 1975). All but five months of the work were conducted at the NASA Johnson Space Center, Houston, Texas during tenure of a Visiting Graduate Fellowship at the Lunar Science Institute; the remaining months were spent at the Department of Geology, St. Andrews University.

Additional material relevant to the thesis has been published and copies of those papers referred to most frequently in the text are enclosed in Appendix III. The conclusion in one of these papers (Donaldson, 1974a), that olivines in Rhum harrisite grew rapidly, is taken as proven for this thesis.

The dual forms of spelling which might appear in the text represent a hazard of crossing the Atlantic and occasionally forgetting one's nationality!

ABSTRACT

There is textural evidence in the Rhum pluton for crystallization of layered ultrabasic rocks ('harrisite') under conditions of massive olivine supersaturation. Some of these rocks are comb layered. This field, petrographic and experimental investigation of harrisite is aimed at determining (1) the degree of supercooling at which different shapes of olivine crystallized in harrisite, (2) how magma in a plutonic environment became massively supersaturated in olivine and (3) whether the parent magma of harrisite was basaltic or ultrabasic. The results have particular relevance to the conditions under which magmas crystallize close to, or on, their margins and enclosures, sometimes to produce comb layers.

Harrisite is here defined as "an ultrabasic, plutonic, igneous rock in layered intrusions which contains >25 vol. percent of olivine. The olivine crystals are characterized by skeletal or dendritic shapes and have larger size than olivines in contiguous layers. Hydrous minerals are essential phases in the rock." Harrisite is a varietal type of peridotite, allivalite or olivine eucrite.

Harrisite layers are mainly confined to the Western Layered Series of the Rhum pluton. They range in thickness from 7 cm to 10 m and have a preferred thickness of about 1 m. Individual layers vary laterally in thickness and olivine crystal shape. A few harrisite layers are intrusive into the Layered Series, but the majority crystallized in conformable sequence with cumulate layers. Five percent of the ultrabasic rock of the island is harrisite; sixty percent of the Transition Series is harrisite.

The shapes of olivines in igneous rocks are classified into thirteen categories (those found in harrisite are underlined): polyhedral, porphyritic, granular, chain-like, parallel-growth, plate, branching (non-crystallographic, crystallographic, linked parallel-unit), randomly oriented, radiate, dendritic, lattice-work, swallow-tail and irregular olivines. Elongate olivines in harrisite

can grow preferentially upwards, downwards, horizontally or in random orientation. There is a gradual, systematic upward change in layers from granular or polyhedral cumulus olivines to skeletal porphyritic olivines, to branching olivines (present only in some layers). This change is accompanied by up to a 10 vol. percent decrease in olivine content and by increases in contents of both chrome magnetite and hydrous minerals; also, olivine crystals increase up to 1000 times in size and plagioclase crystals increase in size up to 10 times. Olivine crystals in harrisite grew as fast as 10^{-4} cm/s.

Olivine in harrisite has a composition range of $Fe_{84} - 73$. Some crystals are reverse zoned (2 - 2.5 mol. percent Fe). Olivines in cumulate layers are up to 2 mol. percent poorer in Fe than those in contiguous harrisite layers. Augite (e.g., $Wo_{46}En_{45}Fs_9$) and rare orthopyroxene crystals (e.g., $Wo_{1.3}En_{79.4}Fs_{19.3}$) indicate crystallization from a transitional magma. Plagioclases range from An_{87} in the generally broad, unzoned cores of crystals, to approximately An_{60} at the extremity of the normally-zoned mantles. Cr-rich kaersutite and phlogopite crystallized by reaction of magma with pyroxene, whereas Cr-deficient varieties of the same minerals crystallized directly from the magma. Chrome magnetite composition is dependent on the enclosing silicate mineral- crystals enclosed in olivine are generally richer in Fe and poorer in Al, Cr and Mg than those enclosed by plagioclase and pyroxene. Variations in olivine, plagioclase and chrome magnetite compositions in one comb layer of harrisite are consistent with upward crystallization of the layer along a thermal gradient in the magma of increasing temperature with height.

The origin of skeletal and dendritic olivines in harrisite is due to growth of edges and corners of crystals and to breakdown of a planar crystal-melt interface into fibres and indentations which are stabilized by a boundary layer of constitutionally supercooled melt. To achieve these conditions, a certain degree of supercooling or supersaturation must be attained. Linked parallel-unit olivines grow in a constrained manner, with latent heat being conducted

through the crystals into the intrusion floor, rather than into the magma.

The shapes of melt-grown olivine crystals vary systematically with increasing cooling rate and degree of supercooling. From hydrous, olivine-rich melts the following sequence of olivine shapes crystallize with increasing supercooling: granular, porphyritic, branching, randomly oriented chain-like, and finally plate. With increasing cooling rate the sequence is: porphyritic or polyhedral, granular + porphyritic, branching, randomly oriented chain-like (\pm lattice-work), plate or porphyritic. From anhydrous olivine-containing melts the following sequence of shapes crystallize with increasing supercooling or cooling rate: porphyritic (\pm linked parallel-unit), chain-like, lattice-work, and finally dendritic. Compositional change of the melt also has a systematic effect on olivine morphology: addition of olivine to a melt reduces the cooling rates at which each morphology of olivine crystallizes, whereas addition of water increases these cooling rates. Water and olivine content of the melt have little effect on the degrees of supercooling at which each olivine morphology crystallizes. Hydrous, ultrabasic melts cooled between 14 and 30 °/hr in the laboratory are differentiated with respect to olivine grain size and shape- small granular olivines form a cumulate at the base of the charge and are overlain by a few large elongate branching olivines with their a axes close to vertical, i.e., the internal layering features of harrisite have been modelled. The temperature must drop between 20 - 50°C below the liquidus to cause growth of the porphyritic and branching crystals in harrisite.

The crystallization experiments indicate that, close to the floor of the Rhum chamber, supersaturation of the magma in olivine increased upwards from cumulate into harrisite, and to this the upward change in olivine shapes is attributed. A detailed consideration of how the Rhum magma became massively supersaturated in a pluton

leads to the conclusion that it is probably due to a combination of cessation of convection of the magma and to loss of water from the water-rich parent magma of harrisite. The magma supercools below the temperature of maximum nucleation rate, at which granular ('cumulus') olivines crystallize and settle, and the growth rate increases, promoting skeletal olivine (porphyritic) growth. If the magma supercools sufficiently, nucleation effectively ceases and olivine crystals on, and just above, the floor grow rapidly with branching shape. Harrisite formation is terminated either when new magma convects to the floor and cumulus crystals settle from it, or when the isotherms in magma at the floor advance slower than the branching olivine. Comb layers form when magma adjacent to the floor or margin of a chamber contains very few suspended crystals and the substrate (wall or floor), on which the elongate crystals grow, is sufficiently cool to promote flow of latent heat through crystals into the substrate. Preferred orientation of crystals results from anisotropic growth rate in thermal and/or chemical gradients in a magma, at specific cooling rates and degrees of supercooling. Enhanced heat flow into the floor of the Rhum intrusion is due to a cycle of warming, by successive influx of new magma into the chamber.

The parent magma of harrisite was a water-rich, olivine-rich eucrite (melting point approximately 1300°C at 1 kb). Similar, unusually hot magmas probably existed in the Cuillin area of Skye and the Blackstones Bank, indicating that these were all particularly hot sites in a hot region (i.e., the Hebridean Province). These hot sites delineate an incipient spreading axis and trace the location of an elongate diapir of mantle peridotite, comparable to current concepts of mid-ocean ridge magmatism.

Currently, most layered igneous rocks are considered to form by gravity sorting and accumulation of crystals (e.g., Jackson, 1971). On the other hand, the origin of layers containing vectorially-oriented crystals, variously known as "comb layers", "Willow Lake layers" and "crescumulate layers" has not been convincingly elucidated. These layers are generally ascribed to in situ crystallization under enhanced supercooling conditions. But how the supercooling is induced, its value and the rate at which the crystallizing magma differentiates have yet to be evaluated.

Some of the layered "harrisitic" rocks (harrisite) of the Rhum pluton resemble "comb-layered" rocks. Since there is controversy regarding the petrogenesis of "comb layering" (Moore and Lockwood, 1973; Leveson, 1973), this type of layering is currently being re-investigated (Van Diver and Magetti, 1973; Lofgren and Donaldson, 1973, in press; Taubeneck, 1974). The large number of harrisite layers in Rhum provide a unique opportunity for detailed examination of this kind of layering. "Comb-layered" rocks are typically highly differentiated and dominated by one phase, as is harrisite, which is an olivine-rich rock. Yet, many of the olivines in harrisite have shapes suggestive of rapid, in situ growth. These conditions may imply crystallization from an ultrabasic liquid (Drever and Johnston, 1972).

There is textural evidence for massive olivine supersaturation of magma at the base of the Rhum magma chamber (Donaldson, 1974a) and for varying degrees of repeated supercooling (Wadsworth, 1961). Textures which may also be attributed to massive supersaturation (of plagioclase and pyroxene respectively) have recently been found in the Hettasch pluton, Labrador (Berg, 1974) and the Greenhills pluton, New Zealand (Mossman, 1973). Fractional crystallization of magmas in the plutonic environment, under conditions far-removed from equilibrium, may therefore be more common than previously recognized. Such metastable crystallization is important because it will have a different effect on the liquid line of descent of a magma than does

crystallization closer to equilibrium. One of the main lines of inquiry of this research is the cause of the metastable crystallization and supercooling in plutons, where slow cooling and slow crystallization are to be expected.

The most common silicate mineral to crystallize early from mafic magmas is olivine. Its crystal shape is extremely variable and sensitive to crystallization environment (Drever and Johnston, 1957). Many olivines, including those in harrisite, have skeletal or dendritic morphologies attributable to crystallization from supercooled magma. The principal objective of this research is to describe the range of morphology of olivine crystals and to deduce from experimental evidence and a theoretical consideration of crystal growth, what parameters control the morphology. Although this objective has wide petrologic relevance to mafic and ultramafic rocks, the study was initiated to solve the problem of how harrisite, and particularly "comb layers" of harrisite, crystallized and whether its parent magma was a basalt (Wadsworth, 1961), or an ultrabasic pegmatite (Harker, 1908b; Drever and Johnston, 1972), or an ultrabasic magma (Donaldson et al., 1973). Detailed examination of the skeletal and dendritic shapes of olivine crystals in harrisite can, by deduction of the crystallization conditions of the olivines, clarify the origin of this unusual rock type.

A detailed petrologic investigation of harrisite has been undertaken, involving petrographic description of the rocks (particularly the shapes of olivine crystals), electron microprobe analyses of minerals in the rocks, chemical analyses of some rocks and phase equilibrium studies. The morphologies of olivine crystals have been investigated experimentally as a function of both supercooling and cooling rate, and the shapes and "comb layering" of olivines in harrisite reproduced. Combination of the experimental and petrographic studies aids in developing a new crystallization model for harrisite by assigning the parent magma a maximum cooling rate and a value for supercooling at the time of growth of particular olivine shapes. From this information, possible mechanisms promoting harrisite crystallization can be constrained and semi-quantitatively evaluated.

Experimental crystallization of rock melts, as an aid to interpreting rock textures, is a relatively new branch of experimental petrology. The techniques used in this thesis have already proved useful in understanding textures in lunar basalts (Lofgren et al., 1974) and in deducing emplacement and thermal histories for igneous rocks. Results indicate that the techniques will also be useful in study of other non-equilibrium processes of petrogenesis, e.g., partial melting and fractional crystallization.

In summary, the thesis has four interrelated aspects:

1. The petrographic features of the rocks containing skeletal and dendritic olivine morphologies in Rhum (harrisite).
2. Determination of what factors control the shapes of olivine crystals in igneous rocks.
3. Laboratory modelling of the crystallization features of harrisite and determination of the degree of magma supercooling at which each olivine morphology grew.
4. The origin of harrisite and its implications for the petrogenesis of the Rhum pluton.

The results of the study provide insight into the relation of olivine crystal shapes to physical and chemical changes in a magma and aid in understanding the origin of supersaturation in layered intrusions. They also have application to the origin of "comb layering" in other layered intrusions and in lavas and to the cause of the rapid solidification recorded in the skeletal and dendritic crystals in these layers.

Chapter II INTRODUCTION TO HARRISITE AND COMB-LAYERED ROCKS

The Rhum lavas, ultrabasic complex and harrisite: previous work

Geologic research on the island of Rhum (fig.1) was initiated by McCulloch (1819) and by Judd (1874,1885,1889). Regional mapping of the island by Harker (1908a) culminated in publication of the "Small Isles Memoir" (1908b) in which he interpreted the Tertiary magmatism. Phillips (1938) and Tomkeieff (1942, 1945) examined the ultrabasic rocks of the layered intrusion and Tomkeieff (1942) and Black (1952) investigated the lavas. The tectonics of the island were discussed by Bailey (1945). In 1950 L.R. Wager initiated further petrologic research of the ultrabasic complex and the surrounding igneous rocks; the results are presented by Wager and Brown (1951), Brown (1956, 1963), Hughes (1960a,b), Wadsworth (1961), Brothers (1964) and Dunham (1964, 1965a,b, 1970), and are summarized by Stewart (1965), Dunham and Emeleus (1967), Wager and Brown (1968) and the Nature Conservancy (1969). Henderson et al. (1971) investigated the distribution of uranium in Layered Series rocks. Ridley (1971a,b, 1973) re-examined the volcanic rocks of Rhum and, in agreement with Brown (1956), considered the lavas to be a residual fraction of the magma which formed the ultrabasic rocks. Distinctive textures in the ultrabasic rocks were discussed by Drever and Johnston (1972), Donaldson et al. (1973) and by Donaldson (1974a). Reaction trends of cumulus spinels in the pluton were studied by Henderson and Suddaby (1971) and by Henderson (1975). The origin of zones of breccia within the pluton was re-interpreted by Donaldson (1975).

The Rhum ultrabasic intrusion is approximately circular in form, 8km in diameter and probably was emplaced 58-60 m years ago (Evans et al., 1973). A geophysical investigation of the pluton by McQuillin and Tuson (1963) indicated that 15.6 km of ultrabasic rocks underlie Rhum. The rocks are conspicuously layered and the layering is predominantly conformable. Macro-units of layered rock range from

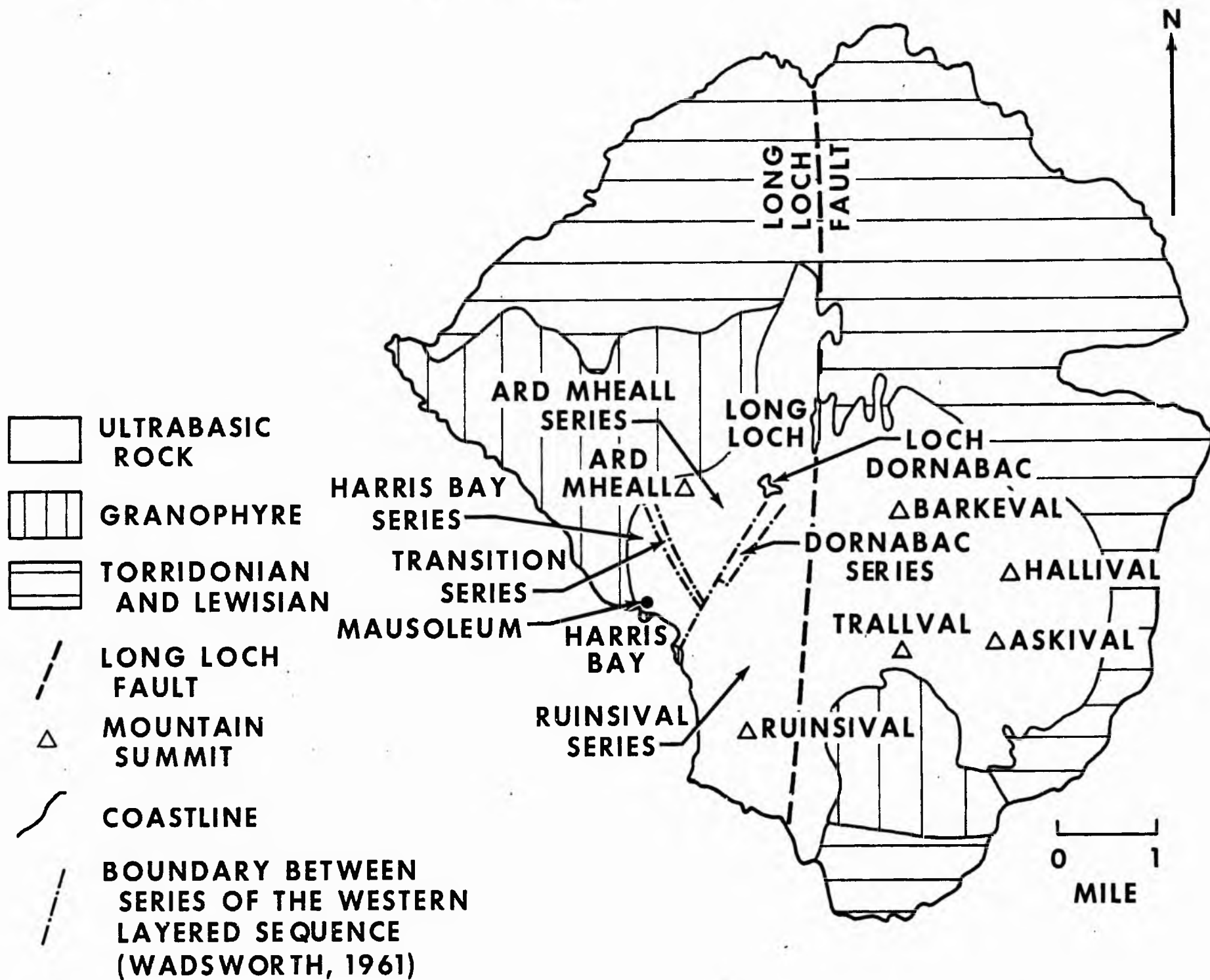


Fig. 1 Geological map of the Isle of Rhum illustrating the form of the ultrabasic pluton, the boundaries between Layered Series of the Western layered sequence (mapped by Wadsworth, 1961) and the location of some prominent geological features mentioned throughout the text. (Adapted from Wager and Brown, 1968, fig. 135.)



Fig. 7. 0.3 cm thick layer of host rock showing graphic, pegmatite texture due to random orientation of elongate, skeletal and parallel growth of quartz. Thin, rounded rock at top and bottom of picture is granitic gneiss. (Archie, 1961, p. 107)

25-130 m in thickness and are internally divisible into layers from 2 cm to 10 m thick. The finer scale layering may involve changes in phase proportions and/or texture. Cryptic layering is not developed. Macro-units either have an overall eucritic or feldspathic peridotite composition. Units of the latter type are commonly differentiated, with dunite (up to 98 vol. percent olivine) at the base, anorthosite at the unit top and rocks gradational in composition between these extremes at intervening heights. Wager et al. (1960) regard the textures of all the layered ultrabasic rocks as cumulus and postcumulus in origin.

A distinctive textural variety of these rocks contains large skeletal and dendritic forsteritic olivines, some with preferred orientation (fig.2) and some of branching shape. The rock was called "harrisite" by Harker (1908b), after Harris Bay (fig.1). Like the other eucrites and feldspathic peridotites, harrisite forms sub-horizontal layers, predominantly conformable with the macro-unit contacts. Harker regarded harrisite as a pegmatite injected, at a late stage in the crystallization of the intrusion, along well-defined planes of contact between the layered ultrabasic rocks. Wadsworth (1961) published some generalized field and petrographic descriptions of harrisite, together with modal analyses and a chemical analysis of one rock. Along with Wager and Brown (1951, 1968), Wadsworth (1961, 1973) considers harrisite to have crystallized from the same parent magma as the contiguous rocks, after the layer below, but before the layer above. A preliminary re-investigation of harrisite caused Drever and Johnston (1972) to revive Harker's concept of the rock as a pegmatite.

Other rocks containing skeletal and dendritic crystals

Textures identical with those in Rhum harrisite have been reported in only one other pluton- the Cambrian, Rognsund intrusion in Seiland, Norway (Robins, 1973). The intrusion is layered and some of the layers contain skeletal and branching olivines up to 1 m long. The layers have a maximum thickness of 3 m and average 1 m. Plagioclase crystals between the large olivines have compositions of An_{92-87} , whereas those

in adjacent cumulate layers are An_{85-73} . This rock type differs from Rhum harrisite in having a more calcic plagioclase and a greater abundance of pyroxene.

Elongate, vectorially oriented crystals of minerals grown in situ have been recorded in other plutons and also in minor intrusions and in lavas (Lofgren and Donaldson, in press). For example, elongate skeletal crystals have been described in the Willow Lake intrusion (Taubeneck and Poldervaart, 1960), the 'Mystery Dyke' (Drever and Johnston, 1972) and Archaean 'spinifex' lavas (e.g., Nesbitt, 1971). The last of these occurrences also contains the unoriented skeletal and dendritic olivines found in some Rhum harrisite (Donaldson, 1974a).

Lofgren and Donaldson (in press) discussed the origin of in situ vectorial crystal growth and described a mechanism by which the growth occurs. Our suggestions apply to all comb layers and to those harrisite layers displaying vectorial crystal growth. They do not apply to randomly oriented skeletal olivines in harrisite. Thus, the harrisite rocks of Rhum represent a unique problem of crystal growth in a plutonic, cumulate-forming environment.

Terminology of layered rocks containing skeletal and branching crystals

Independent investigations of layered igneous rocks containing oriented branching crystals inevitably resulted in a diverse nomenclature, involving descriptive terms, geographic terms and also genetic terms. The result is to obscure the genetic relation of layering in different igneous bodies. Further confusion is provided by the limitation of some terms to acid rocks and others to basic and ultrabasic rocks. Four frequently used terms are discussed here: "Willow Lake layering" (Taubeneck and Poldervaart, 1960), "comb layering" (Moore and Lockwood, 1973), "harrisitic layering" (Wager and Brown, 1951) and "crescumulate layering" (Wager, 1968).

"Willow lake layering" is a geographic term applied to sub-vertical, 'granodioritic' layers, sub-parallel to the margin of the Willow Lake pluton in Oregon. The layers are characterized by vectorial growth of elongate, curved and branching crystals toward the pluton centre.

Recognition that layers with similar textures are common in the Sierra Nevada batholith prompted Moore and Lockwood (1973) to propose the general descriptive term "comb layering". They defined the term as ".... a relatively unusual type of layering in granitoid rocks in which constituent crystals are oriented nearly perpendicular to the planes of layering." "Harrisitic" and "crescumulate" are terms applied to layered basic and ultrabasic rocks; the former is strictly a geographic term, the latter is a genetic term. Unfortunately, "harrisitic" has come to be regarded as a genetic term synonymous with "crescumulate", because the crescumulus hypothesis (Wadsworth, 1961; Wager, 1968) was originated to explain the apparent upward vectorial growth of olivine in harrisite. It will be shown that many harrisite layers contain skeletal and/or dendritic olivines which neither grew upwards nor grew from cumulus crystals, as the crescumulus hypothesis suggests. Unless it can be demonstrated that the elongate crystals grew upwards from cumulus crystals and that the rock represents a magmatic differentiate, the genetic term "crescumulate" should be avoided in describing rocks displaying this type of layering.

There are three differences between the descriptive terms. "comb layering" and "harrisitic layering", as used till now. 1) Unlike comb layers, harrisite need not contain oriented or elongate crystals; 2) only olivine crystals are skeletal in harrisite layers, whereas in comb layers plagioclase, pyroxene, olivine and amphibole may be skeletal in shape and 3) harrisite layers are sub-horizontal and are believed to follow the form of the base of the pluton (Wadsworth, 1961), whereas comb layers are generally sub-vertical and are conformable with the contact of the intrusion.

I propose that "comb layering" should not be restricted to granitoid rocks or to vertical layers. Since it is the skeletal, dendritic and branching crystals of all these layered acid, basic and ultrabasic rocks that makes them so distinctive, I also propose that more accurate description of layers can be achieved by stating the dominant mineral(s) of the layer and its morphological or textural relations. For example,

"plate olivine layer" would specify a layer dominated by plate olivine with no preferred orientation; "plate olivine comb layer" would specify a similar layer with olivine preferentially oriented perpendicular to the plane of the layer. The term "harrisite" or "harrisitic layering" should be confined to Rhum rocks and used to mean rock layers dominated by skeletal or dendritic or radiate olivines. "Comb-layered harrisite" would adequately imply preferred vectorial olivine orientation.

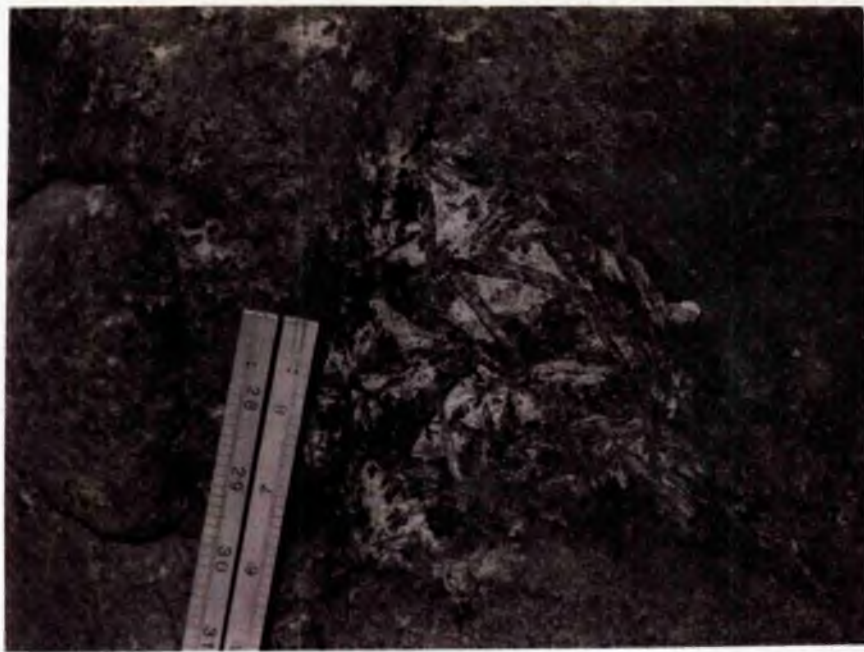
All the layers discussed in this section are dominated by immature (non-polyhedral) crystal morphologies. Hence, the general terms "skeletal crystal layer" and "dendritic crystal layer" could be applied to these rocks. The words "branching" and "comb" could usefully be inserted where appropriate.

Specific petrogenetic conditions are implied when a rock is described as a "crescumulate" or crystals in a rock are said to display "crescumulus" texture. Hence, description of olivines in lunar breccia 14320,4 as showing crescumulus texture (Brown et al., 1972) involves an unjustified genetic assumption. Similar textures are present in chondrules (Keil et al., 1973) and at the margins of basic dykes and sills (Drever and Johnston, 1957, 1972; Platten and Watterson, 1969). They can also be grown in the laboratory (this thesis). A more reasonable conclusion concerning the olivines described by Brown et al., which would not imply an origin in a layered intrusion, would be that they grew rapidly from a significantly olivine-supersaturated melt (Drever and Johnston, 1957).

Harrisite rock types and associated feldspathic veins and pegmatites

Harker (1908b) and Wadsworth (1961) recognized eucritic and peridotitic varieties of harrisite. The former are confined to the Harris Bay Series, which is itself eucritic in composition. The Transition and Ard Mheall Series comprise peridotite and peridotitic harrisite. The proportion of olivine in the eucritic harrisite is 26-45 percent, in the peridotitic harrisite it is 45-89 percent. Many of the peridotitic harrisite layers contain sufficient bytownite to be called feldspathic peridotitic harrisite. Harrisite near Loch

a.



b.

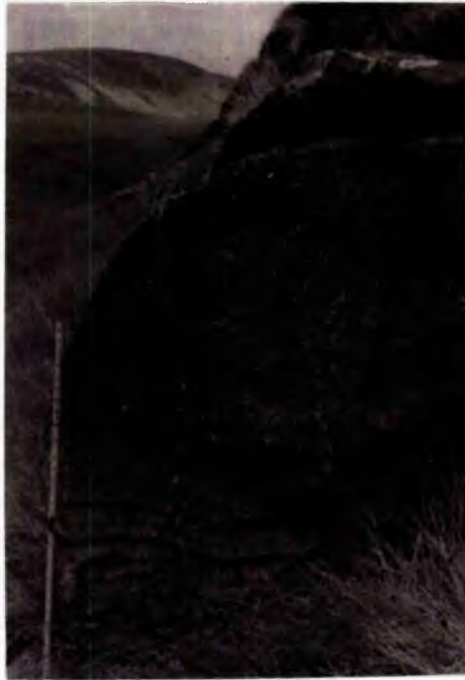


Fig.3 a. Pod of coarse gabbroic pegmatite in a boulder of eucritic harrisite. Large grey, lath-shaped crystals are plagioclase. Ruler is 5 inches (12.5 cm) long. (Harris Bay)

b. Narrow, diffuse vertical anorthosite veins in two harrisite layers and intruding the thin, intervening cumulate layer. Ruler is 3 feet (0.9 m) long. (Ard Mheall Series)

Dornabac contains greater than 50 percent bytownite, the remainder being predominantly olivine. Rocks with these modal proportions are classified as "allivalite" (Brown, 1956).

In most harrisite layers there are patches of olivine-deficient gabbroic pegmatite (fig. 3a). These patches are spherical in shape and 0.02 to 0.3 m in diameter. The plagioclase, augite and ilmenite crystals may be exceedingly coarse grained (Appendix I, samples 204 and 163), giving the rock its pegmatitic character. A vertical dyke (0.5 m wide) of the gabbroic pegmatite cuts eucrite and eucritic harrisite layers near the Harris Bay Mausoleum. Non-harrisitic rocks also contain occasional pods of pegmatite. Some of these pods are apparently isolated from adjacent harrisite layers, whereas others are connected to a harrisite layer by a thin vein.

Donaldson (1975) described thin veins of anorthositic gabbro and gabbroic anorthosite associated with the intrusion breccias of Rhum. Similar veins containing unzoned bytownite crystals are also associated with many harrisite layers. The veins are 1 mm to 2 cm wide and are multiply branching. They have no regular dip or strike and generally are never planar. Veins may connect two harrisite layers by intruding the non-harrisite layer (fig. 3b). Only the thickest veins have sharp contacts, in others contacts are diffuse. The veins appear to have been liquids separated from layers of harrisite and, rather than being considered as intrusive, many of them are best regarded as in situ segregation of feldspathic liquid. It is suggested that, at a certain stage in its crystallization, harrisite became sufficiently rigid to be irregularly fractured and the calcic feldspathic liquid, residual from harrisite crystallization, segregated into the fractures.

A definition of harrisite

In this study I have probably called many more rocks in the pluton "harrisite" than either Wadsworth (1961) or Harker (1908b). This

difference arises principally from lack of a satisfactory definition of harrisite. The AGI Glossary of Geology (1972) defines harrisite as: "A granular igneous rock composed chiefly of olivine and a smaller amount of anorthite and characterized by harrisitic texture."

"Harrisitic" is defined as: "...the texture....in which olivine crystals are oriented approximately at right angles to the cumulate layering of the rock." This definition is unsatisfactory because it alludes to the genesis of the rock and identifies the plagioclase as anorthite and not bytownite. It is also unsatisfactory in stressing preferred perpendicular orientation of olivine. I consider that the definition describes only one variety of harrisite which, although the most distinctive variety, is not the most abundant. For example, some harrisitic olivines show preferred horizontal elongation, while others have no preferred orientation (chapter V) . There is also a significant morphological gradation from round 'cumulus' olivines in normal layers, through subequant, indented, anhedral, skeletal olivines, to the kind of crystals mentioned in the AGI definition.

A more accurate definition of harrisite is necessary and the following one involving field, mineralogic and textural criteria, is preferred. "Harrisite is an ultrabasic, plutonic igneous rock in layered intrusions which contains > 25 vol. percent of olivine. The olivine crystals are characterized by skeletal or dendritic shapes and have larger size than olivines in the contiguous layers. Hydrous minerals are essential phases in the rock."

Terminology of non-harrisitic rocks in Rhum

Throughout this thesis, the terms "normal rock" or "cumulate" are applied to ultrabasic rocks in Rhum which are not harrisite, the latter term following the genetic interpretation of these rocks by Wager et al. (1960). Since it is of little relevance to the present inquiry, the origin of these rocks is not discussed at length. However, it is believed that there were multiple nucleation sites

for crystals in the Rhum pluton, including the floor of the chamber (Appendix I and chapter VII). Many so-called 'cumulus' crystals in 'cumulates' settled only a few cm, while others did not settle at all. My use of the term "cumulate" does not, therefore, imply acceptance of the hypothesis of Wager et al. that cumulus crystals nucleate at the roof of an intrusion, or that all layers of "cumulate" rock in Rhum are the result of gravity settling of crystals.

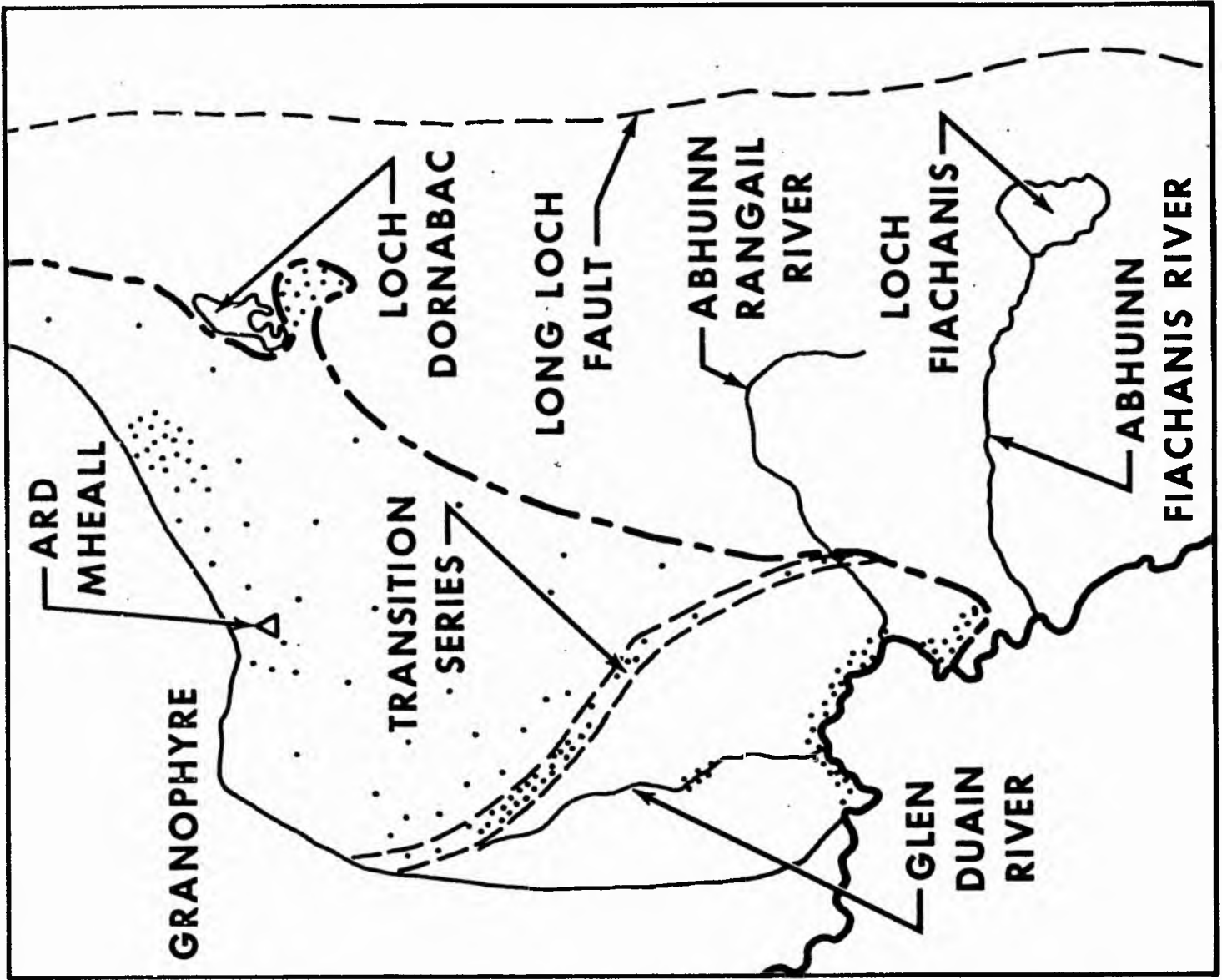


Fig. 4 Sketch map of the principal outcrops of harrisite in the Western Layered Series. Dotted areas contain harrisite layers, undotted areas lack harrisite. Relative density of stippling is proportional to the number of harrisite layers present. (Compare fig. 1)

0.5 MILE

Chapter III FIELD RELATIONS OF HARRISITE LAYERS

Distribution

Harrisite layers exist throughout the Rhum pluton, but are preferentially located in the Western Layered Series, i.e., west of the Long Loch fault (fig. 4). Brown (1956) reports a few layers of harrisite east of the Hallival-Askival ridge and on the north-west slopes of Trollaval. Godfrey (personal communication, 1972) found isolated outcrops of harrisite on the shoulder between Hallival and Barkeval. He considered that the outcrop distribution suggested the presence of a lens of harrisite 10 m thick and 35 m wide. Another previously undocumented harrisite locality was found east of Loch Dornabac during this study (fig. 4). Harrisite is abundant in the Harris Bay and Ard Mheall Series, but is particularly abundant in the Transition Series. The rock is absent from the Ruinsival Series, and from the Dornabac Series as far as mapped by Wadsworth (1961). Traverses I made in Glen Harris failed to locate harrisite. The present field study was confined to the Western Layered Series.

The distribution of harrisite suggests that the rock has a preferred location in the Western Layered Series close to that arc of the pluton margin between bearing 240° and 340° (fig. 4). However, it is not confined to the periphery of the complex.

Layer thickness and the proportion of harrisite in the pluton

A wide range of thicknesses was found on measuring approximately 50 layers of harrisite. The thinnest layer is 7 cm thick, the thickest is 10 m. As shown in fig. 24a, few layers are as thin or as thick as these extremes, and there is a preferred value of thickness of around 1 m. Ninety percent of the layers are between 0.15 and 1.7m thick. There is no evidence that the thickest layers formed by slumping of thinner, unconsolidated harrisite layers. (Details of the variation in layer thickness are discussed in chapter VI).

a.



b.



Fig. 5 a. Harrisite layer (marked by dotted ink lines) thinning from 0.45 m thick to absence (right to left). Length of exposure is 9 m. (Western Harris Bay)

b. Harrisite layer (10 cm thick) abruptly enlarging into a pod (right of picture). (Eastern Harris Bay)

30-35 vol. percent of the exposed Harris Bay Series is harrisite; the proportion rises to 60 vol. percent in the Transition Series and diminishes to 20 vol. percent in the Ard Mheall Series. Thus, although harrisite is a minor rock type in the pluton (less than 5 vol. percent of the total exposure), it is a major rock type in two of the Layered Series and is the dominant type in a third.

Dip and strike

Wadsworth (1961) found that adjacent harrisite and non-harrisitic layers have similar dip and strike. In most parts of the Layered Series, the strike was considered by Wadsworth to be an original depositional feature of crystal settling, related to the form of the floor of the magma chamber and the pluton margin. Dips range from zero degrees in central Harris Bay to 35° in the Transition Series.

Conformity and lateral continuity of layers

The most profitable locality for field study of harrisite is Harris Bay where layers can be examined for conformity and continuity in cliffs and wave-cut platforms. Detailed mapping in Harris Bay reveals the following stratigraphic anomalies between outcrops: 1) Individual harrisite layers vary laterally in thickness; 2) harrisite layers cross-cut cumulate layers; 3) layers of harrisite may laterally disappear; 4) the olivine morphology and crystal size in some layers change laterally. These anomalies are described below.

1) Layer extent and uniformity of thickness

Mapping in Harris Bay indicates a maximum of 350 m in lateral extent for individual layers of harrisite. In the Stillwater stratiform complex, Hess (1960, p. 128) found that the layers were "flat lenses" with lateral extension 100 - 1000 times that of their thickness. Most harrisite layers in Harris Bay have similar length to thickness ratios, being 0.2 to 1 m thick.

Some harrisite layers have non-uniform thickness; either the top or the bottom contact (or both) deviates from a planar contact. Two examples are shown in fig. 5. Occasional layers thin by as much as



Fig. 6 Tongue of eucritic harrisite extending upward into eucritic cumulate. Most tongues in this 0.6 m thick harrisite layer extend 0.3 m above the average level of the top of the layer. Ruler is 9 inches (23 cm) long. (Eastern Harris Bay)

60 percent over one metre lateral distance.

In Eastern Harris Bay (GR 341950) convex lenses of harrisite (0.3-0.45 by 2 m in size) are enclosed in normal (cumulate) eucrite. The conformable tops and bottoms of the lenses, together with their preferred vertically-elongate olivines rules out the possibility of the lenses being xenoliths. Nor do they represent a continuous harrisite layer that has been stretched and deformed into a boudin structure. These ultrabasic lenses unquestionably crystallized in situ. However, field evidence does not permit determination of whether the lenses are intrusive into the Layered Series or are contemporary with it.

In eastern Harris Bay one harrisite layer forms isolated, vertical tongues extending upwards into the normal eucrite (fig. 6). Wadsworth (1961) noted unevenness in the upper contact of harrisite layers due to variation in length of olivine crystals. However, these tongues cannot be attributed to this origin. They appear to have involved diapiric movement of harrisite.

Close to the margin of the pluton in Harris Bay, is an exceedingly thick layer of harrisite (7 m thick). The lateral extent of the layer cannot be determined, but indirect field relations suggest that it may thin, and ultimately disappear entirely, 40 m from the contact. Adjacent to the Mausoleum and 10 m from the granophyre, this thick layer exhibits complex dichotomy, forming five near-horizontal, undeformed, sub-layers of harrisite separated by normal eucrite. Near the granophyre on the opposite side of Harris Bay is a massive harrisite layer of similar thickness to that at the Mausoleum. The two outcrops are assumed to be parts of the same layer. The preferred location of this thick layer and its dichotomy are thought to represent control over the development of harrisite by its proximity to the contact.

2) Cross-cutting relations

A few harrisite layers transgressing normal layers may either be completely transgressive or partially transgressive, e.g., where tongues of harrisite embay or undercut a normal layer. Since some of these harrisite layers and tongues transgress horizontal bands of oriented olivines, their origin cannot be attributed to slumping.

3) Disappearance of layers

Two criteria were used for correlation in the mapping of harrisite layers: a) single marker bands of distinctive harrisitic facies and b) recognizable sequences of both layer thickness and olivine morphology. Application of these criteria revealed minor, unexposed, normal faults. Where correlation fails, the possibilities of faulting or the absence of a layer exist. For example, the stratigraphic sequence west of the mouth of the Glen Duain burn (fig. 4) lacks a harrisite layer that was found to the east, but contains two harrisite layers above and below the horizon of the missing layer. This observation cannot be explained by faulting, but may indicate the loss of a harrisite layer found east of the Glen Duain Burn. A major fault is suspected along the line of the Abhuinn Rangail river, since no correlation could be made across its mouth.

4) Olivine morphology changes

Detailed discussion of the shapes of olivine crystals in harrisite is deferred to a later chapter, only differences in the shape and size of olivines between adjacent harrisite layers and within the same layer are noted here. The descriptive terms "porphyritic olivine", "radiate olivine", "branching olivine" and "randomly oriented olivine" are those used by Donaldson (1974a; see also chapter IV).

The same shapes of olivine crystals may not appear in adjacent harrisite layers. For example, in central Harris Bay three consecutive harrisite layers contain porphyritic olivine, branching olivine and randomly oriented olivine, respectively. Whereas, elsewhere in the bay, three consecutive layers all contain branching olivine. There is no rhythmic or cyclic change in olivine morphology or crystal size between layers, but many harrisite layers show internal, upward textural gradation from small porphyritic olivine to large branching olivine (chapter V).

In Harris Bay the average length of olivines varies along with the morphologies in a single layer of harrisite. For example, a change from thin branching olivines 10 cm long by 0.1 cm wide to stouter, more equant, porphyritic olivines (0.3 cm) was found over a distance of 100 m in the same layer. This change is gradual. In another layer,

porphyritic, branching and radiate olivines were found together in some places, whereas in other outcrops of the layer, radiate olivines are absent.

Just as the difference in olivine shape and size between adjacent harrisite layers may be attributed to differing physical-chemical conditions during crystallization of the layers, so the lateral differences in olivine shape and size in a single harrisite layer suggest areal variation in the physical-chemical conditions prevailing within the magma.

Interpretation and evidence for intrusion of crystal-mush magmas

The differences between my description of harrisite and Wadsworth's (1961) are interpreted as follows. Whereas many of the harrisite layers in the pluton have crystallized after the layer below and before the layer above, this cannot be true of layers that apparently had sufficient mobility to form tongues, isolated reefs, and layers transgressive into the normal layered rocks. Mobility also resulted in thickness variations and marginal dichotomy of layers. Both these features are more common in sills and dykes.

From four sources in the Layered Series there is evidence for mobility and intrusion of crystal mushes. (1) Donaldson (1975) investigated two previously unmapped ultrabasic breccias in the pluton and deduced that probably all the Rhum breccias formed by upward intrusion of crystal-liquid mushes of (olivine + plagioclase + hydrous high-lime liquid) into the Layered Series. (2) At the mouth of the Glen Duain burn there is a complex intrusion of porphyritic 'anorthositic gabbro' into the layered eucrites. A series of irregular dykes of this gabbro invade the eucrites in an area 3 by 5 m. The anorthositic gabbro consists of plagioclase in round clots up to 1 cm in diameter set in fine-grained olivine gabbro. (3) In eastern Harris Bay, one layer of eucrite is intruded by a vertical dyke (0.6 m wide) which is continuous with the underlying, more feldspathic eucrite. The underlying layer either antedated the overlying layer or intruded it as a sill. There is, however, clear evidence for movement and

intrusion of a eucritic crystal mush. (4) In western Harris Bay, eucrite layers up to 1 m thick form horizontal, partially conformable layers. The same layer may outcrop at different stratigraphic horizons, the horizons being joined by an inclined sheet, transgressive to the general layering.

The combined evidence suggests that magmas of various compositions did intrude the Layered Series, and some ultrabasic layers could represent sill intrusions rather than crystal cumulates. These observations suggest for further consideration that harrisite may sometimes have a facility for independent movement, or autointrusion, into the Layered Series.

CHAPTER IV OLIVINE CRYSTAL SHAPES IN IGNEOUS ROCKS

Olivine is the most useful phase for indicating the crystallization conditions of harrisite and extensive petrogenetic interpretation is made in this thesis of its crystal shapes. It is appropriate at this point to digress from the description of harrisite in order to encompass a general discussion of the shapes of olivine crystals in igneous rocks. Using an olivine morphology classification, a more detailed field and petrographic description of harrisite can be presented, including comparison of the olivine shapes observed in it with those in other rocks, and those grown in the laboratory (chapter X).

1. Classification of olivine textures and morphologies

Drever and Johnston (1957) demonstrated the diversity in picritic rocks of growth shapes of forsteritic olivine, particularly of dendritic and skeletal shapes. If the conditions favouring growth of particular morphologies are to be understood, a consistent scheme of classification is necessary.

a) Methods of establishing three-dimensional crystal shape

The three-dimensional shape of skeletal and dendritic crystals can, in some cases, be examined directly: (1) as complete, single crystals fortuitously blown free of lava during vesiculation (Switzer et al., 1972), (2) in experiments where crystal surfaces protrude from the charge free of other crystals and glass (e.g., Lofgren et al., 1974; this study) and (3) where crystals are smaller in size than the thin section thickness and are completely set in glass. Indirect determination of the shape of olivine is achieved by examining a large number of crystals in a thin section and relating the shape of each grain to crystallographic directions established on a Universal Stage. The combined information is used to construct the shape of an "ideal" three-dimensional crystal. This indirect approach

is used extensively in the present study. Statistical populations of crystals were not examined and generally, less than ten crystals were investigated in any one thin section.

The investigation of three-dimensional olivine morphology in harrisite is impeded by the large size and preferred orientation of crystals. Many crystals can be examined in toto only in the field and generally only in flat, two-dimensional surfaces. By sectioning large, single crystals in critical directions and examining the crystallographic orientation with the Universal Stage, and by examining outcrops that have single crystals exposed in more than one outcrop face, it is possible to establish an idealized shape for many of the very large crystals.

b) Scheme of classification

Donaldson (1974a) modified the classification of Nesbitt (1971) and compared olivine morphologies in the harrisite and spinifex rocks. That classification is expanded here and additional illustrations are presented of morphologies in natural rocks and in synthetic, laboratory-crystallized 'rocks'. Some categories of the classification combine both textural and morphologic features, depending on which is the dominant feature. ('Texture' is used here to mean the spatial relationship of one olivine to another, rather than of olivine to other minerals.)

c) Previous work

The following is a brief review of the features of olivine habit recognized by, or inferred from the work of, Drever and Johnston (1957).

1. Equant and tabular (or bladed) crystals are most common; columnar habit is rare.
2. Non-equant crystals are elongate parallel to a or c, but not parallel to b.
3. Faces are generally of the following forms: $\{010\}$, $\{021\}$, $\{101\}$, $\{001\}$, $\{110\}$, $\{100\}$.
4. Skeletal crystals result when a particular form is missing or is only partially developed. The three major crystallographic zones

of olivine lack the following faces, in order of most marked absence:

[100] — {021} followed by {010}

[001] — {110} " " {010}

[010] — {101} " " {110}

These features are used to distinguish categories of morphology in the classification presented here.

d) Thirteen categories of morphology

1. Polyhedral olivine

Crystals have perfect faces (euohedral outline) and are generally equant or tabular.

2. Porphyritic olivine

Crystals are subequant skeletons which retain, with varying degrees of perfection, the gross outline of the common dome and prismatic forms of olivine. They show a combination of planar faces, smooth curvilinear lobes and re-entrants, and may be internally complete (e.g., fig. 7a) or internally skeletal (fig. 7b). The latter type show either regular, symmetrical, skeletal structure (fig. 7d) or irregular internal structure (fig. 7c). The forms {010}, {021} and {110} are absent or incomplete in porphyritic olivines (cf. Drever and Johnston, 1957). Elongation in different crystallographic directions is variable; \underline{a} and \underline{c} are $\geq \underline{b}$, while \underline{a} may be $>$, $<$, or $= \underline{c}$. Hence, though the morphology is commonly equant to subequant (fig. 7d), there is transition to acicular forms (fig. 7n) and to tabular forms (fig. 7m). From the sketches in fig. 7 it is clear that few porphyritic olivines have identical shapes. Some crystals have simple forms (e.g., fig. 7d), others involve growth of complex, irrational, or curved forms (e.g., fig. 7g).

It is common in the literature to see the term "embayed" or "embayment" applied to olivine crystals, particularly those of porphyritic type. The term implies resorption of an originally complete crystal, which is untrue in most skeletal

Fig. 7 Pseudo-three-dimensional sketches of porphyritic olivines in experimental charges and rocks. Axes indicate the crystallographic orientation of each section. Crystals vary from 0.1 to 4 mm in length.

a, c and e: Rhum harrisite sample 17 (Table 2)

b: picrite sill, Soay (fig. 8a of Drever and Johnston, 1957)

d and h: picrite glass crystallized at 40°C below the liquidus temperature

f, g, k, m, n and q: Apollo 12 synthetic glass (analogue of sample 12009) crystallized respectively at 80, 50, 80, 20, 20 and 80°C below the liquidus temperature

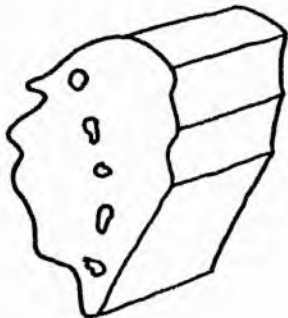
i: Rhum harrisite sample 140 (Table 2)

j and p: Apollo 15 synthetic glass (analogue of "quartz-normative basalt" group) crystallized at 75°C below the liquidus temperature

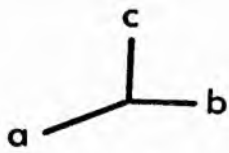
o and r: same glass crystallized by cooling from 20°C above the liquidus at $30^{\circ}/\text{hr}$

l: Rhum harrisite sample 182 (Table 2).

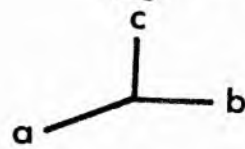
A



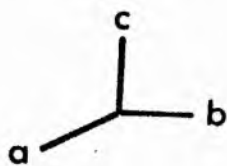
B



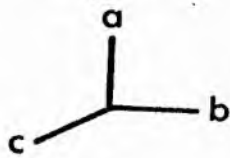
C



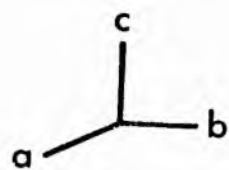
D



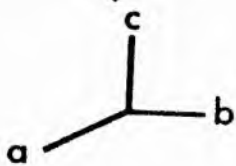
E



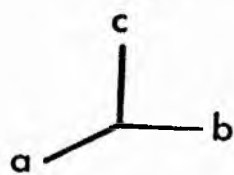
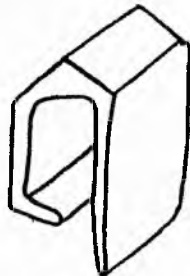
F



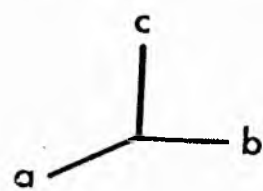
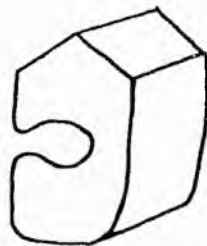
G



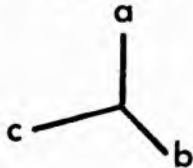
H



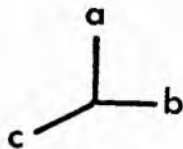
I



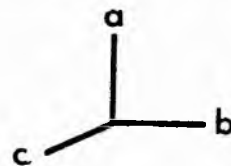
J



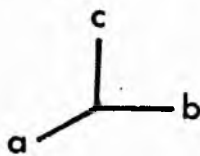
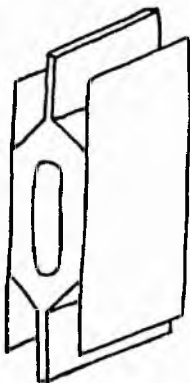
K



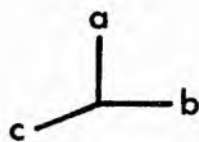
L



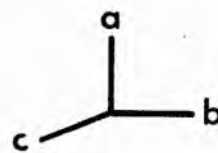
M



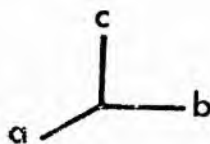
N



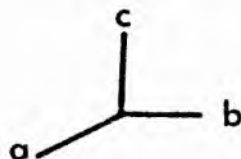
O



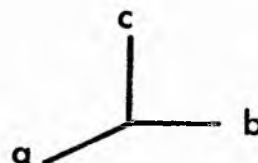
P



Q



R



olivines. The terms "re-entrant" (Martin and McLean, 1973), "cavity" and "indented", which have no genetic connotation, are therefore preferred.

"Porphyritic olivine" is taken from Nesbitt's (1971) term "porphyritic spinifex", and strictly should apply to the texture of a rock, rather than the olivine shapes in it. However, the fact that olivines of this shape are usually larger than all other crystals in a rock (Donaldson, 1974a) justifies this new morphological use of "porphyritic". Description of olivine as "porphyritic", and not "phenocrystal", adequately distinguishes morphological use of the term from all previous use of "porphyritic" as a textural term.

3. Granular olivine

Granular crystals are equant, anhedral and subspherical in shape. They may contain round or oval inclusions of glass or ground-mass material. The cumulus olivines at the base of each harrisite layer and of covering layers are granular. Experimental crystallization of granular olivines (p. 85) indicates that they are not necessarily resorbed forms; some can be growth forms.

4. Chain-like olivine

Crystals of this type are highly elongate skeletons composed of linked units (fig. 8a) or containing glass or mineral-filled holes (fig. 8b). They may be in random orientation or in parallel growths. At their centre, many crystals have an enlarged skeletal unit resembling a lantern or flattened Maltese Cross (Bryan, 1972a, fig. 1b and 1c). In sections cut perpendicular to the c or a axes, units are commonly H shaped, with a small tongue connecting the bar of the H to the next unit (fig. 8a). Growth is apparently effected by repeated nucleation of a new unit on the preceding one. In harrisite many chain-like olivines have lobes and indentations.

Universal Stage study of chain-like olivines establishes that they may be acicular, with $\underline{a} \gg \underline{c}$ and \underline{b} or $\underline{c} \gg \underline{a}$ and \underline{b} , or they may be bladed with $\underline{a} > \underline{c} > \underline{b}$ or $\underline{c} > \underline{a} > \underline{b}$, or they may be thinly tabular with $\underline{a} \approx \underline{c} \gg \underline{b}$. The forms {010}, {021} and {101} are generally well developed.

a.



b.

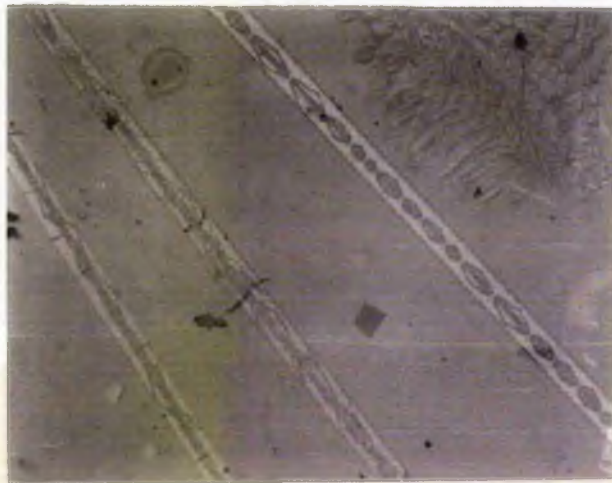


Fig. 8 Chain-like olivines

a. Individual H-shaped units in an olivine, showing the manner of stacking of units and the tongues extending from the cross-bar of each unit. [Crystal grown during cooling of sample E at 29° /hr (Table 17). Length of crystal 1.5 mm. Crystal is elongate parallel to a, short axis is parallel to b.]

b. Glass-filled holes along the length of a chain-like olivine. [Crystal grown during cooling of Apollo 12 basalt at 200° /hr (Table 12a). Same orientation as in fig. 8a. Crystal is 1.2 mm long.]

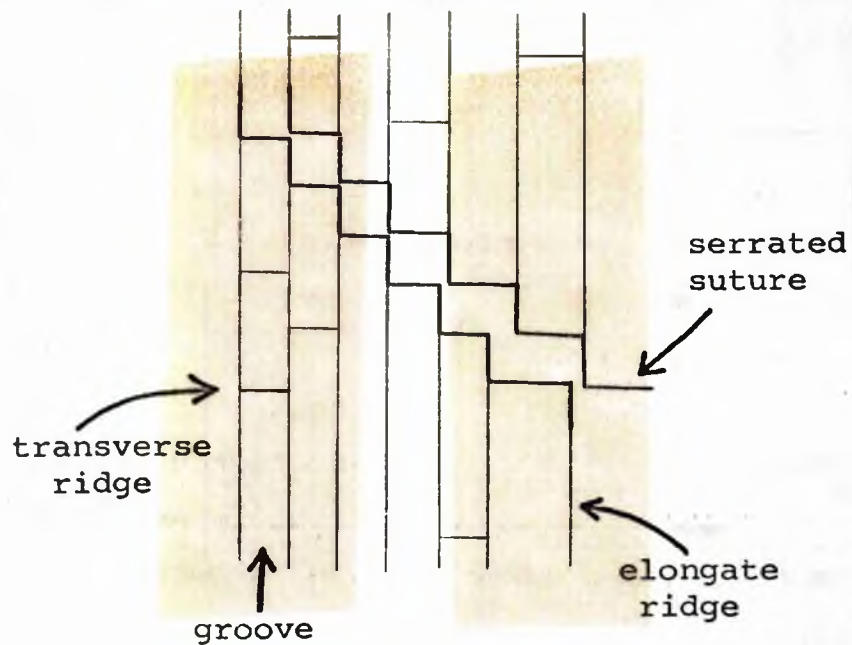


Fig. 9 Sketch of individual plate surfaces in a plate olivine from Western Australia, illustrating the conformity of groove directions in a single olivine plate and the smaller ridges at right angles to the groove. The area between the heavy lines is the surface of the underlying plate, exposed along a suture. (Sketch is approximately 1 cm across.)



Fig. 10 Grooves in an olivine plate in harrisite picked out in a mould of plagioclase. Pencil for scale. (Ard Mheall Series)

5. Parallel growth olivine

Drever and Johnston (1957) illustrated elongate olivines of two, three and four parallel growth units. Their fig. 9 illustrates the relationship of parallel growth olivine to chain-like olivine. Both shapes are elongate parallel to c and/or a and may be acicular, bladed or tabular. The distinction proposed here is that parallel growth olivine lacks the feature of the stacked, skeletal units characteristic of chain-like olivine. But it should be noted that some chain-like olivines display parallel growth (e.g., Lofgren *et al.*, 1974, fig. 2b).

6. Plate olivine

These are complex crystals consisting of two or more parallel, or near-parallel, plates or blades of olivine. Plates are either thinly tabular parallel to (010) or bladed ($c > a \gg b$). Plates of both types are stacked along the b crystallographic axis and individual plates may terminate in dome faces.

Each plate of olivine in spinifex rocks has internal structure. The following description is of a spinifex rock sample from the Ravensthorpe area, Western Australia. Pieces of the thin (0.5 mm) plates have weathered, permitting observation of a number of surfaces belonging to the same set of parallel plates. A series of parallel grooves (< 0.5 mm wide) traverses each surface. All the surfaces show one of two mutually perpendicular groove directions (fig. 9); adjacent plate surfaces need not have different groove directions. At intervals along the length of a groove are narrow ridges (< 0.05 mm wide) perpendicular to the groove lineation. This structure indicates that each olivine plate is composed of near-perfect, flattened parallel growth units (cf. Pyke *et al.*, 1973). Larger-scale grooves are observed in Rhum harrisite (fig. 10), but generally they lack the perpendicular relationship between groove directions found in the Ravensthorpe spinifex rock.



Fig. 11 Crystallographic branching olivine. [Crystal grown during cooling of sample F at $128^{\circ}/\text{hr}$ (Table 17). Crystal is elongate parallel to a and is 3.3 mm long.]

These descriptions emphasize that plates of olivine are not simple solid sheets, but contain an intra-plate structure, the complexity of which is increased in the 'branching olivine' class, described next.

7. Branching olivine

This category was introduced (Donaldson, 1974 a) to replace the "harrisite spinifex" category of Nesbitt (1971). Nesbitt based his description on Wadsworth's (1961) observations of harrisite which stressed the branching or budding nature of olivine parallel growth. Two types of olivine branching were illustrated by Donaldson (1974a). Recognition of one further type of olivine branching in experimental runs renders it necessary to distinguish three morphological sub-groups of the "branching olivine" class.

a. Non-crystallographic branching olivine

From a primary, elongate crystal, secondary elongate branches are inclined at 30° or less to the growth direction of the principal crystal (Donaldson, 1974a, fig. 5). These branches have no fixed orientation with respect to the main crystal, other than having their b crystallographic axes parallel in space to that of the principal crystal. Hence, they are regarded as non-crystallographic branches (Keith and Padden, 1963). The crystals are elongate parallel to c and are all bladed (c > a >> b). The blades lie in a common plane parallel to (010) and each may be internally skeletal.

b. Crystallographic branching olivine

In some experimental runs, there are branching olivines similar in form to non-crystallographic branching olivine. However, the branches are in optical continuity and the whole crystal passes to extinction as a unit (fig. 11). The morphology of these single dendritic crystals is distinguished as "crystallographic" branching. Crystals are bladed parallel to (010) with c > a >> b and the branches inclined at approximately 60° to the c axis are probably growing along directions perpendicular to (101) and $\bar{1}01$. Only one occurrence of this branching form was encountered in Rhum harrisite.

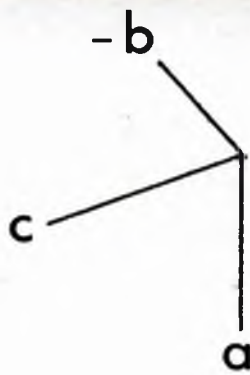


Fig. 12 Block diagrams demonstrating variation in the pattern of linked parallel-unit olivine in harrisite. Each diagram represents one crystal. Olivine is black, plagioclase and augite are white.

- a. Pronounced platey structure of olivine parallel to (010); plates are internally skeletal, composed of units elongate along a.
- b. Less distinct platey structure, more intricate internal plate structure.
- c. Slight platey structure. Individual 'plates' are composed of linked rods. (Scale parallel to a exceeds 15 cm.)

c. Linked parallel-unit olivine

Examples of the appearance of this morphology are shown by Donaldson (1974a, fig. 6) in two dimensions, and in three-dimensional block diagrams in fig. 12. All the examples in harrisite are dominated by abundance of parallel growth units elongate along the a crystallographic axis. Each unit is flattened parallel to (010) and is internally skeletal after the manner shown by Drever and Johnston (1957, fig. 9e). Occasional 'buds' link units, as are shown schematically in fig. 12.

Fig.12a shows that the flattened parallel units may be regarded as substructure of an internally-skeletal plate crystal. Unlike the plate crystals described in section 6, these plates have a more complex internal structure, individual parallel units being linked by 'buds' elongate along the b axis (fig. 12a). In fig.12b the skeletal character and irregularity are increased, but the overall structure still conforms to the model in fig. 12a. In some crystals, evidence for tabularity parallel to (010) may be poor or absent, and a series of irregularly shaped, linked, parallel 'rods' results in a fasciculate intergrowth of olivine and other minerals (fig. 12c). Each 'rod' is still part of one single crystal.

In harrisite, linked parallel-unit olivine grows up to 2.1 mm long. In contrast to linked parallel-unit olivines in the Ard Mheall Series, all of which are equant, the linked parallel-unit olivines in the Transition and Harris Bay Series tend to be bladed with $a \gg c > b$.

This is the most complex morphology of olivine encountered in this study; firstly, because the shape is highly varied (figs. 12a - c) and secondly, because it has the features of, and is transitional between, plate olivine and the simpler, parallel growths of two or three units (Drever and Johnston, 1957). Plate olivine and linked parallel-unit olivine may be regarded as two morphological "end members". Stages in the transition between these extremes are well-displayed by the "barred olivines" in meteorite chondrules (e.g., Dodd and Calef, 1971).



Fig. 13 Randomly oriented olivine in harrisite. Ruler is 27 inches (0.67 m) long. (Eastern Harris Bay)

I have examined occurrences of branching parallel-unit olivine in the 'Mystery Dyke', N. Skye (Drever and Johnston, 1972) and in a banded dolerite dyke from Slemish, N. Ireland (Preston, 1963). The branching olivines in both dykes complicate the features already described in being elongate parallel to the b crystallographic axis, rather than to the a or c axes that are more characteristic of olivine elongation (Drever and Johnston, 1957). Furthermore, they combine aspects of 'radiate' (next section) and non-crystallographic branching morphologies. Therefore the orientation and shape of linked parallel-unit olivines in harrisite are not the only variety of this class of olivine morphology.

8. Randomly oriented olivine

These olivine crystals are randomly arranged, elongate (generally acicular) skeletons. Individual skeletons may be porphyritic, branching or chain-like in shape. Randomly oriented olivines in harrisite (e.g., fig. 13) are acicular to bladed in habit with $c > a \gg b$. Random orientation of elongate skeletons implies either rapid in situ crystallization, with little chance for crystal settling, or accumulation of olivine with another phase in a static magma.

9. Radiate olivine (other phase in a rock)

In his classification, Nesbitt (1971) used the term "radiate" for my "randomly oriented olivine" category. Nesbitt's term contained the erroneous implication of a common nucleus for two or more olivine fibres. Olivines in which fibres or plates radiate from a common nucleus are known, and the term "radiate" should be reserved for these.

Only one occurrence of a spherulite of olivine has been recorded in Rhum -- in Transition Series harrisite. The spherule is 0.22 mm in diameter and is composed of fibres 2 μ m wide. The crystallographic orientation of the fibres has not been determined. Olivine spherulites, up to 0.5 mm in diameter, have been found in the margins of basaltic pillows in Taiwan (Bass, personal communication, 1974). But no other truly spherical olivine spherulites are known to the writer.

a.



b.



Fig. 14 Radiate olivine in harrisite.

- a. Preferred downward growth. Harrisite layer is sandwiched between eucritic cumulate layers which have a well-developed foliation due to preferred orientation of tabular olivines. Ruler is 6 inches (0.15 m) long. (Central Harris Bay)
- b. Downward-forking, radiate olivine in eucritic harrisite. Ruler is 20 inches (0.5 m) long. (Central Harris Bay)

All other radiate forms of olivine in harrisite are fans subtending an angle of 15° or less. Generally, two fibres comprise the fan, but there may be up to six. This textural type was recognized by Lewis (1971) in slag flows, where fayalitic olivines nucleated in the chilled top and bottom of the flows and subsequently grew inwards as fans of olivine plates up to 1.5 cm long (cf., fig. 14a of Harris Bay eucrite). In harrisite, fibres grow up to 0.5 m in length (fig. 14b). Lewis determined that radiate olivines elongate preferentially along the c and a crystallographic axes. The a axes of fibres in a single fan are parallel in space, whereas the c axes diverge from the nucleus. In harrisite, the individual olivines of a fan are bladed ($\underline{c} > \underline{a} > \underline{b}$) or acicular ($\underline{c} > \underline{a} = \underline{b}$) rather than tabular, but they share the crystallographic orientation of crystals in slags. Like plate olivine, the fibres of the fan may have internal skeletal or dendritic structure.

10. Dendritic olivine

This morphology resembles a Cross of Lorraine in sections perpendicular to a, and the veins of a leaf in sections perpendicular to c. Growth involves primary, secondary and tertiary branches. The nucleation site can often be recognized as the thickest portion of the thickest fibre present and this fibre is interpreted as the primary. The locus of fibre terminations trace crystal faces of the forms $\{010\}$, $\{021\}$ and $\{110\}$. In sections cut perpendicular to the a axis, a single primary branch, elongate along c, supports right-angled branches elongate parallel to b which in turn support tertiary branches parallel to the primary fibre (fig. 15). In sections cut perpendicular to c, a single primary branch elongate along a supports secondary branches inclined at approximately 60° to the primary, in turn supporting tertiary branches perpendicular to the secondary ones and lying in the plane of the thin section. It appears that the dendrite is overall tabular parallel to (010) and grows symmetrically from a central primary branch of plate form. Fibres grow predominantly perpendicular



Fig. 15 Dendritic olivine cut perpendicular to c axis and elongate parallel to a. [Crystal grown during cooling of synthetic Apollo 12 basalt at $1250^{\circ}/\text{hr}$ (Table 12a).] Crystal is 1.3 mm long.



Fig. 16 Lattice-work olivine sectioned in a variety of orientations. [Crystal grown during cooling of synthetic Apollo 12 basalt at $650^{\circ}/\text{hr}$ (Table 12a).] Field of view 0.8 mm.

to a, b and c; less common are fibres perpendicular to the forms {021}, {110} and {101}.

11. Lattice-work olivine

This morphology is dominated by a fine-grained dendritic mesh or lattice. Space between the dendritic fibres may be substantially infilled, favouring the suggestion that some crystals originate as dendrites and subsequently fill-in space by overgrowth (Buckley, 1951). The dendrite fibres are straight and all lie in the (010) plane. Examination of {010} sections on the Universal Stage establishes that the dendrite growth directions are approximately along poles to (101) and $\bar{1}01$. If a lattice-work olivine is rotated until it is approximately perpendicular to {010} the shape changes to chain-like. Hence, there exists a gradation in morphology from chain-like crystals which are skeletal and lack dendritic structure in (010) to lattice-work crystals which are skeletal (chain-like) viewed perpendicular to {010}, but dendritic viewed parallel to {010}.

Crystals vary from tabular (a \approx c \gg b) to bladed (c $>$ a $>$ b) in shape. In the former, the locus of the fibre terminations trace edges of the crystal parallel to [100] and [001] and straight extinction results. When the form is bladed (fig. 16), the locus of dendrite terminations define the directions c and [101] or $\bar{1}01$ and inclined extinction up to 40° results.

12. Swallow-tail olivine

From an otherwise euhedral olivine, four gently arcing and flattened fibres extend from the crystal corners formed by intersection of faces of the form {010} and {100} or {010} and {110} (fig. 17a). The space between fibres may be partially filled by secondary fibres on the four primaries (fig. 17b). The secondary fibres are parallel to the direction of the primary adjacent to the primary fibre upon which they grow. None of the fibres shows parallel extinction. The morphology is unusual for olivine in containing curved, irrational dendritic fibres and being tabular parallel to (001) (a $>$ b \gg c) (contrast Drever and Johnston, 1957).

a.



b.

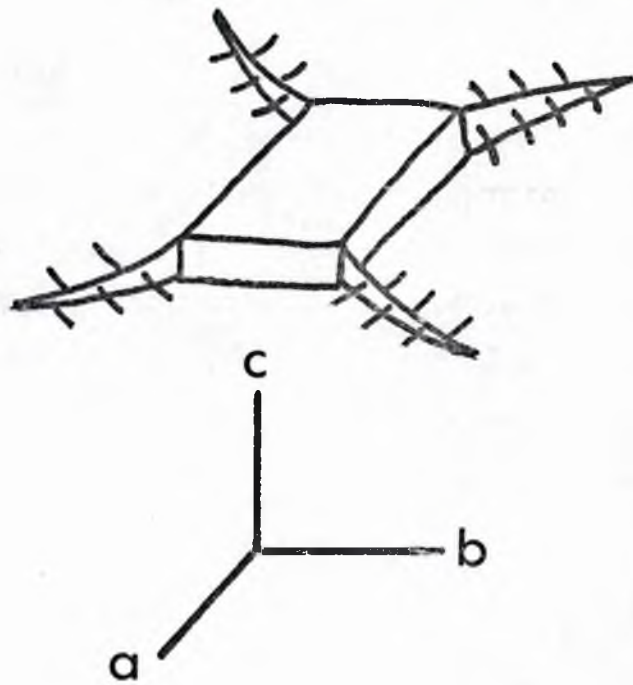


Fig. 17 a. Swallow-tail olivine sectioned perpendicular to c axis; a lies NW - SE. [Crystal grown in the laboratory during quenching of a picrite melt.] Crystal is 0.1 mm long.
b. Sketch of the crystallographic orientation and three-dimensional shape of swallow-tail olivine.

13. Irregular olivines

The crystals of olivine in much of the harrisite exposure at the northern end of the Ard Mheall Series are apparently large (frequently greater than 0.3 m), contain deep indentations and may be curved. While optical examination might permit classification in one of the other categories, this loosely-defined category is erected for those olivines which can adequately be examined only in the field, and yet appear to be unique. In many of the harrisite rocks with irregular olivine the term macrographic intergrowth (of olivine with bytownite and augite) is appropriate.

e) Summary

It is appreciated that these categories fail to cover all possible olivine textures and morphologies and it is not suggested that, given an olivine, it can uniquely be classified. Many crystals must be assigned to combinations of categories. This is made inevitable by the limited number of growth directions in skeletal and dendritic olivine, which presumably reflects the rigid control of growth by the crystal lattice. Nonetheless, only by systematic description can the different morphologies be correlated with variations in crystallization conditions, as discussed in chapter X.

2. Conclusions concerning harrisite olivine morphology

i. Harrisite exhibits seven distinct non-polyhedral olivine morphologies: porphyritic, randomly oriented, chain-like, radiate, parallel growth, irregular and branching. These cannot all be attributed to a growth history of upward elongation by post-depositional overgrowth on an oriented grain of olivine (Wadsworth, 1961; Wager, 1968; next chapter).

ii. Harrisite conspicuously lacks certain olivine morphologies, namely dendritic olivine, lattice-work olivine and swallow-tail olivine.

iii. Those olivines in harrisite which are elongate and oriented perpendicular to the layering are not elongate parallel to b , as are those at the margins of the banded dykes at Slemish and N. Skye.

iv. The very largest olivines are exceedingly complex skeletal crystals composed of flattened parallel units linked together by 'buds' along b and c, and sometimes stacked to form crude, parallel, internally skeletal plates of the form {010}.



Fig. 18 Preferred upward growth of elongate olivines in eucritic harrisite. Note the foliation of crystals in the material between the large olivines. Pencil for scale. (Eastern Harris Bay)

Chapter V ORIENTATION AND DISTRIBUTION OF OLIVINE CRYSTALS
 IN HARRISITE LAYERS: RELEVANCE TO THE
 CRESCUMULUS HYPOTHESIS

This chapter critically examines some of the features of harrisite layers upon which the 'crescumulus' hypothesis (Wager, 1968), currently applied to the rock, is based.

1. Growth direction of olivine

A variety of growth directions of elongate olivines exists in harrisite. The following is a review of these directions.

A. Upward growth

Figure 18 illustrates vertical, elongate, branching olivine in the Harris Bay eucrite. It is the a axis of the olivine which is most commonly vertically oriented. The olivines are of linked parallel-unit type. Other illustrations of upward growth of olivine are shown by Wadsworth (1961, figs. 11, 13 and 14), by Drever and Johnston (1972, fig. 5b), and by Donaldson (1974a, fig. 5).

Many olivines have been located which are not vertically oriented and which cannot be attributed to upward growth. The following are a few examples.

B. Downward growth

The downward-widening, fork shape of radiate olivine in figure 14b indicates the direction of crystal growth. The nucleus of the olivine is located within a harrisite layer and so the crystal cannot have commenced growth from a cumulate crystal mush. The most convincing evidence that harrisitic olivines can grow both downwards and upwards is displayed in figure 14a. Olivines have grown from both the upper and lower margins of the harrisite layer, in contact with horizontally olivine-laminated eucrite. The upper laminated eucrite must have existed before growth of the radiate olivines in the harrisite.

C. Randomly oriented growth

Skeletal olivines of this type are 0.5-10 cm in length in harrisite. Layers containing randomly oriented olivine occur in the Harris Bay, Transition and Ard Mheall Series. The random orientation may indicate homogeneous in situ nucleation.

D. Horizontal growth

Whereas branching olivines frequently grow vertically elongate, many are in random orientation. Examples of branching, horizontally elongate crystals (a crystallographic axis horizontal) have been found. Localities in which horizontally elongate, skeletal olivines dominate the rock texture occur in the laminated eucrites of the Harris Bay Series. The olivines are of flattened porphyritic type, or of parallel growth type, with sub-parallel elongation direction. Like the branching olivines, the a crystallographic axis is located preferentially near-vertical. Wadsworth (1961) regarded this texture as an igneous lamination of cumulus olivines, noting that the tabularity was "considerably obscured by the development of parallel growth structures, similar to those of the harrisitic olivines." Since the olivine crystals are elongate and skeletal, I regard the rock as a variety of harrisite.

E. Cognate skeletal olivine xenocrysts

Isolated olivine crystals typical of harrisitic facies exist in a few outcrops of normal-textured ultrabasic rock. These crystals might be derived as megacrysts from harrisite layers, e.g., they may have been the tops of elongate olivine crystals broken off by motion of magma. This origin cannot be tested since the crystals lack deformation and can never be traced to a source. The possibility cannot be rejected that they nucleated and grew freely within the magma. Clearly, they did not crystallize in situ. The close association of skeletal and non-skeletal (cumulus) olivines suggests that harrisite is an intrinsic part of the development of the layered pluton and that each harrisite layer must be nearly contemporaneous with contiguous layers.



Fig. 19 Thin section of the contact between peridotitic harrisite and overlying cumulate (Ard Mheall Series). Note the changes in olivine grain size and shape and also the train of spinel grains trapped on the underside of the skeletal olivine at the base of the picture. (Plane polarized light. Field of view 8 mm wide.)

2. Changes in olivine shapes within harrisite layers and across layer boundaries- 'anatomy' of a harrisite layer

The contact relations of harrisite layers, and the variation in olivine shapes through the layers, are summarized in this section. It is shown that the layers are internally layered with respect to olivine shapes and grain sizes.

Harrisite layers are consistently bounded by sharp upper contacts. Commonly the contact is undulatory rather than planar. An abrupt textural change, accompanied by a grain size change, marks the contact. Olivine crystals in the underlying harrisite are much larger than those in the overlying facies, and they are also skeletal and dendritic rather than polyhedral or granular (fig. 19). Although the contact is sharp, some irregular-shaped clots of the granular olivine can be found in thin sections of the top of the harrisite layer (fig. 20). These clots may record either local removal of the condition(s) necessary for harrisite crystallization, or active mixing of harrisite and cumulate.

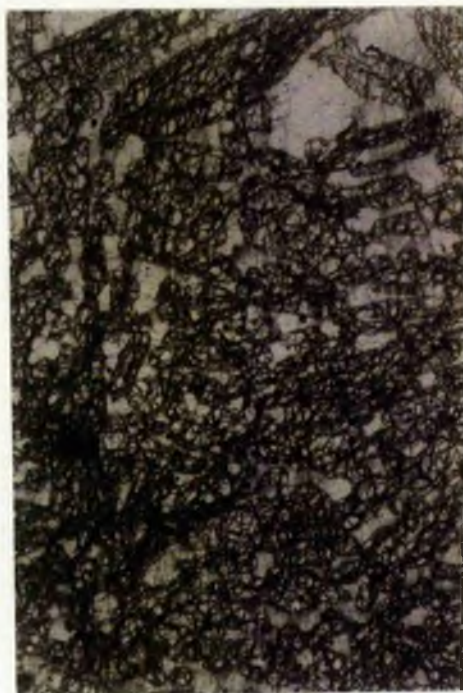
The lower contact of a harrisite layer is always more nearly planar than the upper contact. It is distinguished by a gradational change in texture and grain size (fig. 21a and b). The small, equant, round granular olivines (fig. 21a) of the underlying facies become progressively larger and more deeply indented upwards. A further upward change in olivine shapes is the development of internal skeletal structure, in addition to the indented skeletal shape. At this stage, olivines are porphyritic in shape. Still further upward change of shape in some layers is marked by the presence of parallel growth and branching (usually linked parallel-unit) olivines, which need not be vertically oriented. Hence, a gradational change in olivine morphology is common within harrisite layers and there is no sharp lower contact between granular ('cumulus') olivines and skeletal olivines.

Drever and Johnston (1972, fig. 5a) illustrated gradational change in olivine morphology upwards from non-harrisitic to harrisitic facies. Underlying the skeletal olivines of the harrisite are elongate,



Fig. 20 Mixing of large skeletal olivines in peridotitic harrisite (below) with granular olivines from the overlying cumulate. (Plane polarized light. Field of view 5 mm wide.)

a.



b.



Fig. 21 a. Thin section of the gradational contact between peridotitic cumulate (base) and overlying peridotitic harrisite (Ard Mheall Series; sample 211(2), Table 2). Field of view 2 cm wide.

b. Layer of harrisite in the Transition Series illustrating the change from underlying cumulate to porphyritic olivine to elongate linked parallel-unit olivine. Ruler is 8 inches (20 cm) long.

tabular, polyhedral olivines with prominent horizontal foliation (b perpendicular to the layer). Upwards, the tabular olivines are indented, and less markedly tabular. The complete upward morphology change involves: foliated tabular olivine → foliated, indented, tabular olivine → unfoliated, weakly tabular olivine → unoriented porphyritic olivine → branching linked parallel-unit olivine (vertically oriented). The interval between the first and the last of these changes is approximately 6 cm. The changes suggest a gradual transformation from conditions of crystal settling to dominantly in situ crystallization (branching olivine). Drever and Johnston stressed that the branching olivines had not nucleated on favourably oriented settled (polyhedral or porphyritic) olivines. Nor is there evidence for competitive growth of olivine as the cause of preferred upward growth.

The upward change from abundant, small, granular or polyhedral olivines to porphyritic olivine to branching olivine is observed in many layers. The relative position and grain size of different olivine morphologies within a layer does not vary, only the thicknesses of units of olivine of each type. Thus, the skeletal olivines in some harrisite layers may only be of porphyritic type, branching olivine being absent. These features suggest rhythmic, repetitious induction of olivine supersaturation and that the amount of supersaturation varied between layers, as did the duration of the degree of supersaturation at which each olivine morphology grew.

3. The crescumulus hypothesis

The crescumulus hypothesis assumes that the granular or polyhedral olivines in rocks between harrisite layers represent cumulus crystals that settled from a supersaturated basaltic magma, following convective overturn (Wager and Brown, 1968, p. 295). Crystal settling is envisaged to cease and, without further nucleation of olivine, olivines at the

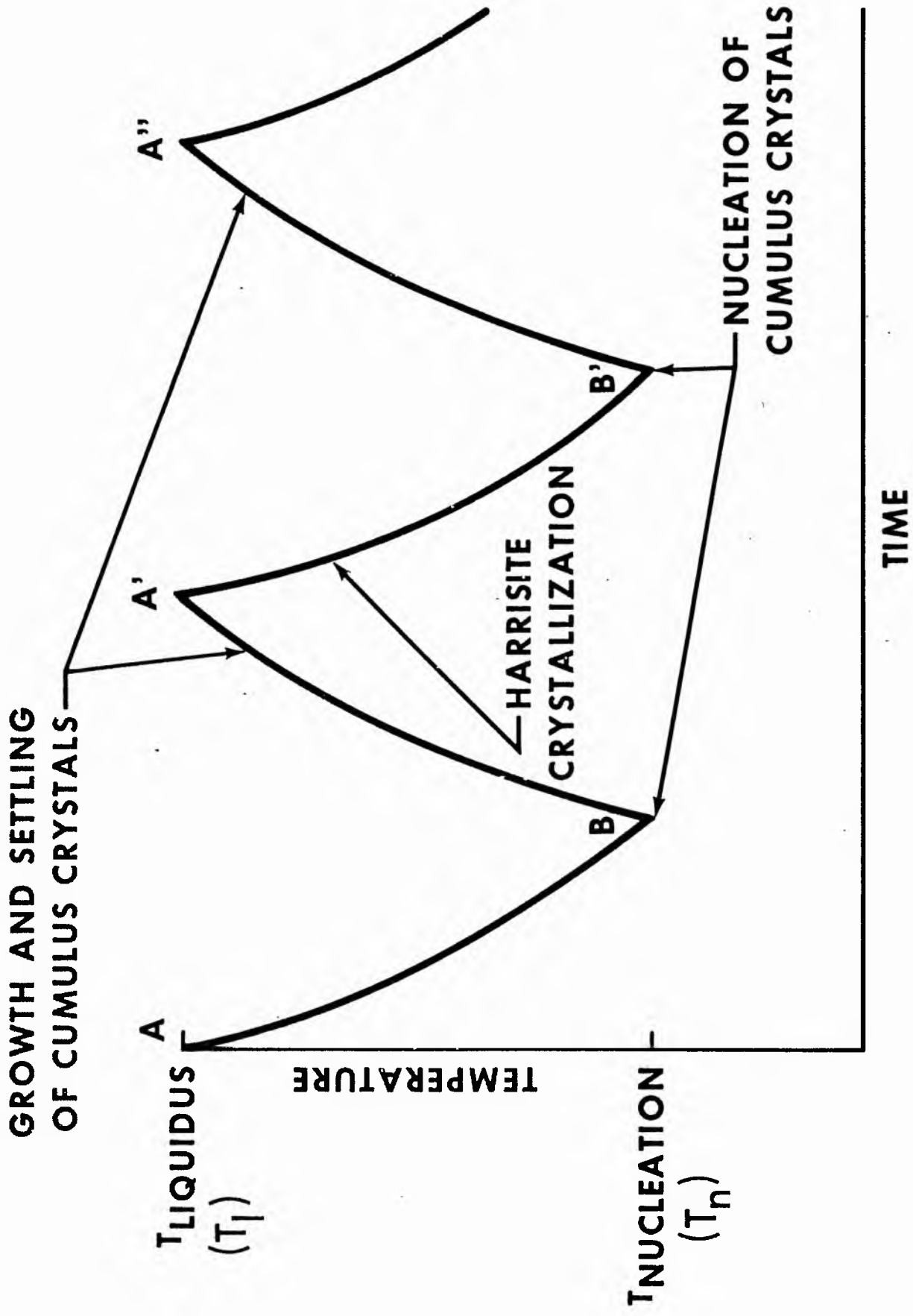


Fig. 22 Schematic temperature-time representation of the crescumulus hypothesis.
 (See text for explanation.)

top of the crystal mush on the floor of the magma chamber grew upwards. ("Crescere", Latin, to grow or increase. Hence, a crescumulate is composed of overgrown cumulus grains.) Initially, growth occurred on all cumulus olivines, but some favourably oriented crystals, with the a crystallographic axis approximately vertical, grew most rapidly, as branching crystals, suppressing other grains by competitive growth. The result is a rock fabric dominated by elongate olivines with (010) sub-vertical. The preferred growth direction is implied to be upward in all harrisite layers. Retention of delicate branching olivines, is attributed to crystallization from stagnant magma. In contrast, the smaller cumulus olivines in the intervening adcumulate layers are regarded as being deposited from flowing magma. Hence, a cyclic condition of magma stagnation, flowage, stagnation,.... is invoked.

The supercooling, supersaturation and nucleation behaviour of the Rhum magma during harrisite crystallization were discussed by Wadsworth (1961) and by Wager and Brown (1968). Wadsworth envisages cyclic conditions involving supercooling of magma, nucleation of olivine at T_n (fig. 22), growth of the olivine until it is large enough to settle as cumulus crystals, and then return of the magma temperature to the liquidus (T_l , fig. 22). Further nucleation of olivine must await renewed supercooling to T_n . As this supercooling is induced, harrisite containing linked parallel-unit olivine crystallizes, if the magma at the floor is stagnant and if it is essentially free of suspended olivines. Formation of harrisite is terminated when T_n is attained and cumulus olivines again settle on to the floor. Thus, the crescumulus hypothesis implies that cumulus olivines grow at greater degrees of supercooling than linked parallel-unit olivines.

Wadsworth does not specify where cumulus olivines nucleate. If it is close to the roof of the intrusion, as Wager and Deer (1939) postulated for the Skaergaard intrusion, the entire Rhum intrusion would have to be supercooled. Wager and Brown (p. 295) suggest that, during convective descent of the unit of magma, which ultimately



fig. 23 Base of eucritic harrisite layer showing the upward textural change from foliated eucrite to elongate, parallel-growth olivines (some growing upwards) in harrisite. Ruler is 11 inches (0.28 m) long. (Eastern Harris Bay)

crystallizes as cumulate overlain by harrisite, the increase in pressure and cooling of the magma causes olivine supersaturation. This implies that olivine probably nucleates close to the intrusion floor. They do not indicate whether supercooling and olivine supersaturation of the magma change, if at all, as cumulate rock gives way to harrisite. If one assumes that crystallization of cumulus olivine near the floor raises the magma temperature (cf. Wadsworth), harrisite must crystallize as magma warms at the floor ($B \rightarrow A'$, fig. 22; contrast Wadsworth), since Wager and Brown imply that the supercooling from $A \rightarrow B$ (fig. 22) results during descent of magma and not at the floor. Wager and Brown do not discuss this difference in mechanism between their hypothesis and that of Wadsworth, but rather, on p. 229 lines 26-27 of Layered Igneous Rocks, they apparently endorse Wadsworth's model. Throughout this thesis, the phrase "crescumulus hypothesis" will refer to Wadsworth's model of harrisite origin.

4. Relationship of the crescumulus hypothesis to olivine crystals in harrisite

i. Growth direction of olivine

Although preferred upward elongation of olivine in harrisite is distinctive (e.g., fig. 23), it is not typical. Layers have been illustrated in which olivine demonstrably grew downwards, horizontally or in random orientation. Clearly, elongate olivines in harrisite grew in any direction. The vertical vector is a common direction of growth, but its importance is overstressed in the crescumulus hypothesis, resulting in a model which explains the origin of only one type of harrisite. Downward growth of olivine is inconsistent with the crescumulus hypothesis and the assumption that solidification of the Rhum pluton occurred only upwards.

ii. Competitive growth

Whereas competitive growth (e.g., Knight, 1967) is observed to cause preferred growth direction of elongate crystals in ice and in metal castings, there is little evidence of it in harrisite (figs. 18 and

23). Furthermore, it fails to explain why olivines in one layer grew preferentially upward, while crystals in another layer grew preferentially horizontal.

iii. Growth centres for harrisitic olivine

The gradual change in olivine shapes observed within harrisite layers does not support a model involving cessation of olivine accumulation followed by upward growth of olivine. Porphyritic olivines probably also settled to the floor and, like granular and polyhedral crystals, nucleated in the bulk of the magma, above the floor.

Within a 10 m thick layer of Transition Series harrisite, there are bladed, branching olivines, 2.1 m in maximum length. Many of the crystals have demonstrably commenced growth within the layer (up to 3.3 m from the contacts; cf. section 1B). They have not grown from the top of a cumulus pile of crystals, nor do 10 m long crystals grow upward from the base to the top of the layer, as the crescumulus hypothesis would predict. Cumulus olivines settling into supercooled magma may have been the growth centres for these branching crystals. However, absence of cumulus-like olivine grains in the layer does not support this suggestion. There is no reason to consider that the branching crystals did not nucleate and grow in situ.

iv. Current action

Normal cumulate layers grade in olivine shape and grain size into harrisite layers. In most layers, there is no textural evidence to indicate that this corresponds to cessation of current action. It is as likely that the olivines in cumulate layers settled from stagnant magma as that both cumulus olivines and those in harrisite grew in a moving magma (see p.16).

v. Termination of harrisite formation

The upper contact of harrisite with cumulate is abrupt in texture and grain size. Whether settling of cumulus crystals terminated harrisite formation, or whether harrisite formation had ceased before deposition of the cumulate, is indeterminable. Intimate mixing

of the two rock types at the top of a layer suggests that the former possibility is most likely.

Summary

Harrisite has been shown to have broader field, and olivine crystal shape characteristics than those described by Wadsworth (1961) and Harker (1908b). As a consequence, the crescumulus hypothesis is found to be inadequate to explain the origin of all harrisite layers. Most significant, is the inability of the hypothesis to explain evidence for downward olivine growth and for the apparent mobility and intrusive nature of some harrisite layers. A hypothesis for harrisite origin cannot ignore the origin of the associated layered rocks; it should not, however, be dictated by it. In the following chapters arguments based on theoretical and experimental crystal growth are combined with petrographic observations and chemical mineralogy to constrain models for harrisite origin.

Chapter VI RHYTHMICITY AND CYCLICITY IN THE THICKNESS OF
HARRISITE LAYERING

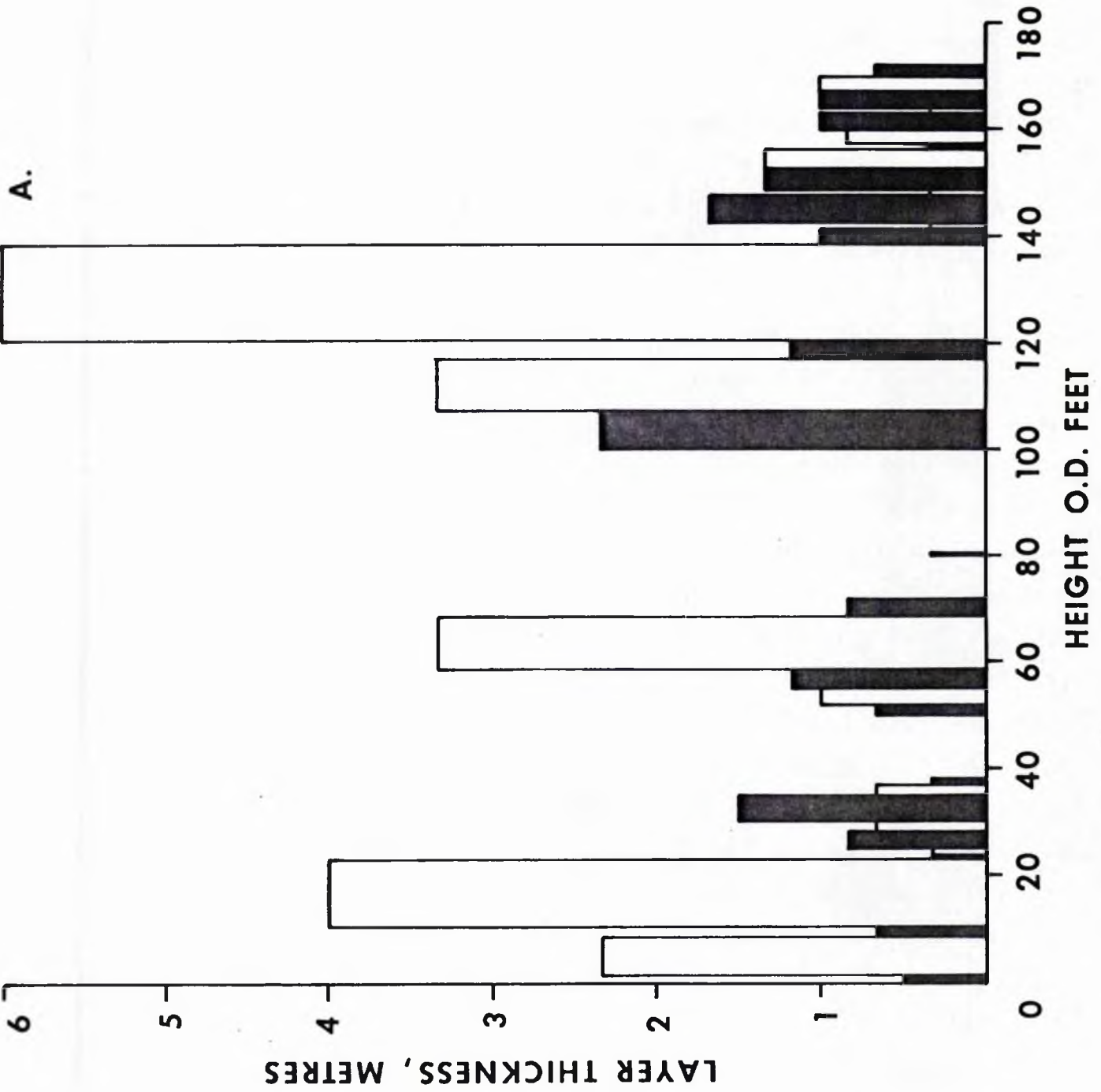
Evidence for the existence of cyclic and rhythmic processes in the origin of harrisite was sought in the thickness of rock layers. These processes could involve the interval between crystallization of adjacent harrisite layers and/or time taken to form each harrisite layer. Assuming that all harrisite layers thicken at a fixed rate and that all inter-harrisite layers also thicken at a fixed rate, though not necessarily at the rate at which harrisite layers thicken, then examination of the thickness of layers permits investigation for both cyclicity and rhythmicity.

The Harris Bay beach exposure, together with the Glen Duain river section through the Harris Bay Series, constitute the most complete stratigraphic section for this study. Nevertheless, approximately 25 percent of the 60 m section is unexposed and only 19 harrisite layers are present. Layer thickness was measured to the nearest 0.3 m. The base of a harrisite layer was taken where olivines first became skeletal, as seen with a hand lens. The height above sea level was measured by pocket barometer (error \pm 30 feet) and checked with the one-inch Ordnance Survey map. Plots of layer thickness against stratigraphic height are shown in figures 24a,b,c.

The following features are apparent from figure 24a.

1. A layer of harrisite may be thicker or thinner than the intervening layer(s); generally it is thinner.
2. Harrisite is most abundant at the top of the stratigraphic section and between 20 to 40 feet O.D.
3. Little rhythmicity in layer thickness is evident. The section between 140 and 170 feet, in which 1 m thick harrisite layers are inter-layered with 0.3 to 1 m thick layers of normal rock, is an exception. No gross cyclic behaviour is present.

To search for a comprehensive pattern in the thickness variation between nearest-neighbour harrisite layers, figures 24b and c were prepared. The former indicates that:



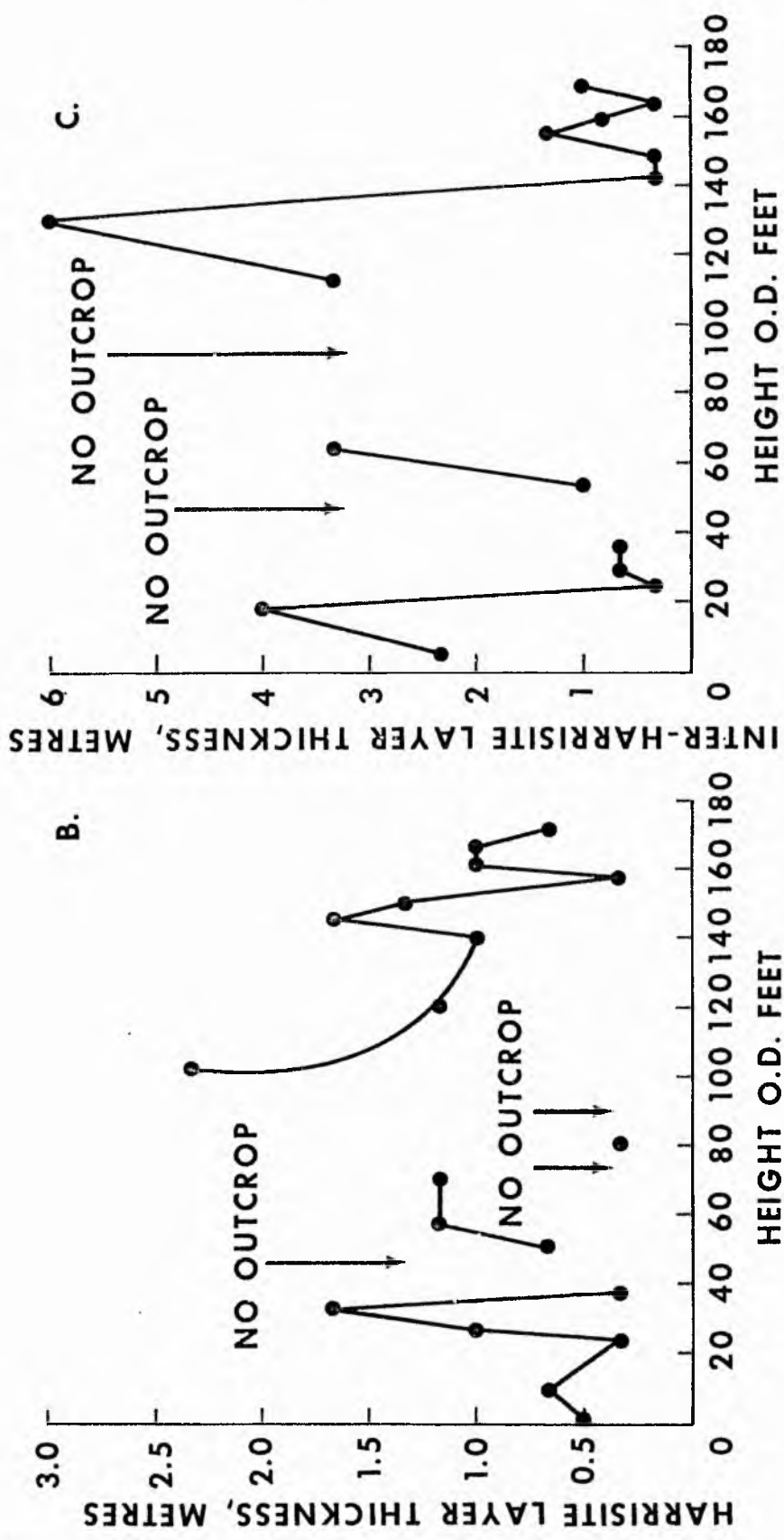


Fig. 24 Thickness of harrissite and inter-harrissite layers in the Harris Bay Series as a function of stratigraphic height.

a. Histogram of layer thickness. Shaded blocks are harrissite layers; blank blocks are inter-harrissite layers; gaps indicate no exposure.

b. Variation in layer thickness of nearest-neighbour harrissite layers.

c. Variation in layer thickness of nearest neighbour inter-harrissite layers.

1. Nearest-neighbour harrisite layers vary widely in thickness.
2. As plotted against stratigraphic height, the layer thickness variation is neither consistently concave nor convex in its decrease or increase.
3. There is no systematic pattern of layer thickness variation.

Figure 24c indicates that:

1. In general, there are even greater changes in the thickness variation of nearest-neighbour inter-harrisite layers than in harrisite layers.
2. No systematic pattern of thickness variation is present.

At the base and top of the section curves of layer thickness against stratigraphic height have a similar pattern of variation in figures 24b and c.

Discussion

If the petrogenesis of harrisite involves repeated episodes of supercooling (Wadsworth, 1961), cyclic or rhythmic variation in the thickness of layering might be expected. On the other hand, a model that requires injection of ultrabasic pegmatite into the Layered Series (Harker, 1908b) would most likely imply intrusions of random thickness. From the field observations made in Rhum, I conclude the following:

1. Comparison of figures 24b and c indicates that intermittently during formation of the Harris Bay Series there existed a relationship between harrisite and inter-harrisite layer thickness. This relation is consistent with the following interpretation: the longer the period of supercooling during harrisite formation, the longer also the period of moderate supercooling when layers of normal rock formed. This interpretation favours the formation of harrisite contemporaneous with, and directly related to, the normal (cumulate) rocks.
2. The preference of harrisite layers for a thickness of approximately 1 m (p. 12) is evidence favouring a model of rhythmic supercooling. It also favours the possibilities that both the

maximum degree of supercooling attained and its duration (period of harrisite crystallization) were of approximately constant values.

3. But, in detail, nearest-neighbour harrisite layers typically differ in thickness. Thus, the periods of supercooling, represented by harrisite layer thickness, varied slightly in duration (fig. 24b), assuming a fixed degree of supercooling for all harrisite layers.

4. No short range or long range cyclicity, which might indicate that separate batches of magma had convected within the magma chamber, can be found.

Each of these conclusions is subject to the caveat that the stratigraphic section studied is thin, and contains a statistically small sample of harrisite layers. Furthermore, these conclusions strictly apply only to the Harris Bay Series and extrapolation to crystallization of harrisite in the Transition Series and Ard Mheall Series would be speculative.

In summary, there is evidence for rhythmic and cyclic increase and decrease in supercooling during crystallization of the Harris Bay Series. This suggests that the origin of harrisite is related to processes which are internal, rather than external, to the magma chamber.

Table 1 Comparison of the ranges of phase content in harrisite and cumulate between three layered series

Layered series	Rock type	Volume percent					
		Olivine	Plagioclase	Pyroxene	Chrome Magnetite	Phlogopite	Other hydrous phases
Harris Bay	Harrisite	45 - 26	57 - 17	22- 7	2.7-0.2	2.8-0	14.8-3.2
	Cumulate	49 - 40	42 - 31	21-15	1.8-0.6	1.0-0.2	-
Transition	Harrisite	71 - 45	44 - 11	28- 4.5	1.5-0.8	0.2-0.1	10.4
	Cumulate	71 - 44	37 - 12	21- 3	0.9-0.6	-	5.2
Ard Mheall	Harrisite	88.5-58	29 - 6.5	3-0.3	10.5-2.5	0.7	10.5-2.5
	Cumulate	99.5-69.5	26.5- 1.5	8-0.5	3.3-0.3	0.0	4 - 3

Modes for harrisite were determined by point counting in thin sections from 4x2 cm to 15x10 cm, with 0.5 mm between counts. For rocks of grain size less than 5 mm, the error is ± 5 percent of the amount reported, for those of grain size exceeding 5 mm, error is 10 - 20 percent. All thin sections were cut perpendicular to the plane of the layering.

A. Mineral proportions

Modes of rocks are presented in Table 2. This table includes analyses for harrisite and for contiguous layers of overlying and underlying cumulate (e.g., sample 213). Selected analyses illustrate the variation in mineral proportions within individual harrisite layers (e.g., samples 211 and 200). Table 1 compares the range in modes of harrisite and cumulate rocks and their variation between the Layered Series. Some of this table comprises data of Wadsworth (1961, Tables 3, 7 and 8).

- (i) Comparison of harrisite and cumulate modes for three Layered Series (Table 1 and analyses 200, 213, 215, and 211 in Table 2)

OLIVINE: Olivine contents are highest in the Ard Mheall Series rocks and lowest in rocks of the Harris Bay Series. The least olivine-rich harrisites in both the Harris Bay and Ard Mheall Series contain less olivine than the least olivine-rich cumulate rocks. The maximum amount of olivine in both harrisite and cumulate rocks is comparable within each Series.

PLAGIOCLASE: In the Harris Bay Series the upper and lower limits of plagioclase content in harrisite are both more extreme than in cumulate rocks. In the Ard Mheall Series and the Transition Series, cumulate and harrisite have a comparable range in plagioclase content. Plagioclase is less abundant in the cumulate contiguous with a harrisite layer (sample 211).

PYROXENE: In the Harris Bay and Transition Series the amount of pyroxene in harrisitic and cumulate rocks is similar; in the Ard Mheall Series it may be higher in the harrisites. The maximum pyroxene content in harrisite rocks is comparable in all three Series; the minimum content decreases from the Harris Bay, to the Ard Mheall Series. In samples 213 and 215 the cumulate overlying harrisite contains more

Table 2 Summary of the field relations, olivine shapes, modal composition and phase compositions of harrissite layers, pegmatites and the Glen Duain gabbro

Sample	Layered Series	Type of layer, position in layer and olivine shape, if harrissite	Volume %													
			Olivine	Plagioclase	Augite	Bronzite	Ore*	Kaersutite	Phlogopite	Green Hornblende	Others†	Olivine	Plagioclase	Mo	En	Fs mol %
17	Harris Bay	Centre of 0.6m thick harrissitic olivine eucrite layer, with randomly oriented olivine (up to 1 cm long) throughout	38.9	33.1	19.9	1.0	2.7	0.2	1.2	Tr.	3.0	76-75	80-55	45-41 1	46-47 79	9-12 20
189	Harris Bay	Centre of 1m thick harrissitic olivine eucrite layer containing 0.8m long linked parallel unit olivine with preferred vertical elongation	45.1	27.2	12.9	0.9	1.7	2.4	1.7	Tr.	8.1	78-77	75-58	44-41 3	46-47 76.5	10-12 20.5
193	Harris Bay	Centre of 1m thick harrissitic olivine eucrite layer, with randomly oriented linked parallel unit olivine up to 5 cm in length	25.9	41.3	21.9	0.0	0.6	0.4	2.8	Tr.	7.1	n.d.	n.d.	n.d.	n.d.	
179	Harris Bay	Sample from outcrop of harrissitic 'allivaltite' west of Abhuinn Fiachan's mouth; sample contains randomly oriented olivine up to 5 cm in length	28.0	57.1	10.8	0.0	0.8	1.5	0.0	0.0	1.8	n.d.	n.d.	n.d.	n.d.	

Tr.- trace n.d.- not determined

*Chrome magnetite, ilmenite and trace sulphide

†Includes tremolite, chlorite, serpentine, clinzoisite, sphene, zeolites, apatite, grossular and prehnite.

Table 2 (Continued)

Sample	Layered Series	Type of layer, position in layer and shape, if harristite	Volume %																
			Olivine	Plagioclase	Pyroxene	Augite	Bronzite	Ore*	Kaersutite	Phlogopite	Green Hornblende	Otherst	Olivine	Plagioclase	An mol %	Wo	En	Fs mol %	
215	Harris Bay	Centre of 1m thick harristitic olivine eucrite layer, with linked parallel unit olivine up to 0.6m long.	45.1	16.6	14.7	0.0	0.3	0.3	0.9	0.3	Tr.	8.3	n.d.	n.d.			n.d.		
200(1)	Harris Bay	Olivine eucrite underlying harristite in section 200(2). Elongate olivines up to 0.3cm lie preferentially in the horizontal plane	35.1	39.3	13.2	0.0	0.8	4.7	0.8	1.1	5.0	77	84-81	44.5	46.5	9.0			
200(2)	Harris Bay	Base of a 0.3m thick harristitic olivine eucrite layer, with randomly oriented olivines up to 1cm long. 200(1) and (2) are continuous with one another	28.8	45.6	7.3	0.0	2.1	3.6	0.9	0.7	11.0	78.5	83-80	45	45	10			
182 _{top}	Harris Bay	Sample from thick harristitic olivine eucrite layer 6.5m from granophyre contact. Elongate parallel growth olivines lie in the plane of layering	36.0	28.8	15.1	0.0	1.8	3.7	1.8	1.7	11.1	82.5-77.5	87-47	45-42	45-43	10-15			
182 _{base}	Harris Bay	Gabbroic pegmatite patch 0.3m in diameter in harristite layer	0.0	47.7	30.1	0.0	2.6	1.2	1.5	3.7	13.2	--	72-47	44	45	11			
204	Harris Bay	7.5cm diameter pegmatite patch between large, randomly oriented olivines in harristitic olivine eucrite	5.1	59.9	11.2	0.7	1.5	0.5	0.4	6.3	14.4	54	79-29	43	45	12	2.5	74.5	23

Table 2 (Continued)

Sample	Layered Series	Type of layer, position in layer, and olivine shape, if harristite	Volume %													
			Olivine	Plagioclase	Augite	Bronzite	Ore*	Kaersutite	Phlogopite	Green Hornblende	Others†	Olivine	Plagioclase	En	Fs mol %	
163	Harris Bay	10cm diameter anorthositic gabbro pegmatite patch in harristitic olivine eucrite	0.0	67.2 (30.3 plagioclase 36.9 albite)	16.4	0.0	2.5	0.5	1.1	6.3	6.0	None	72-1	43	45	11
171	Harris Bay	Centre of 1m wide vertical gabbroic pegmatite dyke	0.0	53.2	28.8	0.0	2.3	2.1	0.1	5.2	8.3	None	71-53	43.5	45.0	11.5
89	Transition	Centre of 0.8m thick layer of harristitic feldspathic peridotite with randomly oriented, linked parallel unit olivine up to 0.4m in size	44.8	43.8	4.5	0.0	1.5	0.9	0.2	0.0	4.3	81-78	87-62	45	45	10
140	Transition	Section through base of a 0.1m thick harristitic peridotite layer containing porphyritic and polyhedral olivines	54.0	11.3	27.8	0.0	0.8	1.1	0.0	0.0	5.0	83.5	85-80	43.5	47.0	7.5
74B	Ard Mheall	Samples from a harristitic peridotite layer of unknown thickness with a single, vertically oriented, linked parallel unit olivine at least 1.2m in length. B-base of outcrop, M-middle, T-top	58.3	11.3	20.0	0.0	1.3	0.8	0.0	Tr.	8.3	80.5	83-61	46.5-42	64 - 47.5	7.5-10.5
74M	Ard Mheall		62.6	20.1	8.4	0.0	1.3	1.0	0.0	Tr.	6.6	82	87-61	46 - 43.5	45 - 47	9 - 9.5
74T	Ard Mheall		61.4	16.3	12.9	0.0	0.9	0.5	0.0	Tr.	8.0	81.5	87-63	45.5-43.5	46.5-47	8 - 9.5

Table 2 (Continued)

Sample	Layered Series	Type of layer, position in layer, and olivine shape, if harristite	Volume %														
			Olivine	Plagioclase	Augite	Bronzite	Ore*	Kaersutite	Phlogopite	Green Hornblende	Others†	Olivine	An mol %	Wo	En	Fs mol%	
213 _{base}	Ard Mhea11	Peridotite with abundant small granular olivine	74.9	15.9	5.6	0.0	0.5	0.0	0.0	0.0	0.0	0.0	2.1	n.d.	n.d.	n.d.	n.d.
213 _{middle}	Ard Mhea11	grading up into harristite feldspathic peridotite with porphyritic olivine.	59.8	23.8	7.8	0.0	2.6	0.0	0.0	0.0	0.0	0.6	5.2	n.d.	n.d.	n.d.	n.d.
213 _{top}	Ard Mhea11	Peridotite with abundant small granular olivine overlying the porphyritic olivine of 213 _{middle}	70.4	11.4	15.2	0.0	0.6	0.0	0.0	0.0	0.0	0.0	2.4	n.d.	n.d.	n.d.	n.d.
214	Ard Mhea11	1.2m thick harristite feldspathic peridotite layer with linked parallel unit olivines. The olivines are preferentially oriented with the direction of elongation in the horizontal plane	58.9	16.6	14.7	0.0	0.3	0.0	0.3	0.3	0.0	0.0	8.3	n.d.	n.d.	n.d.	n.d.
215 _{base}	Ard Mhea11	Top of 0.5m thick harristite feldspathic peridotite layer, with 0.7m long linked parallel unit olivine	59.6	28.1	4.4	0.0	2.7	0.0	0.2	0.2	0.7	0.3	4.0	n.d.	n.d.	n.d.	n.d.
215 _{top}	Ard Mhea11	Peridotite with abundant, small granular olivine. Overlies olivine in 215 _{base}	66.1	20.8	9.1	0.0	1.3	0.0	0.0	0.0	0.0	0.0	2.7	n.d.	n.d.	n.d.	n.d.

Table 2 (Continued)

Sample	Layered Series	Type of layer, position in layer, and olivine shape, if harristite	Volume %										Pyroxene		Plagioclase		Pyroxene							
			Olivine	Plagioclase	Augite	Bronzite	Ore*	Kaersutite	Phlogopite	Green Hornblende	Others†	Olivine	An mol %	Wo	En	Fs mol %	An mol %	Wo	En	Fs mol %				
211(1)	Ard Mhea11	Individual sections upwards through the harristite feldspathic peridotite layer in figure	64.1	19.7	5.2	0.0	2.1	0.2	0.0	0.0	0.0	0.0	0.0	8.7	82	86-82	44 - 45	47.5-47	8.5- 8	86-82	44 - 45	47.5-47	8.5- 8	
211(2)	Ard Mhea11	Sections are contiguous and 2cm long. (1) contains tabular polyhedral olivines weakly oriented in the layering plane;	71.4	23.2	1.0	0.0	2.0	0.0	0.0	Tr.	2.4	83	85-82	2.4	83	85-82	complete range for all five thin sections				85-82			
211(3)	Ard Mhea11	(2) same, plus overlying coarser porphyritic olivine; (3) porphyritic olivine; (4) and (5) contain linked parallel unit olivines	68.6	23.2	1.3	0.0	1.8	1.3	0.0	0.0	3.8	83.5	84-81	3.8	83.5	84-81				84-81				
211(4)	Ard Mhea11		63.2	26.6	2.4	0.0	2.4	1.3	0.0	0.0	4.1	83.5	85-81	4.1	83.5	85-81				85-81				
211(5)	Ard Mhea11		58.8	29.1	3.1	0.0	1.5	0.2	0.0	0.0	7.3	83.5	86-83	7.3	83.5	86-83				86-83				
211	Ard Mhea11	Made from large thin section in vicinity of small sections (4) and (5), but covering 6 times the area of a small section	62.0	27.7	3.3	0.0	2.9	0.4	0.4	0.0	3.3	see above												
22(1)	Glen Duain gabbro intruded into Harris Bay series	Microgabbro layers above and below gabbroic pegmatite [22(2)]	0.0	37.1	21.2	0.0	16.4	0.0	0.0	12.3	13.0	none	47-41	42.5	45	12.5				47-41	42.5	45	12.5	
22(2)	"	Gabbroic pegmatite	0.0	43.7	28.4	0.0	8.2	0.0	0.0	5.2	14.6	none	56-48	43-41	44 - 45.5	13 - 13.5				56-48	43-41	44 - 45.5	13 - 13.5	

pyroxene than the harrisite, whereas the underlying cumulate contains less pyroxene than the harrisite in sample 213. Orthopyroxene is never present in proportions greater than 1 vol. percent.

CHROME MAGNETITE: Excepting rocks of the Ard Mheall Series, harrisite contains slightly more chrome magnetite than cumulate rocks. This is true of contiguous cumulate and harrisite layers. The Ard Mheall Series rocks, both harrisite and cumulate, contain most chrome magnetite, those in the Transition Series contain the least.

HYDROUS MINERALS: These are generally, but not consistently, more abundant in harrisite than in cumulate. Rocks of the Harris Bay Series have larger proportions of hydrous minerals than rocks of the other two Series.

(ii) Modal variation within layers

OLIVINE: The comb-layered harrisite has nearly constant olivine content throughout the layer (samples 74). Upwards through the harrisite layer (sample 211), olivine content increases to a maximum value and then decreases to a constant value in that part of the layer containing branching olivines. The olivine contents in the branching olivine part of sample 211 and in sample 74 are remarkably similar. In sample 200, olivine content increases upwards in the layer.

PLAGIOCLASE: Upwards through each harrisite layer, plagioclase content increases in sample 211, decreases in sample 200 and in sample 74 it varies inconsistently with height. It is often in antipathetic relation to the change in pyroxene content.

PYROXENE, CHROME MAGNETITE AND HYDROUS PHASES: Through harrisite layers there is no consistent change in contents of these minerals.

(iii) Conclusions and interpretation

a) Harrisite rocks with granular and porphyritic olivine are olivine enriched, and were formed in part by crystal settling.

b) The upward textural change from cumulate to harrisite usually involves a decrease of up to 10 vol. percent in olivine content. This

Table 3 Changes in number of crystals and grain-size in harrisite layers

Sample, rock type, layered series		Plagioclase		Pyroxene		Chrome magnetite		Olivine	
		no./cm ²	size mm	no./cm ²	size mm	no./cm ²	size mm	no./cm ²	size mm
212 Ard Mheall	upper cumulate	80	1	1	8	1	0.05	100	0.5
	harrisite	1-6	10	2	8	0-3000	0.1	0.5	50
211 Ard Mheall	upper harrisite	1-4	40	0.25	6	30	0.1	0.1	60
	lower harrisite	10	3	0.25	10	20	0.1	20	20
	basal cumulate	15	4	0.4	8	35	0.2	60	2.8
213 Ard Mheall	upper cumulate	50	4	3	2	30	0.1	1500	0.3
	harrisite	8	6	0.25	8	1	0.2	1	15
	basal cumulate	400	1	1	7	25	0.1	1700	0.3
214 Harris Bay	upper cumulate	6200	2	50	2	100	0.03	100	1
	harrisite	350	5	100	3	3	0.2	0.2	70
200(1), (2) Harris Bay	upper harrisite	30	3	2	3.5	30	0.1	8	10
	lower harrisite	35	4	1	4	20	0.2	20	3

is attributable to 1) a decrease in packing efficiency of grains as granular olivine is replaced by porphyritic olivine, 2) increase in internal skeletal character of olivine grains and 3) a change to in situ crystallization rather than crystal settling.

c) Rocks in which there is definite evidence for in situ crystallization of olivine (e.g., branching crystals) are olivine-rich, either implying extensive in situ crystal-liquid fractionation, if the parent magma were a basalt, or crystallization from an olivine-rich magma.

d) The magmas which formed both harrisite and cumulate rocks in each Series undoubtedly had different normative olivine contents. The parent magma for the Ard Mheall Series rocks was richest in olivine, that for the Harris Bay Series was poorest in olivine.

e) There is a slight preference for hydrous minerals to be located in greater abundance in harrisite rocks than in cumulate rocks. This preference may either reflect more efficient trapping of magma in the initially-formed harrisite crystal mush than in the cumulate crystal mushes, or it may indicate crystallization from a magma richer in water.

f) The greater abundance of chrome-magnetite crystals in harrisite rocks compared to contiguous cumulates might reflect more highly oxidizing conditions during crystallization of the former.

g) In the Ard Mheall Series, cumulate rocks overlying harrisite layers are enriched in pyroxene by a factor of two relative to the harrisite (samples 213 and 215). This fact may be explained by a dense, settling suspension of granular olivines efficiently trapping magma enriched in pyroxene components which were preferentially rejected from the underlying harrisite layer.

B. Crystal abundance and grain size variation

Average values of grain size and abundance of crystals (number per cm^2 in a thin section) of four minerals are tabulated in Table 3. Only rocks from which a large thin section (15 x 10 cm) had been prepared

were studied. For crystals larger than 2 cm, reported crystal abundances are not very accurate.

OLIVINE: The upward and downward changes from normal cumulate to harrisite involve a dramatic decrease in the number of olivine crystals, by up to a factor of 1/1500. The grain size increases by up to 1000 times. Samples 211 and 200 indicate that there is a gradational change in olivine crystal abundance and grain size in passing from normal cumulate into the base of a harrisite layer and up through the harrisite layer.

PLAGIOCLASE: Plagioclase crystals exhibit similar trends in grain size and abundance variation as described for olivine, but the variations are less extreme (Table 3). The upward increase in plagioclase grain size through a harrisite layer is accompanied by a textural change from an interstitial relationship of plagioclase to olivine to a subophitic or poikilitic relationship.

PYROXENE AND CHROME MAGNETITE: The grain sizes of both pyroxene and chrome magnetite crystals generally vary insignificantly through harrisite layers and in passing from harrisite to cumulate facies. The variation in crystal abundance of pyroxene is equally insignificant in three of the rocks (samples 200, 211 and 212, Table 3); in sample 213 the abundance is higher in the cumulate than in the harrisite, whereas in sample 214 the reverse is true. Large changes in chrome-magnetite crystal abundance are related to the degree of development of synneusis amongst crystals and to the formation of diffuse chrome magnetite seams within rocks. No significant upward change in the abundance of chrome magnetites exists within harrisite layers (samples 211 and 200). Samples 213 and 214 show abrupt increase in the number of chrome-magnetite crystals in passing from a harrisite layer into a cumulate layer. The reverse is true in sample 212.

Conclusions and interpretation

1. There are gradations in olivine and plagioclase grain sizes and crystal abundances in passing upwards from normal cumulate into harrisite (compare the change in olivine morphology, p.32, and mode, p.42). These

indicate that the change to conditions favouring harrisite crystallization, rather than formation of normal cumulate, is induced gradually. In contrast, the abrupt upward change from harrisite to normal cumulate implies sudden removal of conditions favouring harrisite crystallization.

2. Grain size and crystal abundance do not change indefinitely upward through layers. Once the olivines become of linked parallel-unit type, grain size and crystal abundances vary insignificantly. The change from cumulate to harrisite formation apparently involves a change in crystallization conditions, and ultimately, when linked parallel-unit olivine crystallizes, establishment of a new steady-state crystallization regime.

3. Assuming that the degree of magma supercooling during harrisite formation is less than the degrees of supercooling at which the nucleation rates of both plagioclase and olivine are maximum (e.g., fig. 33), the decreasing upward abundance of plagioclase and olivine crystals, in passing from a layer of normal cumulate to one of harrisite, should record a decrease in supercooling. On the other hand, if the degree of supercooling is greater than that of the maximum nucleation rates of both minerals, the supercooling must increase.

4. Temperature changes are inferred to have affected pyroxene nucleation rate only slightly. The reason may either be that supercooling with respect to pyroxene was always slight, or that the change in pyroxene nucleation rate as a function of supercooling is less sensitive than that of plagioclase and olivine.

C. Textures of harrisite and associated rocks

To indicate the variety of textures among harrisite and contiguous rocks and the differences in origin of the textures, it is necessary to describe a number of samples. The textures of the rocks selected for electron microprobe analysis are described in Appendix I. From these descriptions, conclusions about the petrogenesis of individual

harrisite layers are reached. This chapter summarizes the textural relations of harrisite and the petrogenetic conclusions reached from the rocks described in the Appendix.

i. General petrographic account of the major mineral constituents

OLIVINE: There is a wide variation in olivine morphology in the ultrabasic rocks (Brown, 1956) from euhedral, equant or tabular crystals (as much as 2 mm across) to anhedral poikilitic crystals (up to 1 cm across) to the skeletal and dendritic crystals of harrisite (up to 2.1 m long). Zoning is never observed optically. The extent of alteration to serpentine and hematite along irregular cracks varies from extensive to negligible in both harrisitic and non-harrisitic rocks. Alteration to chlorite and fine-grained tremolite is pervasive. Some olivine crystals contain inclusions of (1) euhedral chrome magnetite, or (2) round plagioclase (0.1 mm or less across), or (3) an intergrowth of plagioclase, kaersutite and phlogopite. The last two inclusion types occur only in Harris Bay eucrites. In the eucrites, plagioclase, kaersutite and phlogopite may be earlier crystallizing phases than olivine.

PLAGIOCLASE: The plagioclase in the ultrabasic rocks is predominantly bytownite. Crystals have three common shapes: (1) columnar grains ($a \approx c > b$, up to 4 x 1 mm), few of which are zoned; (2) anhedral poikilitic crystals and (3) anhedral interstitial crystals. Crystals with the last two shapes may be zoned or homogeneous. Zoning is of a peripheral type to labradorite. Patchy zoning is common either as elongate strips in crystals, or as isolated irregular patches. The difference in anorthite content between patches and host varies from as little as 3 mol.percent to as much as 30 mol.percent. Finer-grained plagioclase mosaics in some rocks are attributed to partial recrystallization of large plagioclases. The extent of alteration of crystals to clusters of prehnite, scolecite and grossular and veins of thomsonite varies (0-70 percent) between adjacent rocks and between adjacent crystals. Boundaries between plagioclase and olivine are

either fresh, or lined with fine-grained tremolite and green hornblende. Plagioclase crystals contain inclusions of chrome magnetite and, in the Harris Bay eucrites, rare kaersutite.

PYROXENE: Two pyroxenes are present- pale green augite and rare crystals of colourless bronzite, neither having exsolution textures. Augite crystals in the eucrites are variegated greenish brown and dark brown. Plates of the mineral (as much as 2 cm across) enclose olivine and plagioclase crystals poikilitically. Zoning of augite, where present, is slight (Table 2) and consists of a narrow, homogeneous, Fe-enriched mantle around the homogeneous core. Inclusions of kaersutite and phlogopite are abundant, and augites are partially or wholly altered to tremolite or hornblende. Boundaries between augite and plagioclase crystals are either fresh or lined with tremolite, green hornblende and clinozoisite. Augite to olivine boundaries are fresh. Typically anhedral, bronzite is in subophitic relation to plagioclase and olivine, but the textural relation to augite has not been observed. Reaction rims of bronzite on olivine are of uniform thickness, even around lobes and in re-entrants of skeletal olivines. This feature excludes the possibility that the skeletal shapes of olivine in harrisite are the result of reaction of magma and olivine.

KÄERSUTITE AND PHLOGOPITE: Pale brown kaersutite occurs (1) as inclusions in olivine, (2) as replacements after pyroxene, (3) as primary crystals interstitial to olivine and to plagioclase, (4) as round grains (0.5 mm across) in nests also containing ilmenite and tremolite, (5) in randomly distributed late-stage patches and (6) in blebby intergrowth with pyroxene (possibly a primary intergrowth, Prinz and Nehru, 1969). The kaersutite blebs in a single pyroxene crystal generally have common extinction, possibly indicating an epitaxial relation between the two phases.

Chestnut-brown phlogopite shares the first and last of the kaersutite parageneses and also rims ilmenite grains.

CHROME MAGNETITE AND MAGNETITE: In cumulate rocks and harrisite, chrome magnetite is present in diffuse clusters or is disseminated through the rocks. A thin seam of magnetite occurs at the base of some cumulate layers overlying a harrisite layer. Crystals vary from euhedral, equant octahedra to round grains. Those crystals (0.1 mm or less across) enclosed by olivine are consistently smaller by a factor of 3-8 than those at olivine indentations or enclosed by pyroxene or plagioclase. At olivine indentations the oxide grains either abut directly on to the olivine or are separated from it by a thin veneer of plagioclase or pyroxene.

ii. Growth rate of olivine in harrisite

In a few harrisite samples horizontal trains (up to 2 cm long) of chrome magnetite crystals are trapped on the underside of horizontally elongate olivines (fig. 19). These trains are interpreted as diffuse seams which settled through the magma and subsequently were trapped in and below the olivine. Since there is intercumulus plagioclase or pyroxene below the olivine, it is clear that the chrome magnetites could have settled still further, had they not been engulfed by the olivine.

Taking the size of a chrome magnetite as 0.1 mm, the density of chrome magnetite as 4.45 g/cc and assuming a basaltic parent magma of density 2.60 g/cc and viscosity 300 poises (cf. values given by Jackson, 1971), the chrome magnetite may be calculated (Stokes' law) to have settled at 10^{-4} cm/s. In order to engulf the chrome magnetites, the olivine must have grown downwards at a rate exceeding this value. Thus, an average-size olivine in harrisite of 3 cm would grow in approximately 7 hours. (This calculation requires the assumption that the olivine grew wholly in situ. If it settled, it would do so 50 times faster than the chrome magnetite.)

Even allowing an error of 10 in estimation of the viscosity of the magma, this is a rapid crystal growth rate. [Compare and contrast the rate of 10^{-6} cm/s calculated by Donaldson (in press) for olivine in an

oceanic basalt, and also the maximum growth rate of olivine of 10^{-3} cm/s in my crystallization experiments (chapter X).] In a day, a harrisite layer would thicken by approximately 10 cm and an average-sized layer, 1 m thick, would crystallize in 9 days. This rate should be contrasted with the rate of 0.6 mm/day at which layers of cumulate thickened in the Skaergaard intrusion (Wager and Brown, 1968). Thus, harrisite layers may crystallize as much as 160 times faster than the rate of thickening of the cumulate layers, assuming that the mass of crystals accumulating on the floor per unit time is comparable in the Skaergaard and Rhum intrusions.

iii. Evidence for supercooling

The skeletal and dendritic shapes of olivine crystals in harrisite closely resemble those in rapidly-cooled mafic dykes and sheets (Drever and Johnston, 1957) and were therefore attributed by Wadsworth (1961) and Donaldson (1974a) to growth from a supercooled magma. That this interpretation is correct is demonstrated by growth of the same shapes of skeletal and dendritic olivines in the laboratory at varying degrees of supercooling (chapter X). There is also textural evidence that magma supercooled during crystallization of some non-harrisitic rocks, as discussed below.

Donaldson et al. (1973) described massive radiate fibre growths of bytownite poikilitically enclosing oriented olivine crystals. Many of the bytownite fibres share a common nucleus and form a spherulite, up to 1 m in diameter. Plagioclase spherulites grow only under large degrees of supersaturation. For example, Lofgren (1974) demonstrated that, in the water-saturated plagioclase system at 5 kb, plagioclase spherulites crystallize from melts supercooled by more than 250°C , whereas in a basalt at 1 atm they grow at supercooling values greater than 75°C . It seems that during growth of the bytownite macrospherulites, the magma was considerably supersaturated and this, in part, was due to supercooling.

Plagioclase crystals in a few harrisite and cumulate layers have patchy extinction which is irregular in distribution. Some of

these crystals clearly were originally skeletal and were subsequently infilled by plagioclase of slightly different composition. The different plagioclase compositions then partially equilibrated. The original skeleton may have been hollow or cored (cf. Lofgren, 1974, plate 1c). Those crystals with irregular patchy extinction are also interpreted as infilled skeletons, of the type figured by Lofgren, plate 1d. Lofgren grew cored skeletal plagioclases under conditions of moderate supersaturation (approximately 100°C supercooling in the water-saturated plagioclase system at 5 kb).

iv. Conclusions (see Appendix I)

1. The presence of primary kaersutite and phlogopite indicate that the Rhum magma(s) was significantly hydrous. The abundance of hydrous phases and reaction products in harrisite suggests that water was important in formation of the rock. A large water fugacity was also essential to the formation of gabbroic pegmatite differentiates (p. A5).
2. Wager et al. (1960) regard harrisite as a special kind of heteradcumulate, formed by in situ growth on settled olivines and by in situ nucleation of plagioclase and pyroxene under stagnant conditions. In the present study, the observational evidence indicates that plagioclase was a cumulus phase during formation of some harrisite layers and that chrome magnetite or magnetite was always cumulus.
3. Textural relations indicate two paragenetic sequences in harrisite. In the Ard Mheall and Transition Series the sequence is: chrome magnetite, olivine, plagioclase, augite ± bronzite, kaersutite ± phlogopite, ilmenite + alteration products. Minerals in the Harris Bay Series either crystallize in the above order, or in the order: plagioclase, olivine + magnetite, augite + bronzite, kaersutite + phlogopite, ilmenite + alteration products. These paragenetic differences reflect differences in parent magma composition and probably also water fugacity.
4. The concept of variable depth nucleation of minerals in a unit of magma close to the floor of the chamber (Jackson, 1961) has been invoked (Appendix I) to explain the petrographic features of some rocks.

5. Four features indicate that the olivines in harrisite and cumulate crystallized close to the base of the magma chamber (cf. Wager and Brown, 1968, p. 229). a) Olivines in cumulate layers are either granular or polyhedral in shape, the latter being up to 10 times larger than the former. These discrepancies are evidence of different sources for the two shapes of olivine. The granular olivines at the base of most harrisite layers are too small to have crystallized at the top of the chamber and subsequently sunk to the base. Only if these crystals have been transported from top to bottom of the chamber by rapid convective overturn, could they have crystallized at the roof. The large, polyhedral crystals at the base of the harrisite layer shown by Drever and Johnston (1972, fig. 5a) are much more likely candidates for nucleation and growth high in the chamber. b) The olivine morphologies in harrisite are near-perfectly sorted. If crystallization began at the top of the chamber and was followed by either crystal settling or convective overturn, it is unlikely that large porphyritic olivines would consistently overlie much smaller, granular crystals. c) The petrographic features of sample 140 (Appendix I) indicate that olivine crystals in 'normal' (cumulate) layers may also have nucleated and grown close to the floor of the chamber. d) Linked parallel-unit olivine at the top of some harrisite layers unquestionably crystallized in situ, and there is no reason to doubt that these crystals also nucleated in situ.

It is suggested that all harrisite layers are basal crystallization products of the Rhum magma, i.e., the granular and porphyritic olivines nucleated in melt close to the intrusion floor and, as the supersaturation increased, the olivine nucleation decreased to a negligible rate until only crystallization directly on the floor of the magma chamber was possible (chapter XI).

6. All the primary silicate minerals in harrisite underwent low temperature oxidation and hydration reactions. The variable degree of alteration in rocks suggests that the water was not introduced from outside the rock and that it was inhomogeneously distributed.

7. Pods of pegmatite occur in both harrisite and non-harrisite rocks. Hence, hydrous residual liquid may concentrate during formation of both rock types. The more common occurrence of pegmatite in harrisite indicates more efficient entrapment of magma in the harrisite crystal mush than in a cumulate mush.

8. The evidence favouring large supercooling of magma in the Rhum pluton is substantial (Wadsworth, 1961; Donaldson, 1974a,b; Donaldson et al., 1973; this thesis). This property is not unique to Rhum and is being recognised in many plutons (e.g., see lists given by Moore and Lockwood, 1973 and Taubeneck, 1974). Crystal morphologies more commonly found in volcanic rocks, and normally attributed to rapid cooling, result from supercooling. Donaldson (1974a) has argued that the fundamental property common to skeletal, dendritic and spherulitic crystal growth in all crystallization environments is rapid crystal growth rate relative to the value of the melt diffusion coefficient. This does not imply that rapid cooling of magma is essential for crystallization of non-polyhedral olivine crystals (Donaldson, 1974a). Experimental study (chapter X) is used to determine how much supercooling is necessary to produce each of the skeletal and dendritic olivine morphologies and what role magma composition has in accelerating olivine crystal growth rate.

FORSTERITE MOL. PERCENT

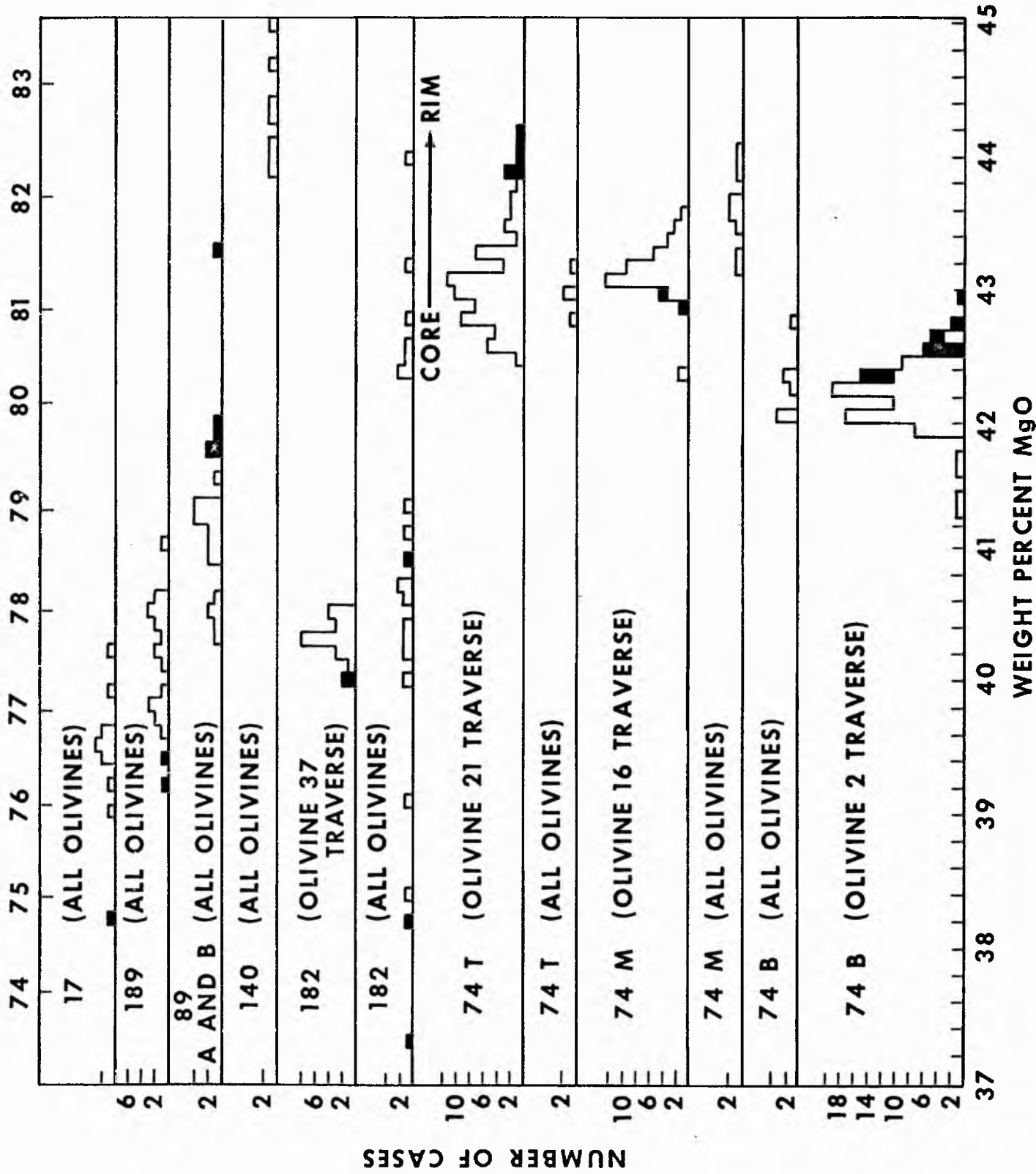


Fig. 25 Histogram of compositions of olivines in eight harrisite samples and of single crystals in four of these samples. Shaded blocks represent analyses at the margin of crystals.

Table 4 Electron microprobe analyses of olivine in selected harrisite and pegmatite samples

Sample	74B		74 M	74T	211(2) Representative of sections 1-5	140	89 A,B	189	182		17	200(1) Representative of sections 1 and 2	204	163
	core	rim												
SiO ₂	38.98	39.28	39.55	39.35	39.44	39.91	38.68	38.54	39.47	38.47	38.40	38.24	37.50	37.09
FeO	17.96	17.17	16.00	16.53	15.94	15.56	19.78	20.06	16.85	23.27	21.46	20.61	23.27	22.66
MnO	0.31	0.30	0.24	0.26	0.24	0.23	0.31	0.31	0.26	0.40	0.35	0.32	0.43	0.34
MgO	42.10	42.79	43.94	42.98	43.59	44.73	41.27	41.16	43.24	38.50	39.57	40.52	38.25	37.23
NiO	0.27	0.25	0.31	0.29	0.26	0.29	0.25	0.24	0.25	0.20	0.22	0.17	0.16	0.13
CaO	0.10	0.07	0.10	0.07	0.14	0.07	0.12	0.02	0.10	0.11	0.00	0.12	0.03	0.02
Total	99.72	99.86	100.14	99.48	99.61	100.79	100.41	100.33	100.17	100.95	100.00	99.98	99.64	97.47
Structural formula: 4 oxygens														
Si	0.997	0.999	0.997	1.001	0.999	0.997	0.991	0.990	0.999	0.996	0.996	0.989	0.986	0.993
Fe	0.384	0.365	0.337	0.352	0.338	0.325	0.424	0.431	0.357	0.504	0.465	0.446	0.512	0.508
Mn	0.007	0.007	0.005	0.006	0.005	0.005	0.007	0.007	0.005	0.009	0.008	0.007	0.010	0.008
Mg	1.605	1.621	1.651	1.630	1.647	1.666	1.576	1.575	1.631	1.486	1.529	1.561	1.500	1.487
Ni	0.006	0.005	0.006	0.006	0.005	0.006	0.005	0.005	0.005	0.004	0.005	0.003	0.003	0.003
Ca	0.003	0.002	0.003	0.002	0.004	0.002	0.003	0.001	0.003	0.003	0.000	0.003	0.001	0.001
Total	3.002	2.999	2.999	2.997	2.998	3.001	3.006	3.009	3.000	3.002	3.003	3.009	3.012	3.000
Atomic ratio														
Mg	80.7	81.6	83.0	82.2	82.9	83.7	78.8	78.5	82.0	74.7	76.7	77.8	74.6	74.5
Fe	19.3	18.4	17.0	17.8	17.1	16.3	21.2	21.5	18.0	25.3	23.3	22.2	25.4	25.5

Series harrisites.

Step-scan analyses (4 micron steps) were made of some olivines. Most of the histograms (fig. 25) summarizing the results of these scans are symmetrical about a maximum, the spread indicating the analytical error. Some histograms (e.g., olivine 21 (sample 74T), samples 74B and 89) distinctly show more magnesian rim compositions. This reverse zoning, which is continuous in olivine 21, is slight (2 - 2.5 mol. percent Fo).

Sample 182 is unique in having a range of olivine compositions ($\text{Fo}_{82.5} - 73.0$) and no preferred composition. However, a traverse across one grain (olivine 37, fig. 25) suggests a uniform composition for individual olivines in the rock. The olivines in sample 182 become more iron rich toward the pegmatite in the sample (Appendix I).

In the comb-layered harrisite, sample 74, olivine composition is $\text{Fo}_{80.5}$ at the base of the outcrop, Fo_{83} at the middle, and Fo_{82} at the top. Large branching olivines in harrisite are apparently slightly zoned, with more magnesian centres and more iron-rich extremities.

Microprobe analyses of olivines in a harrisite layer and the underlying cumulate layer show slight, but significant, compositional change that correlates with texture changes [Table 4, samples 200(1), (2) and 211]. Upwards through these two layers, the olivine becomes more magnesian by 1 - 1.5 mol. percent Fo, as the olivine changes from granular to elongate skeletal crystals.

Reverse zoning of olivine, and upward change in harrisite layers to more magnesian olivines, might reflect increase in temperature during crystallization. An increase in the oxygen fugacity is an alternative cause of the zoning. In the likely range of $f\text{O}_2$ at which harrisite crystallized ($10^{-6} - 10^{-8}$ atm.), a 0.1 log unit increase in $f\text{O}_2$ at constant temperature will cause an increase of 3 mol. percent forsterite in olivine, assuming coprecipitation with magnetite (Speidel and Nafziger, 1968, fig. 4).

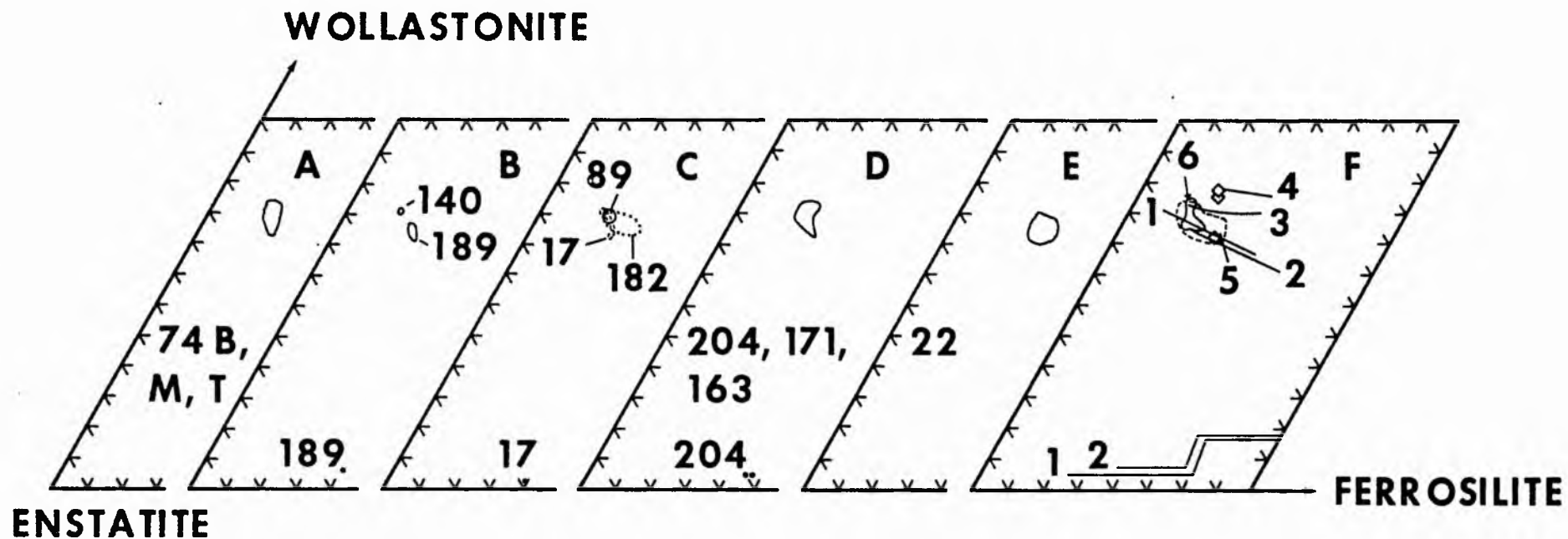


Fig. 26 Compositions of pyroxenes in some harrisite and pegmatite samples. In fig. F the numbers and symbols represent: 1 Bushveld intrusion; 2 Skaergaard intrusion; 3 Shiant Isles sill; 4 Black Jack sill; 5 all Rhum rocks; 6 Eucritic and picritic dykes and sills of Skye; diamonds are pyroxenes in spinifex rocks (Lewis and Williams, 1973). Scale marks at 5 mol. percent intervals.

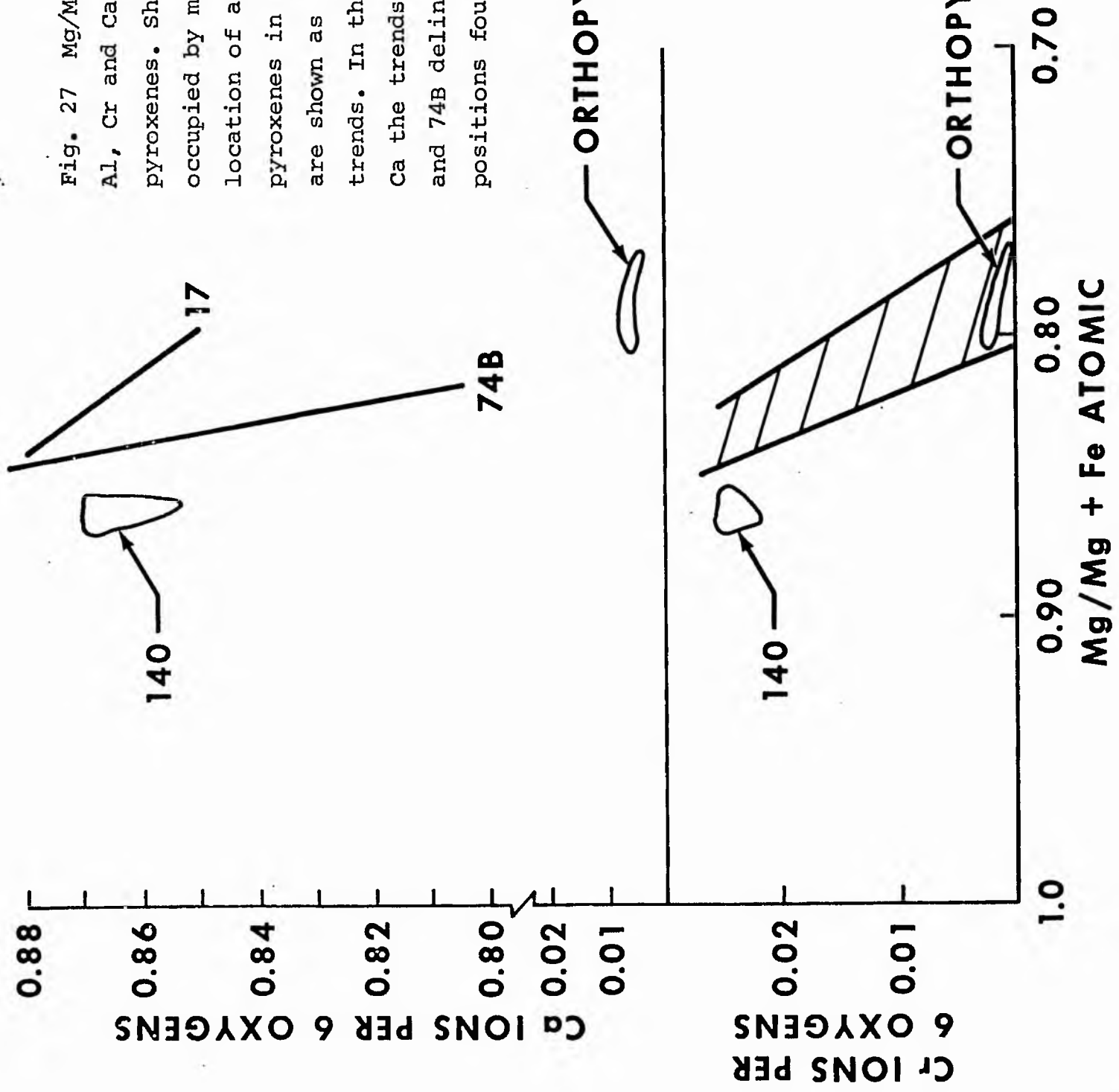
Ni and Mn contents in the olivine correlate with the Mg and Fe content. With a 9 mol. percent decrease in Fo content of the olivine, Ni content decreases by a factor of 2 and Mn increases by the same factor. Ca content is low (500 - 900 ppm), comparable to the content in olivines from the Eastern Layered Series (Simkin and Smith, 1970) and from the Rhum breccia matrices (Donaldson, 1975). There is slight correlation between Ca content and Fo content of olivine; the more Fe-rich olivines of the Harris Bay Series have less Ca than those of the Ard Mheall Series. No Ca zoning has been detected.

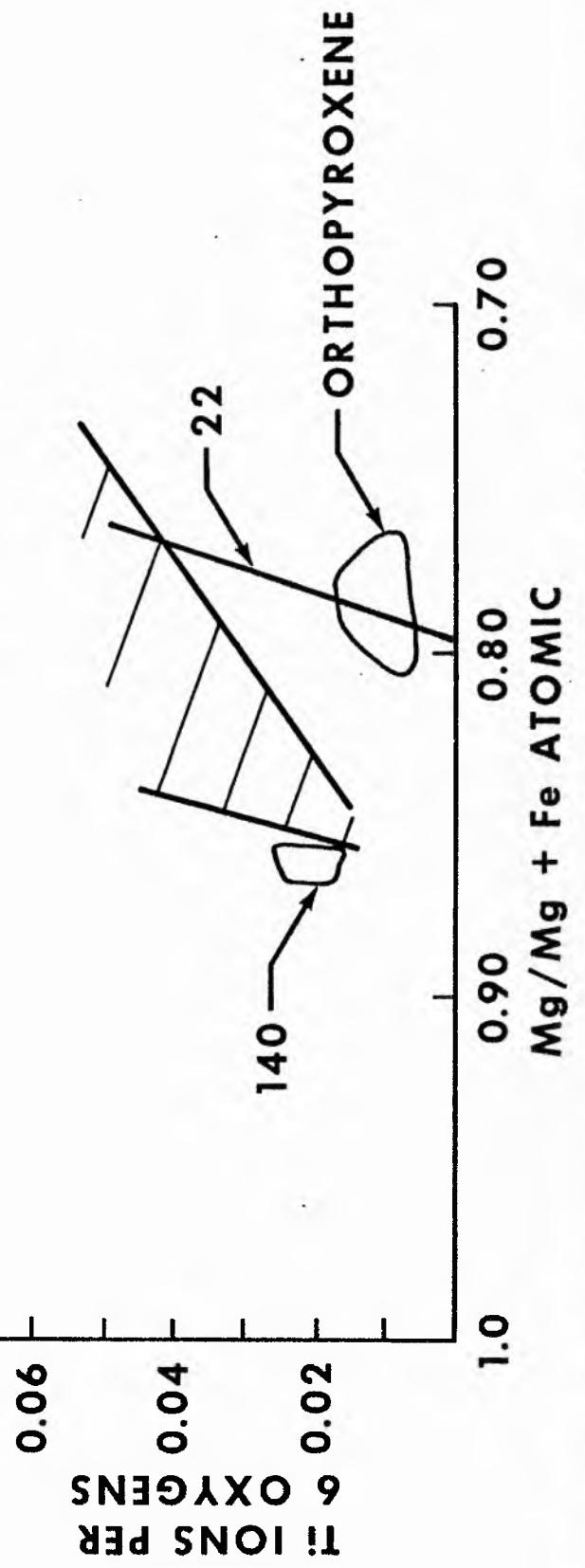
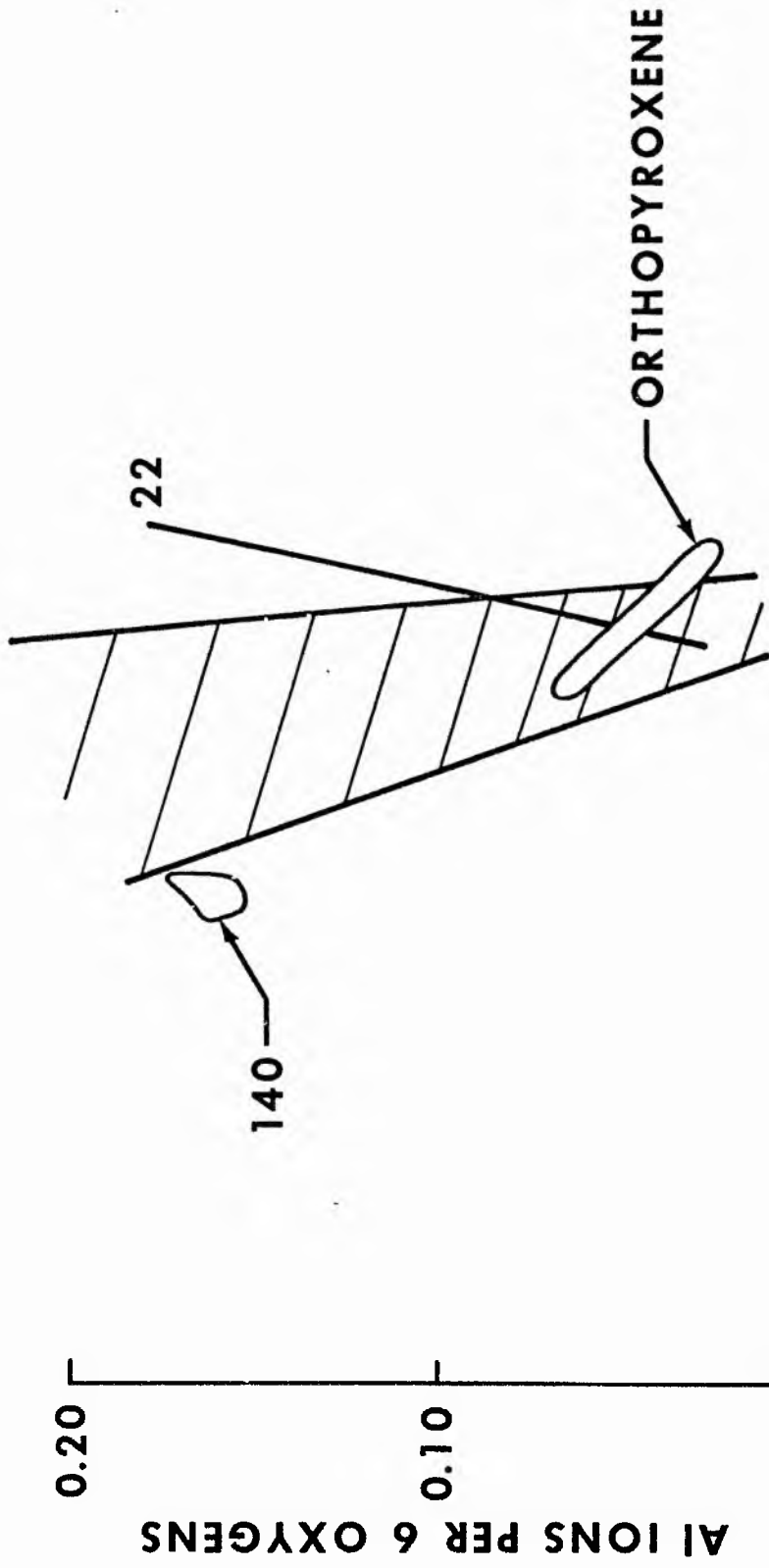
In summary, the following chemical features of olivine are notable: 1) The small range in composition, 2) the existence of reversed zoning, 3) the contrasted extent of olivine zoning between the Harris Bay harrisites and the Ard Mheall and Transition Series harrisites, 4) the zoning pattern of the very large single olivine crystals in comb-layered harrisite, 5) the low Ca contents, possibly suggestive of slow equilibrated crystal growth (Simkin and Smith, 1970), and 6) the upward increase in Fo content of olivine through two harrisite layers. Since olivine in harrisite grew rapidly (Donaldson, 1974a), and at large degrees of supercooling, extensive Mg-Fe zoning might be expected. However, if crystals grow under steady state thermal and chemical conditions from a large reservoir of melt, the composition of the olivine need not be the equilibrium composition, but the crystals can be homogeneous. Only if the crystal growth rate changes, or the volume of the melt decreases significantly, will zoning result. The significance of the low Ca content of harrisitic olivines, despite their rapid growth, is discussed in chapter X.

Pyroxenes

The pyroxenes are remarkable for their limited variation in major element composition within and between samples (Table 5, fig. 26). Most pyroxenes plot in the pyroxene quadrilateral on the corner joining the diopside-enaioopside-salite-augite fields (Poldervaart and Hess, 1951), or just within the augite field. They will be referred

Fig. 27 Mg/Mg+Fe versus Ti, Al, Cr and Ca contents of pyroxenes. Shaded area is that occupied by most analyses. The location of analyses for pyroxenes in individual rocks are shown as areas or linear trends. In the diagram for Ca the trends for samples 17 and 74B delineate the extreme positions found for all samples.





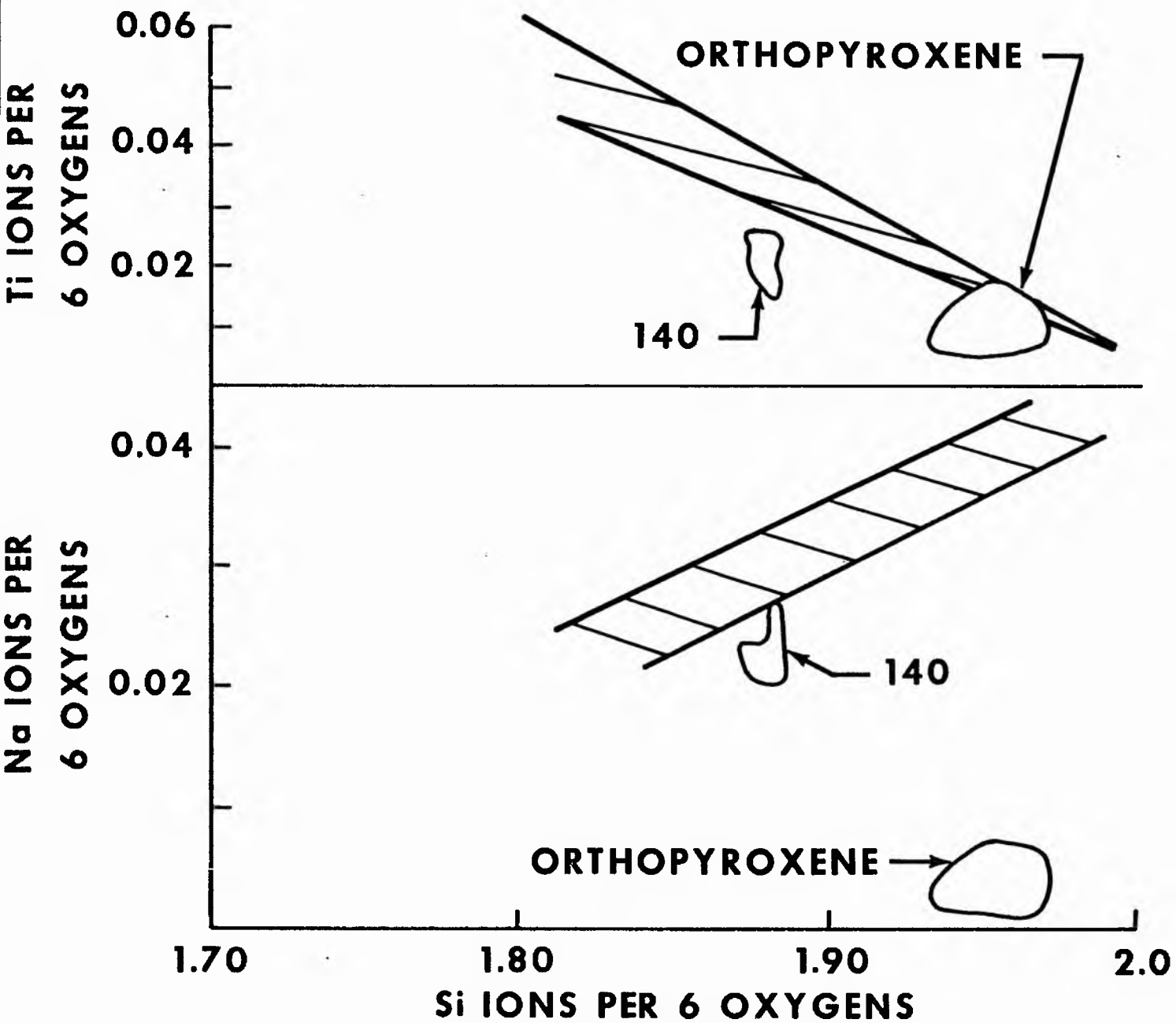
to as augite. All compositions plot in an elongate belt inclined between the Bushveld and Shiant Isles trends. Augites in minor Hebridean intrusions, inferred to have crystallized from eucrite melts (Gibb, 1968), plot in the same area.

Rhum augite compositions plotted in (1) an Al_2O_3 versus SiO_2 diagram (Le Bas, 1962), and (2) a normative nepheline-diopside-quartz-olivine diagram (Coombs, 1963) spread from the non-alkaline to the alkaline fields of both diagrams. These facts together with the location of the augite compositions in the pyroxene quadrilateral relative to those of the Skaergaard intrusion and the Shiant Isles and Black Jack sills suggest that if the Rhum magma(s) was basaltic, it was transitional in composition between a tholeiite and a mildly alkaline basalt. The rare occurrence of orthopyroxene in the eucrites supports this conclusion.

Plots of Ca versus Mg/Mg+Fe ratio for augites in different samples have varied slopes (fig. 27), involving Ca depletion with Fe enrichment. The decrease in Ca content of augite per unit change in Mg/Mg+Fe ratio is greater in Rhum augites than Skaergaard augites, resulting in trends in the pyroxene quadrilateral that more closely resemble those of pyroxenes in rapidly cooled terrestrial basalts (e.g., Evans and Moore, 1968; Donaldson *et al.*, in press) than those in major layered intrusions.

Orthopyroxene was analyzed in two harrisite samples (17, 189). The crystal in sample 17 (Harris Bay Series) has an exceedingly low Wo content (1.3 mol. percent) and is more enstatite-rich than the orthopyroxene in the Transition Series sample (189; Wo content 3 mol. percent). Orthopyroxene was also analyzed in a pegmatite patch in harrisite (Table 5, sample 204). Each orthopyroxene is unzoned and all have lower Mg/Fe ratios than adjacent olivines.

Al and Cr contents decrease with reduction in Mg/Mg+Fe ratio, whereas the Ti content increases (fig. 27). These variations indicate that pyroxene crystallization was always accompanied by plagioclase crystallization, but not by an Fe-Ti oxide. Petrographic observations are in accord with these conclusions. Relative to Si, Na increases



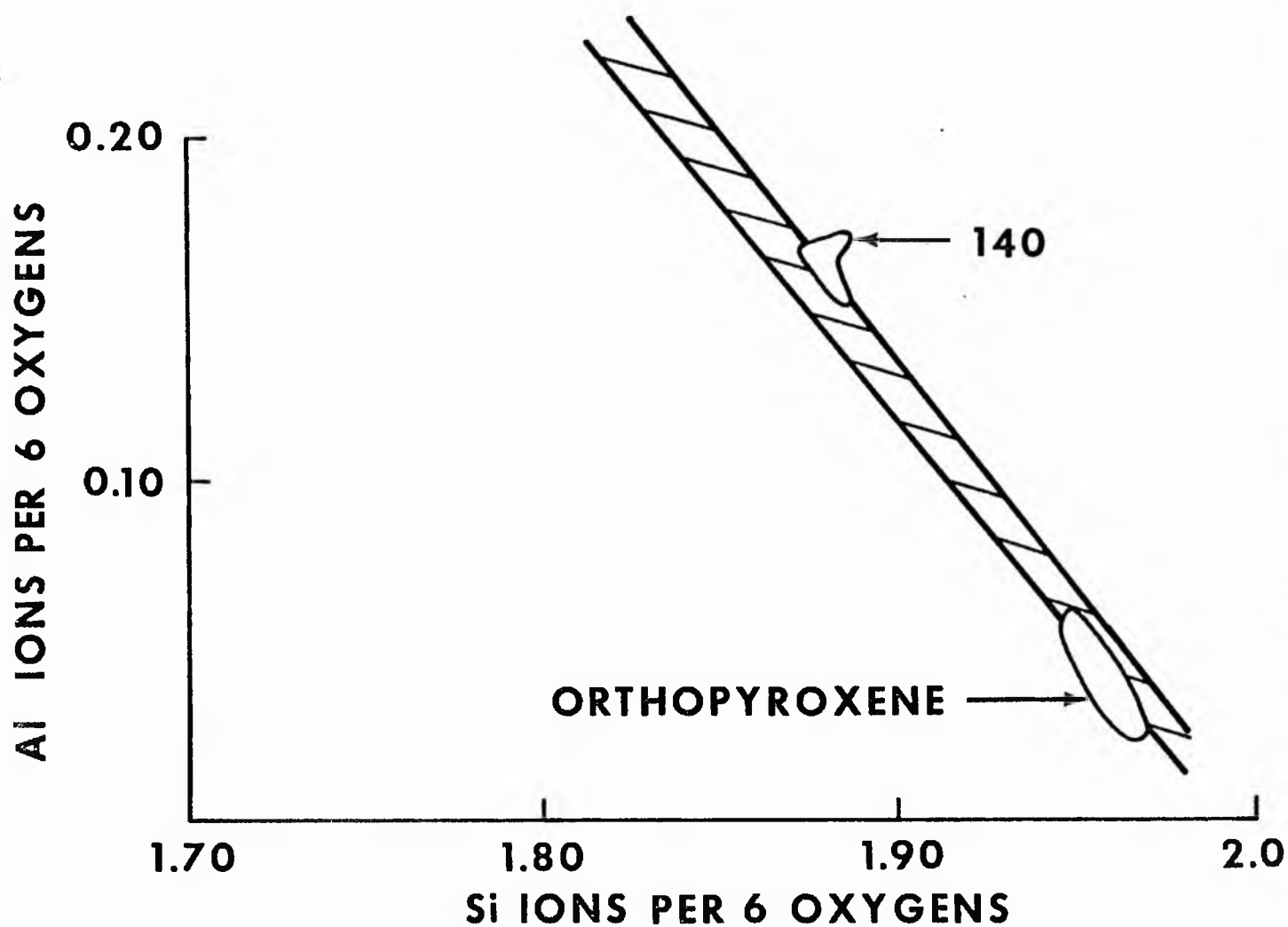


Fig. 28 Variations in Na Ti and Al with Si content of the pyroxenes. Shaded area is that occupied by most analyses.

and Ti and Al diminish (fig. 28). The close approximation of the Al versus Si variation to a 1:1 ratio (fig. 28) indicates that any deficiency in Z is made up by Al. Together with the sympathetic decrease in Ti (fig. 28), this suggests substitution of the type $M_Y^{2+} + 2Si_Z \rightleftharpoons Ti_Y + 2Al_Z$. However, departure of the Ti:Si ratio from 0.5:1 (fig. 28) indicates that there is some substitution of the type $M_Y^{2+} + Si_Z \rightleftharpoons Al_Y + Al_Z$.

The minor element fractionation in augites in harrisite indicates partial or complete entrapment of magma by elongate skeletal olivines and poor diffusional contact between melt in different pores crystallizing pyroxene. The relatively restricted fractionation of these elements in sample 140 (figs. 27 and 28) suggests crystallization of pyroxene while in contact with a large reservoir of melt.

Plagioclase

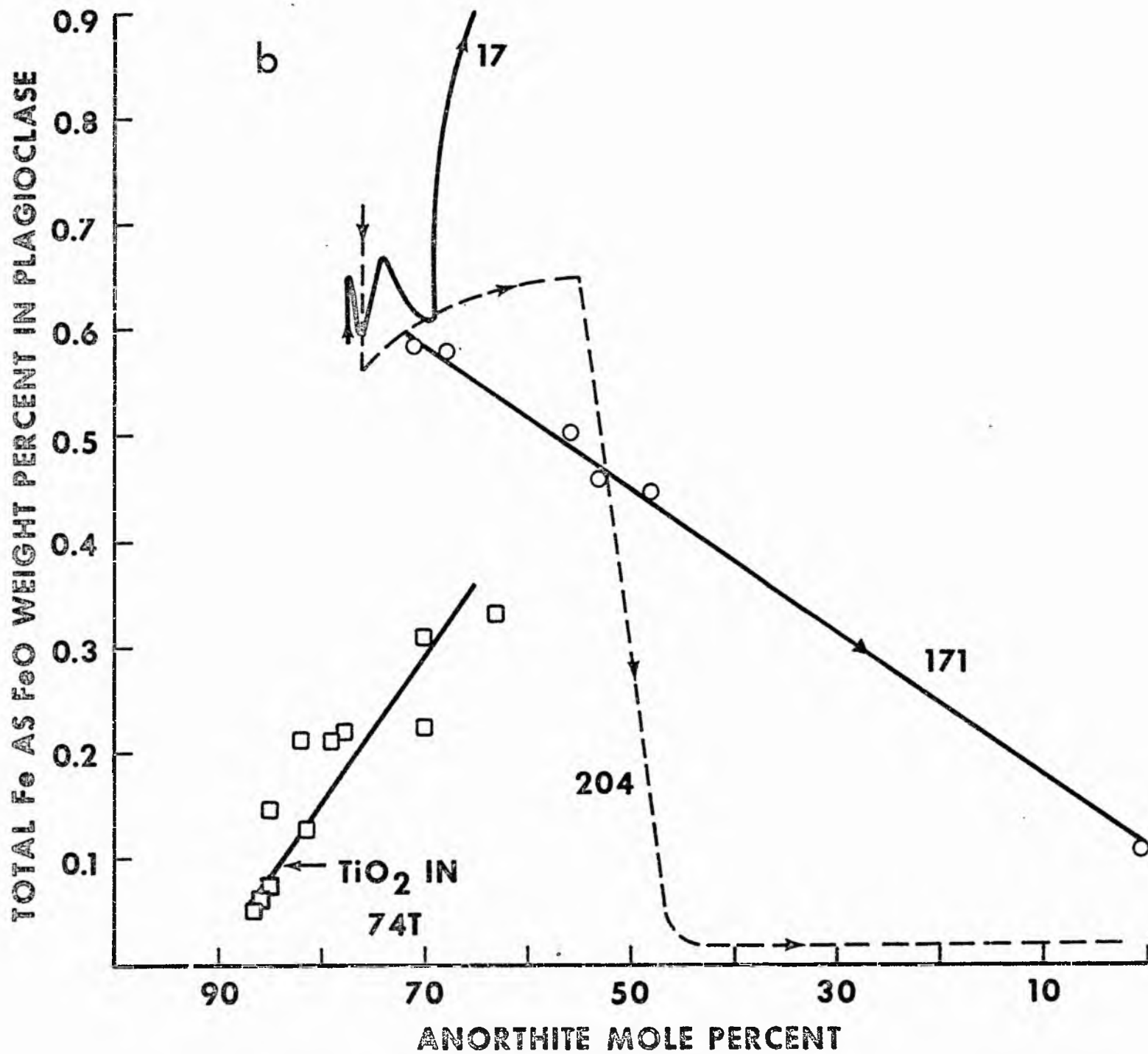
In contrast to the olivines and pyroxenes, major and minor element fractionation is well displayed by the plagioclases. The extremes in plagioclase composition for each rock studied are given in Tables 2 and 6.

The most calcic plagioclase (An_{87}) is in the Ard Mheall Series (samples 74M and T) and in the Transition Series (sample 89). Sample 140 contains a slightly less calcic plagioclase and shows least range in zoning ($An_{85} - An_{80}$) of all samples studied. Of the eucritic samples, number 17 has the most calcic plagioclase cores (An_{80}) and number 182 the least (An_{73}). Cores of Ard Mheall and Transition Series plagioclases are therefore higher temperature varieties than crystals in the Harris Bay Series. Orthoclase content is approximately 0.2 mol. percent at An_{85} , increasing to 1 mol. percent at An_{50} and 2 mol. percent at An_{30} . These values are four times larger than those for plagioclases crystallized from mid-ocean ridge basalts (Donaldson *et al.*, in press).

Most plagioclases in harrisite samples are normally zoned (Table 6), the zoning generally being restricted to the outer margins of crystals. Crystallization of plagioclase rims clearly proceeded under conditions

Table 6 Electron microprobe analyses of plagioclase in selected harristite samples, Glen Druin gabbro and peridotite samples.

Sample	748		74H		74T		211 Range in composition in sections (1) - (5)		140		89 A, B		189		182		17		200		22 (groundmass)		22 (phen)	
	core	r _{im}	core	r _{im}	core	r _{im}	core	r _{im}	core	r _{im}	core	r _{im}	core	r _{im}	core	r _{im}	core	r _{im}	core	r _{im}	core	r _{im}	core	r _{im}
SiO ₂	48.08	53.37	46.81	51.75	46.26	54.32	47.08	48.36	46.83	47.31	46.31	52.44	50.75	53.55	50.76	56.57	49.73	54.95	47.69	56.47	58.44	54.46	54.46	54.46
TiO ₂	0.05	0.05	0.05	0.12	0.02	0.13	n.d.	n.d.	0.04	0.05	0.04	0.05	0.12	0.08	0.06	0.08	0.07	0.12	n.d.	0.08	0.08	0.09	0.09	
Al ₂ O ₃	33.73	30.36	34.10	31.20	34.41	28.84	34.48	33.61	33.80	33.11	34.25	30.24	31.89	30.15	31.59	27.93	31.91	28.86	34.24	27.63	26.25	29.03	29.03	
FeO	0.41	0.49	0.34	0.41	0.37	0.34	0.43	0.51	0.54	0.46	0.47	0.66	0.59	0.50	0.62	0.56	0.49	0.49	0.21	0.59	0.70	0.64	0.64	
MgO	0.02	0.01	0.00	0.04	0.00	0.03	n.d.	n.d.	0.01	0.02	0.03	0.05	0.00	0.00	0.11	0.13	0.10	0.00	n.d.	0.00	0.00	0.06	0.06	
CaO	16.44	12.21	16.99	13.20	16.92	12.62	17.03	16.17	16.87	16.28	17.06	12.34	14.85	11.75	14.43	9.45	15.82	11.04	16.76	9.56	8.60	11.27	11.27	
Na ₂ O	1.85	4.23	1.55	3.74	1.48	3.94	1.61	2.14	1.67	2.07	1.46	4.22	2.76	4.65	3.08	5.98	2.29	4.95	1.87	5.77	6.24	4.76	4.76	
K ₂ O	0.10	0.30	0.06	0.28	0.07	0.33	0.04	0.07	0.04	0.06	0.05	0.14	0.10	0.10	0.05	0.13	0.08	0.13	0.05	0.28	0.35	0.20	0.20	
Total	100.68	101.02	99.90	100.74	99.53	100.55	100.57	100.86	99.80	99.36	99.67	100.15	101.06	100.79	100.70	100.63	100.49	100.54	100.82	100.38	100.66	100.53	100.53	
Structural formula: 8 oxygens																								
Si	2.189	2.395	2.152	2.336	2.136	2.445	2.148	2.198	2.157	2.186	2.137	2.378	2.291	2.406	2.229	2.526	2.265	2.467	2.169	2.532	2.605	2.451	2.451	
Ti	0.002	0.002	0.002	0.004	0.001	0.005	-	-	0.002	0.002	0.001	0.002	0.004	0.003	0.002	0.003	0.002	0.004	-	0.003	0.003	0.003	0.003	
Al	1.810	1.606	1.848	1.660	1.872	1.530	1.855	1.800	1.835	1.803	1.862	1.616	1.697	1.596	1.686	1.470	1.713	1.527	1.836	1.460	1.379	1.539	1.539	
Fe	0.016	0.018	0.013	0.015	0.014	0.013	0.017	0.019	0.021	0.017	0.018	0.025	0.022	0.019	0.023	0.021	0.019	0.018	0.008	0.022	0.026	0.024	0.024	
Mg	0.002	0.001	0.000	0.003	0.000	0.002	-	-	0.001	0.001	0.002	0.003	0.000	0.000	0.007	0.001	0.001	0.000	n.d.	0.000	0.000	0.004	0.004	
Ca	0.802	0.587	0.837	0.639	0.837	0.609	0.832	0.787	0.833	0.806	0.843	0.599	0.718	0.565	0.700	0.452	0.772	0.531	0.817	0.459	0.411	0.543	0.543	
Na	0.163	0.368	0.138	0.327	0.132	0.344	0.143	0.189	0.149	0.185	0.131	0.371	0.242	0.405	0.270	0.517	0.202	0.431	0.165	0.502	0.539	0.415	0.415	
K	0.006	0.017	0.003	0.016	0.004	0.019	0.002	0.004	0.002	0.003	0.003	0.008	0.006	0.006	0.003	0.007	0.005	0.008	0.003	0.016	0.020	0.011	0.011	
Z	4.001	4.003	4.002	4.000	4.009	3.980	4.003	3.998	3.994	3.991	4.000	3.996	3.992	4.005	3.987	3.999	3.980	3.998	4.005	3.995	3.987	3.993	3.993	
X	0.989	0.991	0.991	1.000	0.987	0.987	0.994	0.999	1.006	1.012	0.997	1.006	0.988	0.995	1.003	0.998	0.999	0.988	0.993	0.999	0.996	0.997	0.997	
Mol. %	Ab 16.2	37.3	13.6	32.8	13.1	34.8	85.7	81.0	14.6	18.1	12.9	37.3	24.4	41.0	27.1	52.6	20.0	44.0	83.5	51.0	55.3	42.3	42.3	
	An 83.1	60.9	86.1	65.6	86.5	63.2	14.1	18.6	85.2	81.6	86.8	61.9	75.0	58.4	72.6	46.6	79.5	55.3	16.2	47.3	42.7	56.5	56.5	
	Or 0.6	1.8	0.3	1.6	0.4	2.0	0.3	0.4	0.2	0.3	0.3	0.8	0.6	0.6	0.3	0.8	0.5	0.8	0.3	1.7	2.0	1.2	1.2	



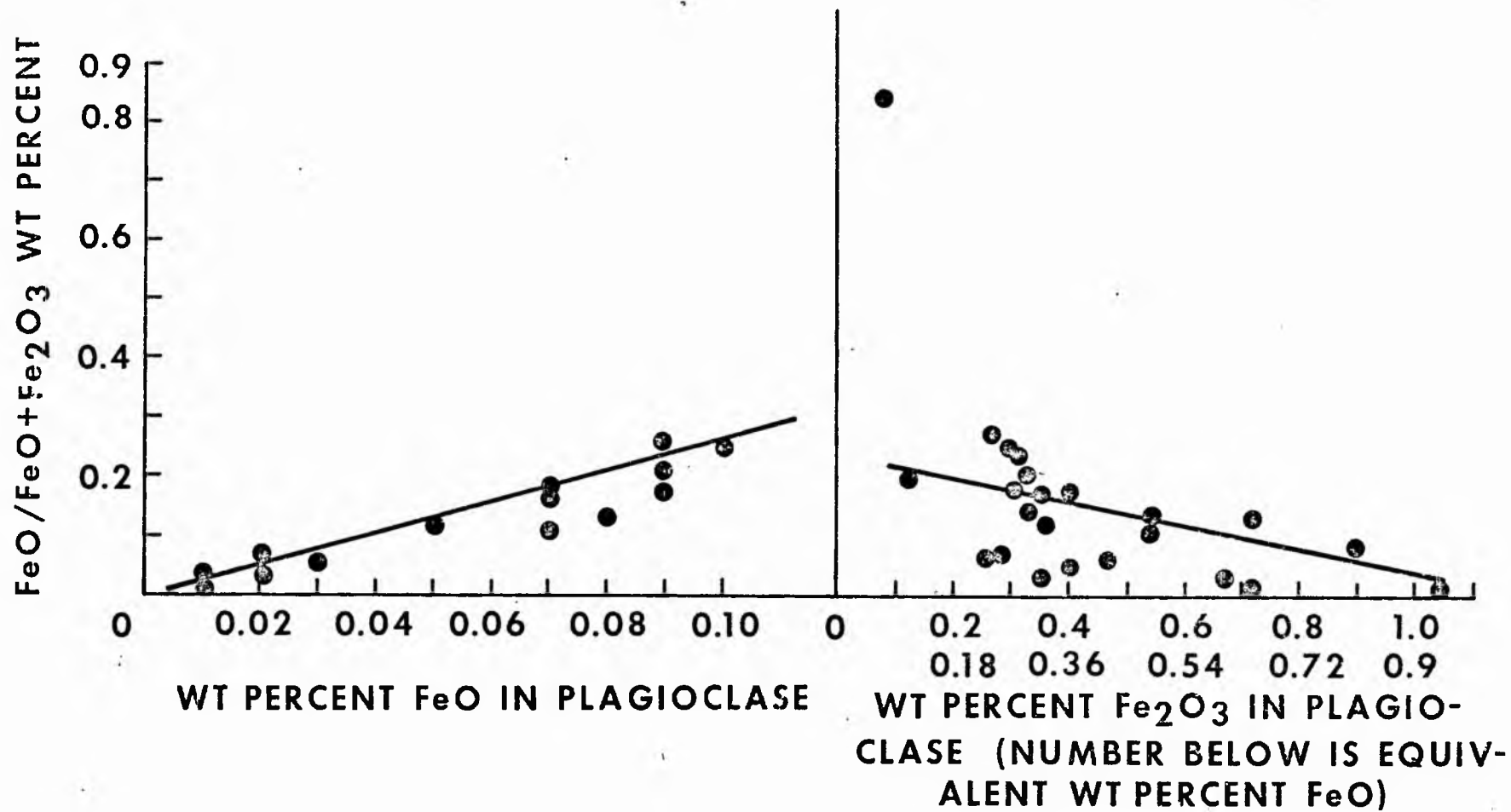


Fig. 30 Fe₂O₃ and FeO contents of plagioclases from the Bushveld intrusion versus FeO/FeO+Fe₂O₃ ratio of the plagioclases. (Data from Ferguson and Wright, 1969)

of non-equilibrium and sluggish reaction between crystal and melt. Pegmatites contain more extensively zoned plagioclases than the harrisites which enclose them (samples 182, 204, 163 and 171, Table 6). These plagioclases probably nucleated at temperatures comparable to those at which plagioclase nucleated in the surrounding harrisite, but continued growth to temperatures well below those at which plagioclase crystallization in harrisite had ceased.

Mg contents of plagioclases are very low and no distinct trends result when they are plotted against anorthite content. Ti increases with decreasing anorthite content of the plagioclase (e.g., fig. 29b). This observation is considered to reflect continuous, smooth increase in the Ti activity of the parent melt with progressive crystallization.

The plagioclases contain approximately 0.4 wt. percent Fe (Table 6). The extent, trend and rate of change of Fe content, as functions of An content are apparently unique to each sample investigated (fig. 29a). The trends of Fe against An for most of the samples are linear. Some samples (e.g., 140 and 182) have trends with steep negative slopes, others (e.g., 74B and M) have positive slopes, whereas others (e.g., 74T) are near horizontal. The trend of decreasing Fe content with An decrease in the crystal from sample 204 (fig. 29b) is reversed between An_{86} and An_{55} ; the abrupt change in Fe content at An_{50} is probably the result of ilmenite crystallization.

The trends of Fe against An indicate (1) that the factor(s) controlling Fe fractionation in plagioclase were operative throughout the crystallization of plagioclase in any one rock, and (2) that the effects were markedly different in individual rocks. The differences in trends for the samples 74B, M and T from the comb-layered harrisite indicate that plagioclase in each part of this layer grew in isolation and out of minor-element equilibrium with adjacent plagioclases and with the supernatant magma. The factor(s) controlling Fe fractionation therefore operate on a very local scale.

The changing Fe/Na ratio of the melt from which the plagioclase crystallizes may control the fractionation trends. For example,

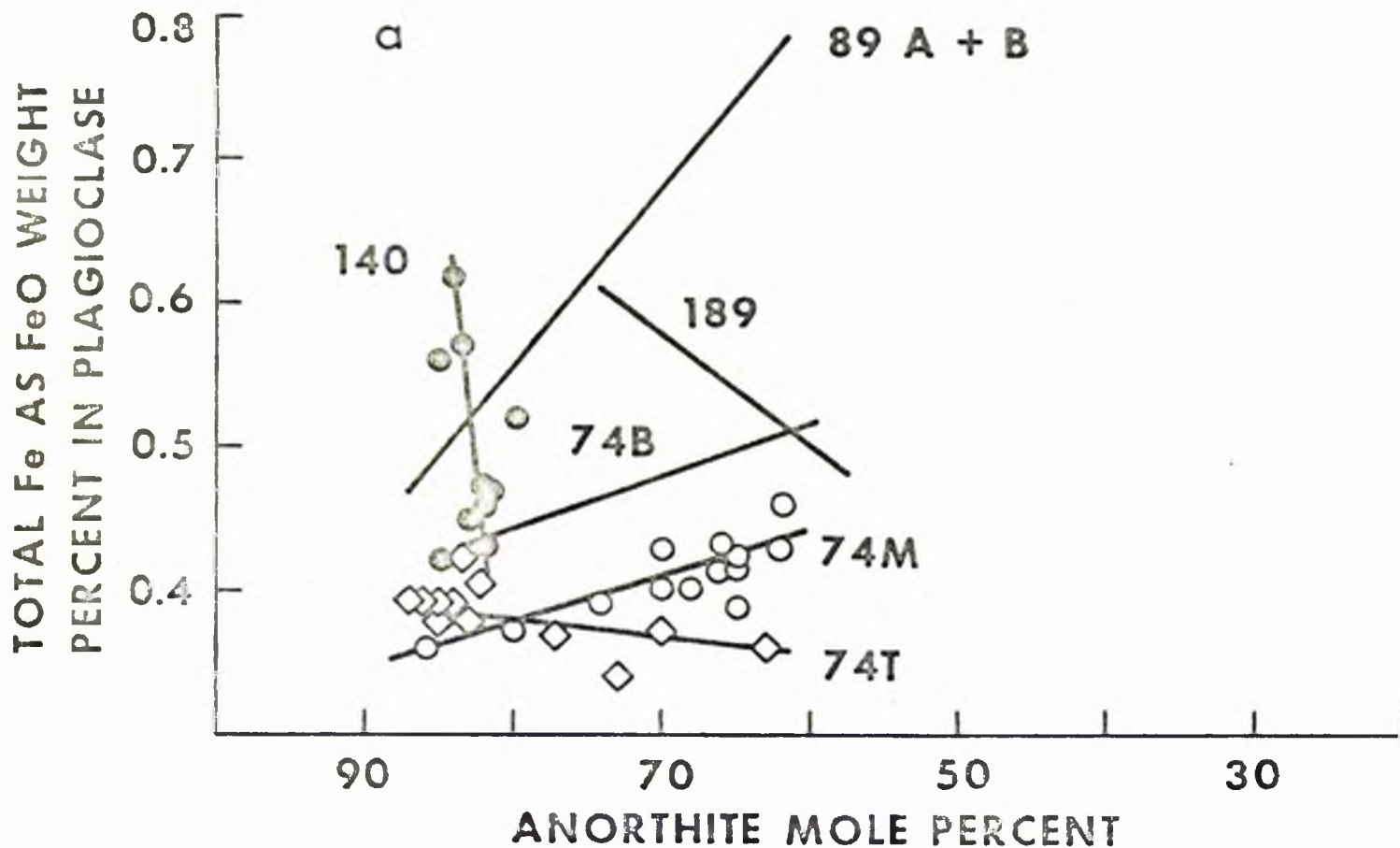


Fig. 29 Anorthite versus FeO content of plagioclases in some Rhum rocks.

a. Trends for crystals in samples 140, 74M and 74T are shown with data points (filled circles, open circles and diamonds respectively).

b. Trends for traverses from core to rim (arrow direction) of individual crystals in samples 17, 204 and 171. The figure also shows the relation of TiO_2 content in plagioclases in sample 74T versus plagioclase composition. TiO_2 scale is the same as for FeO.

decreasing Fe content of the plagioclase with increasing Na content could indicate that the Fe/Na ratio in the melt increased with fractionation, either due to slower Fe enrichment than Na enrichment in the melt, or to decreasing Fe content of the melt.

Alternatively, a change in fO_2 may control the fractionation trends. In terrestrial plagioclases, iron is traditionally considered to be ferric, replacing Al^{3+} ions. However, Ferguson and Wright (1969) have shown that the $FeO/FeO+Fe_2O_3$ ratio of plagioclase from the Bushveld intrusion ranges from 0.08 - 0.84. If the FeO and Fe_2O_3 contents of the Bushveld plagioclases are plotted against $FeO/FeO+Fe_2O_3$ ratio, distinct linear trends result (fig. 30). The greater the FeO content of the plagioclase, the higher the $FeO/FeO+Fe_2O_3$ ratio. Ferguson and Wright attributed trends toward lower $FeO/FeO+Fe_2O_3$ ratios to crystallization from progressively more oxidized magma, and specifically to an increase in pH_2O . The Bushveld data indicate that if the $FeO/FeO+Fe_2O_3$ ratio of plagioclase reflects the ratio in the parent magma, then the more oxidizing the conditions the more total iron that can enter the plagioclase, assuming fixed iron content in the magma. The data also suggest that local pO_2 variations would act as a control of the Fe content of Rhum plagioclases. Trends of Fe depletion against Na enrichment may be ascribed to progressively more reducing conditions occurring during fractionation (the steeper the trend, the more extreme the change in pO_2), while trends in Fe and Na enrichment would reflect progressively increasing pO_2 .

Lacking data on the $FeO/FeO+Fe_2O_3$ ratios of the Rhum plagioclases, the relative importance of pO_2 variation and magmatic fractionation cannot be determined. It seems probable that an interplay of both effects causes the unique Fe-An variation in each sample.

Kaersutite

Representative analyses of the chestnut to pink amphibole are given in Table 7. The presence of a filled A site (Na + K), high Ca content and 2.5 - 1.6 Al ions in the Z group indicates a pargasitic composition. Ti substitution for Al in octahedral sites is sufficiently

Table 7 Electron microprobe analyses of Kaersutite in selected harrisite samples, Glen Duain gabbro, and a pegmatite

Sample	74B	211	89A,B	189	182		17	200	22	204
					core	rim				
SiO ₂	42.52	42.33	43.78	43.43	44.28	53.65	38.09	44.11	44.33	41.56
TiO ₂	5.73	3.21	3.10	3.81	3.90	2.08	7.83	4.29	3.22	3.55
Al ₂ O ₃	12.44	13.55	11.17	10.98	9.95	1.53	14.82	10.51	9.17	13.19
Cr ₂ O ₃	0.69	0.22	0.16	0.16	0.02	0.31	0.17	0.09	0.02	0.16
FeO	9.16	8.51	7.81	8.92	10.26	17.15	9.73	9.10	10.46	10.88
MnO	0.27	0.11	0.11	0.00	0.27	0.35	0.32	0.11	0.13	0.29
MgO	13.93	16.08	16.64	15.64	16.42	12.01	16.06	15.39	15.57	14.50
CaO	12.07	11.96	11.98	11.70	9.81	12.42	10.48	12.42	11.39	11.99
Na ₂ O	2.72	3.17	2.56	2.81	3.10	0.61	1.77	2.57	2.46	3.09
K ₂ O	0.45	0.48	0.92	0.90	0.42	0.24	0.61	0.40	1.22	0.57
F ¹	0.51	0.60	0.78	0.68	0.81	0.54	0.48	0.58	0.98	0.30
Cl ¹	0.10	0.10	0.14	0.13	0.11	0.11	0.17	0.09	0.12	0.02
Total	100.59	100.32	99.15	99.16	99.35	101.00	100.53	99.66	99.07	100.10
Structural formula: 23 oxygens										
Si	6.095	6.046	6.317	6.314	6.410	7.722	5.481	6.344	6.488	6.014
Al	1.905	1.954	1.683	1.686	1.590	0.260	2.513	1.656	1.512	1.986
Al	0.197	0.330	0.217	0.195	0.108	0.000	0.000	0.125	0.070	0.263
Ti	0.618	0.344	0.336	0.417	0.425	0.225	0.847	0.463	0.355	0.387
Cr	0.078	0.017	0.019	0.018	0.003	0.035	0.020	0.015	0.002	0.018
Fe	1.098	1.013	0.943	1.085	1.242	2.064	1.171	1.094	1.280	1.317
Mn	0.032	0.017	0.014	0.000	0.033	0.042	0.039	0.013	0.016	0.036
Mg	2.975	3.427	3.579	3.388	3.543	2.576	3.445	3.299	3.397	3.127
Ca	1.853	1.829	1.851	1.822	1.521	1.916	1.615	1.913	1.785	1.860
Na	0.755	0.876	0.717	0.792	0.871	0.171	0.495	0.717	0.698	0.867
K	0.080	0.086	0.169	0.168	0.078	0.044	0.112	0.073	0.228	0.103
Mg:Mg+Fe	0.73	0.77	0.79	0.76	0.74	0.55	0.75	0.75	0.73	0.70

¹Uncorrected probe analyses

large that many of the compositions exceed the arbitrary minimum 0.45 Ti ions per half formula unit which Leake (1968) considers as the limit of kaersutite compositions. For convenience, all the Ti-rich amphibole in Rhum will be called kaersutite, despite the fact that some of it has less than Leake's limiting Ti content. The amphibole is characterized by substantial substitution of halogens for hydroxyl (Table 7).

The ratio of Mg/Mg+Fe shows remarkably limited variation, and no zoned kaersutite was found. With increasing K_2O content both TiO_2 and Al_2O_3 contents diminish. Cr contents vary in kaersutites from the same rock (0.8 - 0.15 wt. percent Cr_2O_3). The higher of these values is substantial for a phase so late in the paragenetic sequence of the rocks and may indicate that some kaersutite crystallization involves reaction of pyroxene with melt. For comparison, analyses of kaersutite crystals from the type locality give 0.0 - 0.15 wt. percent Cr_2O_3 (Donaldson, in prep.).

Rhum kaersutite is markedly silica undersaturated (11 - 15 wt. percent normative nepheline and 20 - 25 wt. percent normative olivine). All the kaersutite analyses listed by Leake (1968) and by Deer et al. (1963) are from rocks of alkaline, undersaturated affinity and are commonly in association with a titanaugite. The Rhum kaersutite appears to be unusual in being associated with augite and having crystallized from a relatively silica-rich magma (as evidenced by occasional orthopyroxene crystals).

Three conditions favour a high Ti content of pargasite:

(1) High Ti activity in the magma at the time of amphibole crystallization (2) low pO_2 favouring substitution of Ti^{4+} for Fe^{3+} in the amphibole by reducing the Fe^{3+}/Fe^{2+} ratio in the melt (Holloway, personal communication, 1974) and (3) high Ti content in pre-existing pyroxene, if reaction of pyroxene is involved in the amphibole formation. Generally the Ti content of pyroxene adjacent to kaersutite is too low for condition (3) to apply and, since relatively high pH_2O and pO_2 are deduced for the Rhum magma from ilmenite analyses

Table 8 Electron microprobe analyses of phlogopite in selected harrisite samples and one pegmatite sample

Sample	741	89A,B	189	17	200	204
SiO ₂	38.55	38.22	39.21	39.27	38.16	38.47
TiO ₂	7.60	4.24	4.48	4.88	6.70	5.51
Al ₂ O ₃	14.92	16.45	15.37	14.47	14.18	15.06
Cr ₂ O ₃	0.58	0.10	0.13	0.08	0.12	0.01
FeO	6.76	7.50	7.65	9.17	11.11	8.90
MnO	0.05	0.05	0.00	0.00	0.04	0.00
MgO	19.11	20.90	19.75	17.13	17.09	19.37
CaO	0.00	0.00	0.00	0.00	0.00	0.00
Na ₂ O	1.04	1.98	1.04	0.65	0.65	0.75
K ₂ O	8.18	6.54	8.45	8.82	8.59	8.82
Total ¹	96.79	95.98	96.08	96.83	96.64	95.10
Structural formula: 22 oxygens						
Si	5.439	5.406	5.581	5.572	5.509	5.550
Al	2.480	2.594	2.419	2.428	2.413	2.450
Al	8.000	8.000	8.000	8.000	8.000	8.000
Ti	0.806	0.149	0.160	0.019	0.728	0.066
Cr	0.064	0.451	0.479	0.521	0.014	0.443
Fe	0.797	0.011	0.014	0.001	0.014	0.001
Mn	0.006	0.888	0.911	0.975	1.342	1.081
Mg	4.018	5.610	5.591	5.756	5.688	5.830
Ca	0.000	0.000	0.000	0.000	0.005	0.000
Na	0.284	4.407	4.190	4.240	3.677	4.239
K	1.473	0.000	0.000	0.000	0.000	0.000
Mg:Mg+Fe	0.83	0.543	0.286	0.263	0.182	0.210
		1.757	1.780	1.765	1.765	1.842
		1.722	1.596	1.583	1.595	1.632
		0.83	0.77	0.81	0.73	0.80

¹All crystals contain <500 ppm Cl and <500 ppm F

(see below), condition (2) is unlikely to be important.

In summary, kaersutite probably crystallized from Ti-enriched residual melt in crystal-liquid mushes and its formation instead of pyroxene is due to an increase in the volatile content of the melt. It is suggested that those kaersutites with Cr_2O_3 contents comparable to coexisting augite represent products of a reaction between melt and pyroxene, whereas those with lower contents crystallized directly from the magma. Both types co-exist in a single rock.

Phlogopite

All the brown mica crystals analyzed have Mg/Mg+Fe ratios > 0.66 (Table 8) and are classified as phlogopite (Deer et al., 1962a). The Mg/Mg+Fe ratio is both high and limited in range, like that of other mafic minerals in the rocks. Ti content is substantial compared with most phlogopite and biotite analyses listed by Deer et al. As a result, the structural formulae of some of the analyses in Table 8 have Ti in both octahedral and tetrahedral structural sites. Cr content of phlogopite is high in the Ard Mheall harrisite (74M), indicating that, because it is a late-stage crystallizing phase, its formation may have involved reaction of pyroxene (and possibly also chrome magnetite) with the magma.

Opaque minerals (1) Spinel

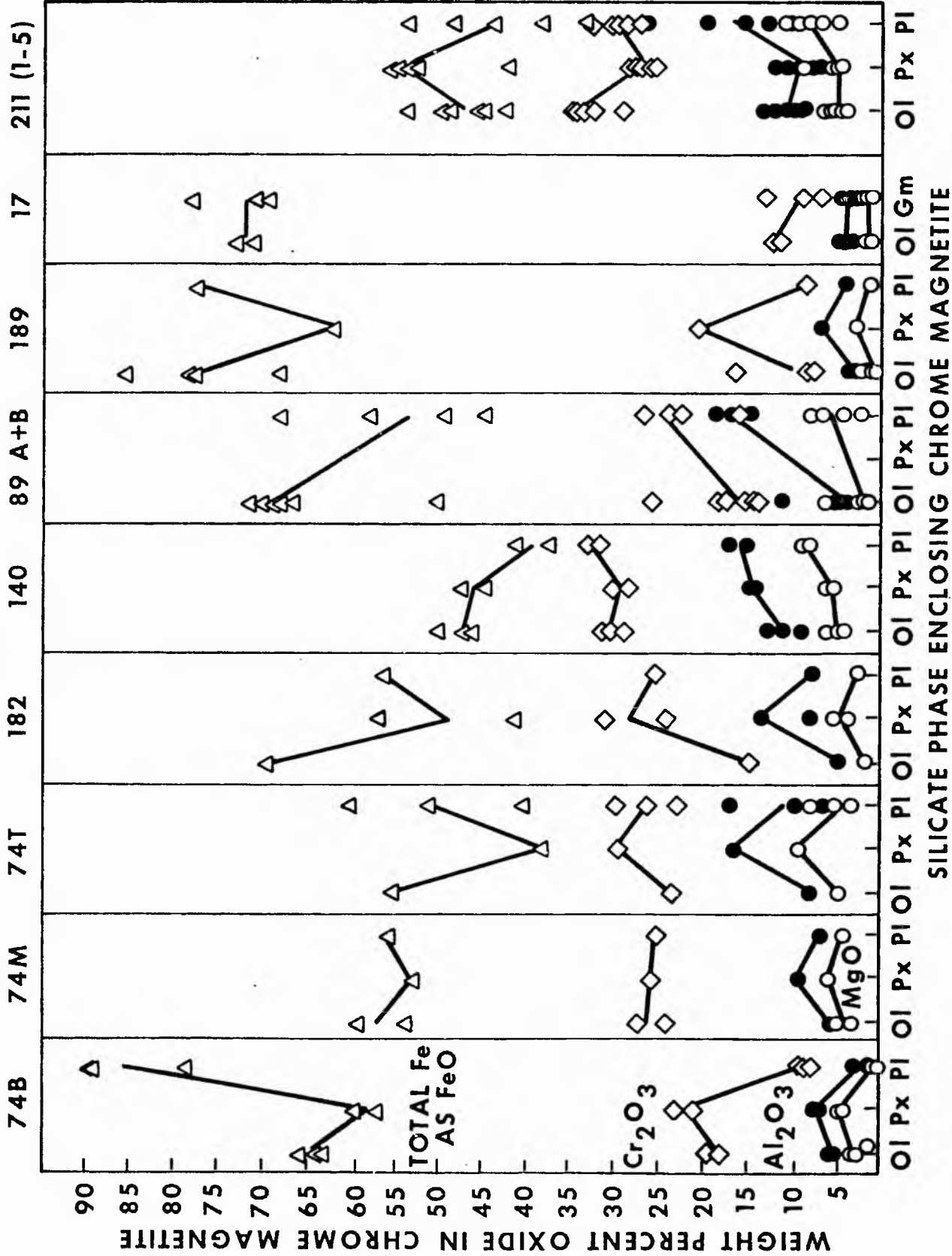
A range of spinel compositions was found both between samples and within samples. Table 9 lists representative analyses of spinels, as a function of the silicate mineral enclosing the spinel. Crystals in the Ard Mheall and Transition Series generally have $\text{Fe} > \text{Cr} > \text{Al}$, though rarely $\text{Cr} > \text{Fe} > \text{Al}$. Fe^{2+} always exceeds Mg^{2+} . These spinels are therefore dominated by solid solution between magnetite and chromite and are conveniently called chrome magnetites. They are relatively Al-deficient compared with most of the spinel analyses reported by Henderson and Suddaby (1971) from rocks of the Eastern Layered Series. Spinel in the Harris Bay Series have smaller Cr contents and are called magnetite.

Table 9 Electron microprobe analyses of sphinels in selected harristite samples and one pegmatite sample

Sample Enclosing mineral	74 B			74 H			74 T			211 Extremes of composition in samples 211 (1) - (5)					140			89 A, B			189			182							
	ol	px	pl	ol	px	pl	ol	px	pl	ol	pl	ol	px	pl	ol	px	pl	ol	px	pl	ol	px	pl	ol	px	pl	ol	px	pl		
TiO ₂	2.53	2.54	1.29	2.60	2.36	2.80	2.96	1.95	2.30	2.58	1.26	0.85	2.37	5.87	2.41	2.61	1.87	1.84	3.90	2.40	4.07	3.45	3.97	4.07	4.07	4.07	4.07	4.07	4.07	1.30	
Al ₂ O ₃	5.72	7.57	3.75	6.00	9.84	7.14	8.30	11.17	10.03	8.83	15.68	26.43	10.09	11.88	10.24	9.20	14.37	17.04	4.25	14.83	3.15	6.95	3.70	3.70	5.78	5.78	5.78	18.05	18.05	18.05	
Cr ₂ O ₃	18.50	21.46	8.81	24.80	26.14	25.34	23.88	28.37	26.52	29.09	33.72	29.65	26.71	28.01	27.21	30.83	28.74	33.32	18.36	24.05	7.89	20.56	8.55	8.55	15.07	15.07	15.07	31.25	31.25	31.25	
Fe ₂ O ₃	41.21	34.90	54.25	33.93	30.36	31.64	31.26	27.12	28.13	26.74	18.18	13.08	27.99	19.22	28.09	24.55	25.93	16.86	38.57	26.84	50.04	35.19	48.79	48.79	41.40	41.40	41.40	16.38	16.38	16.38	
FeO ¹	29.02	26.14	30.52	28.92	25.62	27.50	27.25	26.19	26.23	28.95	25.37	20.98	27.47	24.59	27.80	28.03	27.20	22.41	32.21	25.72	32.89	30.47	33.21	33.21	32.47	32.47	32.47	26.90	26.90	26.90	
MgO	3.66	5.20	1.50	3.71	6.33	4.73	5.00	5.88	5.50	4.09	6.54	10.55	4.87	8.94	4.95	4.71	5.53	8.97	1.93	6.85	1.48	3.25	1.24	1.24	2.19	2.19	2.19	5.56	5.56	5.56	
MnO	0.33	0.34	0.34	0.37	0.31	0.34	0.35	0.33	0.36	0.40	0.39	0.27	0.44	0.29	0.42	0.37	0.33	0.26	0.38	0.28	0.26	0.40	0.31	0.31	0.35	0.35	0.35	0.40	0.40	0.40	
Total	100.97	98.15	100.46	100.33	100.96	99.49	99.00	101.01	99.07	100.68	101.14	101.81	99.94	98.80	101.12	100.30	100.97	100.70	99.60	100.97	99.78	100.27	99.77	99.77	100.73	100.73	100.73	99.85	99.85	99.85	
Structural formula: 4 oxygens																															
Ti	0.07	0.07	0.04	0.07	0.05	0.07	0.08	0.05	0.06	0.07	0.03	0.02	0.06	0.15	0.06	0.07	0.05	0.04	0.11	0.06	0.11	0.09	0.11	0.11	0.11	0.11	0.11	0.11	0.03	0.03	0.03
Al	0.24	0.32	0.16	0.25	0.40	0.30	0.35	0.45	0.41	0.36	0.61	0.95	0.41	0.47	0.41	0.38	0.57	0.65	0.18	0.58	0.14	0.29	0.16	0.16	0.22	0.22	0.22	0.71	0.71	0.71	
Cr	0.52	0.61	0.25	0.70	0.70	0.71	0.67	0.76	0.73	0.80	0.88	0.71	0.73	0.75	0.74	0.85	0.76	0.85	0.53	0.63	0.23	0.88	0.25	0.25	0.43	0.43	0.43	0.82	0.82	0.82	
Fe ²⁺	1.10	0.94	1.51	0.91	0.78	0.84	0.83	0.69	0.74	0.70	0.45	0.30	0.73	0.49	0.72	0.64	0.58	0.41	1.07	0.67	1.40	0.94	1.36	1.36	1.13	1.13	1.13	0.41	0.41	0.41	
Fe ³⁺	0.86	0.78	0.94	0.86	0.73	0.81	0.80	0.74	0.76	0.84	0.70	0.53	0.80	0.69	0.80	0.81	0.76	0.61	0.99	0.71	1.02	0.91	1.03	1.03	0.98	0.98	0.98	0.75	0.75	0.75	
Mg	0.19	0.28	0.08	0.20	0.32	0.25	0.26	0.30	0.29	0.21	0.32	0.48	0.25	0.45	0.25	0.24	0.28	0.43	0.11	0.34	0.08	0.17	0.07	0.07	0.12	0.12	0.12	0.27	0.27	0.27	
Mn	0.01	0.01	0.01	0.01	0.01	0.01	0.01	0.01	0.01	0.01	0.01	0.01	0.01	0.01	0.01	0.01	0.01	0.01	0.01	0.01	0.01	0.01	0.01	0.01	0.01	0.01	0.01	0.01	0.01	0.01	
R ³⁺ + ⁴⁺	1.93	1.94	1.97	1.93	1.94	1.92	1.93	1.95	1.94	1.93	1.97	1.98	1.93	1.86	1.93	1.94	1.96	1.95	1.89	1.94	1.88	1.90	1.88	1.88	1.89	1.89	1.89	1.97	1.97	1.97	
R ²⁺	1.06	1.07	1.03	1.07	1.06	1.07	1.07	1.05	1.06	1.06	1.03	1.02	1.06	1.15	1.06	1.06	1.05	1.05	1.11	1.06	1.11	1.09	1.11	1.11	1.11	1.11	1.11	1.03	1.03	1.03	
Mg/Mg+Fe ²⁺	0.18	0.26	0.08	0.19	0.30	0.24	0.25	0.29	0.28	0.20	0.32	0.47	0.24	0.39	0.24	0.23	0.27	0.41	0.10	0.32	0.07	0.16	0.06	0.06	0.11	0.11	0.11	0.26	0.26	0.26	
Fe ²⁺ /Fe ²⁺ +Al+Cr	0.59	0.50	0.78	0.49	0.41	0.45	0.45	0.36	0.39	0.38	0.23	0.15	0.39	0.29	0.39	0.34	0.30	0.21	0.60	0.36	0.79	0.52	0.77	0.77	0.63	0.63	0.63	0.21	0.21	0.21	

¹Calculated assuming perfect analysis and perfect stoichiometry

SAMPLE NUMBER



SILICATE PHASE ENCLOSING CHROME MAGNETITE

Unlike the spinels reported by Donaldson (1975) from the matrices of Rhum ultrabasic breccias, the grains in harrisite are unzoned. However, they are not homogeneous, since many contain rods and blebs of exsolved ilmenite.

To facilitate comparison of analyses between different rocks and within the same rock, fig. 31 has been constructed showing the behaviour of each analyzed element. It is apparent that considerable differences in spinel composition exist between different rocks. Spinel in sample 140 are the least Fe rich. Fe content in the following samples increases in the order 211, 74T, 74M, 74B, 182, 89A and B, 17 and 189 ('averaging' the composition of the spinel in the rock). This increase in Fe content is accompanied by decrease in Mg, Al, and Cr. As the Fe content of spinel increases in the order 211, 182, 89, 17 and 189, so does the Ti content. As the Fe content of spinel increases in the order 74T, 74M and 74B, the Ti content decreases. Spinel in the former group of samples crystallized from magmas progressively more enriched in Fe and Ti. Those in the comb-layered harrisite (sample 74 B, M and T) indicate that the magma with which spinels at the bottom of the layer equilibrated was more Fe and Ti rich than that at the top of the layer. Apparently the magma was cooler at the base of the layer compared to the top (Evans and Wright, 1972).

Figure 31 also demonstrates that spinel composition in any rock is a function of the silicate mineral enclosing the spinel grain (cf. Donaldson, 1975). The most Fe-rich spinel is not always enclosed by the same silicate phase. Spinel enclosed by pyroxene are always the most depleted in Fe and richest in Mg, Al and Cr, except for those in samples 140 and 211. In samples 74B, 182, 89A and B and 189, spinels in olivine come next in degree of Fe enrichment, followed by those enclosed by plagioclase. In samples 74M and T, these relations are reversed, while in sample 140, spinels in pyroxene are more Fe rich than those in plagioclase, but are less Fe rich than those in olivine. Thus, the trends in spinel composition, as a function of the enclosing

Table 10 Electron microprobe analysis, equilibration temperatures and oxygen fugacities of ilmenite, titanomagnetite and magnetite in selected harristite samples, Glen Duan gabbro and pegmatite samples.

Sample	74 B.M.T	189	182	200	22	204	163						
TiO ₂	53.40	49.92	1.51	49.24	51.35	28.21	4.09	48.96	50.04	1.73	49.58	0.97	47.45
Al ₂ O ₃	0.00	0.36	1.60	0.00	0.72	1.20	2.62	0.19	0.00	0.42	0.00	0.97	0.00
Cr ₂ O ₃	0.39	0.29	0.00	0.22	0.07	0.05	0.21	0.41	0.00	0.18	0.03	0.04	0.08
FeO	38.79	43.65	90.17	49.53	47.91	67.70	82.37	45.00	48.81	89.27	49.39	90.98	51.09
MnO	0.51	0.40	0.14	1.13	0.14	0.20	0.21	0.57	0.90	0.03	0.39	0.04	0.74
MgO	7.69	5.43	1.00	1.46	0.12	0.22	1.78	3.95	0.13	0.10	0.38	0.26	0.41
Total	100.78	100.05	94.42	101.58	100.31	97.58	91.28	99.08	99.88	91.73	99.77	93.26	99.77
Ilmenite basis													
FeO ¹	33.81	34.81		40.53	45.81			36.41	43.85		43.50		41.19
Fe ₂ O ₃ ¹	5.52	9.82		10.01	2.32			9.54	5.51		6.55		11.00
Total	101.32	101.03		102.59	100.53			100.03	100.43		100.43		100.87
Mol. % ilmenite	93.16	88.17		90.0	96.73			89.16	94.65		93.65		89.28
Ulvsöspinel basis													
FeO ¹			30.26			56.21	29.31			32.00		31.48	
Fe ₂ O ₃ ¹			66.59			12.76	58.95			63.64		66.12	
Total			101.1			98.85	97.17			98.10		99.88	
Mol. % ulvsöspinel			-1.93			81.19	1.05			4.48		1.21	
-log f _{O₂}		<25			11.2	<25				23		<25	
T°C		<500			1040	<500				525		<500	

¹Calculated after the method of Carmichael (1967)

mineral, are not the same for all rocks. This study establishes that the composition of spinel, in addition to being a function of pressure, temperature and magma composition (Brown, 1968) is also markedly dependent on the identity of the enclosing or adjacent mineral.

Henderson and Suddaby (1971) found a systematic compositional variation in spinels upwards through a 1.5 mm thick oxide seam in Rhum. Cr, Fe, Ti and Mn contents of the spinels increased at the expense of Mg and Al. They suggested that this was due to in situ reaction of cumulus chromite crystals with olivine and plagioclase crystals and with interstitial liquid in the crystal-liquid mush. Henderson (1975) has identified two reaction trends of cumulus chromite, one involving Al enrichment at the expense of Cr, and the other involving Fe³⁺ enrichment at the expense of Cr and Al. Both of these trends are also found in harrisite. My results indicate that a third reaction trend exists, involving Cr and Al enrichment at the expense of Fe³⁺ (samples 182 and 89, fig. 31). The reaction trend of Fe³⁺ enrichment for Cr and Al was also found to occur during cooling of Hawaiian basalts (Evans and Wright, 1972). Enrichment of spinel in Cr and Al at the expense of Fe³⁺ therefore suggests a rise in temperature during reaction, as does the increase in Mg at the expense of Fe²⁺ reported by Henderson and Suddaby (1971). These reaction trends to spinels of apparently higher temperature varieties than the cumulus spinel are anomalous and, like the compositional control exerted by the mineral enclosing a spinel, have yet to be explained.

(2) Ilmenite

Two features of the ilmenite analyses in Table 10 are noteworthy. One is the wide variation in the amount of Mg substitution for Fe and the other is the very large content of Mg in some grains (cf. Donaldson, 1975). The analyses in Table 5 of Deer et al. (1962b) indicate that ilmenite in igneous rocks generally contains less than 3 wt. percent MgO. With MgO contents ranging from 0.1 - 8 wt. percent, some ilmenites in harrisite contain substantial giekelite component.

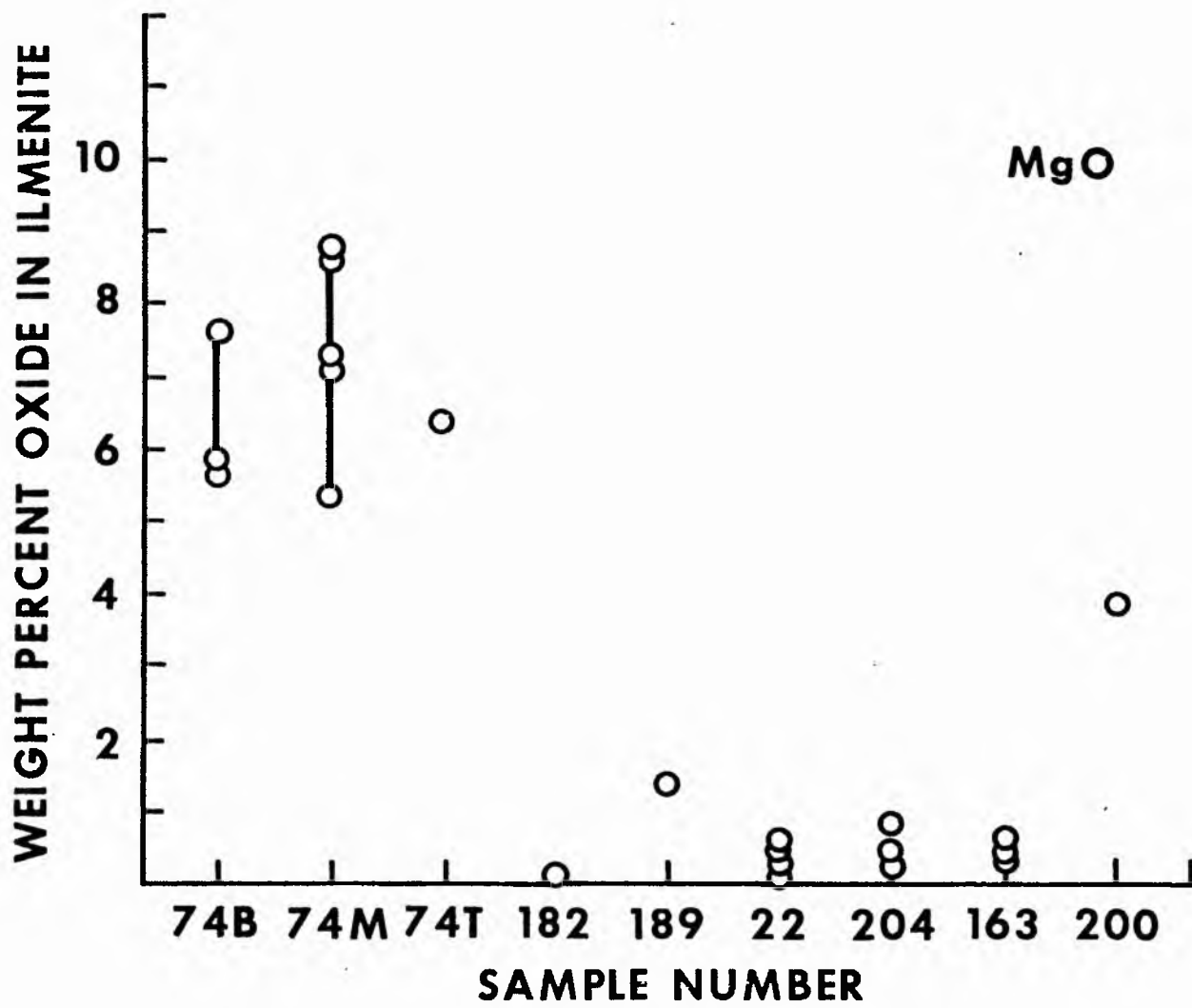
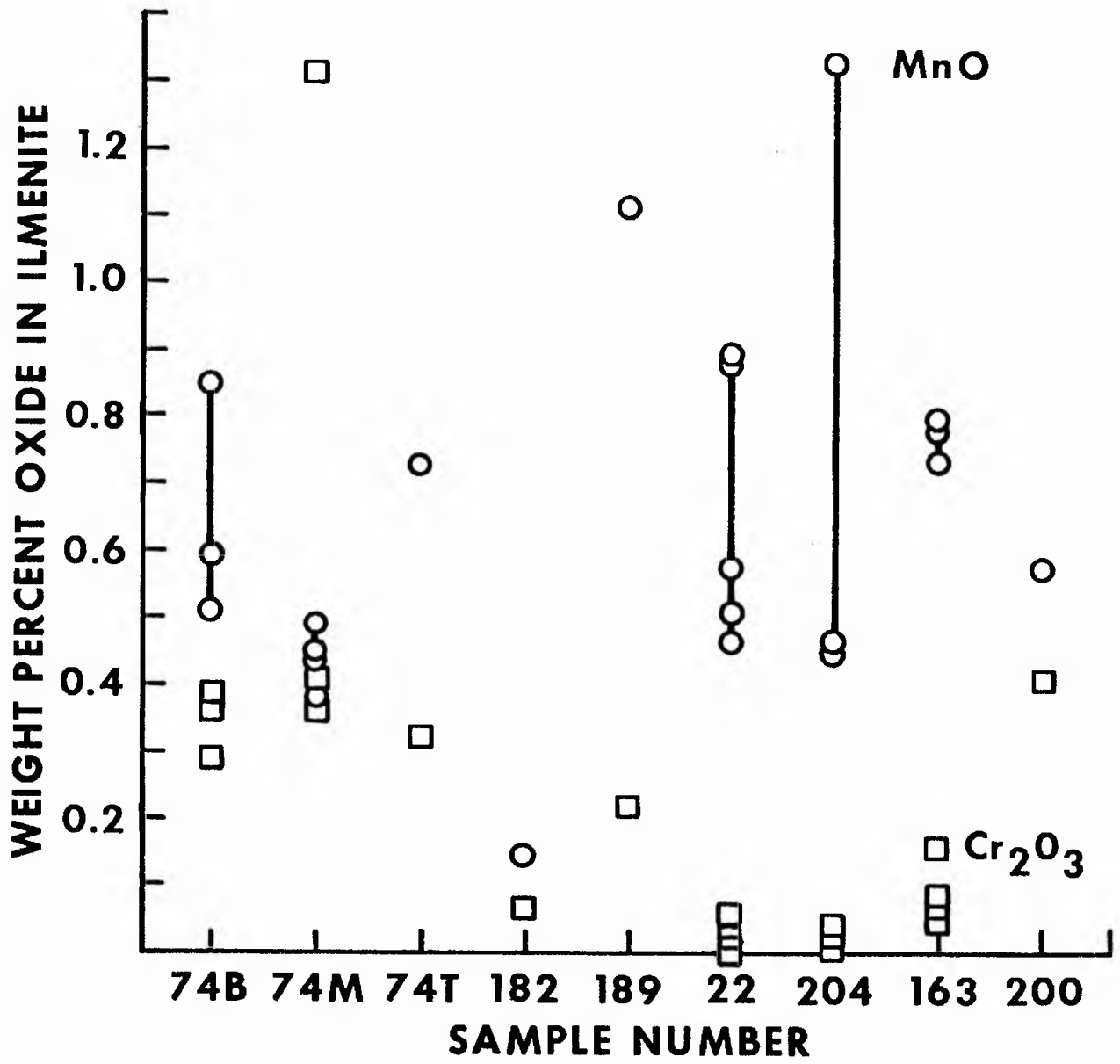


Fig. 32 Summary diagrams of the ranges in minor element contents of ilmenite in some Rhum rocks.



Details of the minor element chemistry of the ilmenites in each rock are shown in fig. 32. The most magnesian ilmenites are in the Ard Mheall harrisite (most magnesian harrisite) and the least magnesian ilmenites in the Harris Bay eucritic harrisite and gabbroic pegmatite (highest Fe/Mg+Fe ratios of the samples investigated). This change is accompanied by a decrease in Cr content in the ilmenite. Mn content shows no consistent trend between rocks; in the same rock, the most magnesian ilmenite generally has lowest Mn. All these features suggest that the composition of the melt from which the ilmenite crystallized, or the composition of the rock (if the ilmenite is the result of a solid state reaction) controls the ilmenite composition.

Substantial giekelite component in ilmenite is a feature of very high pressure crystallization [e.g., in kimberlites (Mitchell, 1973)], but not of the low pressure crystallization environment of Rhum. Since pure giekelite melts at a higher temperature than ilmenite, higher crystallization temperature should promote solid solution of Mg in ilmenite. Speidel (1970) and Helz (1973) have shown that both high Mg/Fe ratio of the parent melt of ilmenite and high fO_2 favour Mg substitution for Fe in ilmenite. The higher MgO content of the Ard Mheall ilmenites compared to those in Harris Bay may, therefore, be attributed to any or all of the effects of higher Mg/Fe (or Mg/Fe²⁺) ratio of the parent melt or rock, higher crystallization temperature and higher fO_2 .

Only one magnetite grain was found to have sufficient Ti (Table 10) for meaningful use with ilmenite as a geothermometer and fO_2 index (Buddington and Lindsley, 1964). This is in harrisite sample 182. The assumed equilibration of ilmenite and titanomagnetite took place at 1040°C and 10^{-10} atm oxygen. If it is assumed that in cooling from 1200°C (assumed crystallization temperature) the Fe²⁺/Fe³⁺ ratio of sample 182 was internally buffered by a gas phase of fixed composition, then the liquidus fO_2 was 10^{-8} atm.

Table 11 Representative electron microprobe analyses of accessory phases in harristite

Phase	Sphene	Grossular	Clinzoisite	Scolecite	Thomsonite	Gomardite	Prehnite	Chlorite	Cummingt
Sample	74B	140	74B	74M	74T	182	89A	89A	74E
SiO ₂	30.49	39.10	38.78	44.59	37.48	40.62	44.02	31.58	56.8
TiO ₂	34.70	0.34	0.19	0.16	0.07	0.11	0.14	0.14	0.4
Al ₂ O ₃	5.04	22.81	30.79	26.30	30.55	30.46	24.82	17.26	2.5
Cr ₂ O ₃	0.02	0.02	0.14	0.13	0.11	0.10	0.02	0.01	0.0
FeO	1.59	0.95	6.19	0.67	0.45	0.22	0.89	12.86	8.5
MnO	0.21	0.21	0.18	0.21	0.01	0.13	0.18	0.33	0.2
MgO	1.57	0.03	0.26	0.26	0.38	0.14	0.00	24.74	29.7
CaO	27.01	36.19	24.60	17.26	13.12	2.24	26.94	0.05	0.5
Na ₂ O	0.13	0.12	0.12	0.14	3.23	10.10	0.16	0.11	1.1
K ₂ O	n.d.	n.d.	n.d.	0.00	0.00	0.15	0.25	0.25	0.0
Total	100.76	99.77	101.25	89.72	85.40	84.27	97.42	87.33	100.5
Structural formula									
Number of oxygens	19.5	12	12.5	10	20	20	22	28	23
Si	3.836	2.849	2.945	2.862	5.087	5.487	5.976	6.228	7.5
Al	0.164	0.151	0.055	1.990	4.888	4.848	0.024	1.772	0.5
Al	0.583	1.973	2.699	-	-	-	3.946	2.239	-
Ti	3.283	0.018	0.011	0.008	0.007	0.011	0.014	0.022	0.0
Cr	0.002	0.001	0.008	0.006	0.011	0.010	0.002	0.001	0.0
Fe	0.168	0.058	0.393	0.036	0.051	0.025	0.101	2.121	0.5
Mn	0.023	0.014	0.012	0.011	0.001	0.014	0.020	0.056	0.0
Mg	0.294	0.003	0.029	0.025	0.077	0.028	0.000	7.273	5.5
Ca	3.641	2.882	2.002	1.186	1.909	0.324	3.918	0.009	0.0
Na	0.031	0.016	0.018	0.017	0.850	2.645	0.042	0.044	0.0
K	-	-	-	0.000	0.000	0.025	0.053	0.077	0.0
Mg:Mg+Fe	0.64	0.05	0.07	0.41	0.60	0.53	0	0.77	0.0

Accessory minerals

Compositions of the minerals serpentine, chlorite, sphene, clinozoisite, scolecite, thomsonite, gonnardite-natrolite, apatite, anorthite, albite, grossular and assorted amphiboles are given in Table 11. Neither muscovite nor hydrogrossular were identified (contrast Wadsworth, 1961). All these minerals, with the exception of apatite and sphene, indicate that silicates in the ultrabasic rocks and pegmatites underwent hydration and oxidation reactions with a fluid phase between the solidus temperature, possibly to a temperature as low as 200°C. In harrisites, which contain 3 - 15 vol. percent hydrous minerals, the extent of reaction was very variable.

Pyrite and chalcopyrite are present in all samples (less than 0.5 vol. percent), but no detailed analytical work was undertaken. These minerals are always associated with hydrous minerals and are apparently late in the paragenetic sequence. They are interpreted as hydrothermal in origin.

Conclusions

This investigation of the mineral chemistry of harrisite has compounded the petrologic complexity of the rock type. Some observations of direct petrogenetic significance are:

1. Branching olivines may show slight reverse zoning across the narrowest dimension; very large crystals show significant compositional variations (e.g., sample 74).
2. The common upward change in olivine morphology (p. 32) can be accompanied by an increase in forsterite content. The major element composition of other phases generally remain uniform through a layer.
3. Ca content in harrisitic olivine is apparently incompatible with rapid crystal growth rate.
4. Augite compositions tend to a metastable crystallization trend, if they crystallized from a basaltic magma. The compositions are compatible with those of pyroxenes crystallized from high-lime liquids.
5. The limited range in olivine and pyroxene compositions and plagioclase core compositions in most harrisite layers can be attributed

to one of two causes. Either diffusional contact between the supernatant magma and the melt within the olivine-liquid mush (partially consolidated harrisite) was maintained or, if it was not maintained, permeability of melt within the crystal mush was sufficiently rapid to keep the interstitial melt homogeneous. Donaldson (in press) concluded that diffusion contact between supernatant magma and interstitial melt in a crystal-liquid mush is effective only over a few microns. The large, melt-filled pores between elongate olivines in harrisite ensured high porosity of the crystal-liquid mush, and hence high permeability (Krumbein and Pettijohn, 1936), until the pores were substantially filled with pyroxene and plagioclase. While the permeability was high, broad, unzoned crystals grew. As the permeability decreased with progressive crystallization, contact between pores decreased and peripheral normal zoning resulted, crystals in each pore zoning to different rim compositions.

6. Plagioclase Fe content and Fe against An trends have been ascribed, in part, to the value and change in value of p_{H_2O} and f_{O_2} . During plagioclase crystallization in some harrisite layers the nascent rock tended to behave like an open system (Fe increases with increasing albite), in others like a closed system (Fe decreases with increasing albite).

7. Crystals of amphibole and mica indicate that the magma chamber was open with respect to water, and therefore f_{O_2} was maintained at a high value (Osborn, 1959).

8. The relative compositions of the olivine, plagioclase and chrome magnetite in samples from the comb-layered harrisite (sample 74) are all consistent with the conclusion that the temperature in magma at the floor of the chamber increased upwards through a distance of only 1.2 m (Table 2).

Chapter IX CRYSTAL GROWTH THEORY AND THE ORIGIN OF OLIVINE SHAPES

The following review of crystal growth from the melt discusses the topics of crystal growth rate, diffusion in the melt and crystal-melt interface stability only in sufficient detail for understanding the origin of olivine crystal shapes and for interpreting the crystallization experiments discussed in the next chapter. A more detailed account of the theory of crystal growth of silicates is presented in a review by Kirkpatrick (1975).

Nucleation

Initiation of crystal growth of a phase from a melt requires the existence of a nucleus of the phase of sufficient size ('critical nucleus') to stimulate deposition. At any temperature, the melt contains a distribution of sizes of molecular clusters (Jackson *et al.*, 1967). At, and above, the equilibrium liquidus temperature, the critical nucleus is infinite in size, thus nucleation rate is zero. With progressive supercooling, the size of the critical nucleus decreases, while the average size of molecular clusters in the melt increases. Ultimately, at a temperature below the liquidus, some clusters exceed the size of the critical nucleus and grow spontaneously. Hence, a crystal-free melt will not spontaneously crystallize until it has attained, or exceeded, a certain degree of supercooling.

The actual nucleation temperature is dependent on the type of nucleation. Spontaneous nucleation directly from the melt is said to be 'homogeneous'. When nucleation is on another phase (including the walls of the melt container), it is referred to as 'heterogeneous'. Nucleation of the former type occurs at greater supercooling than the latter.

In the experiments described in chapter X, melts are homogenized at temperatures above the liquidus and then are cooled at 0.5 to 14,000°C/hr to temperatures below the liquidus. If the crystallization temperature is maintained isothermal following cooling, a period of

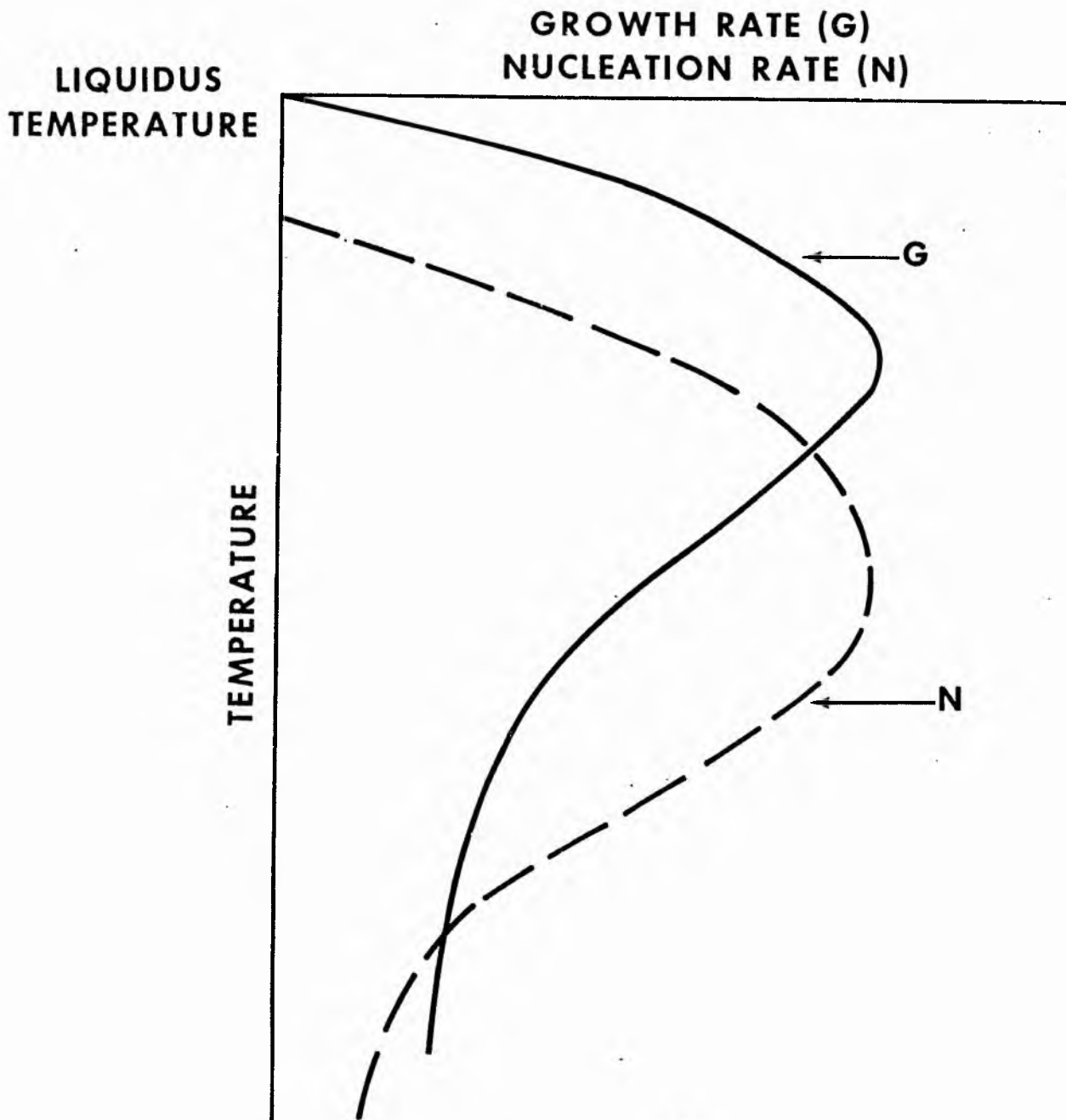


Fig. 33 Forms of the growth rate and nucleation rate versus supercooling curves for a phase crystallizing from a melt of its own composition.

time elapses before nucleation, during which the melt undergoes structural rearrangement and a larger average molecular cluster size forms. Homogeneous nucleation ensues once clusters larger than the critical nucleus for that temperature are attained. The time interval between attainment of the crystallization temperature and onset of nucleation is called the 'incubation period' (Turnbull, 1948). Winkler (1947) reports an incubation period of 97 minutes before growth of nepheline crystals at 30°C supercooling in a silicate melt. In the experiments conducted for this thesis incubation times for olivine nucleation of as much as 9 hours were deduced. As long as the time taken to cool to the crystallization temperature is less than the incubation time, nucleation will not occur during cooling. Hence, the faster the cooling rate, the smaller the chance of homogeneous nucleation during cooling and also the larger the degree of supercooling attained, if nucleation does occur (Donaldson, 1974a).

Crystal growth rate and nucleation rate as functions of supercooling, number of crystals and melt composition- relation to harrisite origin

The equations for crystal growth rate (G) and nucleation rate (N) include two exponential terms, one related to the bulk free energy of crystallization and the other related to the activation energy necessary to move an atom, ion or molecule across the interface between the crystal and the melt. The first term increases with supercooling, whereas the second term decreases with supercooling, being proportional to the atomic mobility. Consequently, both growth rate and nucleation rate have maximum values at specific degrees of supercooling, where one exponential term balances the other. This behavior is shown by all crystals grown from melts of their own composition and it is generally found that the maximum in nucleation rate occurs at a larger supercooling than the maximum in the growth rate (fig. 33; Tammann, 1925).

The curves of N and G in figure 33 are idealized and do not

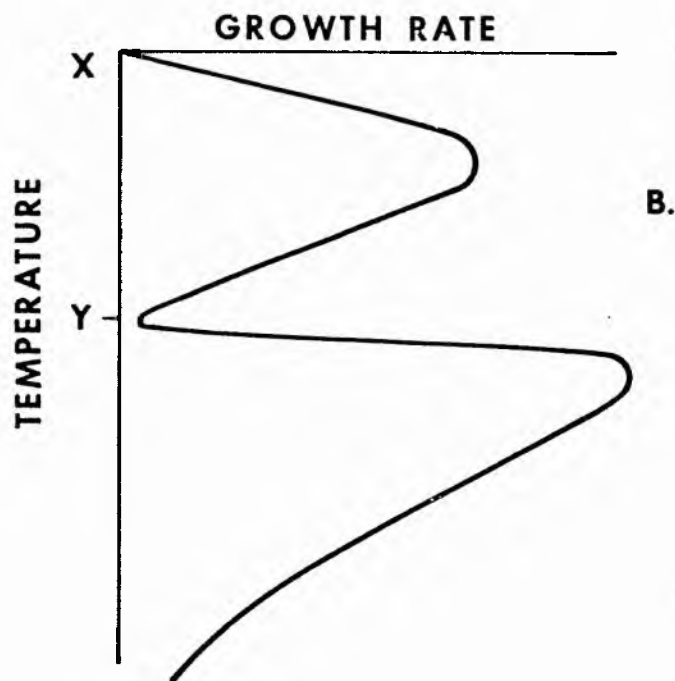
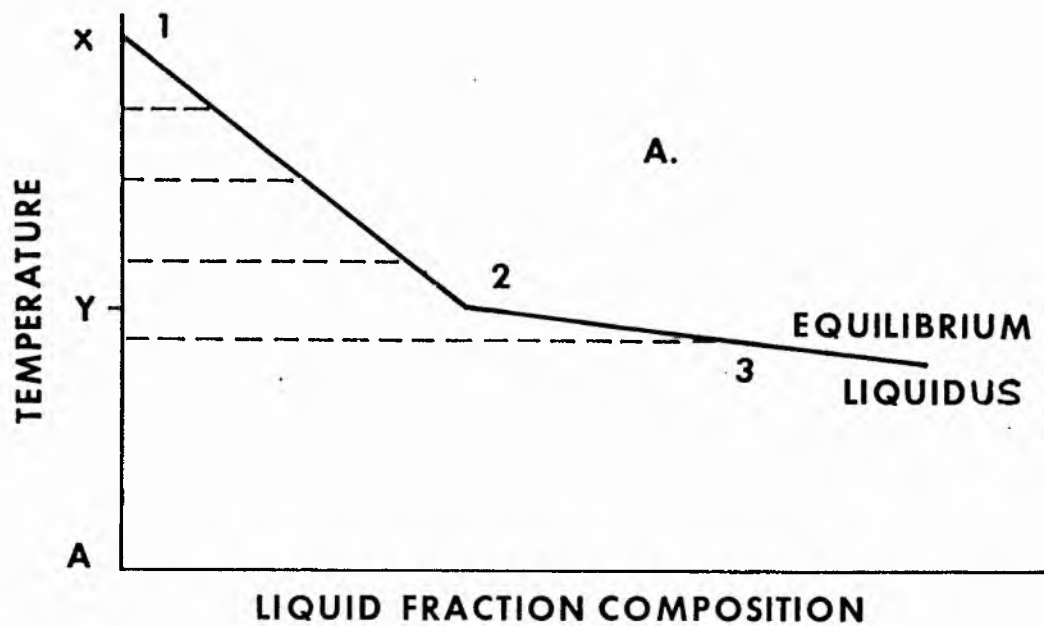


Fig. 34 A. Schematic T-X plot of the liquidus of a multicomponent system. Between 1 and 2, only phase M can crystallize in equilibrium with the melt; between 2 and 3, two phases, M and N can crystallize. Length of hachures is proportional to supersaturation of melt of composition A in phase M at various degrees of supercooling.

B. Growth rate of phase M versus supercooling for melt of composition A.

take into account the reduction in G when a large number of crystals compete for diffusing material. Thus, the more nuclei of a phase, the slower G (Doremus, 1973). The reverse of this behaviour suggests an origin for harrisite (p. 117). If slightly supercooled magma becomes sufficiently cleared of granular and polyhedral olivines that the remaining crystals in suspension have to compete less for solute, those crystals will grow faster. The increase in G could be sufficient to promote skeletal growth. This mechanism might not require change in the degree of supercooling to enhance olivine supersaturation of the magma, only a decrease in abundance of settling crystals (cf. petrographic observations, chapter VII).

In multi-component systems, the form of the nucleation and growth rate curves as functions of supercooling are more complex than those shown in figure 33. If the equilibrium temperature-composition ($T - X$) liquidus of a magma is traced (fig. 34A), it is seen to have breaks in slope when an additional phase crystallizes from the system (Wyllie, 1963). Consider the growth rate of phase M in melt A , as a function of supercooling. Assume that between temperatures X and Y G passes through a maximum. At Y , the supersaturation suddenly increases, because of shallowing of the liquidus. The result is to greatly enhance the force driving molecules across the crystal-melt interface toward crystals and cause a sudden increase in G (fig. 34B) which could promote skeletal growth. Depending on the change in free energy for the phase with increased supersaturation, N may increase or decrease (Lofgren *et al.*, 1974). It is possible that cumulus olivines in Rhum crystallize during cooling between X and Y and that if the melt cools below Y , with supersaturation in plagioclase and consequent decrease in liquidus slope, olivine nucleation diminishes, growth rate increases favouring skeletal growth, and harrisite forms. While any change in the physical-chemical conditions of a supersaturated melt instantly affects the growth rate of crystal phases, there is not an instant change in the nucleation rate. The reason is the re-establishment of an equilibrium

distribution of molecular cluster sizes, which takes a finite time. This could explain the gradational change in olivine crystal abundance and crystal shape at the base of harrisite layers.

Crystallization on the molecular scale- crystal growth rate control of morphology

When a crystal grows, material is transported from the surrounding melt, rearranged to conform to the crystal structure and eventually precipitated onto a surface. The slowest step in this sequence determines the crystal growth rate, which is dependent on five factors, discussed below.

- i) At high supersaturation (supercooling), diffusion is probably the dominant process controlling crystal growth rate (Gray, 1971). Donaldson (in press) showed that convection and turbulent movement of melt are ineffective transporting mechanisms in moving components to the crystal-melt interface of growing olivines. I found that diffusion must occur across a layer of melt at least 1 -20 microns wide. Mg, Fe, Cr and Mn diffuse preferentially toward olivine and all other ions diffuse away.
- ii) At low supersaturation, growth rate may be limited by the rate of nucleation of new growth sites on a crystal (steps, edges or dislocations). This nucleation rate depends principally on the structure of the crystal and its entropy of fusion (Jackson, 1958).
- iii) At the interface between a crystal and melt, reaction involving rupture and creation of chemical bonds occurs as the melt structure is rearranged prior to precipitation of material on the crystal. The rate of this reaction may be the growth rate controlling step, usually at slight supersaturation. Olivine has a simple crystal structure consisting of individual SiO_4^{4-} tetrahedra with Mg^{2+} and Fe^{2+} ions octahedrally coordinated to six oxygens. The structure of a silicate melt probably includes single network-forming ions (e.g., SiO_4^{4-} , AlO_4^{5-}) and some polymeric species (Hess, 1970). Hence, the basic structural elements of an olivine already exist in silicate melts and no structural rearrangement is necessary.

iv) Because of the large amount of energy which would be expended in orienting a unit of crystal in a melt to fit into a crystal structure, Chalmers (1964) has argued that silicates grow by addition of ions to the crystal, rather than by addition of small units of crystal. Thus, olivine is likely to grow by addition of Mg^{2+} , Fe^{2+} and SiO_4^{4-} ions rather than by attachment of $n[(Mg\ Fe)_2SiO_4]$ units. Time will be required to orient SiO_4^{4-} ions to fit into the crystal lattice and this will limit the growth rate.

v) The possibility exists of 'poisoning' growth sites on a crystal by addition of unwanted ions (Moore, 1965). Growth rate will then depend on the proportion of sites 'poisoned' and the rate at which the 'poison' is removed. The importance of this property in silicate crystal growth from magmas is unknown.

Any of the above factors can limit olivine growth rate under different growth conditions (supercooling, supersaturation, heat flow). It should be anticipated that there are transitions in growth rate of olivine as a function of melt composition and supercooling, depending on which growth factor is important for the given growth conditions. Also, the factor controlling growth of each particular face of a crystal may differ, causing anisotropic growth rate. If there is no difference in growth rate between faces of a crystal, faces do not develop and granular crystals grow; if the relative difference in growth rate between faces is small, faceted crystals grow, whereas if it is large, skeletons and dendrites grow (Jackson, 1974).

Compared with diffusion coefficients of components in organic melts and metal melts, from whose crystallization most of the above growth rate control factors were deduced, the diffusion coefficients of ions in silicate melts are $10^4 - 10^5$ cm^2/s smaller. Thus, it seems likely that the dominant factor controlling olivine growth rate, at all but the smallest degrees of supercooling, is diffusion rate (cf. Kirkpatrick, 1975).

Thermal and chemical behaviour at the crystal-melt interface- the origin of dendrites and skeletons

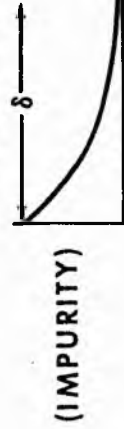
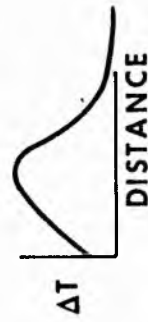
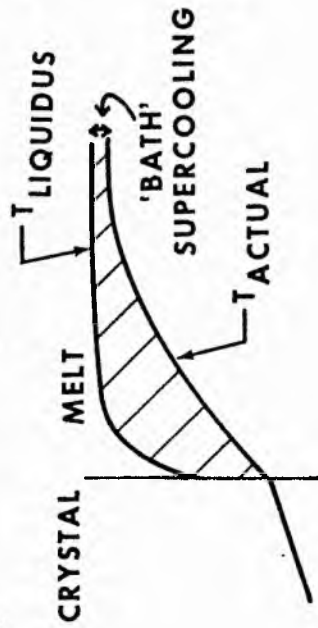
It is generally assumed that in the melt adjacent to a growing crystal face there exists a gradational boundary condition represented by either a thermal gradient, a chemical gradient, or both (Rutter and Chalmers, 1953; Tillier, 1964).

When a crystal grows, latent heat is evolved at the growth site. Two situations are of petrologic interest. If the crystal grows totally enclosed by melt ('unconstrained growth'), latent heat of crystallization is removed into the melt by transport processes [diffusion, convection, conduction; fig. 35(2B)]. The result is that the crystal remains close to its melting temperature, but there is a decreasing temperature gradient in the liquid away from the crystal. If the crystal is anchored to a cool substrate ('constrained growth'), latent heat is conducted away from the interface through the crystal and the resultant thermal gradients in the crystal and melt are as shown in fig. 35(1B).

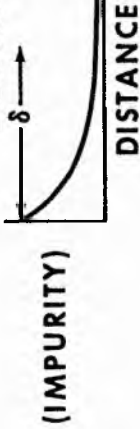
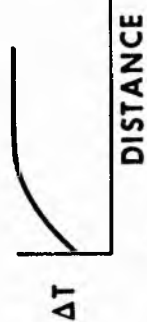
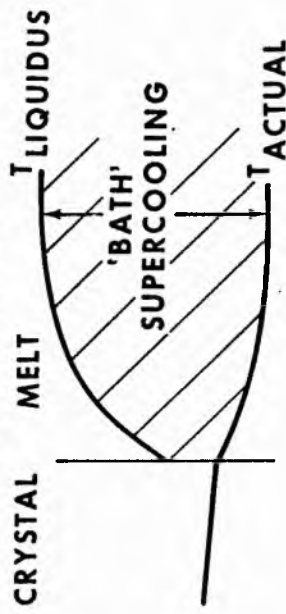
In multicomponent systems, the rate of advance of a crystal face depends upon an interplay of heat transport and the transport of melt components. At the interface, the growing crystal preferentially rejects components not required in its structure. Under steady state growth conditions these rejected components accumulate in the melt adjacent to the crystal, and the melt becomes depleted in components required by the crystal. The effect of these chemical gradients is to locally decrease the liquidus temperature of the melt toward the crystal [fig. 35(1A,2B)]. Under constrained and unconstrained growth conditions, the configuration of liquidus temperature relative to actual temperature is shown in figs. 35(1A) and (2A) respectively. The hachured area between $T_{\text{equilibrium liquidus}}$ and T_{actual} is said to be "constitutionally supercooled" (Knight, 1967). Comparison of curves of supercooling against distance from the interface (fig. 35) shows how the changing $T_{\text{equilibrium liquidus}}$ alters the supercooling relative to growth from a pure melt. Since

MULTICOMPONENT SYSTEM (A)

1. CONSTRAINED GROWTH



2. UNCONSTRAINED GROWTH



PURE SYSTEM (B)

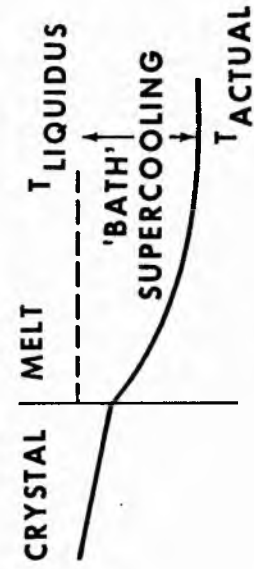
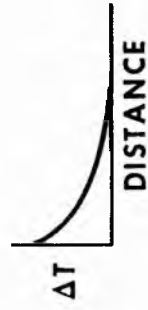
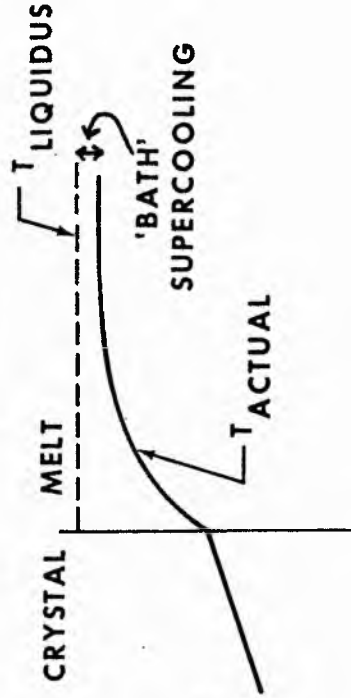


Fig. 35 Form of the liquidus temperature, melt temperature, crystal temperature, supercooling and impurity concentration adjacent to the crystal-melt interface during growth. Left hand column (A) is for crystallization in a multicomponent system, right hand column is for crystallization from a melt whose composition is that of the crystal. Upper set of diagrams (1) is for constrained growth, lower set (2) is for unconstrained growth. Hachures show region of melt which is constitutionally supercooled. " ΔT " is the difference between T_{liquidus} and T_{actual} at any distance in the melt from the crystal-melt interface. "Bath supercooling" is the value of ΔT far from the interface. "(impurity)" is the concentration of a component in the melt which is rejected by the growing crystal. " δ " is the effective thickness of the impurity gradient.

magmas are multicomponent systems and the thermal diffusivity of silicate melts exceeds the chemical diffusivity by a factor of $10^3 - 10^5$ (Bottinga et al., 1966) impurity gradients adjacent to olivines must form during growth, and have been shown to exist by Anderson (1967) and Donaldson (in press). Hence, only curves in figs. 35(1A and 2A) are relevant to petrologic systems. Furthermore, since most magmas nucleate away from the margins of their enveloping container (Harker, 1909), growth of most crystals in magmas is unconstrained. Constrained growth is limited to crystallization of elongate crystals on the walls of some igneous bodies (Lofgren and Donaldson, in press) and on xenoliths in magmas (Moore and Lockwood, 1973), i.e., to comb layers.

The exact form of the curves in fig. 35 depends on the growth rate of the crystal, the diffusion coefficients of all the ions in the melt and, therefore on the temperature of the system. Large growth rate and small diffusion coefficients favour narrower concentration gradients. Donaldson (in press) showed that gradients adjacent to skeletal olivines in a basalt are 1 - 20 microns wide. No measurements of the thickness of the thermal gradient in the melt adjacent to a growing crystal have yet been made.

If we consider a projection resulting from some chance fluctuation on the planar growth surface of a crystal undergoing unconstrained growth, the projection reaches into melt of increased constitutional supercooling and grows at an accelerated rate relative to the planar surface (Keith and Padden, 1963). Hence, constitutional supercooling not only stabilizes projections on originally planar surfaces, but it also promotes their growth. The projection may be regarded as a new crystal nucleus and is subject to the same stability control as normal homogeneous nucleation, i.e., only if it exceeds a critical size for the given supercooling conditions will it grow. Keith and Padden (1963) showed that, for stable growth, a projection should have a diameter approximately equal in size to the thickness of the concentration gradient δ (fig. 35). Hence, as supercooling increases, diffusion coefficients decrease, and both critical nucleus size

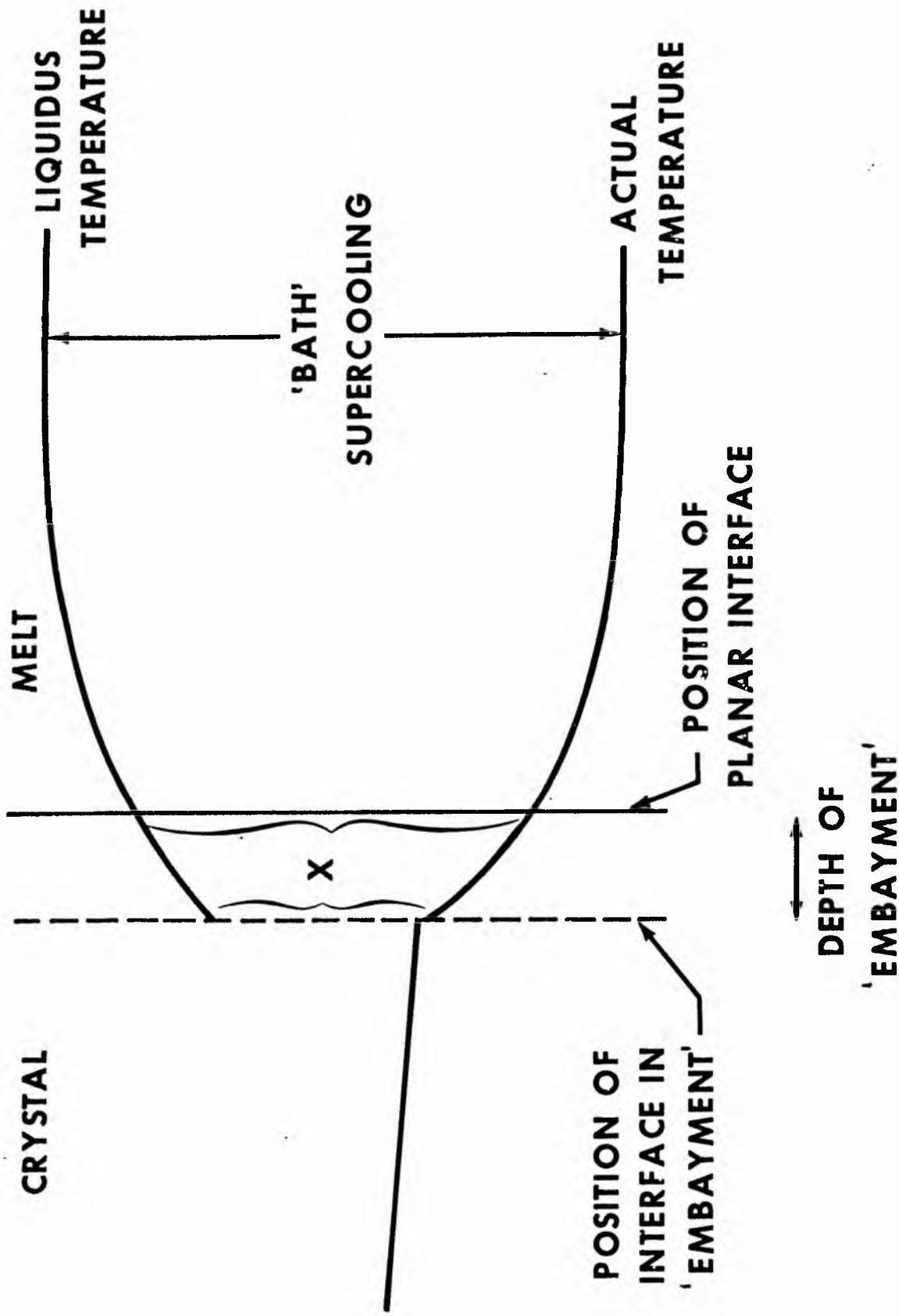


Fig. 36 Form of the liquidus temperature and actual temperature at the interface of a crystal growing in an unconstrained manner, illustrating the smaller degree of constitutional supercooling in an indentation, compared to that part of the crystal-melt interface which is planar. X represents degree of constitutional supercooling.

and δ decrease, the size of these projections should become smaller. This change has been observed in the crystallization of plate olivine during this study. For example, plates grown in composition E (Table 16) at 100°C supercooling are 50 microns thick, those grown at 200°C supercooling are 15 microns thick.

Using this model, Keith and Padden (1963) explained the origin of spherulites under large degrees of supercooling. The model works equally well for growth of olivine dendrites. In olivine dendrites, the projection could be a lump on a face, or a corner or an edge of the crystal. If the projection is of comparable size to the δ in the melt, it will grow rapidly by reaching into more highly supercooled melt. (This explains the origin of swallow-tail olivine, lattice-work olivine, branching olivine and dendritic olivine.)

The reverse of this argument explains the origin of re-entrants ("antiskeletal projections") in olivine and growth of certain types of skeletal olivine. If we consider a planar interface growing by unconstrained growth (fig. 36), and if growth of part of that face slows down, or ceases (e.g., due to poisoning, insufficient dislocations etc.), a cavity develops. The melt in the cavity is enriched in impurities and warmed by latent heat evolved from those parts of the crystal face still growing. Hence, the melt in the cavity is less constitutionally supercooled than that at the planar interface (fig. 36). This reduces growth rate of the crystal in the cavity and stabilizes the cavity. Hence, the lobes and cavities in skeletal olivines are readily explained as due to enhanced growth of a projection on a planar interface (lobe) and diminished growth of a gap on a planar interface (cavity).

The origin of dendritic and skeletal olivine growth forms are, therefore, related, a conclusion which is in accord with the gradational change in morphology between dendrites and skeletons. The model predicts the stability of various crystal morphologies as functions of supercooling. At low supercooling, the planar interface is stable, because the critical radius of a projection is very large. Hence,

polyhedral crystals are favoured at low supercooling. At moderate supercooling, moderate-sized cavities and projections are stable and skeletal growth results. With further supercooling, corners and edges are capable of stable growth as narrow crystallographically oriented fibres (cf. crystallographic branching olivine) or plates or dendrites. These are geometrically favourable sites on a crystal for rapid growth, since they extend into supercooled melt more than a planar interface. Further, they do not require nucleation for growth, as do projections growing from a planar interface. This is clearly demonstrated by swallow-tail olivine (p. 27). At lesser supercooling, corners and edges do not grow as rapidly, because they are too large. At even higher degrees of supercooling, small projections of random orientation (non-crystallographically oriented branches) on a crystal or new nuclei in the interfacial melt are stabilized and spherulitic growth results (Keith and Padden, 1963).

The predicted variation in crystal shape as a function of supercooling also correlates with a progressive increase in the ratio of crystal growth rate to melt diffusion coefficient, as discussed by Knight (1967) and Donaldson (1974a).

Linked parallel-unit branching olivine and the origin of comb-layered harrisite

This morphology is remarkably similar to what Chalmers (1964) calls "cellular dendrites", grown during crystallization of many metal and organic melts. Chalmers (p. 164) states that "The alignment of the dendrites to form a square array....of dendritic growths may arise from the fact that, if the branches join to form webs, they provide a better conducting path for heat flow from the liquid to the crystal than would exist if the crystals were separate". He further indicates that cellular dendritic structures are produced if there is a very shallow positive temperature gradient in the liquid adjacent to the crystal (i.e., the crystals grow in a constrained manner). This shallow gradient means that melt, a large distance from the crystal,

is constitutionally supercooled. Hence, large projections on the crystal are stabilized and these grow readily into the supercooled melt. Since growth is constrained, each of the projections has a positive temperature gradient in the melt around it and can also grow projections. In the case of olivine, growth of projections parallel to a, b or c is favoured over other directions.

Saratovkin (1959) distinguished this type of crystallization as "antiskeletal growth", because growth of projections on crystal faces is promoted in addition to growth of corners and edges, as in true skeletal crystallization. In linked parallel-unit olivine, growth of the edge between $\{021\}$ and $\{0\bar{2}1\}$ is promoted, as are projections on $\{100\}$ and $\{010\}$, parallel to a and b respectively.

From this comparison of linked parallel-unit olivine with other cellular dendrites three petrogenetic conclusions are reached for comb-layered harrisite:

1. Chalmers' suggestion that cellular dendrites crystallize under constrained growth conditions is in accord with field observations on this olivine morphology. There is therefore textural evidence that during growth of linked parallel-unit olivine in harrisite, latent heat flowed into the intrusion floor, not into the magma.
2. Even those linked parallel-unit olivines in the Ard Mheall harrisite that are 1 m across grew from a single nucleus (cf. Bochvar, 1935). Each unit does not grow competitively from suitably oriented olivines (contrast Wadsworth, 1961), but this does not imply that competitive growth of some elongate olivines in harrisite has not occurred.
3. The nucleation density of olivine during crystallization of linked parallel-unit olivine was as small as 1 per 0.45 m [cf. the low nucleation density of poikilo-macrospherulitic plagioclase in Rhum (Donaldson et al., 1973)].
4. The upward increase in magma temperature at the floor of the Rhum chamber, inferred from the compositions of minerals in the comb-layered harrisite (sample 74; p. 66) is in accord with the

condition of Chalmers for a positive thermal gradient during cellular dendrite growth.

5. Lamellar intergrowth of two or more phases, similar in style to linked parallel-unit olivine are common in metal alloys (e.g., Chalmers, 1964). These are usually ascribed to cotectic or eutectic crystallization. In experiments conducted for this thesis (chapter X), both plate and linked parallel-unit olivine have been grown with only interstitial glass or quench amphibole. This observation rules out a cotectic origin for both morphologies.

Summary

Crystal growth theory provides a phenomenological explanation of skeletal and dendritic olivine morphologies and also predicts the relative departures from equilibrium, polyhedral growth conditions. Each shape may be explained by the predominance of either corner and edge growth over facial growth, or more generally, by fibrillation of a planar interface, stabilized by a large degree of constitutional supercooling. The presence of an ever-larger degree of constitutional supercooling away from the interface promotes growth of perturbations on the planar interface during unconstrained growth. Growth of olivine in magmas at all but the slightest degrees of supersaturation is probably diffusion rate dependent. Formation of dendrites and skeletons requires both a large ratio of crystal growth rate to melt diffusion coefficient and a large difference in growth rate between crystal faces.

Whereas the granular and porphyritic olivines in harrisite undoubtedly grew by unconstrained growth, the branching crystals have grown by constrained growth, using the underlying crystal mush as a heat sink. This behaviour indicates a change in latent heat flow conditions, as the harrisite layer develops. Downward heat flow into the base of the intrusion is contrary to the usually-accepted hypothesis for cumulates of upward diffusion of latent heat into the overlying magma (Wager and Brown, 1968), but is in accord with the ideas of Jackson (1961) for crystallization of the ultramafic unit of the Stillwater intrusion.

In this chapter the results are discussed of an experimental investigation of olivine morphology. The systematic controls exerted by the degree of supercooling, the cooling rate and the olivine and water contents of the melt on olivine morphology are demonstrated. Some of the experiments have reproduced the variation of olivine shapes and sizes in harrisite layers and these are used to further elucidate the origin of the rock.

i) Previous work and introduction

Experimental investigation of olivine morphology began with the studies of Fouqué and Michel-Lévy (1881), Vogt (1884), Morozewicz (1899) and Lenarcic (1903). Much of this work involved devitrification of glasses at temperatures close to the transition temperature of each glass. A more extensive investigation was made by Portevin (1928) who melted and cooled an olivine basalt, producing elongate, skeletal olivines in parallel groups. These experiments were repeated by Drever and Johnston (1957) using picritic melts.

Despite the fact that magmatic crystallization is polythermal (and sometimes also polybaric), and despite the indications from early researchers that rock texture modelling was possible in the laboratory, modern experimental petrologists have been reluctant to follow the example, favouring equilibrium studies. Reluctance to undertake textural study may have been due to an inability to grow crystals sufficiently large for petrographic analysis. Recently, Lofgren (1968) has demonstrated that large crystals (up to 3 mm long) can be grown from silicate melts, if the experimental charge is melted above its liquidus temperature before crystallization is initiated. This technique has proved useful in crystallization studies in mineral systems (Fenn, 1973), in simple rock systems, e.g., haplogranodiorites (Lofgren and Donaldson, in press) and in rock melts (Lofgren et al., 1974; Donaldson, 1974b; this thesis). The

techniques, conditions and rock compositions used in the present study of olivine shapes are outlined in Appendix II.

ii) Aims

Experimental crystallization of olivine under known conditions of temperature, cooling rate, p_{H_2O} and p_{O_2} (some experiments) permits investigation of the following petrographic features and petrogenetic applications:

1. The interrelation of each of the morphologies used in the olivine classification (chapter IV) as a function of supercooling, superheating, cooling rate, composition and water content of the melt.
2. The degree of supercooling necessary to crystallize in a magma a particular olivine shape. This information is essential to understanding the origin of non-polyhedral olivine shapes in harrisite.
3. Comparison of the textures of isothermal and cooling rate runs, to estimate the degree of pre-nucleation supercooling achieved in the cooling rate runs.
4. Investigation of whether some morphologies grow only under isothermal or under cooling conditions.
5. An estimate of the form of the olivine nucleation rate and growth rate curves as functions of supercooling is possible. This information is critical in understanding the olivine grain size and morphology distributions in harrisite layers.
6. The experiments provide material for microprobe investigation of olivine composition and zoning, as functions of cooling rate. Of particular importance is the Ca content of olivine which Simkin and Smith (1970) suggested is positively correlated with increasing cooling rate and which is anomalously low in harrisitic olivines (chapter VIII).
7. Initiation of a means of ascribing a semi-quantitative crystallization history (cooling rate, supercooling at time of nucleation of olivine, growth rate to diffusion rate) to a rock, based solely on its petrographic characteristics. The rock compositions investigated could be used to assess the thermal histories and origin

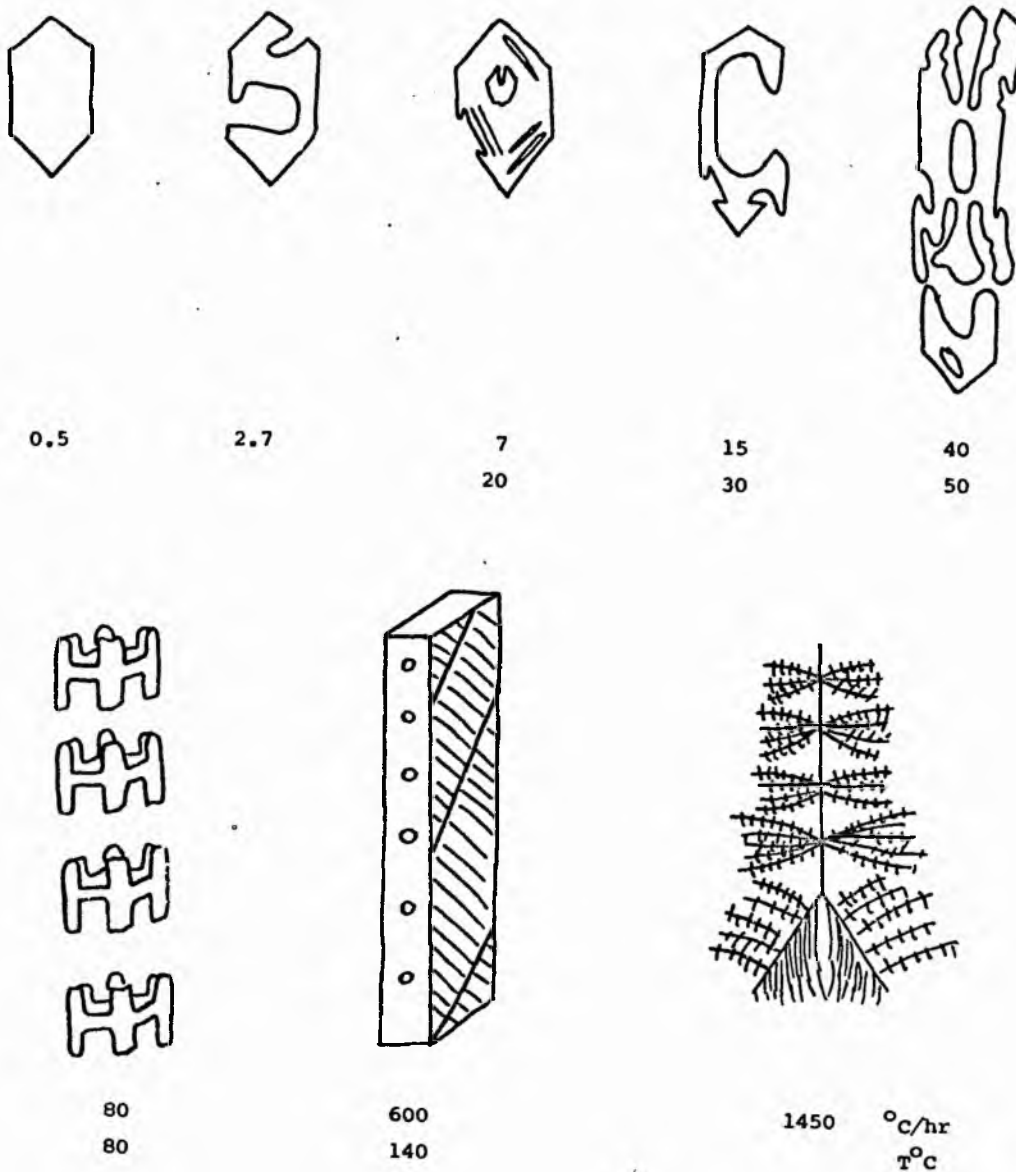


Fig. 37 Summary of the change in shape of olivine crystals in cooling rate and isothermal crystallization experiments on anhydrous rock compositions. Numbers refer to cooling rates and degrees of supercooling at which particular shapes were grown in melt the composition of lunar sample 12009.

of the skeletal and dendritic olivines in spinifex rocks (Donaldson, 1974a), in the margins of picritic sills and dykes (Drever and Johnston, 1958), in submarine basalts (Bryan, 1972b; Donaldson, in press), in lunar mare basalts and in meteorite chondrules.

iii) Anhydrous experiments (see figs. in chapter IV for illustrations)

Isothermal and cooling rate crystallization experiments at 1 atm. pressure were conducted on a variety of anhydrous melt compositions (Table 21; Appendix II). Three of these melts are synthetic lunar basalts; the other is a harrisitic olivine eucrite from Rhum. The range of fO_2 used during crystallization of each melt composition is given in Table 21. Summaries of the olivine shapes grown in each melt at various cooling rates and degrees of supercooling are presented in Tables 12 - 15a,b.

a) Cooling rate crystallization

The change in olivine morphology with increasing cooling rate is systematic and this pattern is common to all four melts investigated (fig. 37). For example, in melt 12009, olivines grown at $0.5^\circ/\text{hr}$ are solid, subequant, polyhedral crystals; those grown at $3^\circ/\text{hr}$ are indented, whereas those grown at $7^\circ/\text{hr}$ are externally subhedral to euhedral, but are internally skeletal (porphyritic, fig.37); at $15^\circ/\text{hr}$ olivines are externally euhedral, but internally hollow (porphyritic); at $40^\circ/\text{hr}$ they are skeletal, typically lacking crystal faces (porphyritic); at $80^\circ/\text{hr}$ crystals are acicular and chain-like in shape, both in sections parallel to (010) and perpendicular to the face; as the cooling rate increases to $650^\circ/\text{hr}$, the chain-like olivines become more bladed parallel to (010) and develop internal dendritic structure (lattice-work olivine); at $1450^\circ/\text{hr}$ olivines are dendritic. Parallel growth of chain-like and lattice-work olivine is favoured by faster cooling rates. For example, parallel growths are well developed in 12009 runs cooled at $650^\circ/\text{hr}$, but are absent in runs cooled between 80 and $350^\circ/\text{hr}$, where the olivines are in random orientation. Lattice-work and dendritic olivines were not grown in

Table 12a. Olivine morphology in synthetic Apollo 12
basalt: Cooling rate experiments. (See Table 22
for melt composition.)

<u>Cooling rate °C/hr.</u>	<u>Olivine morphology</u>
0.5	Large polyhedral
2.7	Large polyhedral
7	Equant porphyritic (indented)
15	Porphyritic and linked parallel-unit olivine (open skeletons)
40	Elongate porphyritic
86	Chain-like
200	Chain-like + lattice-work
380	Chain-like + lattice-work
650	Chain-like + lattice-work
1430	Dendrite

Table 12b. Olivine morphology in synthetic Apollo 12 basalt:
isothermal experiments.

<u>Temperature °C*</u>	<u>Olivine morphology</u>
1205	Porphyritic
1203	Porphyritic
1190	Porphyritic (more elongate)
1179	Porphyritic (cf. 40°/hr)
1150	Chain-like
1110	Chain-like + lattice-work
1058	Lattice-work
1000	Very fine chain-like and lattice-work

*Olivine liquidus approximately 1250°C.

Table 13a. Olivine morphology in synthetic Apollo 15 basalt:
Cooling rate experiments. (See Lofgren et al., 1974, for fuller
descriptions and photographs.) (See Table 22 for melt composition)

<u>Cooling rate °C/hr</u>	<u>Olivine morphology</u>
1260	Dendrite
430	Lattice-work plus dendrite
220	Parallel growth chain-like plus lattice-work
115	Chain-like
60	Porphyritic (tabular crystals)
20	Porphyritic (subequant crystals)
5*	Porphyritic

*No olivine in runs cooled at 4, 2.5 and 1.2°/hr.

Table 13b. Olivine morphology in synthetic Apollo 15 basalt:
isothermal experiments.

<u>Temperature °C*</u>	<u>Olivine morphology</u>
1215	None
1204	Porphyritic (tabular)
1188	None
1160	Porphyritic (subequant)
1145	Chain-like
1130	Chain-like
1110	Lattice-work
1070	Chain-like
1000	Dendrite

*Olivine liquidus approximately 1215°C.

Table 14a. Olivine morphology in synthetic Apollo 11 basalt:
cooling rate experiments. (See Table 22 for melt composition)

<u>Cooling rate °C/hr</u>	<u>Olivine morphology</u>
* 2	Porphyritic and linked parallel-unit branching
* 7	Porphyritic and linked parallel-unit branching
* 18	Elongate porphyritic to chain-like
* 86	Chain-like
* 210	Chain-like
† 18	Porphyritic and linked parallel-unit
† 86	Chain-like

*All runs 0.3 log f_{O_2} units more reducing than the iron-wüstite buffer.

†All runs 1.4 log f_{O_2} units more reducing than the iron-wüstite buffer.

Table 14b. Olivine morphology in synthetic Apollo 11 basalt:
isothermal experiments.

<u>Temperature °C[#]</u>	<u>Olivine morphology</u>
* 1157	Porphyritic
* 1108	Chain-like
* 1058	None
† 1150	Porphyritic
† 1105	Chain-like
† 1100	Chain-like to elongate porphyritic
† 1060	None

*All runs 0.3 log f_{O_2} units more reducing than the iron-wüstite buffer.

†All runs 1.4 log f_{O_2} units more reducing than the iron-wüstite buffer.

[#]Olivine liquidus approximately 1170°C.

Table 15a. Olivine morphology in olivine eucrite: Cooling rate experiments. (See Table 22, analysis 89(E) for composition.)

<u>Cooling rate °C/hr</u>	<u>Olivine morphology</u>
3	Chain-like + lattice-work
14	Chain-like
29	Chain-like + lattice-work
58	Chain-like + lattice-work
2760	Spherulitic aggregates of dendrites

Table 15b. Olivine morphology in olivine eucrite: Isothermal experiments.

<u>Temperature °C*</u>	<u>Olivine morphology</u>
1350	Porphyritic
1320	Branching to porphyritic (linked parallel-unit)
1303	Branching to porphyritic (linked parallel-unit)
1272	Branching (linked parallel-unit)
1250	Lattice-work
1200	Parallel lattice-work to plate
1100	Dendrite

*Olivine liquidus approximately 1360°C.

the Apollo 11 basalt. They may grow if the melt is cooled faster than $210^{\circ}/\text{hr}$ (Table 14a).

Comparable cooling rates are required to grow dendrites, lattice-work olivines and chain-like olivines in the Apollo 15 and 12 melts. These morphologies grow at considerably slower cooling rates in the olivine eucrite melt. In the Apollo 11 melt, chain-like olivines grow at cooling rates intermediate between those at which the morphology grows in the olivine eucrite melt and in the Apollo 15 and 12 melts.

b) Isothermal crystallization

A similar pattern of variation in olivine shapes is found in isothermal crystallization experiments (fig. 37). For example, in melt 12009, crystals grown within 60° of the liquidus temperature are porphyritic or linked parallel-unit in shape- the greater the supercooling, the more pronounced the elongation of the olivine; crystals grown between 60° and 230° supercooling are acicular and chain-like in shape; those grown between 100° and 230° supercooling are bladed in form and have lattice-work shapes, as viewed parallel to (010); at greater supercooling, olivine fails to nucleate during 24 hour runs. In all the melt compositions, polyhedral crystals never grow in isothermal runs which were melted above the liquidus temperature. They do grow in runs in which a glass is raised to a temperature within 50° of the liquidus, but is not melted above the liquidus prior to crystallization at the growth isotherm. In these runs the nucleation density of olivine is much greater than in the runs first melted above the liquidus, Thus, as noted by Klein and Uhlmann (1974), the thermal history of the charge affects nucleation rate and the shapes of crystals grown under isothermal conditions. The Apollo 11 composition never crystallized lattice-work olivines. Dendrites crystallize only from the olivine eucrite and Apollo 15 basalt melts and always at larger degrees of supercooling than lattice-work olivines.

c) Linked parallel-unit olivine

Branching olivines of linked parallel-unit type grow in some isothermal and cooling rate runs (e.g., Table 12a), and frequently are associated with porphyritic olivines. The branching crystals are consistently located at the margin of each charge, whereas porphyritic olivines always crystallize within the bulk of the melt. These observations indicate that the interface between the melt and the gas atmosphere is a site of preferred nucleation of olivine for certain melt compositions (notably 12009) and that olivines which nucleate at the margin of the charge grow as linked parallel-unit crystals at the same cooling rates and degrees of supercooling at which porphyritic crystals grow. This preferred, marginal location of linked parallel-unit olivines, where the gas flowing round a charge can conduct latent heat away from the crystal (i.e., act as a heat sink) is consistent with the suggestion that linked parallel-unit olivines grow in a constrained manner (p. 76).

d) Effect of melt olivine content

With increased olivine content in a melt the minimum cooling rate at which chain-like and lattice-work olivines grow decreases. For example, lattice-work crystals grow at $3^{\circ}/\text{hr}$ in the olivine eucrite melt (40 percent normative olivine content), but at $300^{\circ}/\text{hr}$ in the Apollo 12 olivine basalt (9 percent normative olivine). This observation is critical to interpretation of the shapes of olivine crystals in the Archaean spinifex lavas (Nesbitt, 1971). Growth of skeletal and dendritic olivine from these olivine-rich lavas (up to 40 percent normative olivine) is not an index of unusually rapid cooling rate (quenching), as suggested by Brooks and Hart (1974). The experiments support the conclusion of Donaldson (1974a) that these ultramafic flows cooled no faster than basaltic lavas of the same thickness. For example, porphyritic olivines in spinifex rocks probably crystallized during cooling at less than $3^{\circ}/\text{hr}$. The rapid growth rate of olivine recorded in the crystal shapes in spinifex rocks is not the result of rapid cooling, but rather of large olivine content in the melt.

a.



b.



Fig. 38 a. Three shapes of olivine crystals in lunar olivine vitrophyre 12009. (See text for description.) Plane polarized light. Field of view 2.5 mm.

b. Olivine crystal grown during cooling of a melt of 12009 composition at $7^{\circ}/\text{hr}$. Plane polarized light. Field of view 1.2 mm.

In contrast, the olivine content does not significantly affect the degree of supercooling at which olivine morphologies grow in different melts (Tables 12b, 13b, 14b, 15b).

e) Petrogenetic application of the experiments

Because variation in olivine shapes as a function of both cooling rate and degree of supercooling is systematic, comparison of the crystals grown in the laboratory with those in rocks permits deduction of the cooling history of a natural rock, during the period that olivine was crystallizing from the magma. As an example of this application, the crystallization of olivine in lunar basalt 12009 is discussed. The same principles are later applied to the more complex case of harrisite crystallization.

Sample 12009 contains three shapes of olivine crystals (fig. 38a):

1. Glomerocrysts of subhedral crystals, some with chain-like overgrowths on edges and corners.
2. Large, single, subequant, porphyritic crystals with essentially euhedral outline, but internal skeletal structure resulting from incomplete crystallization of faces of the form $\{021\}$.
3. Crystals of elongate porphyritic, chain-like and occasionally lattice-work shapes.

Olivine crystals of comparable size and shape as the second variety listed above grow when melt 12009 is cooled at $7^{\circ}/\text{hr}$ (fig. 38b). Chain-like and lattice-work olivines grow at cooling rates of $80^{\circ}/\text{hr}$, or more (Table 12a). Subhedral crystals grow when the melt is cooled at $0.5^{\circ}/\text{hr}$, or less. These cooling rates are considered to be the approximate values at which each crystal shape grew in a magma of 12009 composition. From this comparison, the following crystallization and emplacement history is suggested for sample 12009. Polyhedral olivines grew as melt of 12009 composition rose in the lunar crust and cooled from its liquidus temperature at less than $0.5^{\circ}/\text{hr}$. Turbulence in a narrow conduit caused synneutic accretion of these crystals into glomerocrysts (Vance, 1969). Following eruption, the magma cooled at a continuously increasing rate. Initially the rate was less than $10^{\circ}/\text{hr}$ and large skeletal olivines (type 2 crystals) crystallized.

As the rate increased to greater than $100^{\circ}/\text{hr}$, the skeletal crystals became more elongate and were replaced by chain-like and lattice-work shapes.

All the experiments indicate that rapid cooling of mafic melts promotes crystallization of olivine at the expense of pyroxenes. In very rapidly cooled runs, the amount of modal olivine in a charge may exceed the normative olivine content by as much as 15 vol. percent. With progressively slower cooling, the excess of modal olivine relative to normative olivine diminishes. One side of sample 12009 lacks chain-like and lattice-work olivine, the place of olivine being taken by groundmass pyroxene. The experiments indicate that this variation is attributable to a slower rate of cooling in the area containing groundmass pyroxene.

Sample 12009 is among the most rapidly cooled Apollo 12 olivine basalts. Others, of which sample 12009 is a likely parental magma composition (Green et al., 1971), lack groundmass olivine (except 12008) and probably cooled at rates less than $80^{\circ}/\text{hr}$.

In the Apollo 15 basaltic melt (Table 13) olivine is a stable phase at the liquidus temperature (1215°) and to 35° below the liquidus. If the melt cools below 1180° , the olivine reacts with the melt to form pigeonite. In experiments cooled faster than $5^{\circ}/\text{hr}$ olivine persists metastably at temperatures below 1180° . Apparently, all the olivine can react with the melt if the cooling rate is $5^{\circ}/\text{hr}$, or less. Retention of groundmass olivine, in basalts in which reaction is expected, may therefore be used as a sensitive thermal index (cf. Evans and Moore, 1968).

iv) Crystallization of hydrous eucrite and peridotite melts

Run conditions and the variation in olivine shape, grain size, nucleation density and growth rate, as functions of isothermal crystallization temperature and cooling rate, are summarized in Tables 16 and 17. Reference is made in the tables to figures 39, 42 and 45 which depict particular olivine morphologies, and textural features, in the runs.

a) Isothermal crystallization

The general transition in olivine morphology with increasing supercooling in rocks A, E and F is:

porphyritic → granular → branching → randomly oriented chain-like → plate. Some morphologies are stable only within a narrow range of supercooling values ($\leq 50^\circ$). Hence, the absence of granular olivine in experiments on composition E and of branching olivine in compositions A and F is understandable. Randomly oriented chain-like olivine first appears at approximately 1100° in all compositions (fig. 40) and, between 1100° and 950° , chain-like olivine and plate olivine morphologies are stable in compositions A, E and F.

The stability of each morphology varies as a function of the normative olivine content of the original rock. As the olivine content increases (E → F; Table 22), the range of chain-like olivine stability increases at the expense of plate olivine.

Composition B, which is exceedingly olivine-rich, is apparently complex in its morphology variation; the orthodox morphological transition is followed at low values of supercooling, but is partially repeated below 1075° (fig. 40) and perhaps also below 925° . It is possible that this composition cannot be cooled sufficiently fast to prevent olivine nucleation and growth of granular olivine, before the growth isotherm is attained.

b) Cooling rate crystallization

The pattern of olivine morphology variation in cooling rate runs is more confused than that deduced from isothermal runs. Large, single skeletons (porphyritic olivine) grow at the slowest cooling rate investigated (fig. 41). In composition Z these crystals are replaced at progressively greater cooling rates by abundant olivine of porphyritic shapes, then by granular olivine, then by branching olivine, then by a mixture of plate, lattice-work and chain-like olivine, and finally by plate olivine (fig. 41). When cooled at rates less than $7^\circ/\text{hr}$, a similar variation is found in composition F, up to

Table 16. Run conditions, olivine morphology and crystal growth parameters of harrisite isothermal experiments.

Run no.	Rock	Melting		Crystallization			H ₂ O wt. %	Olivine morphology	Average olivine size (mm)	No. of olivines per cm ²	Maximum growth rate cm/s x 10 ⁷	
		P, kb	T, °C	Time hrs.	P, kb	T, °C						Time hrs.
1	A	5.3	1250	4	5.1	1200	20	14.7	None	---	---	---
	B							14.9	Porphyritic	0.45	1.1 x 10 ³	6.2
	E							15.4	None	---	---	---
	F							14.9	None	---	---	---
8	B	5.5	1250	4	5.3	1175	20	15.1	Porphyritic	1.2	8	16
	F							15.1	None	---	---	---
2	A	5.4	1250	4	5.2	1150	20	16.3	None	---	---	---
	B							14.9	Branching (linked parallel unit) (fig. 39h)	4.5	6	62
	E							15.0	Porphyritic	0.25	20	3.5
	F							14.8	Single porphyritic crystal	2.5	8	34
9	A	5.5	1250	4	5.2	1125	20	15.2	Upward gradation from abundant small granular olivine to randomly oriented porphyritic	0.09 at base 0.6 at top	6.1 x 10 ³ 160	1.2 8.3
	E							14.9	Branching (linked parallel unit)	0.75	180	10
	F							15.0	Upward gradation from fine-grained granular to coarse-grained granular and porphyritic	0.16	3.1 x 10 ³	2.2
3	A	5.5	1250	4	5.1	1100	21	15.0	Randomly oriented chain-like	1.4	120	18
	B							15.6	Randomly oriented chain-like	0.4	680	5.3
	E							14.8	Elongate chain-like and lattice-work	2.8	47	37
	F							13.9	Randomly oriented chain-like	0.9	1.10 ³	11
4	A	5.6	1250	4	5.2	1050	21	15.4	Randomly oriented chain-like (fig. 39g)	1.1	290	14
	B							16.0	Granular	0.1	10.8 x 10 ³	1.3
	E							13.9	Plate	3.4	19	44
	F							15.0	Upward change from abundant small granular to randomly oriented chain-like	1.6	600	21
5	A	5.5	1250	4	5.1	1000	20	14.4	Plate	2.5	33	34
	B							14.7	Randomly oriented chain-like	0.25	2.8 x 10 ³	3.5
	E							14.9	Plate	3.5	11	48
	F							14.9	Chain-like and bladed lattice-work	2.5	139	34
6	A	5.5	1250	4	5.1	950	21	14.9	Plate (narrower than 1000°)	3.2	30	42
	B							15.3	Elongate chain-like	2.5	203	33
	E							15.0	Plate	3.8	10	50
	F							14.9	Plate	2.8	64	37
7	A	5.4	1250	4	5.0	900	21	14.9	None	---	---	---
	B							15.3	Abundant subequant anhedral	0.08	10.4 x 10 ³	1.1
	E							15.2	None	---	---	---
	F							14.7	None	---	---	---
10	A	5.5	1250	4	5.1	1100	21	5.0	Upward gradation from abundant granular to randomly oriented chain-like	0.10 at base 0.7 at top	5.8 x 10 ³ 200	1.3 9.3
	B							5.1	Abundant granular	0.4	700	5.3
	E							4.9	Lattice-work plus chain-like	4.0	30	52
	F							5.0	Granular plus randomly oriented chain-like	0.10 at base 0.4 at top	6 x 10 ³ 400	1.3 5.3
11	A	5.6	1250	4	5.2	1050	21	5.1	Upward gradation from abundant porphyritic to chain-like and lattice-work	0.08 at base 2.0 at top	6 x 10 ³ 85	1.1 26
	B							4.9	Abundant granular	0.5	650	8.0
	E							5.0	Plate	9.0	4	119
	F							5.0	Upward gradation from abundant granular to chain-like	0.08 at base 2.0 at top	5.7 x 10 ³ 60	1.1 26

Table 17. Run conditions, olivine morphology and crystal growth parameters of harrisite cooling rate crystallization experiments.

Run no.	Rock	Melting		Crystallization		H ₂ O wt. %	Cooling rate °C/hr	Olivine morphology	Average olivine size (mm)	No. of olivines per cm ²	Minimum growth rate cm/s x 10 ⁷		
		P, kb	T, °C	Time hrs.	Final T, °C							Time hrs.	
7	A	5.5	1250	4	5.0	960	140	15.1	2.0	Single porphyritic (f.g. 39a)	4.0	1	8.0
	B							14.7		Euhedral skeletons	1.0	2 x 10 ²	2.0
	E							14.7		Single porphyritic	3.6	8	7.1
	F							14.8		Single porphyritic	2.4	5	4.8
4	A	5.6	1250	4	3.5	980	72	15.3	3.7	Elongate columnar	2.0 x 0.25	5	7.7
	B							14.7		Abundant granular	0.15	4.5 x 10 ³	0.6
	E							14.4		Porphyritic	1.5	98	5.8
	F							15.3		Porphyritic	0.4	1.3 x 10 ³	1.5
3	A	5.4	1250	4	4.4	1000	36	14.8	7.0	Polyhedral	1.0	7	7.7
	B							14.4		Abundant granular	0.10	5 x 10 ³	0.7
	E							15.2		Porphyritic	2.7	90	20
	F							15.2		Polyhedral	0.5	250	3.9
2	A	5.4	1250	4	4.7	995	18	14.9	14.3	Upward gradation from abundant small granular olivine to few, large porphyritic and crystallographic branching olivines (Fig. 4-5)	0.1 - 0.2 at base 1.8 at top	1.5 x 10 ² at base 5 at top	2.3 27
	B							15.5		Abundant small granular crystals, coarsening upward to porphyritic	0.07 at base 0.75 at top	6.3 x 10 ³ at base 1.4 x 10 ³ at top	1.1 11
E								14.8		No olivine recovered	---	---	---
	F							15.2		Similar to B	0.12 at base 0.54 at top	5.8 x 10 ³ at base 1.4 x 10 ³ at top	1.9 8.3
A								45.6		Upward gradation from abundant small granular crystals to fewer, larger porphyritic crystals	0.3 at base 1.0 at top	1.0 x 10 ² at base 10 at top	4.6 15
	B							46.5		Similar to A (15% H ₂ O)	0.1 at base 1.5 at top	1.5 x 10 ⁴ at base 2 x 10 ³ at top	1.5 23
E								46.4		Polyhedral and porphyritic	0.9	110	13
	F							46.0		Branching (linked parallel unit)	2.7	16	416
10	A	5.6	1250	4	5.0	985	17.8	5.1	14.6	Similar to 2A (f.g. 39b)	0.06 at base 1.5 at top	5 x 10 ⁴ at base 5 at top	0.93 23
	B							5.2		Similar to 2B	0.1 at base 1.0 at top	3 x 10 ³ at base 5 x 10 ² at top	1.6 15

Harristite cooling rate experiments (contd.)

Run no.	Rock	Melting		Crystallization		H ₂ O wt. %	Cooling rate °C/hr	Olivine morphology	Average olivine size (mm)	No. of olivines per cm ²	Minimum growth rate cm/s x 10 ⁷
		P, kb	T, °C	Time hrs.	Final T, °C						
10	E			5.1			Branching, crystallographic and linked parallel unit Similar to 2F	4.3	25.6	67	
	F			5.0				0.10 at base 0.5 at top	2.9 x 10 ³ at base 1.3 x 10 ³ at top	1.6 7.8	
1	A	5.4	1250	4	5.0	985	8.9	29	2.0	10	62
	B			15.1				2.4	22	74	
	E			14.6				0.13	4.8 x 10 ³	4.1	
	F			15.3				0.5	2.2 x 10 ³	15	
9	A	5.6	1250	4	5.1	975	9	30	0.1 at base 2.0 at top	6 x 10 ³ at base 10 at top	3.1 61
	B			15.2				0.1 at base 0.75 at top	1.1 x 10 ⁴ at base 2.2 x 10 ³ at top	3.1 23	
	E			15.0				1.9	15	58	
	F			15.0				---	---	---	
	A			5.0				0.1 at base 1.0 at top	9 x 10 ³ at base 15 at top	3.1 30	
	B			5.1				0.1	1 x 10 ⁴	3.1	
	E			5.2				0.08 at base 1.9 at top	5.8 x 10 ³ at base 64 at top	2.5 58	
	F			5.0				0.08 at base 0.25 at top	1.2 x 10 ⁴ at base 2.2 x 10 ³ at top	2.5 7.7	

Harrisite cooling rate experiments (contd.)

Run no.	Rock	Melting		Crystallization		Cooling rate °C/hr	Olivine morphology	Average olivine size (mm)	No. of olivines per cm ²	Minimum olivine growth rate cm/s x 10 ⁷			
		P, kb	T, °C	Time hrs.	Final T, °C						Time hrs.	H ₂ O wt. %	
5	A	5.7	1250	4	5.0	990	4	15.1	60	Skeletal box-work shape (fig. 39f)	3.0	1	208
	B							15.3		Abundant porphyritic olivine	0.1	3.6 x 10 ³	6.9
	E							14.9		Plate, lattice-work and chain-like	3.0	45	208
	F							15.2		Porphyritic	3.0	45	208
6	A	5.7	1250	4	4.9	980	2	15.1	118	Single plate olivine	>6 long	1	833
	B							14.9		Abundant granular	0.1	4 x 10 ³	13
	E							14.9		Plate	4.9	34	680
	F							14.6		Porphyritic	0.4	2.4 x 10 ³	55
13	A	5.6	1250	4	4.9	975	1.8	15.1	128	Upward gradation from abundant small granular olivine to rare, large, porphyritic olivine	0.1 at base 0.4 at top	3 x 10 ³ at base 103 at top	15 61
	B							15.1		Same as A	0.15 at base 0.55 at top	3.5 x 10 ³ at base 5 x 10 ² at top	23 84
	E							15.3		Dendritic	4.9	7	756
	F							14.8		Upward gradation from abundant small granular olivine to large chain-like to crystallographic branching form	3.2	65	493
14	A	5.5	1200	4	4.8	*1150-855	4.4	15.0	66	Upward gradation from abundant small granular olivine to chain-like crystals elongated perpendicular to the layering	0.08 at base 1.4 at top	5 x 10 ³ 3 at top	5.1 8.8
	E							15.3		Chain-like	4	20	252
	F							15.2		Chain-like	2.3	90	145
15	E	5.4	1250	4	5.0	985	8.9	1.2	29	Bladed plate	2.0	20	62
	E							U 2.0		Bladed branching (linked parallel unit).	6.5 x 0.5	7	203
	E							U 3.0		Bladed branching (linked parallel unit)	3.0 x 0.8	10	94
	E							S 4.1		Chain-like and branching (crystallographic) (fig. 39c)	4.5 x 1.5	10	140

* Temperature dropped from 1200 to 1150° in 15 minutes, from 1150° to 855° in 4.4 hr.

U = water undersaturated
S = water saturated



a.



e.



b.



f.



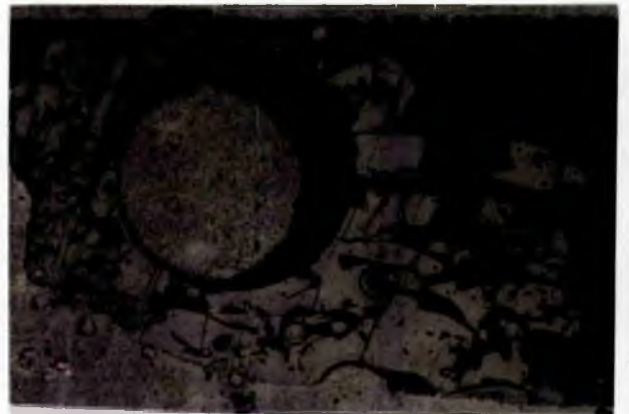
c.



g.



d.



h.

Fig. 39 Olivine shapes in cooling rate and isothermal crystallization experiments on rocks A, B, E and F (Tables 16 and 17). Where complete charge is shown, width is 3 mm; others as specified.

- a. Rock E with 5 percent H_2O cooled at $14^\circ/hr$ - branching olivine of crystallographic and linked parallel-unit types.
- b. Rock A with 5 percent H_2O cooled at $14^\circ/hr$ - granular olivine at base, changing to porphyritic. Field of view 1.3 mm.
- c. Rock E with 4 percent H_2O cooled at $29^\circ/hr$ - chain-like and crystallographic branching olivine.
- d. Rock B with 15 percent H_2O cooled at $29^\circ/hr$ - linked parallel-unit branching olivine. Crystal is 2.4 mm long.
- e. Rock A with 15 percent H_2O cooled at $2^\circ/hr$ - porphyritic olivine. Crystal is 4 mm long.
- f. Rock A with 15 percent H_2O cooled at $60^\circ/hr$ - box-work skeletons.
- g. Rock A crystallized at 1050° - chain-like olivine. Field of view 3 mm.
- h. Rock B crystallized at 1150° - linked parallel-unit branching olivine.

	A	B	E	F
1200	None	Porphyritic	None	None
		Porphyritic		
1150	None	Branching (LPU)	Porphyritic	Porphyritic
	Granular + porphyritic		Branching (LPU)	Granular + porphyritic
1100	Randomly oriented chain-like	Randomly oriented chain-like	Chain-like + lattice-work	Randomly oriented chain-like
1050	Randomly oriented chain-like	Granular	Plate	Randomly oriented chain-like
1000	Plate	Randomly oriented chain-like	Plate	Chain-like + lattice-work
950	Plate	Randomly oriented chain-like	Plate	Plate
900	None	Granular	None	None

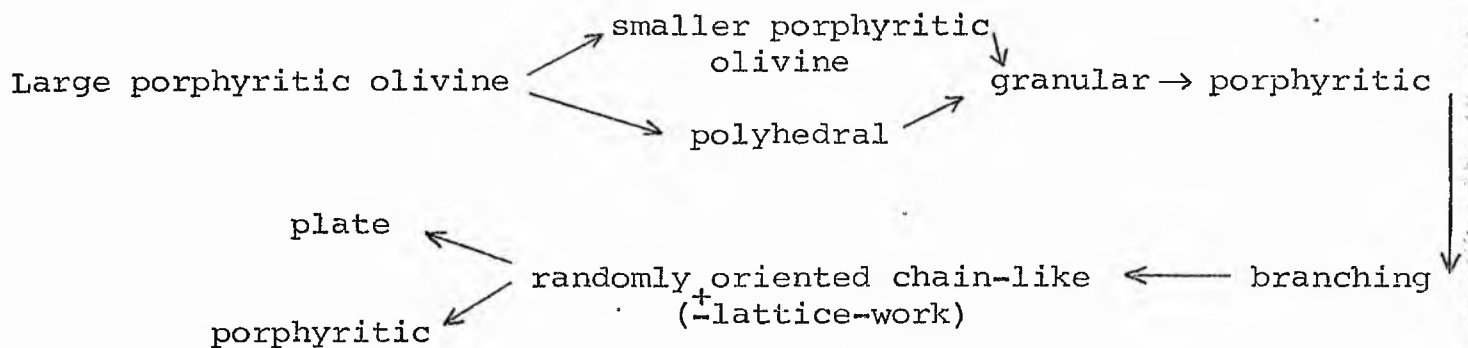
Fig. 40 Summary of olivine shapes in isothermal crystallization experiments on rocks A, B, E and F at $p_{H_2O} = p_{total} = 5 \text{ kb.}$

	A	B	E	F
2	Single porphyritic crystal	Porphyritic	Single porphyritic crystal	Single porphyritic crystal
4	Polyhedral	Granular	Porphyritic	Porphyritic
7	Polyhedral	Granular	Porphyritic	Polyhedral
14	Granular + porphyritic and crystallographic branching	Granular + porphyritic	—	Granular + porphyritic
28		Branching (LPU)	Granular	Randomly oriented chain-like
30	Granular + porphyritic and crystallographic branching	Granular + porphyritic	Branching (LPU)	—
60	Box-work skeletons	Granular + porphyritic	Chain-like + lattice-work + plate	Porphyritic
118	Plate	Granular	Plate	Porphyritic

Fig. 41 Summary of olivine shapes in cooling rate crystallization experiments on rocks A, B, E and F at $p_{H_2O} = p_{total} = 5 \text{ kb.}$

the stage where porphyritic olivine crystallizes. At $7^{\circ}/\text{hr}$, polyhedral crystals grow and are replaced at $14^{\circ}/\text{hr}$ by a combination of granular and porphyritic olivine morphologies. At $28^{\circ}/\text{hr}$ randomly oriented chain-like olivine crystallizes, while at rates greater than $60^{\circ}/\text{hr}$ the morphology reverts to porphyritic in type. At $60^{\circ}/\text{hr}$, a run of sample A contains branching olivine. At $118^{\circ}/\text{hr}$, A contains plate olivine. Composition B is dominated in the experiments by porphyritic and granular olivines, either alone or in combination (Table 17). Only at $28^{\circ}/\text{hr}$ is branching olivine encountered. At the cooling rates investigated, all the rock compositions are dominated by porphyritic and granular olivine morphologies. Additional morphologies apparently grow only at restricted cooling rates.

The results suggest the following morphological variation as a function of cooling rate:



Many of the cooling rate runs display morphological, as well as compositional, differentiation in the run products. In these runs a layer of granular olivine occupies one side of the charge and is covered by porphyritic olivine (fig. 42), itself sometimes covered by branching olivine or chain-like olivine. The change from granular olivine to porphyritic olivine is gradational, involving a grain size increase and crystallization of less round, and more inlaid, olivines. Only occasional isothermal runs display these differentiation features, and usually much less dramatically than do cooling rate runs.



Fig. 42 Experimental charge containing granular olivine overlain by large branching olivine. The a axis of all three branching olivines is within 20° of the vertical. (Rock E with 5 wt. percent H_2O at $p_{total} = 5$ kb and cooled at $30^{\circ}/hr$. Plane polarized light.) Height of charge 3 mm. (Compare fig. 21b of harrisite.)

c) Comparison of isothermal and cooling rate runs

Comparison of figures 40 and 41 shows that the sequence of morphologies, as a function of increasing supercooling, is only in partial accord with the sequence of morphologies grown in cooling rate runs. The single, large porphyritic olivines grown at slow cooling rate did not crystallize in isothermal runs, and neither did polyhedral crystals. Chain-like and lattice-work olivine are apparently more abundant in isothermal crystallization runs than in cooling rate runs. There is, however, a similarity in pattern of morphological variation in both types of experiment which indicates that the faster the cooling rate, the greater the degree of supercooling required to grow the same morphology in isothermal runs. This conclusion supports the argument of Donaldson (1974a) that to grow dendritic or skeletal olivines requires more rapid induction of olivine supersaturation than is necessary to grow polyhedral olivine.

The isothermal experiments indicate that, in a given melt composition, crystal morphologies are only stable within specific temperature intervals. When the same morphology appears in both isothermal and cooling rate experiments, the olivine in the cooling rate run must have grown sufficiently rapidly to exhaust olivine components in the melt during cooling through the stability interval of the morphology. Alternatively, once a particular morphology is established, it continues to grow, even at temperatures below its stability range, unless there is a sudden change in cooling rate. Since more than one morphology is found in some cooling rate runs, the former alternative seems most likely. Hence, it should be possible to estimate an approximate value of the supercooling attained in a cooling rate experiment prior to nucleation of olivine. For this purpose, the data are reorganized in figure 43 to show at which temperatures and cooling rates identical morphologies crystallize. Only for composition E is a complete calibration of morphology in terms of cooling rate and approximate nucleation temperature possible. To grow plate olivine in composition E, the melt has to be supercooled by about 100° prior to olivine nucleation. This condition may also

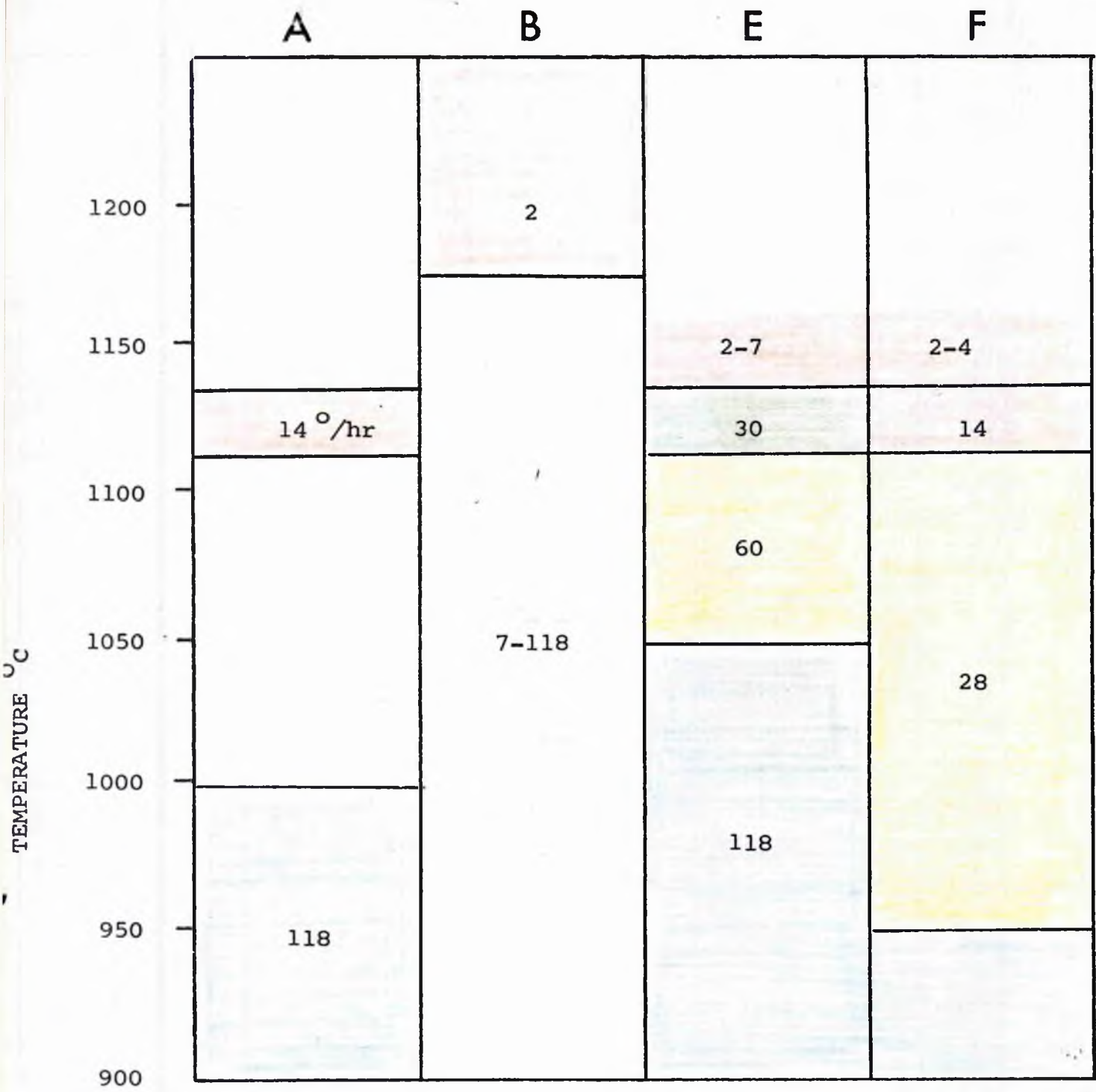


Fig. 43 Comparison of the cooling rates and isothermal crystallization temperatures at which similar olivine shapes crystallize from rocks A, B, E and F run water saturated at 5 kb. Colour scheme same as that in figs. 41 and 42.

be achieved by cooling at a rate $> 60^{\circ}/\text{hr}$. Hence, if cooled at $60^{\circ}/\text{hr}$, composition E may be held in a metastable, supercooled state without olivine nucleation for at least 1.5 hours. Comparison of all the morphologies produced in composition E, as functions of supercooling and cooling rate, suggests a similar length of time for retention of a supercooled state, prior to nucleation. In contrast, compositions A and F apparently remain supercooled for twice as long before nucleation of olivine. This period represents the incubation time of nucleation (p. 68), and apparently the larger the olivine content of the melt, the longer it is.

d) Effect of water on olivine morphology

Most runs were made with 15 wt. percent water. This value was arbitrarily chosen to ensure saturation with water (Appendix II). A few runs were made with 5 wt. percent and 45 wt. percent water, to examine the effect of excess water above the saturation level. From the limited data at these water contents (Table 17) it is tentatively deduced that olivine morphology, nucleation density and growth rate are all insensitive to the amount of excess water in the charge.

Runs with samples of rock E containing 1, 2, 3, 4 and 5 wt. percent water were made, cooling being at $28^{\circ}/\text{hr}$ (Table 17). Despite the fact that only charges with greater than 3 wt. percent added water evolved water at the end of the experiment (i.e., were water saturated), all five charges contained similar olivine morphologies, numbers of crystals and grain sizes (Table 17). Hence, the effect on olivine morphology of water contents below the saturation level is apparently also slight.

e) Olivine growth rate (G) and nucleation density (N)

The number of olivines per cm^2 (Tables 16 and 17) in each run was determined by counting the number of crystals in thin section photographs of the charges and dividing by the area occupied by the crystals. The maximum growth rate (Tables 16 and 17) was estimated

by measuring the longest olivine in a charge and dividing by the duration of the run (time below the liquidus temperature) in seconds.

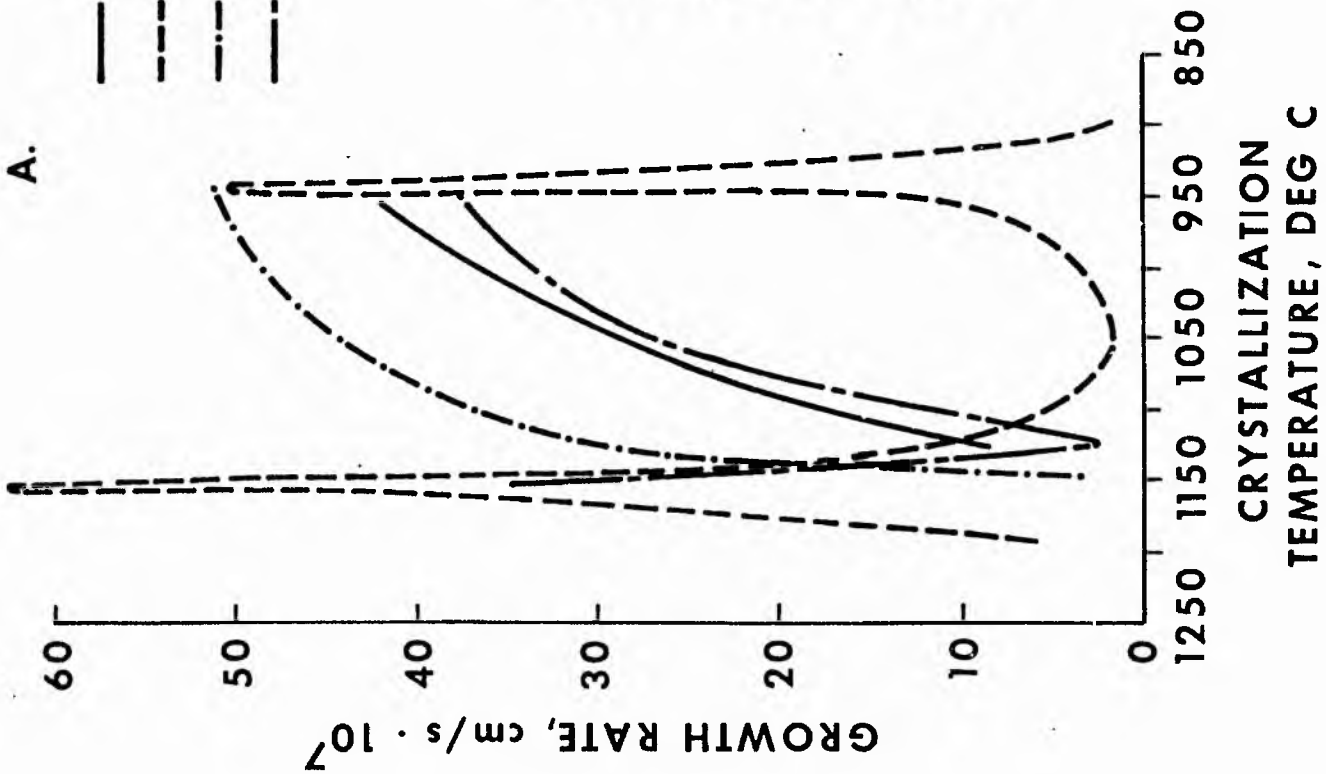
In most discussions of crystal nucleation, the rate of nucleation (number of nuclei/s/cm³) is the parameter used in analysis of nucleation. In experimental petrology nucleation of crystals cannot be observed, so this type of data cannot be obtained. It must be assumed that the "nucleation densities" determined from my experiments are proportional to the true rates of nucleation. In determining N for granular olivine and porphyritic olivine, the effect of gravity differentiation is ignored and in situ nucleation is assumed. If, as seems likely, olivine nucleated throughout the charge, the reported N values for granular and porphyritic olivine are 5 - 10 times too large.

The growth rate is in error because without being able to see when nucleation occurs, the period of incubation and, hence the actual growth time, are unknown. Furthermore, the growth rate may not be linear, and the crystals may stop growing before the run is quenched, resulting in underestimation of the true growth rate.

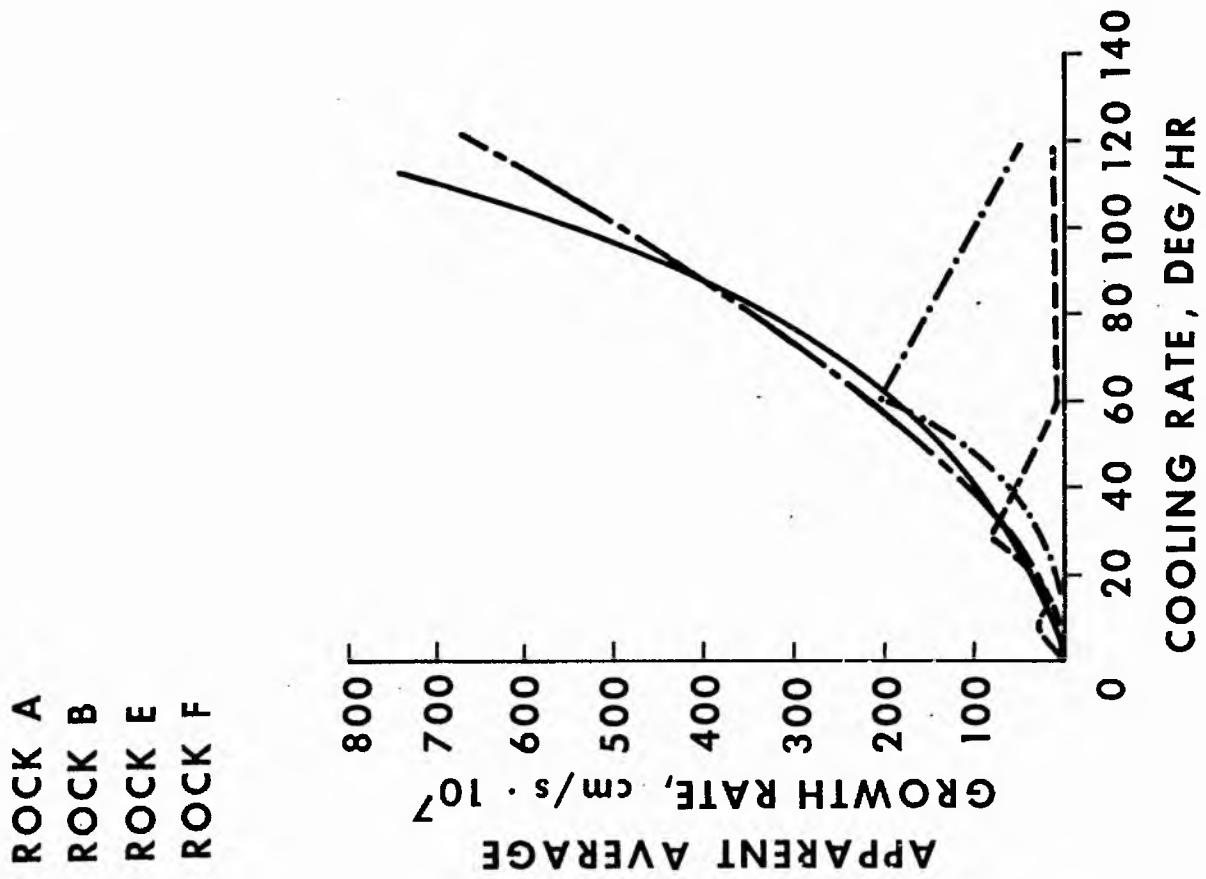
The above errors do not defeat the aim of this section, which is not accurate determination of olivine growth rate and nucleation density, but establishment of the form and relative positions of the maxima of each of these parameters as functions of supercooling. The nucleation density and growth rate curves against cooling rate can be considered of similar form to those against supercooling, since the supercooling attained at nucleation is proportional to the cooling rate.

In graphs of G against cooling rate (fig. 44b) growth rate of olivine in rock A peaks at approximately 110 °/hr, while maxima for E and F were not located. Crystals in rock B have comparatively low and constant growth rate at all cooling rates. In contrast, the nucleation density (fig. 44d) shows a distinct maximum in all the rocks at 20 - 40 °/hr. Curves for N and G in the isothermal experiments are shown in figs. 44a and c. If we ignore rock B, there is a very large difference

A.

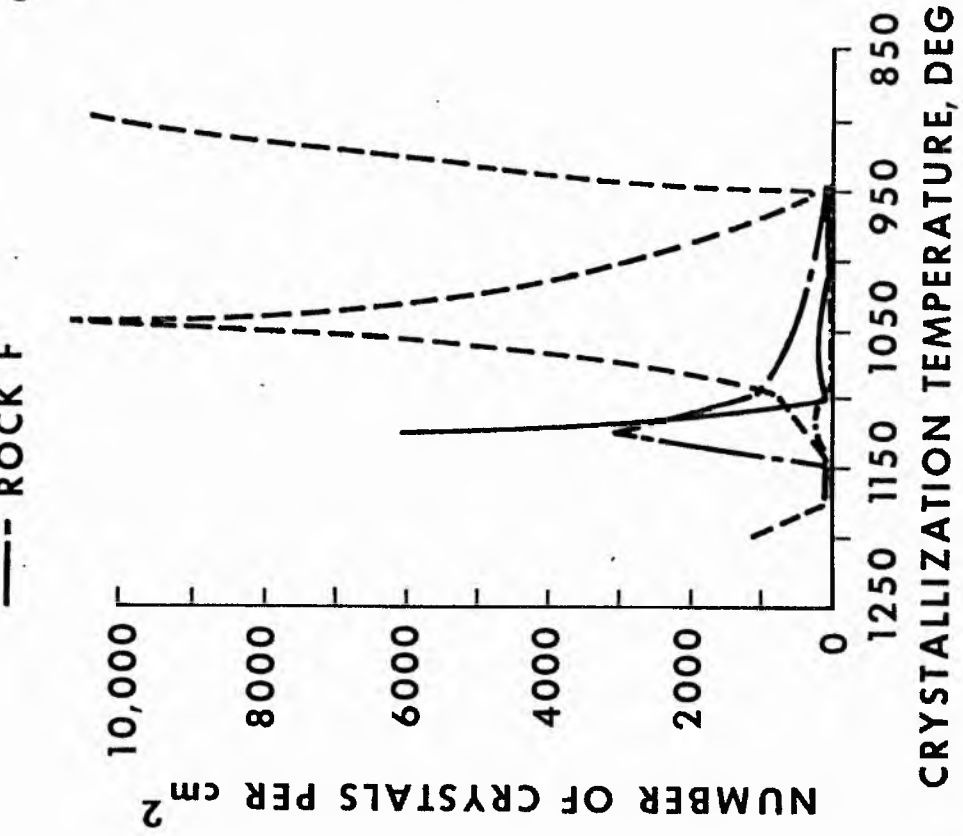


B.



- ROCK A
- - - ROCK B
- · - · - ROCK E
- - - - - ROCK F

C.



D.

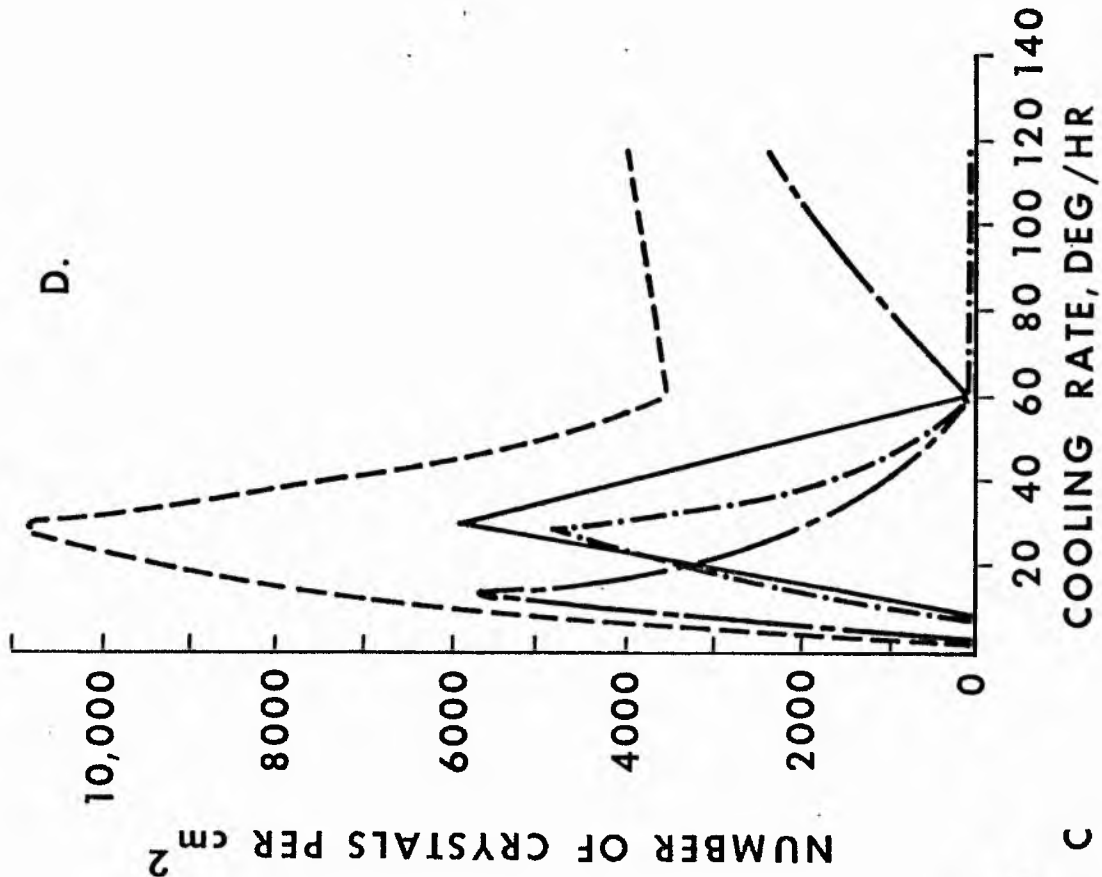


Fig. 44 Maximum growth rate (A and B) and number of crystals (C and D) of olivine as functions of isothermal crystallization temperature (A and C) and cooling rate (B and D) for rocks A, B, E and F run water saturated at 5 kb. Data in Tables 16 and 17.

in temperature between the maximum for N and the maximum for G (which is never attained). The maximum N value typically occurs within 25° of the liquidus temperature.

In summary, both isothermal and cooling rate experiments indicate that the maximum value of N for olivine occurs at low supercooling and rapidly diminishes with increasing supercooling, whereas the growth rate increases steadily with increase in supercooling. This property is apparently unique to olivine, for the maximum value of N occurs at greater supercooling than the maximum value of G in all mineral systems hitherto investigated (e.g., Carmichael et al., 1974). The property has considerable importance for petrogenetic interpretation of the upward change in olivine grain size and shape in harrisite layers, as discussed later.

f) Resemblance of run textures to harrisite

i. Similarity of olivine morphology

Many olivine morphologies in harrisite have been reproduced, suggesting that the natural olivine skeletons grow from a melt and not during a recrystallization event (Donaldson et al., 1973). Porphyritic olivine grows at low supercooling and cooling rate, branching olivine of both linked parallel-unit and crystallographic types grows at similar and greater degrees of supercooling and cooling rate. Randomly oriented olivine crystallizes at still greater supercooling or a faster cooling rate. Clearly, harrisite layers did not all crystallize under unique conditions. Instead, each morphology indicates the supercooling value attained at the time of olivine nucleation and also the rate at which the supercooling was induced. The experiments give an indication of the relative degree of supercooling between different harrisite layers, leading to the possibility of investigation for thermal rhythmicity in the layering.

A feature of many run products was the crystallization of granular olivine similar, except for the inclusions, to that in 'cumulate'

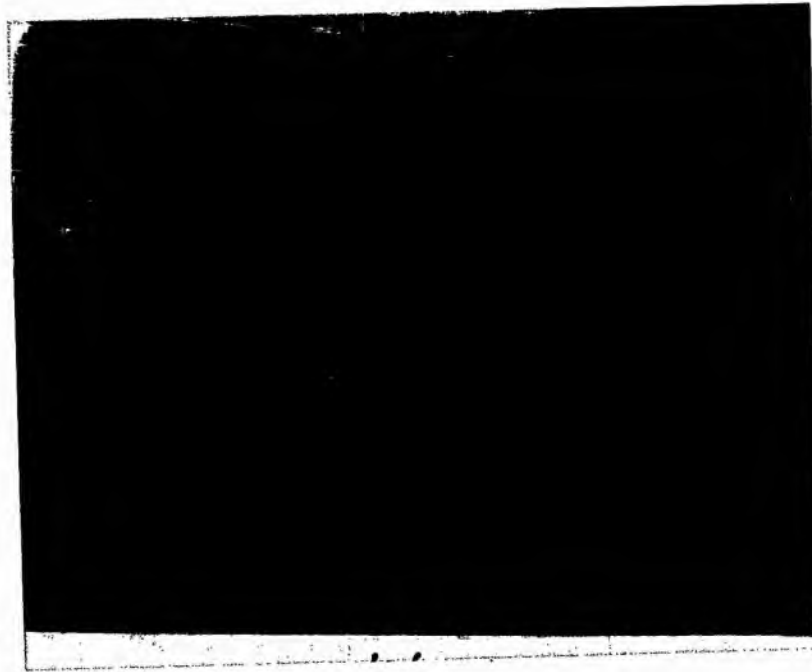


Fig. 45 Differentiation of a cooling rate run with respect to olivine grain size and shape. Note the preferred upward growth of the largest crystals in each charge. Rock A with 15 wt. percent H_2O cooled at $14^\circ/hr.$ Charge is 2 mm wide.

at the base and cumulate overlying many harrisite layers (fig. 41). This feature confirms that the gradation from cumulate to harrisite crystallization is caused by a continuous change in some intensive parameter of the natural system. An origin for harrisite involving emplacement of new magma for each layer can, therefore, be rejected.

ii. Olivine growth direction and distribution of morphology and grain size

Many charges in cooling rate runs are stratified according to olivine morphology and grain size in a manner identical to harrisite layers. For example, the upward succession from fine granular olivine to coarse granular olivine to coarse porphyritic olivine to branching olivine in fig. 42 closely resembles the morphology and relative grain size change observed in harrisite (p. 32).

The preferred upward growth of branching olivine in harrisite has also been reproduced in a few experiments (e.g., fig. 45). Universal Stage examination of these crystals reveals preferential growth with a elongate and close to vertical (cf. harrisite). Elongation is either parallel to a or c; crystals with a elongation are more common than those with c elongation by a factor of 3:1.

Thus, four petrographic features critical in explaining the origin of harrisite have been modelled: olivine morphology, morphology distribution, relative grain size distribution and also preferred upward growth parallel to a.

g) Composition of olivine in hydrous experiments

Microprobe analyses in a few isothermal and cooling rate experiments were obtained for comparison with those in natural harrisite and the Rhum cumulates and to aid interpretation of crystallization of the charges (next section). The following is a summary of the results.

The range of compositions is $\text{Fo}_{96} - 81$ (most olivines are $\text{Fo}_{93} - 91$.) The content of water in the charge has no effect on the composition of olivine, and crystals grown in isothermal runs are essentially unzoned.

In charges differentiated with respect to olivine grain size and shape distribution (e.g., A at $30^{\circ}/\text{hr}$), granular olivines at the

base of the charge are reverse zoned ($\text{Fo}_{90 - 92}$), and those 1 mm above the base are normally zoned ($\text{Fo}_{92 - 86}$). Branching crystals above the granular olivines are normally zoned along their length and across their width ($\text{Fo}_{93 - 82}$). The most magnesian portion of these elongate crystals is usually 1/5 of the length above their lowest point.

Ca content of the olivines ranges from 550 ppm to 1700 ppm. In isothermal experiments, the greater the supercooling during crystallization, the greater the Ca content. Ca content generally increases with Fe content of the olivine, but the reverse-zoned crystals at the base of some charges have higher Ca contents toward the periphery. The cores of elongate crystals typically have 600 - 800 ppm of Ca, and the rims have 1000 - 1700 ppm. Granular olivines contain 500 - 1000 ppm Ca. There is no correlation between Ca content of an olivine and the cooling rate of a run.

Discussion

The olivine compositions are considerably more magnesian than those in the natural rocks. This is to be expected, because the $f\text{O}_2$ of the experiments is probably $10^6 - 10^7$ orders of magnitude larger than that at the liquidus temperature of the rocks in nature. Granular crystals at the base of some charges are reverse zoned, presumably, because at the time of crystallization, H_2 was still being released from the capsules, due to H_2O dissociation, and Fe^{2+} in the melt continued to be oxidized to Fe^{3+} . Since later-crystallizing granular olivines are normally-zoned, either loss of H_2 had ceased or (and this is more likely) the rate of Fe^{2+} depletion in the melt, due to olivine fractionation, was faster than Fe^{2+} depletion due to oxidation. The same is true of the normal zoning in elongate, branching crystals. The zoning behaviour of these crystals suggests that they grew both upwards and downwards from a growth centre close to the interface between the crystal mush to melt, but not in, or on, the mush.

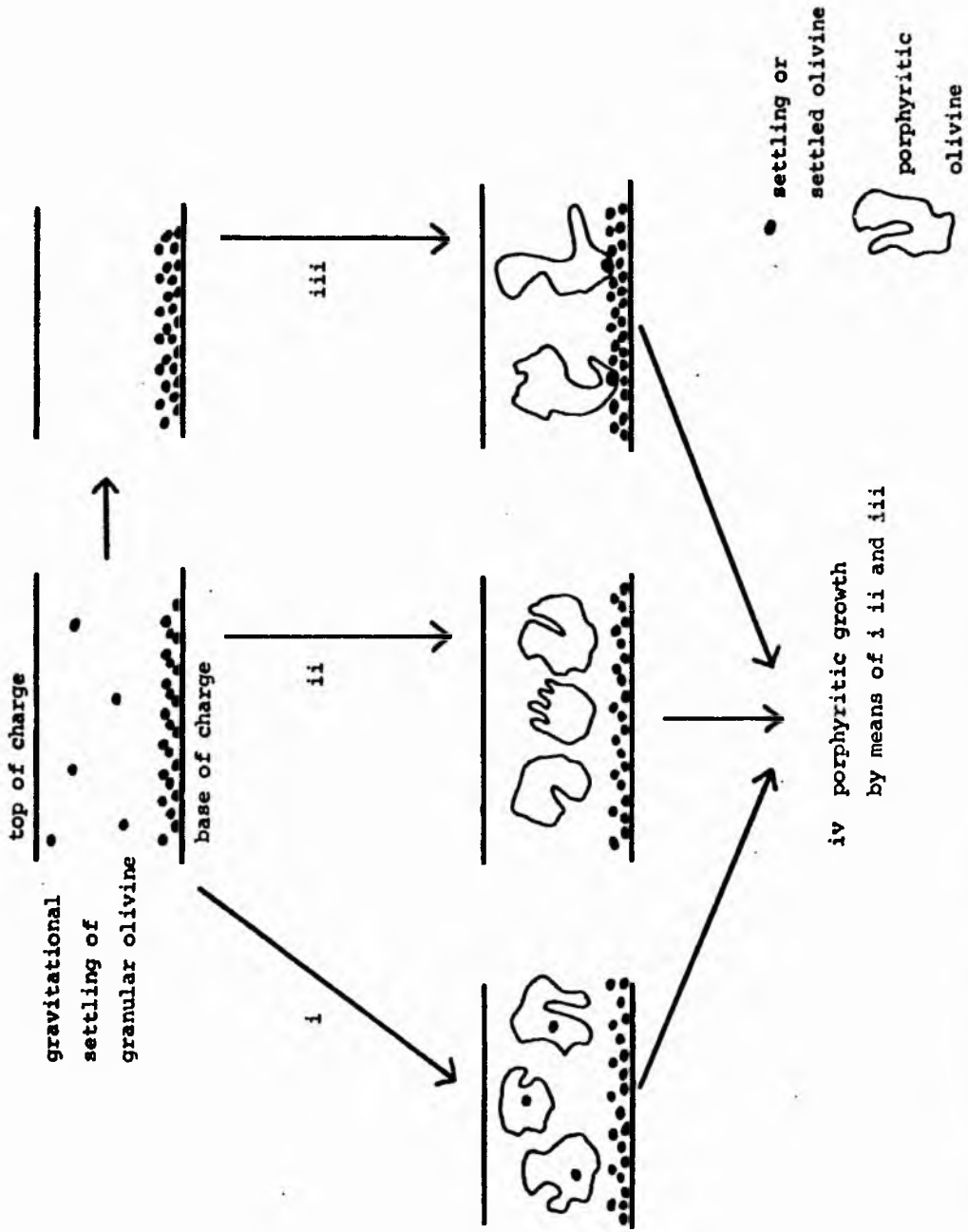


Fig. 46 Three possible origins of porphyritic olivine in hydrous cooling rate crystallization runs.

Many of the olivines grown in these experiments grew very fast (in a few hours or less) and yet have the very low Ca contents typical of slowly grown olivines in plutonic rocks [≤ 1000 ppm (Simkin and Smith, 1970)]. These results indicate that even though the olivines in harrisite crystallized rapidly, their low Ca contents are not anomalous (see p. 65). In anhydrous, 1 atm. crystallization experiments with rock E no olivine with less than 1000 ppm Ca has been grown, even though the olivine growth rates are comparable between hydrous and anhydrous experiments. These results imply that water under pressure in a melt influences Ca content of crystallizing olivine.

h) Crystallization of differentiated runs (cf. harrisite)

For the purpose of discussing the progressive crystallization of olivine in differentiated runs, crystallization of composition E with 5 wt. percent water run at 30° /hr (fig. 42) is discussed.

Cooling commences from 100° above the liquidus, before nucleation of olivine. At the nucleation temperature, the nucleation rate of olivine is very high, being close to the maximum, and abundant growth centres form. The olivine growth rate is low, so the crystals remain small. A granular olivine (0.1mm) which nucleated at the top of the charge will sink to the base at 2.6×10^{-3} cm/s in 2 minutes [calculated from Stokes' Law, $\eta_{1125^{\circ}} = 4.2$ poise (determined using Shaw's (1972) method and assuming 5 wt. percent H_2O for melt saturation), $\rho_{\text{olivine}} = 3.3$ g/cc, $\rho_{\text{eucrite}} = 2.8$ g/cc]. These crystals form a 'cumulate' up to 1 mm thick containing as much as 80 vol. percent olivine. With further cooling, the nucleation density greatly decreases and the growth rate steadily increases. Both changes promote growth of larger crystals than the original granular crystals. When the ratio of growth rate to diffusion rate reaches a critical value, porphyritic olivines form. Further increase in supercooling promotes growth of larger porphyritic crystals. Yet further increase in supercooling reduces both the nucleation density and melt diffusion coefficients and increases the growth rate, with production of branching crystals.

Porphyritic olivines could grow from any of three possible nuclei (fig. 46): i. from settling crystals which originally were

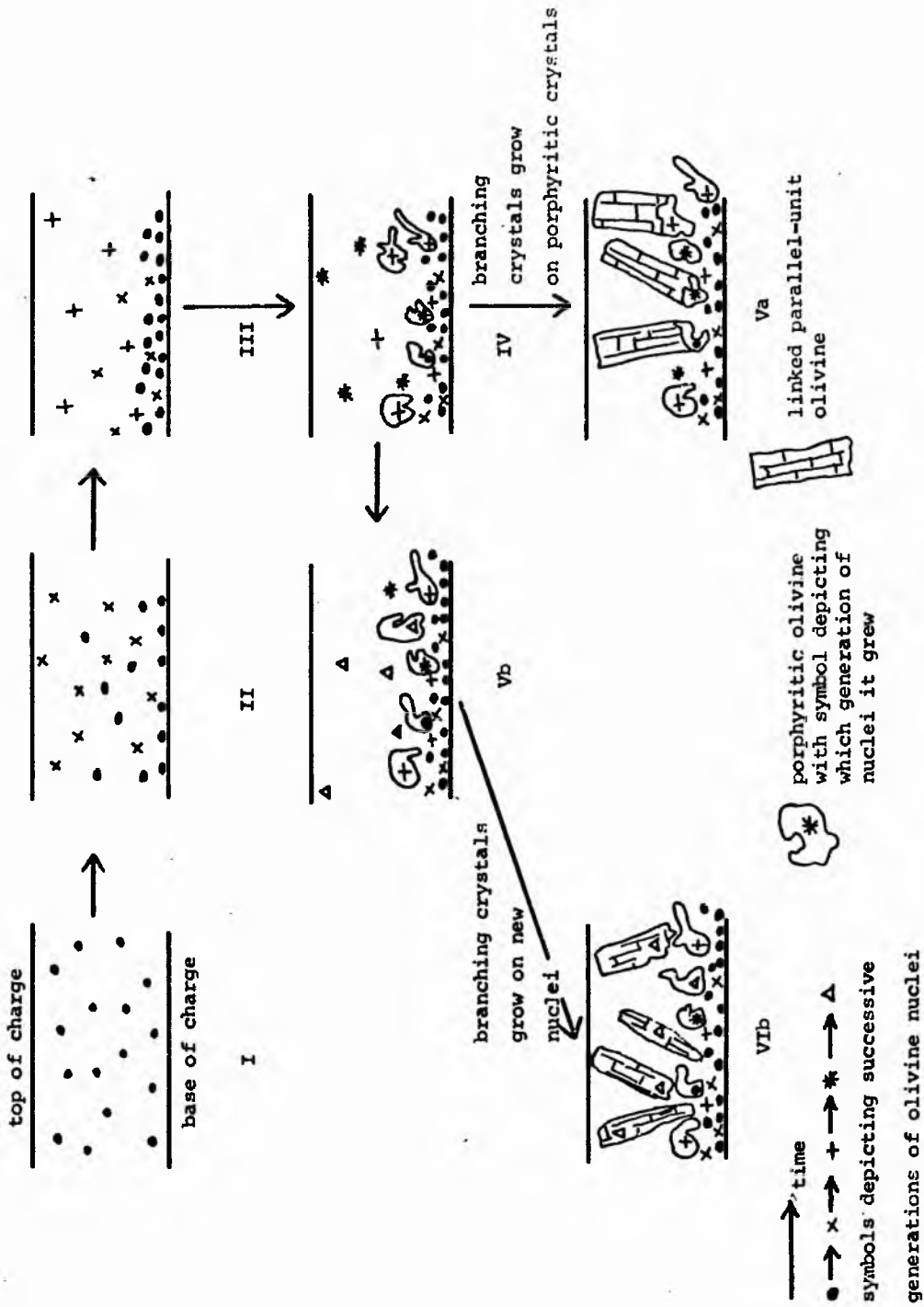


Fig. 47 Schematic representation of olivine nucleation and growth in hydrous cooling rate crystallization runs and two possible origins of branching crystals.

granular in shape, ii. from new nuclei and iii. from the uppermost granular crystals in the mush of settled crystals. Since granular olivines grade into porphyritic olivines, the validity of suggestion iii, on the crystallization of porphyritic olivine, is probably slight. A combination of the other two crystallization schemes is more valid.

The preferred elongation and crystallographic orientation of branching olivine (e.g., fig. 42), together with the zoning pattern in the crystals (p. 92) strongly suggests that these crystals grew in situ. Otherwise, the preferred elongation direction must be attributed to the unlikely possibility of a preferred settling direction for branching crystals. Whether the branching crystals grew on porphyritic olivines or from nascent nuclei (fig. 47, stages IV to Va or IV to VIb) is indeterminable. However, the zoning pattern of crystals establishes that the growth centre lay just above the mush of settled olivines.

Three types of nucleation history which might explain the sorting and stratification of olivine morphologies in certain cooling rate runs seem consistent with these conclusions and observations. 1) There may be continuous nucleation throughout the charge (fig. 47); 2) nucleation may be continuous, but decreasing in rate with time, and all nuclei, other than the initial ones, form only at the top of the charge where the olivine supersaturation is greatest, and 3) there may be discontinuous nucleation involving crystallization and settling of granular olivine, followed by cessation of nucleation and then by renewed nucleation at a lower rate providing growth centres for porphyritic olivines. Only in composition B does the form of the nucleation density against supercooling curve (fig. 44c) have two maxima; in compositions A, E and F there is a maximum at low supercooling, related to the formation of granular olivine. Therefore, the possibility of discontinuous nucleation (explanation 3) can be rejected. Nucleation may, however, be effectively discontinuous, since a sharp decrease in nucleation density below the maximum value occurs with further supercooling (fig. 44c). Thus, after abundant nucleation of the olivines which grow with granular morphology, further, but relatively slow, nucleation will continue. Whether or not subsequent nucleation is

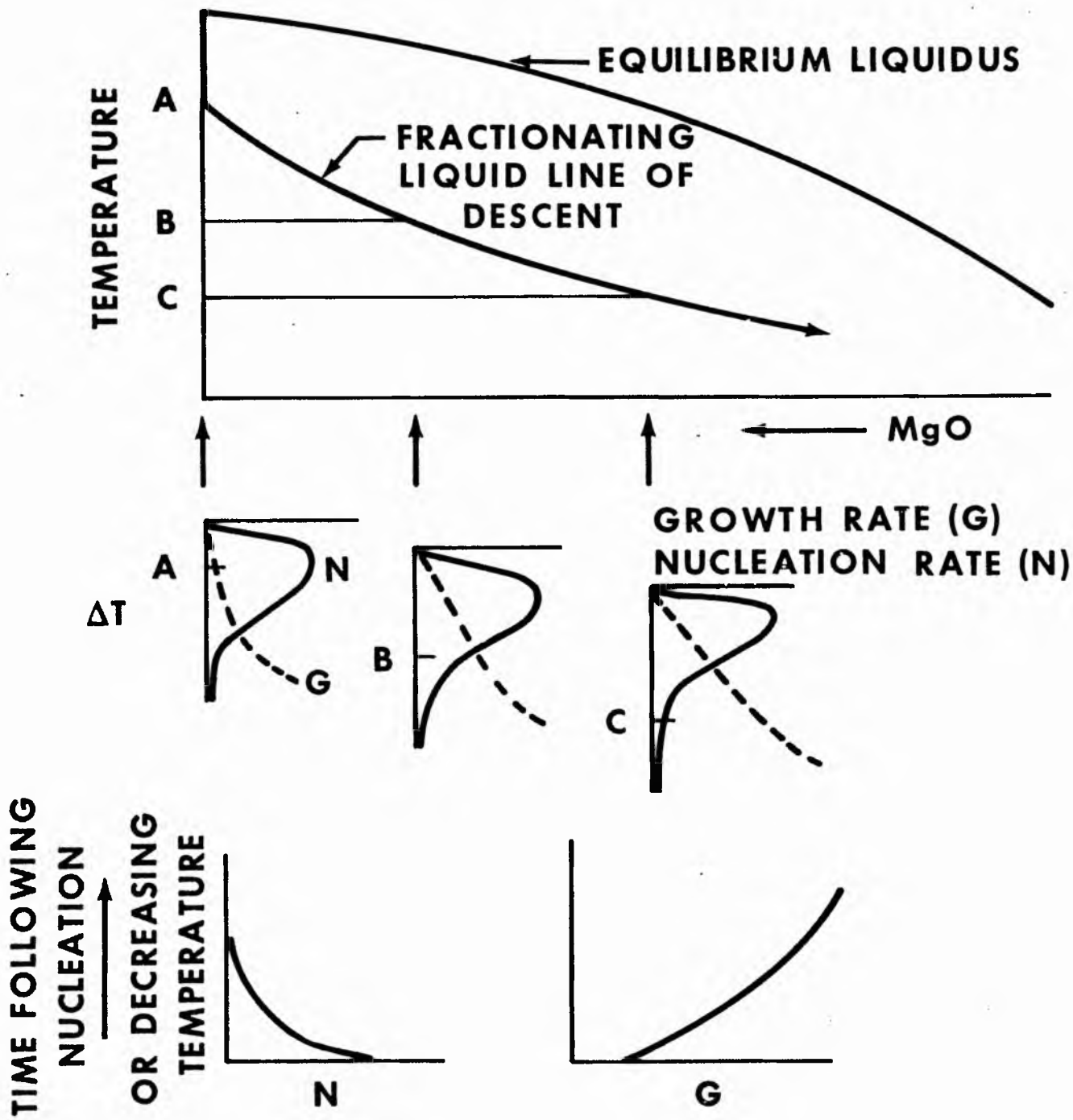


Fig. 48 Pseudobinary phase diagram to illustrate the relation of the actual (fractionating) liquid line of descent to the equilibrium liquidus in a cooling rate experiment and the possible relation of the liquid line of descent to the olivine growth rate and nucleation rate curves for various liquid compositions. Lowermost sketches illustrate the forms of the olivine nucleation and growth rate curves for liquids formed by progressive fractionation of the original liquid.

confined to the top of the charge cannot be determined, because olivine settles so rapidly in these low viscosity melts. It seems most likely that nucleation continued to occur throughout the charge but that, at any instant, the rate of nucleation and the number of nascent nuclei decreased from the top of the charge to the base. This model of crystallization is depicted in fig. 47 .

In summary, olivine nucleation occurred throughout cooling, following a period of incubation. The rate of nucleation decreased with time, and all olivine settled under gravity. If nucleation first occurred close to N_{maximum} , granular olivine crystallized, this being an attempt by the system to relieve supersaturation by abundant nucleation. With further cooling, the nucleation rate rapidly diminished. In order to continue relief of supersaturation, the growth rate increased and larger, porphyritic olivines grew. With further supercooling, the nucleation rate tended to zero, but the growth rate being high, growth on any available olivine crystal occurred readily. Those crystals with a approximately perpendicular to the layering grew most rapidly.

This discussion has ignored the fact that with progressive fractionation of granular olivine in the cooling rate experiments, the supersaturation of the melt in olivine might be reduced so that polyhedral olivine crystallized. However, by comparison with isothermal runs, crystallization of porphyritic olivine, and then branching olivine, after granular olivine indicates that the supersaturation continued to increase. The pseudobinary phase diagram in fig. 48 shows in principle how the supersaturation might increase, despite rapid crystallization of olivine. It further shows how the crystallization path must be related to the curves of growth rate and nucleation rate against supercooling along the fractionating liquid line of descent. The nucleation rate decreases and the growth rate increases with time (fig. 48).

v) Effect of superheat on olivine shapes

Superheat must be regarded as a potential control of textures in runs, since the experimental charges are melted above the liquidus

Table 18. Comparison of the olivine morphologies in hydrous and anhydrous isothermal and cooling rate runs on olivine eucrite (rock E, Table 21).

ISOTHERMAL EXPERIMENTS °C	HYDROUS	ANHYDROUS
0	{ Porphyritic and granular Linked parallel-unit Chain-like and lattice-work Plate ↓	{ Porphyritic Linked parallel-unit Lattice-work Plate
20		
40		
60		
80		
100	↑ Porphyritic Porphyritic and granular Branching (linked parallel-unit) Chain-like and lattice-work Plate	↓ Chain-like and lattice-work
120		
130		
COOLING RATE EXPERIMENTS °C/hr		
0		
7		
14		
30		
60		
118		

temperature, destroying possible heterogeneous nuclei and altering the melt structure. A few cooling rate experiments and isothermal experiments have been conducted, both of hydrous and anhydrous types, at melting temperatures 30° and 100° above the liquidus. There is no significant difference in olivine morphologies between runs identical except for melting temperature. Therefore, nucleation of olivine cannot be significantly delayed in highly superheated runs.

vi) Comparison of the olivine shapes in anhydrous and hydrous experiments

The systematic sequence of olivine shapes as a function of cooling rate and supercooling is comparable in both anhydrous and hydrous experiments- solid, faceted crystals grow at the slowest cooling rates and smallest degrees of supercooling, and they are replaced by skeletal olivines and then by dendrites at progressively larger cooling rates and degrees of supercooling. There are two major differences in olivine shapes between the anhydrous and hydrous experiments:

1) granular olivine crystallizes only in the hydrous experiments, whereas at similar cooling rates and degrees of supercooling, polyhedral or porphyritic olivines grow in the anhydrous experiments and 2) whereas dendrites grow in anhydrous experiments, plate olivine grows in hydrous runs. The origin of these differences is probably due to differences in physical properties of the wet and dry melts. Indented olivine crystals in hydrous melts commonly have rounder indentations and lobes than olivines in anhydrous experiments. Hence, water appears to disfavour growth of angularities on crystals, resulting in granular, rather than faceted, crystals and round indentations, rather than angular ones. Because some cumulate contains granular olivines, this conclusion is consistent with the suggestion that the Rhum magma was hydrous (p. 50).

Table 18 compares the olivine shapes in melt E crystallized wet and dry in both isothermal and cooling rate experiments. Equivalent degrees of supercooling are required to grow the same shapes of olivine

in wet and dry runs. However, at similar cooling rates there is no correspondence of olivine shapes in the two types of experiment. The dry experiments are dominated by chain-like and lattice-work shapes, whereas the hydrous experiments display a wider variety of olivine shapes. Addition of water to a melt therefore results in greater diversity of olivine shapes in cooling rate experiments. Also, chain-like and lattice-work olivines appear at faster cooling rates in the hydrous experiments than in the anhydrous ones.

The layering in hydrous experiments, caused by differentiation of olivine shapes and sizes, is not reproduced in anhydrous runs. This is most likely due to the considerably lower viscosity (by a factor of 10) of hydrous melts and, hence, to more rapid settling of olivine.

vii) Summary and relevance to harrisite

1) Relationship of the olivine morphology classification to experiments

The most important conclusions of this experimental work are that a consistent relationship exists between most of the olivine shapes classified in chapter IV, as a function of both cooling rate and degree of supercooling, and that each shape has a specific range of temperature stability for each melt. With increasing cooling rate or degree of supercooling the following changes in olivine shapes occur: polyhedral or granular → porphyritic (indented; e.g., fig. 7i) or linked parallel-unit → porphyritic (internally skeletal; e.g., fig. 7b) or linked parallel-unit → crystallographic branching → randomly oriented chain-like → parallel growth chain-like → chain-like + lattice-work → plate or dendritic → (pseudo-spherulitic). Linked parallel-unit olivines crystallize at comparable degrees of supercooling and cooling rate as porphyritic olivine, but they grow in a constrained manner.

As demonstrated for rock 12009, these differences in olivine shapes can be used to distinguish relative cooling rates and degrees of supercooling at which differently-shaped olivines in the same rock

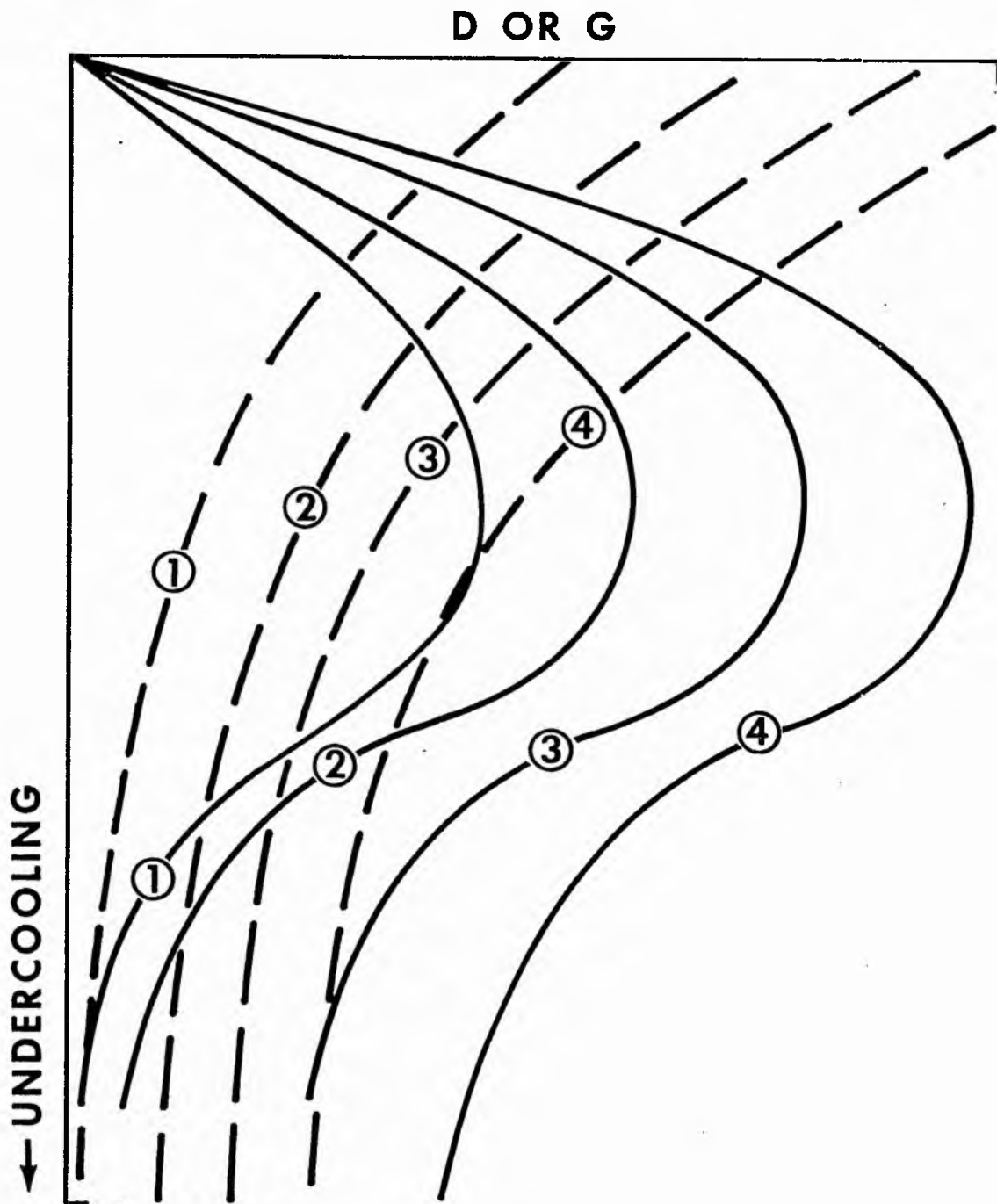


Fig. 49 Form and relative position of olivine growth rate, G (solid lines) and diffusion coefficient, D (dashed lines) curves as functions of olivine and water contents of melts. ①→④ corresponds to increasing water and/or olivine content. (Origin of the temperature axis is the liquidus temperature.)

crystallized. In section 3 (p. 99) this approach is used to distinguish the relative degrees of supercooling at which differently-shaped olivines in cumulate and harrisite crystallized.

All the morphologies listed in chapter IV have been synthesized, except radiate olivine and swallow-tail olivine. Swallow-tail olivine did crystallize in experiments "devitrifying" a picritic glass (results not discussed here). The dendritic projections grow on polyhedral crystals, probably during quenching. This suggests that the morphology is favoured by very rapid cooling rate and the presence of crystals with well-formed corners and edges, i.e., polyhedral crystals. Conditions favouring radiate olivine crystallization remain unknown, but a substrate for constrained growth and low nucleation density of olivine probably aid this type of olivine growth.

2) Summary of the effects on olivine shapes of water and olivine contents in the melt

Irrespective of the water and olivine contents of the melt, the same shapes of olivine crystals grow at similar degrees of supercooling. This observation indicates that, although at the same degree of supercooling there are differences in olivine growth rate (G) and in diffusion coefficients (D) of components between different melts, the form and relative position of the G and D curves, as plotted against supercooling, are comparable for all the melts investigated (fig. 49). Hence, the ratio of G/D, so critical in determining crystal shapes (Keith and Padden, 1963), is similar in different melts, supercooled to the same extent.

These conclusions are consistent with examination of T - X sections of many olivine-bearing experimental systems which reveals that the liquidus surface between olivine and liquid is convex to the liquid side. Hence, as the melt becomes progressively olivine enriched, it will be more highly supersaturated for a given degree of supercooling. More olivine-enriched melts should, therefore, display higher G values for a given degree of supercooling, assuming that

nucleation rate varies little as a function of composition.

Addition of water to a melt and higher olivine content have dissimilar effects on olivine shapes in cooling rate experiments-- the former increases the cooling rate at which each morphology in the experimentally-determined sequence of shapes grows, the latter reduces it. Since the temperature range at which each olivine shape is stable is essentially independent of the water and olivine contents of the melt, the differences in olivine shapes in cooling rate experiments caused by variation in water and olivine contents of the melt must reflect differences in incubation time of olivine nuclei. The lower the olivine content, the shorter the incubation time. Presumably the more olivine-rich the melt the slower the melt structure rearranges to form olivine nuclei during cooling (p. 68). Hence, the longer it takes to form a critical nucleus and the deeper the supercooling achieved before nucleation in a cooling experiment. The opposite is apparently true of water addition to a melt.

3) Application of the experiments to the origin of harrisite

Reproduction of harrisite layering has been effected in hydrous, ultrabasic melts cooled at constant rates. Thus, continuous rather than abrupt changes are likely in the intensive parameters of the natural harrisite-forming magma. Harrisite and associated cumulate are two textural extremes of ultrabasic rock linked by changes in crystal growth parameters, attributable to differences in degree of magma supercooling. Olivines in harrisite crystallized at greater supercooling than those in cumulate (contrast Wadsworth, 1961). By comparison of experiments with harrisite, it is clear that the upward transition from cumulate to harrisite is the result of a continuous increase in olivine supersaturation. In the hydrous runs showing differentiation of olivine morphologies, olivine crystals always grew under water-saturated conditions, indicating that the origin of harrisite cannot be ascribed to a change from water-undersaturated to water-saturated conditions (or vice versa). Complete absence of plagioclase and pyroxene in the hydrous runs also testifies that a change in liquidus slope, due to supersaturation

with a second phase (p. 69), cannot be the origin of harrisite.

Synthesis of the textural features and phase chemistry (low Ca content of olivine) of harrisite in hydrous experiments does not imply that the cooling rate found to produce 'harrisite' in the laboratory also caused its crystallization in nature. The sizes of crystals in harrisite are larger than those in the experiments and the olivines are less extensively zoned. Since harrisite crystallized from a larger volume of magma than did the laboratory-crystallized 'harrisite', the dimension of the system and the mass of the melt are vastly different in the magma chamber in comparison with the same parameters in the experiments. The extent of fractionation of the natural magma must be considerably less than that of the experimental one. Part of the cause of the change in olivine nucleation rate and growth rate with time in the cooling rate experiments [i.e., the extreme fractionation of the liquid (fig. 48)] is not experienced to any significant extent in the harrisite parent magma. Therefore, the effect of changing liquid composition is of little importance, in explaining the crystallization of harrisite in Rhum, when compared with this effect in the experiments. Increased supercooling alone, of a magma of essentially fixed composition, must be the cause of natural harrisite crystallization, and this supercooling must extend beyond the maximum in nucleation rate (fig. 44c) to a level where nucleation rate is low and growth rate high (i.e., greater than 25 - 30° supercooling in rocks A, E and F, fig. 44).

Differentiation, in both the experiments and in the harrisite-forming magma, involves some crystal settling. In nature, these crystals may settle a greater distance than those in the experiments and this takes more time. The cooling rate for natural harrisite crystallization must therefore be less than that in the experiments. How much less is unknown; it must, however, be a rate compatible with the settling rate of granular and porphyritic olivines.

In summary, olivines from hydrous ultrabasic melts, cooled

between 15 and 30°/hr, most closely resemble the shapes and distribution of olivines in harrisite. However, the experimental cooling rates are not typical of those at which harrisite crystallized in nature. They represent maximum natural cooling rate values. In contrast, the values of supercooling for crystallization of particular growth shapes, deduced from the isothermal experiments, are probably representative of those for harrisite, particularly those for the olivine eucrite (sample E). Granular olivines crystallize at approximately 25° supercooling, porphyritic olivines at approximately 30 - 50° supercooling and linked parallel-unit olivines at 40 - 50° supercooling. The polyhedral olivines underlying some harrisite layers (p. 33) probably crystallized at similar degrees of supercooling to (or lesser than) those at which granular olivine crystallized. Variations in water and olivine contents have little effect on the degree of supercooling at which each olivine morphology crystallizes; they do affect the cooling rate. Hence, if the parent magma of harrisite were a basalt and not an olivine eucrite (p. 127), faster cooling rates than those determined in the laboratory will cause harrisite to crystallize.

The previous chapter has shown that harrisite crystallized from a strongly supersaturated magma and has illustrated how the olivine morphology distribution within harrisite layers forms. This chapter discusses how the Rhum magma, in its plutonic crystallization environment, became so greatly supercooled, and how the supercooling affected crystallization.

I Origins unrelated to the crescumulus hypothesis

1. Water-saturated origin (Harker, 1908b; Drever and Johnston, 1972)

The AGI Glossary of Geology defines "pegmatite" as "An exceptionally coarse-grained (most grains one cm or more in diameter) igneous rock, with interlocking crystals...." Those harrisite layers containing giant olivine crystals are therefore ultrabasic pegmatites. Current opinion considers pegmatites to "represent the last and most hydrous portion of a magma to crystallize...." (AGI); the relative proportions of silicate and volatile components in the pegmatite parent fluid are, however, in dispute, so that it is unknown whether pegmatites crystallize from water-saturated magmas or from the free vapour phase [supercritical fluid (Burnham, 1967)] separated from such a magma. It is impossible to know which of these conditions Harker favoured, but Drever and Johnston specifically use the phrase "supercritical fluid". The partition coefficients of elements between a water-saturated magma and its associated supercritical fluid (vapour) favour enrichment of the fluid in Si, Fe and alkalis (Burnham, 1967 and Holloway, 1969). These enrichments render the fluid inappropriate as an origin of ultrabasic rock, particularly as harrisite is not significantly enriched in these elements relative to adjacent cumulate layers. Calculations indicate that if harrisite did crystallize from a supercritical fluid, each 1 m thick layer of rock would require a layer of parent fluid 0.3 km thick (calculated at S.T.P.). Since it is unlikely that such large quantities of water were concentrated in the Rhum

magma, a supercritical fluid origin for harrisite is unacceptable. On the other hand, crystallization from a water-saturated magma is consistent with the petrographic evidence for a water-bearing magma, though there is no way of determining whether or not the magma was saturated with water. (See also Appendix II, p. A10.)

2. 'Metamorphic' origin

If there were a rhythmic build-up of volatiles in cumulate crystal mushes, the cumulus olivines might recrystallize under the influence of metasomatism, to form skeletal and dendritic crystals (Drever, personal communication, 1972). The sharpness of the upper contact, and the planar character of the lower contact, of harrisite to cumulate do not favour such a 'metamorphic' origin. Were it possible, pockets, rather than layers of harrisite would be expected.

3. Postcumulus recrystallization origin

In the Bushveld intrusion, Cameron (1969) has documented postcumulus recrystallization of cumulus crystals into larger crystals, with supplementary adcumulus growth. Physical chemists refer to this process, whereby the larger crystals in a saturated solution or melt grow at the expense of the smaller ones, as an "ageing effect" or "Ostwald ripening" (Doremus, 1973). Although the solution may remain of constant composition, the number of crystals diminishes with time. It is, however, doubtful that the formation of skeletal and dendritic crystals could be attributed to this property.

Attempts in the laboratory to synthesize harrisite by modelling origins 2 and 3 failed. The rest of this chapter therefore examines how the crescumulus hypothesis must be modified to account for the petrographic features and field relations of harrisite.

II Modification of the crescumulus hypothesis

A number of field and petrographic features of harrisite which are inconsistent with the crescumulus hypothesis have been noted in the descriptive chapters. These include: field relations only explicable

by intrusion; gradational rather than abrupt changes in grain size, crystal abundance and shape upwards from cumulate into harrisite; elongate olivines not growing upward, and not commencing growth from the underlying layer of cumulate; evidence for constrained growth of linked parallel-unit olivines along a thermal gradient; and experimental evidence for crystallization of harrisite at greater supercooling than cumulate. In particular, five questions concerning the origin of harrisite and its relationship to crystallization of the Rhum pluton need answering:

- 1) Why is there a change in the shape of olivine crystals within harrisite layers?
- 2) Why is olivine supersaturation apparently confined to the floor of the magma chamber?
- 3) If settling of 'cumulus' olivines is to be assumed, why did the settling terminate during crystallization of harrisite?
- 4) Why is harrisite absent from all, but one, other layered intrusions.
- 5) How are large degrees of supercooling ($40 - 50^{\circ}\text{C}$) caused in a plutonic magma chamber?

Any model for the origin of harrisite must supply the answers to these questions and remove the inconsistencies of the crescumulus hypothesis, or invalidate it.

A. Constraints and some introductory comments

The following constraints on the petrogenesis of harrisite are indicated by the field and petrographic features of the rock and by the olivine crystallization experiments.

i. Harrisite is limited to certain stratigraphic horizons in the pluton. Eucritic harrisite is never associated with peridotitic cumulate, nor peridotitic harrisite with eucritic cumulate. The compositions of the phases in harrisite show only slight, or no, differences from those in the underlying and overlying cumulate. These facts suggest that the parent magma of harrisite is not randomly injected into the Layered Series or into the magma chamber.

- ii. Most harrisite layers crystallized upwards, as part of the progressive upward solidification of the intrusion. This does not imply that olivines in harrisite necessarily grew upwards, e.g., one layer definitely crystallized olivine from both the top and bottom of the layer (fig. 14a). This layer is one of the few which unquestionably intruded the layered sequence.
- iii. The reverse 'bedding' in harrisite in which larger olivines overlie smaller ones, and the internal textural changes in harrisitic layers are the results of (a) the changes in olivine nucleation and growth rates as functions of supercooling and (b) the change from unconstrained to constrained crystal growth. These changes in olivine morphology, grain size, and olivine morphology distribution, are more accurately reproduced in the laboratory by continuous increase in supersaturation (i.e., cooling rate crystallization) than by sudden induction of supersaturation (isothermal crystallization).
- iv. Harrisite containing granular and porphyritic olivines is olivine-enriched due to crystal settling. The differentiation necessary to form comb-layered harrisite (sample 74, Appendix I) must be due to transport in situ of ions in the parent magma by chemical diffusion, thermal diffusion, or convection.
- v. The crystallization experiments indicate that the magma supercooled up to 50^oC during harrisite formation.
- vi. Either the parent magma of harrisite is richer in water than that of the 'normal' cumulates, or water is more effectively trapped in the rock during harrisite crystallization. The latter suggestion seems less likely when it is considered that diffusion and convection were sufficiently effective, during formation of some harrisite layers, to remove much of the pyroxene component from the rock.
- vii. Olivines in harrisite and cumulate crystallized close to the base of the magma chamber (cf. Wager and Brown, 1968, p. 229) at less than 2.5 kb (Appendix II).
- viii. The number of olivines accumulating on the floor of the magma chamber decreases upwards through a harrisite layer. Accumulation

essentially ceases during growth of branching crystals. If cumulus olivines nucleate near the intrusion roof, and if the processes causing harrisite formation affect the whole magma chamber (?Wadsworth, 1961; see p. 34), then the disappearance of cumulus olivines is understandable. However, if they affect only a layer of magma at the floor of the chamber, settling of crystals from the chamber roof to the floor should continue. Thus, the absence of cumulus olivine in branching olivine harrisite must result from either: (a) melting of cumulus crystals before they reach the floor, or (b) assuming that harrisite crystallizes from a discrete unit of magma spread across the floor of the chamber by convection (Wager and Brown, 1968), and that magma reaches the floor by undercutting magma containing settling cumulus crystals, cumulate rock will not form again until cumulus crystals settle through the unit of harrisite-forming magma. Alternatively, the cumulus olivine underlying and overlying harrisite may crystallize only from magma near the base of the chamber (cf. Jackson, 1961) and, as indicated on p.51, this model is more in accord with available evidence.

In summary, a very restrictive set of conditions for harrisite formation emerges from this petrographic and experimental study. These are that supercooling and magmatic temperature increase continuously upwards and that conditions favouring crystal accumulation are removed. These changes take place essentially in situ, on the chamber floor.

B. Mechanisms of supersaturation induction

Four types of mechanism which may cause supersaturation of a magma are examined below:

- i. conductive cooling at the margins of the magma body.
- ii. cooling due to intrusion into a cooler and larger unit of magma.
- iii. cooling due to vesiculation of a gas phase.
- iv. elevation of the liquidus temperature relative to the actual temperature

i. Cooling at the margins of a magma chamber

Marginal conductive cooling is possible at three localities within a magma chamber- the roof, the sides and the floor. Although the magma crystallizing as harrisite may have reached the floor in a supersaturated state, due to cooling at the chamber roof and sides during convection, it must have increased in supersaturation (supercooling) at the floor. Conductive cooling at the floor is therefore of most relevance to the present inquiry.

a. Form of the thermal gradient at the base of the chamber

In the Ard Mheall and Transition Series, pyroxene is never, and plagioclase is rarely, a cumulus phase (Wadsworth, 1961). Hence, the temperature of the magma (at least close to the floor of the chamber) exceeded the liquidus temperatures of both plagioclase and pyroxene. However, both phases occur as intercumulus crystals. Thus, the actual temperature in a crystal mush on the floor of the chamber must, at some depth in the mush, be less than the liquidus temperatures of both the plagioclase and the pyroxene. The magma temperature, therefore, increases upwards through the mush into the overlying magma. Since cooling also occurs from the top of the chamber, the vertical thermal gradient in the chamber must at some level change to one of decreasing temperature with increasing height, i.e., magmatic temperature increases from the roof and the floor of the chamber to a maximum value near the centre. If there is convection of magma, the thermal gradient increases with depth at $0.3^{\circ}/\text{km}$ (Jackson, 1961) and the maximum in the gradient is close to the floor of the chamber. Cessation of convection, either throughout the chamber or in a unit of magma at the base of the chamber (cf. Jackson, 1961), alters the thermal gradient at the base of the chamber. The magma at any given height in the chamber will become progressively cooler than that at the same height during convection.

Table 19 Maximum cooling rates of magma at various distances above the floor of the Rhum chamber. The floor is assumed to have fixed coordinates with time.

Distance above floor, cm	Maximum cooling rate, °/hr	Time to reach maximum cooling rate, hours
10	9	1.23
100	$9 \cdot 10^{-2}$	123 (5days)
1000	$9 \cdot 10^{-4}$	12345 (514 days)
10000	$9 \cdot 10^{-6}$	1234500 (140 years)

b. Rate of magma cooling following cessation of convection

After cessation of convection, an infinitely thick and broad sheet of magma is assumed to be in sharp contact with underlying, cooler cumulates. The heat flow equation for this condition is

$$v = \frac{1}{2} V \left\{ 1 + \operatorname{erf} \frac{x}{2\sqrt{kt}} \right\} \quad (1) \quad \text{Carslaw and Jaeger (1959)}$$

where v is magma temperature, V is the temperature difference between the magma and the cumulate, x is the distance from the boundary, k is thermal diffusivity of the cumulate and t is time.

Differentiation of equation (1) with respect to time gives

$$\frac{dv}{dt} = \frac{v}{2\sqrt{kt}} \cdot e^{-\frac{x^2}{4kt}} \cdot \frac{V}{t\sqrt{\pi}} \quad (2)$$

Carslaw and Jaeger (1959) show a graph (fig. 5) of $\frac{x}{2\sqrt{kt}} \cdot e^{-\frac{x^2}{4kt}}$ which can be used to evaluate equation (2). The curve is Gaussian in shape with a maximum value of $\frac{x}{2\sqrt{kt}} \cdot e^{-\frac{x^2}{4kt}}$ at $\frac{x}{2\sqrt{kt}} = 0.75$. The cooling rates reported here are for this value and are therefore the maximum values experienced by magma at a given height above the floor.

Temperature in the cumulates decreases with depth below the boundary between magma and cumulate. For the calculations it is assumed that there is a temperature difference of 50° across the magma to cumulate boundary. (The value of 50° was chosen as this is the maximum supercooling deduced experimentally for harrisite.) k is taken as $0.01 \text{ cm}^2/\text{s}$ (Jaeger, 1968). Maximum cooling rates and the times necessary to attain these at different heights above the floor are shown in Table 19. Hence, assuming the level of the floor remains stationary, magma 10 cm above the floor may cool as fast as $9^\circ/\text{hr}$, whereas magma 10 m above the floor cools at only $10^{-5}^\circ/\text{hr}$. (Contrast the average Skaergaard cooling rate of $10^{-6}^\circ/\text{hr}$.) Close to the

chamber floor (10 cm and below) rapid cooling rates, of the order of those determined in the experiments simulating harrisite, are achieved.

Combining these calculations with the cooling rate experiments, it can be postulated that granular crystals grow at some height above the floor, porphyritic crystals grow closer to the floor and branching crystals grow at or near the floor. This situation is, however, unsatisfactory, since the stratigraphic succession of crystal morphologies is opposite to that in harrisite. Clearly, another factor causes the sequential change in olivine shapes and the reduction in olivine nucleation rate. However, the calculations of cooling rate do confirm the petrographic conclusion that porphyritic and branching olivine crystals grow closer to the floor than granular crystals and that substantial heat flow into the floor accompanies branching olivine growth.

ii. Injection of fresh (hotter) magma into the magma chamber

If fresh magma is injected into the Rhum chamber, and if it is both hotter and has a higher olivine liquidus temperature than the magma already in the chamber, the fresh magma will cool and ultimately crystallize olivine. If cooling is sufficiently rapid, enough supersaturation may be induced prior to nucleation to promote skeletal olivine crystallization. [Note that this is not the same proposition as random intrusion of magma into the Layered Series, which has already been rejected as an origin of harrisite (p. 104).]

This origin of harrisite is in accord with the postulate (Brown, 1956) of periodic replenishment of the Rhum chamber with fresh magma. However, Brown suggests that the replenishment occurred on a large scale (units of magma greater than 100 m thick), rather than as periodic small influxes of magma capable of forming layers of approximately 1 m thickness. Furthermore, harrisite is not found at the junctions between units in the Eastern Layered Series, where Brown considers that the overlying unit crystallized from a new

batch of magma. Other circumstantial objections against this intrusive origin of harrisite are summarized below:

1) It is most unlikely that influx of fresh magma into the chamber would involve spreading of the magma over the floor to form a perfect layer from which harrisite crystallized.

2) The preference for harrisite layers to be 1 m thick is an unlikely consequence of this intrusive model.

3) There is no textural or structural evidence for intrusive movement of magma prior to crystallization of harrisite.

iii. Cooling due to vesiculation of a gas phase

If the parent magma of harrisite is water saturated, bubbles of water-rich gas may nucleate and, being less dense than the magma, float upwards. For every gram of water that separates from the magma, 100 - 150 calories of heat are absorbed from the magma (Kadik, 1971). The change in magma temperature following vesiculation is given by

$$\Delta T = \frac{H}{m \cdot S}$$

where ΔT is the temperature change, H is the heat evolved, m is the mass of the system and S is the specific heat of the magma. Consider a unit of magma of mass 100 g from which 0.1 g (0.1 wt. percent) of water separates as a gas phase. Taking S as 0.3 cal/g. $^{\circ}$ C (Hess, 1960) and H as 500 cal/g, the decrease in temperature of the magma is approximately 1 $^{\circ}$ C. Loss of 1 g (1 wt. percent) of water would decrease the temperature by 10 $^{\circ}$ C.

The rate of cooling resulting from vesiculation cannot be calculated, since neither the nucleation rate of the bubbles, nor their size could be estimated. Even if the nucleation rate is as fast as the vesiculation rate in basalts, the likely supercooling induceable by this means (1-10 $^{\circ}$ C) is still too small to promote harrisite crystallization.

iv. Supersaturation induction by elevation of olivine liquidus temperature

The liquidus temperature of a magma may be altered in three ways: a) by change in the confining pressure, b) by change in water content (Donaldson, 1974a) or c) by change in the partial pressure of oxygen in the magma. Each of these possibilities as the cause of the supersaturation promoting harrisite formation is discussed below.

a) Change in P_{total}

If the parent magma of harrisite is water-undersaturated, supercooling could be induced in a descending batch of magma due to elevation of the liquidus temperature (Wager and Brown, 1968). The greater the change in height, the greater the cooling that might be attained. Also, the more rapid the movement of the magma, the more likely will it reach the floor without nucleation of olivine. If the harrisite parent magma is water-saturated, supersaturation caused by change in confining pressure can only be effected by movement from a depth greater than that at which it crystallized. This means that the magma would always have to rise from a level in the pluton below the mush to magma interface, and is equivalent to suggesting emplacement of fresh magma into the chamber for each harrisite layer. It is therefore an unsuitable mechanism, as discussed in section ii.

Such movements of magma could initiate harrisite crystallization, but cannot be the cause of the inferred in situ increase in supersaturation through harrisite layers (section IIA). For the same reason, the suggestion of Donaldson (1974a), that slight adiabatic cooling might occur due to expansion of the magma on emplacement, is also unsuitable as a cause of increasing in situ supersaturation.

b) Change in magma water content

The water content of a magma may decrease in two ways. If the magma is water saturated, 'bubbles' of water-rich gas can separate by vesiculation. This process does not alter the liquidus temperature.

Once water undersaturation is achieved, loss of water can occur only by diffusion along a pressure, temperature or composition gradient.

Two types of situation under which water diffusion may operate are:

1. throughout a column of magma and
2. in a stratified magma chamber in which relatively water-enriched magma, spread across the intrusion floor, underlies relatively water-deficient magma.

In the following paragraphs the water flow rates for each situation are discussed and the rate of supercooling evaluated.

1. In a magma with an initially uniform water content, the chemical potential of water increases with depth (Goranson, 1937), causing water diffusion along the chemical potential gradient. The flow rate of water in magma depends on the magnitudes of the diffusion coefficient and the chemical potential gradient of water. Assuming that water solution in a magma is approximately ideal, the chemical potential gradient of water is approximately proportional to the concentration gradient. Then according to Fick's law,

$$J = -D \cdot dc/dx$$

where J is the flow rate of water per unit surface area per unit time, D is the diffusion coefficient of water in the magma and dc/dx is the gradient in water concentration through the chamber.

If there is no chemical interaction between water and the magma, a value for D_{H_2O} may be calculated from the Stokes-Einstein equation

$$D = \frac{RT}{6\pi\eta r N_0}$$

where r is the water molecule radius, η is the magma viscosity, N_0 is Avogadro's number, T is the absolute temperature and R is the gas constant (Donaldson, 1974c; in press). η may be calculated by the method of Shaw (1972). Taking T as 1250°C , and magma of composition 89 (E) in Table 22, η is 1.6 poises and $D_{H_2O} = 6.3 \times 10^{-7} \text{ cm}^2/\text{s}$.

Assuming that the equilibrium water concentration gradient is 0.3 wt. percent per km (Burnham, 1967), water will diffuse upwards from an initially homogeneous magma at a rate of $3.5 \times 10^{-13} \text{ moles/s.cm}^2$.

Table 20. Time required for 1 wt. percent water to diffuse from harrisite-forming magma into adjacent non-harrisite-forming magma. (See text for explanation.)

Difference in water content between harrisite forming and non-harrisite forming magmas (grad c), wt. percent	Grad c, moles/cm ⁴	Flow rate (J) of water, moles/cm ² .s (J = -D grad c)	Time (t) for 1 wt. percent water to diffuse across the boundary between the two magmas, days
5	7.48 $\cdot 10^{-3}$	4.7 $\cdot 10^{-9}$	3.7
4	6.00 $\cdot 10^{-3}$	3.8 $\cdot 10^{-9}$	4.6
3	4.50 $\cdot 10^{-3}$	2.8 $\cdot 10^{-9}$	6.1
2	3.00 $\cdot 10^{-3}$	1.9 $\cdot 10^{-9}$	9.3
1	1.50 $\cdot 10^{-3}$	9.4 $\cdot 10^{-10}$	18.6
0.5	7.50 $\cdot 10^{-3}$	4.7 $\cdot 10^{-10}$	37.2

2. In this situation a unit of water-enriched magma (parent of harrisite) is assumed to cover the floor of the chamber and to be in sharp contact with overlying, drier, bulk magma. The flow rate of water from the wetter to the drier magma is dependent on:

- a) the diffusion coefficient of water in the magma,
- b) the temperature difference between harrisite-forming magma and the overlying magma, and
- c) the difference in water content between harrisite-forming magma and the overlying magma.

In the following calculation it is assumed that there is no temperature difference between harrisite-forming and non-harrisite-forming magma. In reality, the former is probably cooler than the latter and diffusion of water will be slower than calculated. It is also assumed that the flow of water between the two magmas is uniaxial, i.e., that it flows perpendicular to the boundary between the harrisite-forming and the non-harrisite-forming magmas.

The rate of water flow is again calculated from Fick's law, where dc is the difference in water content between the two magmas and dx is the distance over which diffusion occurs. Initially, the wet and dry magmas are juxtaposed. J_{H_2O} will then be a maximum, since dx is zero. As the content of water at the top of the harrisite-forming magma decreases, the rate of flow of water decreases, because dx increases in value. The values of J_{H_2O} calculated here are for dx equals 1 cm. As dx increases, the value² of J decreases proportionately.

Taking the diffusion coefficient of the H_2O molecule as $6.3 \times 10^{-7} \text{ cm}^2/\text{s}$ (p.112), the flow rate of water across the boundary between the relatively wet and dry magmas is given in Table 20. The table also indicates the time required to decrease the water content of the harrisite-forming magma by 1 wt. percent at various values of dc . If $dc = 5$ wt. percent, the time required is 3.7 days.

The rate of water flow in situation 2 is therefore 10^4 times faster than the rate in situation 1.

Scarfe (1973) gives the maximum solubility of water in a tholeiite magma at 2 kb as 4 ± 0.5 wt. percent and in a picrite magma as 2.5 ± 0.5 wt. percent. If the harrisite-forming magma were of either of these compositions, these values would represent the maximum possible difference in water content between the harrisite-forming and the non-harrisite-forming magmas, assuming neither is superheated. If the harrisite-forming magma were a basalt, the water content at the upper 1 cm of the magma layer would reduce by 1 wt. percent in 4 - 5 days; if the magma were picritic, it would take 9 - 12 days (these values are for situation 2). A 1 wt. percent decrease in the water content of a basalt magma would result in an induced supercooling of 25 - 35 °C (Khitarov and Kadik, 1973, fig. 1c). Combining these data with the computed rate of water flow, an equivalent cooling rate of 0.1 - 0.3 °C/hr is calculated, *i.e.*, smaller than the cooling rates found necessary to crystallize "harrisite" in the laboratory.

It is tentatively concluded that a mechanism involving diffusional loss of water, either by situation 1, or more rapidly by situation 2, could cause the supersaturation promoting harrisite crystallization and the textural changes within harrisite layers.

This model explains certain field and textural observations on harrisite. Heterogeneous water content in the harrisite-forming magma would account for the lateral variation in olivine facies, since olivine morphology is cooling rate (or liquidus elevation rate) dependent. Differences in water content between batches of harrisite-forming magma, and hence in rate of water diffusion, account for the textural variation between certain adjacent harrisite layers (p. 15). Similarly, variation in the water content of the overlying, non-harrisite-forming magma, and the vigour of convection in this magma, could result in olivine morphology differences.

Harrisite formation requires a change in physical and/or chemical conditions of the Rhum magma. Brown (1956) has suggested a mechanism whereby a change in the rate of flow of water (in situation 1) can result. He proposed that refluxing of magma occurred in the Rhum chamber.

Each major unit of ultrabasic rocks is considered to crystallize from a single unit of magma which periodically was extruded from a volcano overlying the chamber and was replaced by fresh magma. It is also possible that magma was intermittently ejected from the chamber during formation of major ultrabasic units. Eruption decreases the volatile content in magma near the top of the chamber and triggers faster diffusion of water through the chamber, due to the increased value of dc/dx . This raises the liquidus temperature at the chamber base (assuming a water-undersaturated parent magma).

Situation 2 will result if water-enriched magma from the top of the chamber convects to, and spreads across, the floor of the chamber.

The origin of the hypothetical water-rich magma is more speculative. It might form at the top of the chamber and convect to the base, or form by absorption of water from the country rocks during convection down the sides of the chamber, or form in situ. In situ formation could result from a period of rapid crystallization near the floor or in the mush, enriching the magma in water more rapidly than diffusion or convection can remove it (cf. Weedon, 1960). Of these possibilities, the first two seem most likely. However, it is noted that there is little evidence for vigorous convection of magma during formation of the Western Layered Series.

c) Change in oxygen fugacity in the magma

It is conceivable that fO_2 changes at the base of the magma chamber, thereby altering the liquidus temperature. Phase relations of the margins of some layered intrusions as a function fO_2 have been determined by Biggar (1974). The olivine liquidus at 10^{-12} atm. is typically 5°C higher than that at 10^{-8} atm., and 12°C higher than that at 10^{-6} atm. Hence, even if the fO_2 of the harrisite parent magma decreased by six orders of magnitude, the supercooling induced would only be 12°C . Furthermore, decrease in fO_2 has the effect of reducing the forsterite content of olivine, contrary to the trend found for olivine in harrisite. If the forsterite content is to increase, the fO_2 must increase and this lowers, rather than raises,

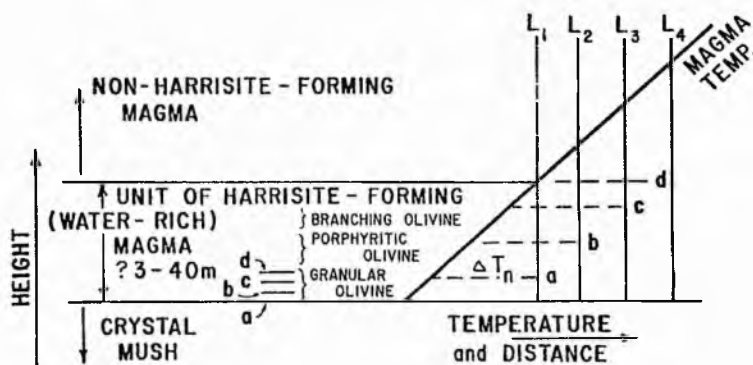


Fig. 50 Schematic representation of changes in liquidus temperature ($L_1 - L_4$) and the level of the chamber floor, during harrisite crystallization. Horizontal dashed lines are of uniform length (ΔT_n) and correspond to the degree of supercooling at which olivine nucleation rate is a maximum. Horizontal lines on left, labeled a, b, c and d, represent successive levels of the interface between the crystal mush and the magma and correspond to the heights at which ΔT_n has reached levels a, b, c and d. The type of olivine shape at each level in the resultant rock is indicated. (The slope of the liquidus temperature is ignored.)

the liquidus temperature. Hence, if fO_2 does increase during crystallization of harrisite, this cannot be the cause of the olivine supersaturation.

C. Summary of the conditions during formation of harrisite layers

The change in harrisite layers from unconstrained to constrained olivine growth implies that the thermal gradient in the magma did change in a manner consistent with removal of convection conditions. Hence, there is good evidence that this mechanism operated during harrisite formation. The relative values of the cooling rate due to convection cessation, and the liquidus temperature elevation due to water diffusion, are such that the former is a more rapid way of inducing supersaturation. From the detailed examination above, it is concluded that cessation of convection is the primary cause of supersaturation, and that water diffusion is of lesser importance.

The following sequence of events is suggested. During periods when the Rhum volcano was dormant, water-rich (but not saturated) magma formed at the chamber-top and, when it had cooled sufficiently, convected down the sides of the chamber to the floor. The magma cooled as it descended and the liquidus temperature increased. As it spread across the floor, any crystals in suspension settled (probably spinel and granular or polyhedral olivine). Convection ceased, causing heat to flow more rapidly into the floor. The cooling induced sufficient supersaturation of olivine in the hydrous magma to form granular olivines which sank to the floor (fig. 50). As water was evolved from the magma, the liquidus temperature rose ($L_1 \rightarrow L_4$, fig. 50) and the height at which abundant olivine nucleation took place (to yield granular olivines) also increased. Ultimately, ΔT in the unit of water-rich magma increased beyond the degree at which abundant olivine nucleates (ΔT), and far fewer olivines nucleated in the magma. These new crystals grew with externally skeletal shapes, and settled as porphyritic olivines. As the floor of the chamber rose further, and more water was evolved from the magma, nucleation of

olivine became very slow and linked parallel-unit olivine grew from the few olivines still suspended in the magma and on crystals at the rapidly-cooled boundary between the magma and the crystal mush (p. 108). Assuming that the level of the floor rose faster than the isotherms in the magma, the composition of the olivines in the harrisite layer become more magnesian upwards. (Cf. this model with the summary of constraints on harrisite petrogenesis, p. 106.)

It should be noted that supercooling below the level at which the maximum number of olivines nucleates (ΔT_n , fig. 50) always exceeds ΔT_n . The reason that this does not result in an anomalous, upward stratigraphy of branching olivine, porphyritic olivine, granular olivine (p. 109) is that such a large number of crystals settle into the more highly supercooled magma and compete for solute, thereby reducing the olivine growth rate relative to its true value for that degree of supercooling. Only once the number of crystals has reduced to the value more typical of spontaneous nucleation at these supercoolings, does the growth rate increase and skeletons and dendrites grow (see p. 69).

Occasional units of convected harrisite-forming magma were intruded below the interface between the crystal mush to magma into the Layered Series. These would immediately experience supercooling. Because the temperature in the mush is consistently less than that in the magma, these layers tend to show olivine morphologies typical of large supercooling (e.g., randomly oriented olivine).

The thickness of the layer of convected magma must remain conjectural (fig. 50). If the parent magmas of harrisite have the composition of each layer, then the layer of magma could be as thick as each rock layer. Since most harrisitic rocks probably represent differentiates of less mafic magma, the unit of supercooled magma must exceed the thickness of a harrisite layer. If the parent magma is a basalt with 24 wt. percent olivine (Brown, 1956), the 60 vol. percent of branching olivine in some Ard Mheall Series layers must

crystallize from a unit of magma at least 2.5 times thicker than the layer.

This model of harrisite formation differs from the crescumulus hypothesis in three respects. 1. Cooling of the magma occurs at the floor of the chamber due to enhanced heat flow into the floor. 2. The parent magma of harrisite was water-rich. 3. Skeletal and dendritic olivine in harrisite crystallized from a unit of supersaturated magma and not from cumulus crystals at the interface between magma and the floor. The term 'crescumulate' (p. 34) is therefore inappropriate to harrisite.

D. Absence of harrisite in other plutons

Jackson (1961) concluded that in sizeable magma bodies convection is inevitable. It seems reasonable to anticipate that in other layered plutons periods of stagnation alternated with periods of convection (e.g., Jackson, 1961). Why then is harrisite found in only one other pluton (Seiland; Robins, 1973)? Clearly there is something almost unique about solidification of the Rhum magma which promotes harrisite crystallization. I suggest three factors.

1. The water-rich character of the parent magma of harrisite which ensures low viscosity, and hence high diffusion rates and olivine growth rates.
2. The parent magma of the Rhum ultrabasic rocks was unusually olivine-rich (chapter XII) which favours growth of olivine skeletons and dendrites at slow cooling rates (p. 82).
3. The other factor stimulating harrisite formation is the apparently increasing temperature of the parent magmas of the Harris Bay Series, the Transition Series and the Ard Mheall Series. Wadsworth (1961) postulated that each Layered Series crystallized from a fresh influx of magma to the chamber. Thus, during crystallization of the Transition Series and the Ard Mheall Series, the magma chamber was undergoing a phase of warming following crystallization of the lower temperature Harris Bay Series cumulates. When convection did cease, the parent magma of the Transition Series overlaid cooler, eucritic rocks of the Harris Bay Series. This would promote heat loss

from the magma into the chamber floor and a resultant formation of harrisite, during stagnation. The Transition Series is considered to represent the first crystallization products of a fresh influx of magma to the chamber which later crystallized rocks of the Ard Mheall Series (Wadsworth, 1961). Dominance of the Transition Series by harrisite (p. 13) is consistent with this petrogenesis. In layered intrusions which crystallized from only one batch of magma, the residual magma becomes progressively cooler and the underlying cumulates are of comparable temperature. Heat flow into the floor is therefore much slower than that during harrisite formation and the cooling rate following cessation of convection is much smaller. (The presence of eucritic harrisite in the Harris Bay Series invites the speculation that the Harris Bay Series overlies a still less-refractory hidden Series of, for example, gabbroic rocks.)

Regional metamorphism precludes estimation of the original water content of the 'harrisite' in Seiland. However, Robins' (1973) statement that the Seiland pluton "possibly originated from at least two separate magma pulses and open system differentiation" is in accord with the the third of the three conditions considered necessary for the formation of harrisite in Rhum.

III Origin of vectorial crystallization in comb-layered rocks

To complete this chapter, the origin of the preferred elongation direction of olivine in comb-layered harrisite, and of elongate crystals in comb layers in general, is discussed and the essential conditions for vectorial crystal growth identified.

Wadsworth (1961, p. 60 - 61) ascribed the preferred elongation direction and crystallographic orientation of olivines in harrisite to competitive growth, suggesting that settled, cumulus crystals, oriented with (010) vertical, grew upward faster than crystals of other orientations. By "budding", these crystals expanded laterally, obstructing growth of adjacent crystals. In view of the lack of growth competition between oriented olivines in experiments simulating

harrisite (e.g., fig. 42) and in many harrisite layers (e.g., fig. 23), another cause of preferred elongation of crystals in comb-layered rocks is needed.

In comb-layered rocks, there is never evidence for unconstrained growth of the parallel, branching, elongate crystals within the magma chamber; instead they always crystallized at the walls and margins of magma bodies, or on cognate xenoliths (resulting in "orbicular" rocks; Van Diver and Magetti, 1973). These facts indicate that a substrate is necessary for branching crystal growth and also that a thermal gradient probably must exist in the magma. The value of the cooling rate at the crystallization location is critical to maintainance of conditions for comb layer formation. If the cooling rate increases, magma ahead of the advancing comb layer will supercool sufficiently to cause homogeneous nucleation in the bulk of the magma. By removing growth components from the magma, these new crystals will terminate elongate crystal growth in the comb layer. On the other hand, if the cooling rate decreases, the elongate crystals may reach into magma that is too little supercooled to permit continued elongate branching growth. Thus, the rate of advance of the isotherms in the magma should be comparable to the crystal growth rate. (It is possible that the upward textural change from comb-layered harrisite to cumulate might be the result of the isotherms advancing more rapidly than the elongate crystals).

Preferred elongation direction of crystals is consistently associated with directional crystallization (Knight, 1967). Therefore, in examining the petrogenesis of comb layering, both the cause of the uni-directional solidification (A), and the cause of preferred crystallographic orientation (B) require explanation.

(A) Uni-directional solidification results from (1) directed heat flow along a thermal gradient and/or (2) directed solute flow along a compositional gradient. To prevent disturbing these flow regimes, turbulence and convection in the magma must be negligible.

(1) When heat is withdrawn from a magma through a planar boundary, a thermal gradient is established at right angles to the boundary.

Along the gradient, elongate crystals grow in constrained fashion, from low temperature to high. This is the cause of the preferred elongation of crystals in ingots of rapidly cooled metals (e.g., Walton and Chalmers, 1959). In geological literature, crystal growth in which preferred elongation direction is dictated by a thermal gradient is called "thermotactic" (e.g., Drever and Johnston, 1972).

(2) With regard to concentration gradients as a cause of crystal orientation by directing solute flow, it is necessary to distinguish between conditions initiating elongate crystal growth and those maintaining it. The most likely location for directed solute flow in a magma chamber, resulting in initiation of oriented growth, is in magma just beyond a solidifying crystal mush at the floor or margins of the chamber. Here, flow of components exists, as ions within the mush exchange with those from the supernatant magma. Because the elongate crystals in comb layers grow in constrained fashion, the concentration gradient in the magma adjacent to each crystal will ensure continued directed flow of components toward the crystal (Lofgren and Donaldson, in press).

In cooling rate experiments reproducing comb-layered harrisite (e.g., fig. 42) elongate olivines did not grow along an externally applied thermal gradient. Neither can there have been a thermal gradient within charges, because the heat removal from charges is isotropic. Olivines, therefore, can grow vectorially for reasons other than directional heat flow. However, the marginal location of comb layers in magma bodies indicates that most of the layers did crystallize in a thermal gradient. There is unambiguous evidence that olivines in at least one layer of comb-layered harrisite (sample 74) crystallized along a marked thermal gradient.

(B) Preferred crystallographic orientation can be of two types: either (a) all three crystallographic axes of crystals have common orientation (e.g., linked parallel-unit olivine) and, hence, only one crystal (nucleus) exists (see p. 76) or (b) only one crystallographic direction, the elongation direction, is common to all crystals (e.g., olivines in the 'Mystery Dyke', Skye, and individual linked

parallel-unit olivines in a layer). The preferred crystallographic orientation of the units in each linked parallel-unit olivine in comb-layered harrisite is the result of fibrillation and repeated branching of an olivine which originally had a stable, planar interface with the magma (chapter IX). If, by branching, two upwardly growing linked parallel-unit olivines of different orientation (except for nearly parallel a axis elongation) expand sufficiently to interfere, one will inhibit further development of the other by competitive growth. However, it was not competitive growth that initiated the upward growth of olivine along the a axis.

Linked parallel-unit olivines in harrisite expand extensively because of their ability to branch. Elongate crystals in most comb layers branch less extensively, each crystal growing from a separate nucleus. Hence, the preferred crystallographic orientation must result from preferred nucleation orientation, or from preferred orientation as crystals become attached to a substrate, or from competitive growth. Published accounts of comb-layered rocks do not permit discrimination between these suggestions.

At particular growth conditions, the growth rate of olivine is markedly anisotropic. Presumably during comb layer formation the anisotropy is greatly enhanced when a particular crystallographic axis lies closely parallel to the direction of heat and/or solute flow. No satisfactory explanation can be offered for the difference in crystallographic orientation of elongate olivines between comb-layered harrisite and comb layers in the Mystery Dyke and the Slemish dyke (p. 25). Perhaps the thermal gradient and degree of supercooling were larger in the dykes and these affected the anisotropy.

In summary, certain criteria have to be fulfilled to cause formation of the oriented crystals in comb layers:

1. Cooling of the magma should be sufficiently rapid to form a thermal gradient at the margin of the magma body.
2. The isotherms and elongate crystals should advance at comparable rates.

3. The magma should be stagnant.
4. A planar substrate must exist within, or at the margin, of the magma body.
5. Suspended crystals of the phase growing in an elongate manner on the substrate should be absent or of low concentration in the magma.
6. The supercooling of the magma should be of the appropriate value to promote skeletal, branching crystal growth, i.e., the growth rate to diffusion coefficient ratio should be within a certain range (p. 77). It should also have a value at which the rate of homogeneous nucleation is low.

It is concluded that most comb layers, including comb-layered harrisite, are examples of thermotactic crystallization, but that crystallization in the absence of a thermal gradient can also cause the columnar, oriented crystal growth.

Chapter XII COMPOSITION OF THE RHUM MAGMA AND ITS
 REGIONAL SIGNIFICANCE

Because many harrisite layers contain only slightly zoned bytownite between the olivines, and since a high-alumina olivine tholeiitic magma was inferred to be parental to the Rhum Layered Series (Brown, 1956), olivine growth in harrisite was considered by both Wadsworth (1961) and Wager and Brown (1968) to proceed sufficiently slowly to permit adcumulus growth of plagioclase (i.e., to permit diffusion between the supernatant magma and the melt surrounding the growing olivines). In this manner, harrisite was believed to crystallize as a basaltic differentiate. This chapter considers the suitability of high-alumina olivine tholeiite as the parental magma of harrisite and of Rhum Layered Series rocks in general.

Olivine content and rate of fractional crystallization

Donaldson (1974a) argued that because the olivines in harrisite grew rapidly, a magma, with only 24 percent normative olivine [the high-alumina olivine tholeiite of Brown (1956)], would be an unlikely parental liquid for those peridotitic harrisites which contain linked parallel-unit branching olivines grown wholly in situ (e.g., sample 74). Calculations in this section demonstrate that this argument is wrong and that even at the fastest growth rates deduced for harrisitic olivines, it is possible to form a rock of 60 percent olivine which crystallized totally in situ from a basaltic parent magma.

Consider a linked parallel-unit olivine growing vertically upwards into supersaturated magma at a rate of 10^{-4} cm/s (chapter VII). Assume that the resultant rock contains 60 vol. percent olivine of composition Fo_{100} and that olivine is deposited only at the tips of the elongate crystals. The mass of crystalline olivine produced per second per cm^2 of floor area is 2.4×10^{-4} g; i.e., 2.6×10^{-6} moles of Mg is fixed in olivine per cm^2 .s. Assume that the parent magma contains 10.9 wt. percent MgO (Brown, 1956) and that all the MgO in the liquid becomes fixed as olivine. This magma contains 4.2×10^{-3} moles of Mg

per cm^3 ; one cm^3 of peridotite contains 2.3×10^{-2} moles of Mg. Therefore, at least 1.9×10^{-2} moles of Mg must diffuse into each cm^3 of rock during formation of the peridotite. This corresponds to a flow rate of Mg into the rock of 1.9×10^{-6} moles/ $\text{cm}^2 \cdot \text{s}$ (for a crystal growth rate of 10^{-4} cm/s).

Mg flows toward the growing olivines at a rate given by

$$J = \frac{(C_B - C_A) D}{\delta} \quad (\text{Donaldson, in press})$$

where J = flow rate

C_B = concentration of Mg in melt distant from the olivine

C_A = concentration of Mg in melt adjacent to the olivine

δ = concentration gradient thickness

D = diffusion coefficient of Mg at a given temperature

Donaldson (in press) found Mg concentration gradients 6 to 20 microns in thickness in basaltic glass adjacent to skeletal olivines. From the Stokes-Einstein equation, the diffusion coefficient of Mg at 1260° in this basalt was calculated as 1.5×10^{-8} cm^2/s . Taking δ as 10 microns, D_{Mg} as 1.5×10^{-8} cm^2/s , C_B as 10.9 wt. percent MgO and C_A as 1 wt. percent MgO, $J_{\text{Mg}} = 5.7 \times 10^{-8}$ moles/ $\text{cm}^2 \cdot \text{s}$. This value is 33 times smaller than the required flow rate of Mg. Medford (1973) has measured D_{Ca} in a mugearite melt. He reports a value 15 times greater than that calculated from the Stokes-Einstein equation at the same temperature. If it is assumed that the calculated value of D_{Mg} is also low by a factor of 15, then the value is only 2.2 times smaller than the required Mg flow rate. Reduction in the value of δ readily explains this remaining discrepancy. For example, if $\delta = 1$ micron, $J_{\text{Mg}} = 8.6 \times 10^{-6}$ moles/ $\text{cm}^2 \cdot \text{s}$. If C_A is then increased to 8.6 wt. percent MgO, J_{Mg} decreases to 1.9×10^{-6} moles/ $\text{cm}^2 \cdot \text{s}$; i.e., the required flow rate. This value of $C_B - C_A$ is more closely similar to that measured by Donaldson (in press) than the value calculated assuming C_A is 1 wt. percent MgO.

These calculations indicate that even if the parent magma of the Rhum intrusion were a basalt, it would be possible to form peridotite layers by rapid, directed, in situ crystallization. This rate of fractionation is probably many times faster than most petrologists would anticipate. However, formation of feldspathic peridotite by directed crystal growth at the margins of the 'Mystery Dyke' (Drever and Johnston, 1972; Lofgren and Donaldson, in press) and the Slemish dyke (Preston, 1963) testifies that this rate of fractionation is indeed possible. So also does the peridotite formed by branching olivine growth in cooling rate experiments (e.g., fig. 42). The key to rapid fractional crystallization is directed crystal growth.

I suggest that the radiate branching olivine in the harrisite layer in fig. 14a crystallized wholly in situ from a magma intruded into the Layered Series (p.30). The rock contains 28 wt. percent of branching olivine (determined by point counting on fig. 14a). Assuming that there is no lateral diffusion contact between the intrusion and a larger reservoir of supernatant magma, all the olivine must have crystallized from the intruded magma. Hence, the parent magma of the layer contained 28 wt. percent of normative olivine. This is 4 wt. percent more olivine than in the hypothetical magma of Brown (1956) and 3 wt. percent more than the maximum value of olivine normally considered to crystallize from a basalt (Wilkinson, 1968).

Normative plagioclase composition

Donaldson et al. (1973) and Donaldson (1975) argued that the normative plagioclase composition of the Rhum parent magma was bytownite rather than labradorite. The arguments respectively concerned the crystallization of poikilo-macrospherulites of bytownite in Rhum peridotite and the calcic nature of the plagioclase in the matrices of the ultrabasic breccias intruding the Layered Series and in the anorthosite veins associated with the breccias (cf. the calcic anorthosite veins in harrisite, p. 9).

A similar case in favour of calcic liquids in Rhum can be made from the bytownite in harrisite layers, particularly in those layers

containing branching olivine. It is clear that plagioclase always nucleated after olivine in Ard Mheall harrisite layers (cf. Wager, 1968, p. 160). Yet, much of it occupies narrow gaps between and within olivines and is still unzoned bytownite. Wager and Brown (1968) suggested that adcumulus (unzoned) crystal growth is restricted to the contact of a crystal mush with supernatant magma. Only if plagioclase growth occurred at the same rate as olivine growth, would it be possible to satisfy this condition for adcumulus crystallization of bytownite. It is more likely that plagioclase grew more slowly than olivine, most plagioclase thus growing within the framework of branching olivine. Diffusional contact between plagioclase and supernatant liquid would then be unlikely. Hence, in situ crystallization of unzoned bytownite can only occur if the trapped liquid is bytownite-normative. This liquid must have a higher Ca/Ca+Na ratio than basaltic magma. The normative plagioclase content of Brown's (1956) hypothetical Rhum magma is more sodic (An_{65}).

Summary and discussion

Textural features of the Rhum rocks suggest that they crystallized from olivine- and bytownite-enriched magmas. It seems that an olivine-rich eucritic magma was present in Rhum (cf. Donaldson 1974a, 1975); however, accurate determination of the parent magma composition for any of the Series is impractical. Brown's (1956) method of estimating the composition from the pore material in an olivine-plagioclase orthocumulate requires subjective discrimination between cumulus crystals and pore material and cannot allow for reaction between the cumulus crystals and the pore material. That his estimated composition is inaccurate is manifest by the unreasonably low normative pyroxene content (11.8 percent) of the melt, which results in a high normative olivine content (24 percent).

Of the analyses made of Rhum rocks in this study (Table 22), sample 28(C) is the most reasonable representative of a melt composition. In terms of the normative requirements of the melt for approximately 28 percent olivine (last page), a composition between samples 28(C) and 89(E) is most likely. There is no more

accurate way of estimating the composition.

Such a composition has characteristics transitional between the picritic and the high-lime liquids recognized by Drever and Johnston (1966). A similar magma was probably the parent of the Sgurr Dubh intrusion (Gibb, 1968) and the White Allivalite (Hutchison, 1968), Skye. However, the greater fayalite content of the olivines in Rhum compared with those in the Skye rocks suggests that the Rhum magma was more fractionated with respect to Mg/Mg+Fe ratio.

Certain properties of the magma can be deduced from this study.

1. It fractionates to form Ti-rich, undersaturated liquids which precipitate silica-unsaturated minerals (kaersutite and phlogopite).
2. The likely liquidus pO_2 of the magma was approximately 10^{-8} atm. (p. 64), which compares well with the value determined by Gibb and Henderson (1971) for an olivine eucrite dyke in Skye.
3. The temperature of the magma could have ranged between 1135° and 1385° (Appendix II).
4. The fractionation trend of pyroxenes from this magma (fig. 26) is different from that of basaltic pyroxenes.
5. The magma has closer affinity to the Hebridean low alkali tholeiite (Thompson, 1974) than the alkali olivine basalt suite.

Regional significance of the magma

Another Tertiary ultrabasic pluton has been identified in the Blackstones region, 60 miles south-west of Rhum (McQuillin and Binns, 1973). If it is assumed that this also crystallized from an olivine-rich eucritic magma, there are three closely spaced, co-linear plutons (Skye, Rhum and Blackstones) at the centre of the Hebridean Province in which are represented hotter parent magma types than any of those toward the periphery of the province. This means that these magma types are generated at particularly hot localities in a regionally hot area. This conclusion is compatible with Thompson's (1974) suggestion that the Hebridean tholeiite represents a more extensive upper mantle partial melt than the alkali olivine basalt which dominates the Province. The following tectonic interpretation is attempted. The belt of Tertiary magmatism extending from western Scotland into N. Ireland

delineates a location of tension and continental rifting (i.e., an incipient spreading axis). Following modern theory of mid-ocean ridge magma genesis (e.g., Green, 1971), an elongate, wedge-shaped diapir of mantle peridotite, oriented NE-SW, rose below western Scotland in the early Tertiary. From various localities along the diapir, magmas were tapped off from the partially molten peridotite to yield the basalts of Skye, the Inner Hebrides and Ireland. It is suggested that the eucritic magmas segregated from areas of extensive partial melting along the apex of the diapiric wedge. These would also represent the locations of maximum tension, where rifting of western Scotland would have begun, if the magmatic activity (and presumably the mantle diapirism) had not suddenly ceased.

The narrow, linear nature of the Hebridean magmatic belt, the short duration of magmatic activity and its contemporaneity with opening of the Atlantic, all indicate that the magmatism must be related to the tension associated with opening of the Atlantic. One line of future research in this area should be a synthesis of the different magmatic styles and magma compositions throughout the Hebridean Province, in terms of a common event of mantle upwelling. The change from alkali basalt to tholeiitic magmas with age of the Province (Thompson, 1974) and its relation to, and implications for, the cessation of mantle diapirism, also merits investigation. As more becomes known, through drilling, about the origin and fractionation of magmas at the Mid-Atlantic Ridge (e.g., Melson et al., 1974), the Scottish Tertiary Igneous Province may provide crucial petrogenetic evidence for comparison with mid-ocean ridge volcanism and prediction of its evolution with time.

CHAPTER XIII IMPORTANCE OF METASTABLE CRYSTALLIZATION IN
PLUTONS AND FUTURE USE OF NON-EQUILIBRIUM
EXPERIMENTAL PETROLOGY

The theme of this thesis has been a reinvestigation of the origin of harrisite by means of the shapes of the olivine crystals in the rock. The conclusions are relevant to the origin of all comb-layered rocks and the differentiation mechanisms by which they are produced. The experimental methods used suggest new approaches for the study of non-equilibrium (dynamic) crystallization of igneous rocks. In this chapter the implications of deep-seated, metastable fractional crystallization are summarized and the aspects of layered plutons still needing research are identified. The prospects for further non-equilibrium experimental studies are also considered.

1. Comb layers and metastable fractional crystallization

It has been shown that rapid crystallization on the bottom and near the bottom of a major plutonic magma chamber is possible. The crystallization takes place under large, and initially increasing, supersaturation conditions. Once steady state crystallization is achieved and directed, in situ crystallization begins, fractional crystallization is rapid. Similar large degrees of supersaturation and rates of crystal growth and fractional crystallization probably occur during crystallization of comb layers in other plutons and in minor intrusions and lavas. Necessary conditions for comb layer formation are: cessation of magma convection, a sufficiently large contrast in temperature between magma and rocks at the margin or floor of a magma body, and comparable rates of crystal growth and isotherm advance into the magma. If it is the cessation of convection which promotes harrisite formation, other layered intrusions probably contain layers of branching minerals, for temporary cessation of convection is a likely event in large chambers of convecting magma (Jackson, 1961). These layers will most likely be found close to the margin of the body, but chambers into which magma has repeatedly been injected may show

comb layering parallel to the floor.

The fractional crystallization of olivine, and possibly of other minerals, from the Rhum magma during harrisite formation took place under conditions of significant departure from equilibrium (large degree of supercooling). This disequilibrium must change the composition of the residual liquids relative to those resulting from near-equilibrium (near-liquidus temperature) crystallization and fractionation. If these residual liquids are expelled from the magma chamber as lavas, dykes and sills, the metastable fractional crystallization will increase the 'noise' (Carmichael et al., 1974) in chemical trends determined from the lavas and minor intrusions. Metastable plutonic crystallization may be responsible for anomalous rock compositions in other petrologic provinces.

2. Questions concerning the crystallization of large bodies of magma

This work highlights current ignorance of the crystallization of large bodies of magma in respect of nucleation, growth rate and controls of the supersaturation of phases. Each of these parameters is critical in development of the various types of cumulate distinguished by Wager et al. (1960). The following questions are of particular importance. How are the growth rate, nucleation rate and supersaturation of a phase affected as the concentration of crystals in suspension in a magma decreases due to crystal settling (p. 69)? How does preferential settling of olivine from a magma affect the crystallization (nucleation, growth rate, growth mechanism and composition) of more slowly settling pyroxene and plagioclase crystals? How does the proportion of each phase in a suspension of crystals affect crystallization of other phases? How rapidly, and over what distance can diffusion between intercumulus melt and supernatant magma take place to prevent zoning of cumulus crystals? Further crystallization experiments in which crystal settling and its effects can be studied should help understand these kinetic aspects of the crystallization of magmas and explanation of the petrographic features of rocks.

3. Application of non-equilibrium experiments

By cooling melts from above the liquidus temperature, the textures and mineral chemistry features of igneous rocks can be modelled (Donaldson et al., 1975; this thesis). For example, the morphologies and morphology distributions of olivine in harrisite were reproduced, together with the low Ca content of the olivine. This type of experiment aids deduction of the crystallization history of the natural rock.

Cooling experiments have enabled interpretation of the crystallization, thermal and emplacement histories of lunar basalts (Lofgren et al., 1974). Similar experiments on ternary feldspar melts were used by Lofgren and Donaldson (in press) to investigate crystallization of curved and branching crystals in comb layers and to reject a hydrous fluid as the parent material (Moore and Lockwood, 1973). This type of experiment is, therefore, useful in obtaining thermal information about the crystallization of natural rocks and their mineral chemistry. It also can be used to obtain kinetic data on the nucleation rates, incubation times and growth rates of minerals in igneous rocks. Specific petrogenetic problems or controversies can be examined (e.g., Lofgren et al., 1974) and information about the origin of rock textures obtained. Thus, non-equilibrium experimentation is as powerful a petrogenetic tool as is 'equilibrium' experimental petrology. The difference between the two types of experiment is the difference between a dynamic system and a static system.

4. Further types of non-equilibrium experimentation

Non-equilibrium experiments can be of petrogenetic use in three further ways.

i. By cooling a melt at a fixed rate and quenching it at various temperatures, the fractional crystallization path of the liquid (residual glass) can be ascertained. By examining this fractionation path at various cooling rates, it will be possible to predict the effect of cooling rate on fractional crystallization and liquid line of descent.

ii. By combining two internally heated pressure vessels in series, one containing samples and the other acting as a 'pressure reservoir', it is possible by heating or cooling the reservoir vessel at a controlled rate to effect controlled, polybaric or isobaric crystallization. If the sample vessel can also be varied in temperature, controlled polybaric and polythermal crystallization can be achieved. A few runs, not reported in this thesis, have been made at constant temperature crystallizing water-saturated peridotite melts by decreasing pressure at a controlled rate. A layered run product like harrisite and like that in fig.42 resulted. This type of experiment could be useful in studying polybaric fractional crystallization of magmas as they rise in the crust. As O'Hara (1968) has noted, fractionation of mantle-derived liquids is dependent on the rates at which they rise and cool in the crust. Only by polybaric, polythermal crystallization experiments can the chemical evolution of rising magmas be examined.

iii. The technique can also be applied to partial melting experiments. Until now, experimental investigation of the compositions of magmas generated in the mantle by partial melting have involved isothermal, equilibrium-type experiments (e.g., Kushiro et al., 1972). It seems likely that the rate at which the parent rock is heated and decompressed affects the composition of the partial melt. This possibility could be examined using the experimental approach described here.

It is the aim of the petrologist to understand the origin of rocks. As illustrated by the laboratory synthesis of harrisite, one of the most satisfactory ways of achieving this aim is to model the petrographic features of rocks, and the processes by which they form. Encouragement for attempting to model other aspects of petrogenesis by the above experimental techniques may be found in the present study.

ACKNOWLEDGMENTS

I am grateful to my supervisors, Professor H.I. Drever and R. Johnston, for their guidance, their patience and their suggestion that I go to the Johnson Space Center.

The advice, interest, discussion and kindness of friends in 'Building 31' and the Lunar Science Institute, Houston will always be remembered. To R. Brett, J. Chamberlain, G. Lofgren, R. Pepin, A. Reid (who nobly acted as American supervisor) and R. Williams, I owe sincere thanks for the opportunities and freedom given me to develop my own research and become involved in their work. The chance to study problems apparently unrelated to my own topic was critical in providing stimulation and preventing stagnation in personal studies.

Much of the data presented could not have been obtained without the technical genius of O. Mullins and the care taken of the microprobe by R. Brown. J.M. Rhodes kindly gave instruction in the techniques of XRF'ing, Fe³'ing and H₂O'ing and D. Blanchard performed the neutron activation analyses for Na. The equations for heat flow treatment were suggested by W. Mendell.

I am indebted to the Natural Environment Research Council for a NATO Studentship and to the Lunar Science Institute for a Visiting Graduate Fellowship. The Director of the Nature Conservancy (Scotland) kindly permitted visits to Rhum and free collection of samples. The help of P. Wormell and his staff in moving the samples is gratefully appreciated. Mrs. L. Mager kindly typed numerous, impeccable drafts of the papers written while at the LSI. For access to the facilities of the NASA Johnson Space Center, I am grateful to the American people.

H. I. Drever, R. Johnston, G. Lofgren, A. Reid and R. Williams kindly reviewed early drafts of this manuscript.

Finally, I wish to thank the Reids, Arch, Mary, Karen, Gavin and Shona, for 'adopting' me into their family. They are greatly missed in Houston.

REFERENCES

- Anderson, A.T. 1967. Possible consequences of composition gradients in basalt glass adjacent to olivine phenocrysts. EOS (Trans. Amer. Geophys. Union), **48**, 227-228.
- Bailey, E.B. 1945. Tertiary igneous tectonics of Rhum (Inner Hebrides). Q. J. Geol. Soc. Lond., **100**, 165-191.
- Bence, A.E. and Albee, A.L. 1968. Empirical correction factors for the electron microanalysis of silicates and oxides. J. Geol., **76**, 382-403.
- Berg, J.H. 1974. Snowflake troctolite and crescumulate layering in the Hettasch Intrusion. EOS (Trans. Amer. Geophys. Union), **55**, 486.
- Biggar, G.M. 1974. Phase equilibrium studies of the chilled margins of some layered intrusions. Contrib. Mineral. Petrol., **46**, 159-167.
- Black, G.P. 1952. The Tertiary volcanic succession of the Isle of Rhum, Inverness-shire. Trans. Edin. Geol. Soc., **15**, 39-51.
- Bochvar, A.A. 1935. The Mechanism and Kinetics of Crystallization in Eutectic-type Alloys. Moscow.
- Bottlinga, Y., Kudo, A. and Weill, D. 1966. Some observations on oscillatory zoning and crystallization of magmatic plagioclase. Amer. Min., **51**, 792-806.
- Brooks, C. and Hart, S.R. 1974. On the significance of komatiite. Geology, **2**, 107-110.
- Brothers, R.N. 1964. Petrofabric analyses of Rhum and Skaergaard layered rocks. J. Petrol., **5**, 255-274.
- Brown, G.M. 1956. The layered ultrabasic rocks of Rhum, Inner Hebrides. Phil. Trans. R. Soc., **B**, **240**, 1-53.
- Brown, G.M. 1963. Melting relations of Tertiary granitic rocks in Skye and Rhum. Min. Mag., **33**, 533-562.
- Brown, G.M. 1968. Mineralogy of basaltic rocks. In H. H. Hess and A. Poldervaart (eds.): Basalts, vol. 1, 103-162. New York.
- Brown, G.M., Emelius, C.H., Holland, J.G., Peckett, A. and Phillips, R. 1972. Mineral-chemical variations in Apollo 14 and Apollo 15 basalts and granitic fractions. Proc. 3rd Lunar Sci. Conf. (Suppl. 3, Geochim. Cosmochim. Acta), **1**, 141-157.
- Bryan, W.B. 1972a. Morphology of quench crystals in submarine basalts. J. Geophys. Res., **77**, 5812-5819.
- Bryan, W.B. 1972b. Mineralogical studies of submarine basalts. Carnegie Inst. of Washington, Ann. Rept. Dir. Geophys. Lab., **71**, 396-403.
- Buckley, H.E. 1951. Crystal Growth. New York.
- Buddington, A.F. and Lindsley, D.H. 1964. Iron-titanium oxide minerals and synthetic equivalents. J. Petrol., **5**, 310-357.
- Burnham, C.W. 1967. Hydrothermal fluids at the magmatic stage. In H. L. Barnes (ed.): Geochemistry of Hydrothermal Ore Deposits, p. 14-76. New York.
- Cameron, E.N. 1969. Postcumulus changes in the Eastern Bushveld complex. Amer. Min., **54**, 744-779.
- Carmichael, I.S.E., Turner, F.J. and Verhoogen, J. 1974. Igneous Petrology. New York.
- Carlaw, H.S. and Jaeger, J.C. 1959. Conduction of Heat in Solids. Oxford.
- Chalmers, B. 1964. Principles of Solidification. New York.
- Compston, W., Berry, H., Vernon, M.J., Chappell, B.W. and Kaye, M.J. 1971. Rubidium-strontium chronology and chemistry of lunar material from the Ocean of Storms. Proc. 2nd Lunar Sci. Conf. (Suppl. 2, Geochim. Cosmochim. Acta), **2**, 1471-1485.
- Conroy, D.S. 1963. Trends and affinities of basaltic magmas and pyroxenes as illustrated on the diopside-olivine-silica diagram. Min. Soc. Amer. Spec. Paper, **1**, 227-250.
- Deer, W.A., Howie, R.A. and Zussman, J. 1962a. Rock-Forming Minerals. Vol. 3 Sheet Silicates. London.
- Deer, W.A., Howie, R.A. and Zussman, J. 1962b. Rock-Forming Minerals. Vol. 5 Non-Silicates. London.
- Deer, W.A., Howie, R.A. and Zussman, J. 1963. Rock-Forming Minerals. Vol. 2 Chain Silicates. London.
- Dodd, R.T. and Calef, C. 1971. Twinning and intergrowth of olivine crystals in chondritic meteorites. Min. Mag., **38**, 324-327.
- Donaldson, C.H. 1974a. Olivine crystal types in harrisitic rocks of the Rhum pluton and Archean spinifex rocks. Geol. Soc. Amer. Bull., **85**, 1721-1726.
- Donaldson, C.H. 1974b. Experimental investigation of olivine morphology. Geol. Soc. Amer. Ann. Meeting Abstracts with Programs, v. 6, 712.
- Donaldson, C.H. 1974c. Calculated diffusion coefficients and the growth rate of olivine. EOS (Trans. Amer. Geophys. Union), **55**, 460-461.
- Donaldson, C.H. 1975. Ultrabasic igneous broccias in layered intrusions — the Rhum complex. J. Geol., in press.
- Donaldson, C.H. In press. Calculated diffusion coefficients and the growth rate of olivine in a basalt magma. Lithos.
- Donaldson, C.H., Drevor, H.I. and Johnston, R. 1973. Crystallization of poikilo-macrospherulitic feldspar in a Rhum peridotite. Nature Phys. Sci., **241**, 69-70.
- Donaldson, C.H., Brown, R.W. and Reid, A.M. In press. Petrology and chemistry of basalts from the Nazca Plate; Part I - Petrography and mineral chemistry. Initial Reports of the Deep Sea Drilling Project.
- Donaldson, C.H., Williams, R.J. and Lofgren, G.E. 1975. A sample holding technique for study of crystal growth in silicate melts. Amer. Min., in press.
- Doramus, R.H. 1973. Glass Science. New York.
- Drevor, H.I. and Johnston, R. 1957. Crystal growth of forsteritic olivine in magmas and melts. Trans. Roy. Soc. Edin., **63**, 289-315.
- Drevor, H.I. and Johnston, R. 1958. The petrology of picritic rocks in minor intrusions - A Hebridean Group. Trans. Roy. Soc. Edin., **63**, 459-499.
- Drevor, H.I. and Johnston, R. 1966. A natural high lime liquid more basic than basalt. J. Petrol., **7**, 414-420.
- Drevor, H.I. and Johnston, R. 1972. Metastable growth patterns in some terrestrial and lunar rocks. Meteoritics, **7**, 327-340.
- Drevor, H.I., Johnston, R., Butler, P. and Gibb, F.G.F. 1972. Some textures in Apollo 12 lunar igneous rocks and in terrestrial analogs. Proc. 3rd Lunar Sci. Conf. (Suppl. 3, Geochim. Cosmochim. Acta), **1**, 171-184.
- Dunham, A.C. 1964. A petrographic and geochemical study of back-veining and hybridization at a gabbro-felsite contact in Coire Dubh, Rhum, Inverness-shire. Min. Mag., **33**, 887-902.
- Dunham, A.C. 1965a. The nature and origin of the groundmass textures in felsites and granophyres from Rhum, Inverness-shire. Geol. Mag., **102**, 8-23.
- Dunham, A.C. 1965b. A new type of banding in ultrabasic rocks from central Rhum, Inverness-shire, Scotland. Amer. Min., **50**, 1410-1420.
- Dunham, A.C. 1970. The emplacement of the Tertiary igneous complex of Rhum. In G. Newall and N. Rast (eds.): Mechanism of Igneous Intrusion, Geol. J. Spec. Issue, **2**, 23-32.
- Dunham, A.C. and Emelius, C.H. 1967. The Tertiary geology of Rhum, Inner Hebrides. Proc. Geol. Assn., **78**, 391-418.
- Evans, B.W. and Moore, J.G. 1968. Mineralogy as a function of depth in the prehistoric Makaopuhi tholeiitic lava lake, Hawaii. Contrib. Mineral. Petrol., **17**, 85-115.
- Evans, B.W. and Wright, T.L. 1972. Composition of liquidus chromite from the 1959 (Kilauea Iki) and 1965 (Makaopuhi) eruptions of Kilauea volcano, Hawaii. Amer. Min., **57**, 217-230.

- Evans, A.L., Fitch, F.V. and Miller, J.A. 1973. Potassium-argon age determinations on some British Tertiary igneous rocks. J. Geol. Soc., **129**, 419-444.
- Fenn, P.M. 1973. Nucleation and growth of alkali feldspars from melts in the system $\text{NaAlSi}_3\text{O}_8\text{-H}_2\text{O}$. Ph.D. thesis, Stanford Univ. 145 pp.
- Ferguson, J. and Wright, I.H. 1970. Compositional variation of plagioclases in the Critical Series, Bushveld complex. In J. Willense (ed.): Bushveld Igneous Complex and Other Layered Intrusions, Symposium. Geol. Soc. S. Afr., Spec. Publ. 1, 59-66.
- Fouqué, F. and Michel-Lévy, A. 1881. Réproduction des Basalts d'melaphyres labradoriques, des diabases et dolerites à structure ophitique. Bull. Soc. Min. Fr., **5**, 277-279.
- Frazier, J.Z., Fitzgerald, R.W. and Reid, A.M. 1966. Computer programs EMX and EYX2 for electron microprobe data processing. Scripps Instn. of Oceanography Rept.
- Gibb, F.G.F. 1968. Flow differentiation in the xenolithic ultrabasic dykes of the Cullins and the Strathaird Peninsula, Isle of Skye, Scotland. J. Petrol., **9**, 411-443.
- Gibb, F.G.F. 1971. Crystal-liquid relationships in some ultrabasic dykes and their petrological significance. Contrib. Mineral. Petrol., **30**, 103-118.
- Gibb, F.G.F. and Henderson, C.M.B. 1971. The magmatic oxygen fugacity of an ultrabasic dyke. Contrib. Mineral. Petrol., **30**, 119-124.
- Goranson, R. 1937. Silicate-water systems: The 'osmotic' pressure of silicate melts; Amer. Min., **22**, 485-490.
- Gray, N.H. 1971. A parabolic hourglass structure in titanite. Amer. Min., **56**, 952-958.
- Green, D.H. 1971. Composition of basaltic magmas as indicators of conditions of origin: application to oceanic volcanism. Phil. Trans. R. Soc., A, **268**, 707-725.
- Green, D.H., Ringwood, A.E., Ware, N.G., Hibberson, W.O., Major, A. and Kiss, E. 1971. Experimental petrology and petrogenesis of Apollo 12 basalts. Proc. 2nd Lunar Sci. Conf. (Geochim. Cosmochim. Acta, Suppl. 2), **1**, 601-615.
- Harker, A. 1908a. Geological Survey of the United Kingdom one-inch map of Scotland, Sheet 60.
- Harker, A. 1908b. The Geology of the Small Isles of Inverness-shire. Mem. Geol. Surv. Scotland.
- Harker, A. 1909. The Natural History of the Igneous Rocks. London.
- Holz, R.T. 1973. Phase relations of basalts in their melting range at $P_{\text{H}_2\text{O}} = 5 \text{ kb}$ as a function of oxygen fugacity. Part I. H_2 Mafic phases. J. Petrol., **14**, 249-302.
- Henderson, P. 1975. Reaction trends shown by chrome-spinels of the Rhum layered intrusion. Geochim. Cosmochim. Acta, in press.
- Henderson, P. and Suddaby, P. 1971. The nature and origin of the chrome-spinel of the Rhum layered intrusion. Contr. Mineral. Petrol., **33**, 21-31.
- Henderson, P., MacKinnon, A. and Gale, N.H. 1971. The distribution of uranium in some basic igneous cumulates and its petrological significance. Geochim. Cosmochim. Acta, **35**, 917-925.
- Hess, H.H. 1960. Stillwater igneous complex, Montana: a quantitative mineralogical study. Geol. Soc. Amer. Mem., **80**, 230 pp.
- Hess, P.C. 1970. Polymer model of silicate melts. Geochim. Cosmochim. Acta, **35**, 289-306.
- Holloway, J.R. 1969. Composition of fluid phase solutions in a basalt- H_2O - CO_2 system. Geol. Soc. Amer. Bull., **82**, 233-237.
- Holloway, J.R. 1971. Internally heated pressure vessels. In G.C. Ulmer (ed.): Research Techniques for High Pressure and High Temperature, 217-258. New York.
- Hughes, C.J. 1960a. The Southern Mountains igneous complex, Isle of Rhum. Q. J. Geol. Soc. Lond., **116**, 111-138.
- Hughes, C.J. 1960b. An occurrence of Tilleyite-bearing limestone in the Isle of Rhum, Inner Hebrides. Geol. Mag., **97**, 384-388.
- Hutchison, R. 1968. Origin of the White Allivalite, western Cullin, Isle of Skye. Geol. Mag., **105**, 338-347.
- Jackson, E.D. 1961. Primary textures and mineral associations in the Ultramafic Zone of the Stillwater Complex, Montana. U. S. Geol. Surv. Prof. Paper, **358**, 1-106.
- Jackson, E.D. 1971. The origin of ultramafic rocks by cumulus processes. Fortschr. Miner., **48**, 128-174.
- Jackson, K.A. 1958. Interface Structure. In R. H. Doremus, B. W. Roberts and D. Turnbull (eds.): Growth and Perfection of Crystals, 319-323. New York.
- Jackson, K.A. 1974. The present state of the theory of crystal growth from the melt. J. Crystal Growth, **24/25**, 130-136.
- Jackson, K.A., Uhlmann, D.R. and Hunt, J.D. 1967. On the nature of crystal growth from the melt. J. Crystal Growth, **1**, 1-36.
- Jaeger, J.C. 1968. Cooling and solidification in igneous rocks. In H. H. Hess and A. Poldervaart: Basalts, vol. 2, 503-536.
- Judd, J.W. 1874. The secondary rocks of Scotland. Second paper. On the ancient volcanoes of the Highlands and the relations of their product to the Mesozoic strata. Q. J. Geol. Soc. Lond., **30**, 220-301.
- Judd, J.W. 1885. On the Tertiary and older peridotites of Scotland. Q. J. Geol. Soc. Lond., **41**, 354-418.
- Judd, J.W. 1889. The Tertiary volcanoes of the Western Isles of Scotland. Q. J. Geol. Soc. Lond., **45**, 187-218.
- Kadik, A.A. 1971. Heat effects of separation of water and melting of silicates in hydrous silicate melts at high pressures. Geochim. Int., **8**, 179-185.
- Koel, K., Prinz, M., Planner, H.N., Skaggs, S.R., Dowty, E., Nelson, L.S., Richardson, N.L. and Blander, H. 1973. A qualitative comparison of textures in lunar chondrules and CO_2 laser-formed synthetic chondrule-like spherules. Spec. Publ. Univ. New Mexico Inst. of Meteoritics, **7**, 16 pp.
- Keith, H.D. and Padden, F.J. 1963. A phenomenological theory of spherulitic crystallization; J. Appl. Phys., **34**, 2409-2421.
- Khitrov, N.I. and Kadik, A.A. 1973. Water and carbon dioxide in magmatic melts and peculiarities of the melting process. Contrib. Mineral. Petrol., **41**, 205-215.
- Kirkpatrick, R.J. 1975. Crystal growth from the melt: A review. Amer. Min., in press.
- Klein, L. and Uhlmann, D.R. 1974. Crystallization behavior of anorthite. J. Geophys. Res., **79**, 4869-4874.
- Knight, C.A. 1967. The Freezing of Supercooled Liquids. New York.
- Krumbein, W.C. and Pettijohn, F.J. 1936. Manual of Sedimentary Petrography. New York.
- Kushiro, I., Shimizu, N., Nakamura, Y. and Akiyama, S. 1972. Compositions of coexisting liquid and solid phases formed upon melting of natural garnet and spinel ilmenites at high pressure: a preliminary report. Earth and Planet. Sci. Lett., **14**, 19-25.
- Leake, B.E. 1968. A catalog of analyzed calciferous and sub-calciferous amphiboles together with their nomenclature and associated minerals. Geol. Soc. Amer. Spec. Paper, **98**, 210 pp.
- Le Bas, M.J. 1962. The role of aluminium in igneous clinopyroxenes with relation to parentage. Amer. J. Sci., **260**, 267-288.
- Lonarcic, J. 1903. Über gegenseitige Löslichkeit und Ausscheidungsgänge der Mineralien im Schmelzflusse. Zbl. Miner. Geol. Paläont., **A**, 743-751.

- Leung, I.S. 1974. Sector-zoned titanagites; morphology, crystal chemistry, and growth. Amer. Min., 59, 127-138.
- Loveson, D.J. 1973. Origin of comb layering and orbicular structure, Sierra Nevada Batholith, California: Discussion. Geol. Soc. Amer. Bull., 84, 4005-4006.
- Lewis, J.D. 1971. "Spinifex texture" in a slag, as evidence for its origin in rocks. Western Australia Geol. Surv. Ann. Rept., 60-68.
- Lewis, J.D. and Williams, I.R. 1973. The petrology of an ultramafic lava near Murphy Well, Eastern Goldfields, Western Australia. Western Australia Geol. Surv. Ann. Rept., 60-68.
- Lofgren, G.E. 1968. Experimental devitrification of rhyolite glass. Ph.D. thesis, Stanford Univ. 99 pp.
- Lofgren, G.E. 1974. An experimental study of plagioclase crystal morphology; isothermal crystallization. Amer. J. Sci., 274, 243-273.
- Lofgren, G.E. and Donaldson, C.H. 1973. Experimental evidence bearing on the origin of "Comb (Willow Lake) layering". Geol. Soc. Amer. Annual Meeting Abstracts with Programs, v. 5, 716.
- Lofgren, G.E. and Donaldson, C.H. In press. Curved branching crystals and differentiation in comb-layered rocks. Contr. Mineral. Petrol.
- Lofgren, G.E., Donaldson, C.H., Williams, R.J., Mullins, O. and Usselman, T.M. 1974. Experimentally reproduced textures and mineral chemistry of Apollo 15 quartz normative basalts. Proc. 5th Lunar Sci. Conf. (Suppl. 5, Geochim. Cosmochim. Acta), 1, 549-568.
- Martin, R.F. and MacLean, W.H. 1973. Crystal growth forms in hawaiitic lavas of Heimay, Iceland. Geol. Soc. Amer. Ann. Meeting Abstr. with Programs, v. 5, 726-727.
- MacCulloch, J. 1819. A Description of the Western Isles of Scotland. London.
- McQuillin, R. and Dinns, P.E. 1973. Geological structure in the Sea of Hebrides. Nature Phys. Sci., 241, 2-4.
- McQuillin, R. and Tuson, J. 1963. Gravity measurements over the Rhum Tertiary plutonic complex. Nature, 199, 1276-1277.
- Medford, G.A. 1973. Calcium diffusion in a mugearite. Can. J. Earth Sci., 10, 394-402.
- Melson, W.G. et al. 1974. Leg 37 - the volcanic layer. Geotimes, 19, 16-18.
- Merrill, R.B. and Wyllie, P.J. 1973. Absorption of iron by platinum capsules in high pressure rock melting experiments. Amer. Min., 58, 16-20.
- Mitchell, R.H. 1973. Magnesian ilmenite and its role in kimberlite petrogenesis. J. Geol., 81, 301-311.
- Moore, W.J. 1965. Physical Chemistry. New Jersey.
- Moore, J. G. and Lockwood, J.P. 1973. Origin of comb layering and orbicular structure, Sierra Nevada Batholith, California. Geol. Soc. Amer. Bull., 84, 1-20.
- Morozewicz, J. 1899. Experimentelle untersuchungen über die bildung der minerale in magma. Miner. Petrogr. Mitt., 18, 177-197.
- Mossman, D.J. 1973. Geology of the Greenhills ultramafic complex, Bluff Peninsula, Southland, New Zealand. Geol. Soc. Amer. Bull., 84, 39-62.
- Nature Conservancy, 1969. Geology of the Isle of Rhum National Nature Reserve. Booklet published by Natural Environment Research Council.
- Nesbitt, R.W. 1971. Skeletal crystal forms in the ultramafic rocks of the Yilgarn Block, Western Australia: Evidence for an Archean ultramafic liquid. Spec. Publ. Geol. Soc. Austral., 1, 331-347.
- Nesbitt, R.W. and Hamilton, D.L. 1970. Crystallization of an alkali-olivine basalt under controlled P , P_{O_2} , P_{H_2O} conditions. Phys. Earth Planet. Interiors, 3, 309-315.
- O'Hara, M.J. 1968. The bearing of phase equilibria studies in synthetic and natural systems on the origin and evolution of basic and ultrabasic rocks. Earth Sci. Rev., 4, 69-133.
- O'Hara, M.J., Biggar, G.M., Richardson, S.W., Ford, C.E. and Jamieson, B.G. 1970. The nature of seas, mascons and the lunar interior in the light of experimental studies. Proc. 1st Lunar Sci. Conf. (Suppl. 1, Geochim. Cosmochim. Acta), 1, 695-710.
- Osborn, E.F. 1959. Role of oxygen pressure in the crystallization and differentiation of basaltic magma. Amer. J. Sci., 257, 609-647.
- Phillips, F.C. 1938. Mineral orientation in some olivine-rich rocks from Rhum and Skye. Geol. Mag., 75, 130-135.
- Platten, I.M. and Watterson, J.S. 1969. Oriented crystal growth in some Tertiary dykes. Nature, 223, 286-287.
- Foldervaart, A. and Hess, H.H. 1951. Pyroxenes in the crystallization of basaltic magma. J. Geol., 59, 472-489.
- Portevin, A. 1928. Le basalte fondu. Mém. Soc. Ing. Civ. Fr., 4, 266-300.
- Preston, J. 1963. A columnar crystallization of olivine and plagioclase. Geol. Mag., 100, 1-6.
- Prinz, M. and Mehru, C.E. 1969. Comments on "Kaesutite from San Carlos, Arizona, with comments on the paragenesis of this mineral" by Brian Mason. Min. Mag., 37, 333-337.
- Pyke, D.R., Naldrett, A.J. and Eckstrand, O.R. 1973. Archean ultramafic flows in Munro Township, Ontario. Geol. Soc. Amer. Bull., 84, 955-978.
- Ridley, W.I. 1971a. Some chemical features of basalts from the British Tertiary Province. Earth Planet. Sci. Lett., 11, 435-439.
- Ridley, W.I. 1971b. The petrology of some volcanic rocks from the British Tertiary Province: The islands of Rhum, Eigg, Canna and Muck. Contr. Mineral. Petrol., 32, 251-266.
- Ridley, W.I. 1973. The Petrology of Volcanic Rocks from the Small Isles of Inverness-shire. Rep. Inst. Geol. Sci. No. 73/10, 55 pp.
- Robins, B. 1973. Crescumulate layering in a gabbroic body on Seiland, northern Norway. Geol. Mag., 109, 533-542.
- Rutter, J.W. and Chalmers, B. 1953. A prismatic substructure formed during solidification of metals. Can. J. Phys., 31, 15-39.
- Saratovkin, D.D. 1959. Dendritic Crystallization. New York.
- Sato, M. 1971. Electrochemical measurements and control of oxygen fugacity and other gaseous fugacities with solid electrolyte systems. In G. C. Ulmer (ed.): Research Techniques for High Pressure and High Temperature.
- Scarfe, C.M. 1973. Viscosity of basic magmas at varying pressure. Nature Phys. Sci., 241, 101-102.
- Shaw, H.R. 1972. Viscosities of magmatic silicate liquids: An empirical method of prediction. Amer. J. Sci., 272, 870-893.
- Simkin, T. and Smith, J.V. 1970. Minor element distribution in olivine. J. Geol., 78, 304-325.
- Spidel, D.H. 1970. Effect of magnesium on the iron-titanium oxides. Amer. J. Sci., 268, 341-353.
- Spidel, D.H. and Nafziger, R.H. 1968. P-T-f_{O₂} relations in the system Fe-O-MgO-SiO₂. Amer. J. Sci., 266, 361-379.
- Stewart, F.H. 1965. Tertiary Igneous Activity. In G. Y. Craig (ed.): The Geology of Scotland, 420-466. Edinburgh.
- Switzer, G., Melson, W.G. and Thompson, G. 1972. Olivine crystals from the floor of the Mid-Atlantic Ridge near 22°N latitude. In W. G. Melson (ed.): Mineral Sciences Investigations, 1969-1971. Smithsonian Contributions to Earth Sciences, 9, 43-46.

- Tammann, G. 1925. The States of Aggregation. New York.
- Taubeneck, W.H. 1974. Petrologic implications of comb (Willow Lake) layering in the Skaergaard Intrusion, East Greenland, and in other selected intrusions in Northern Ireland and western North America. Research Proposal to the National Science Foundation.
- Taubeneck, W.H. and Poldervaart, A. 1960. Geology of the Elkhorn Mountains, northeastern Oregon; Part 2. Willow Lake intrusion. Bull. Geol. Soc. Amer., 71, 1295-1322.
- Thompson, R.N. 1974. Primary basalts and magma genesis. I Skye, north-west Scotland. Contrib. Mineral. Petrol., 45, 317-341.
- Tiller, W.A. 1964. Dendrites. Science, 146, 871-879.
- Tomkeleff, S.I. 1942. The Tertiary lavas of Rhum. Geol. Mag., 79, 1-13.
- Tomkeleff, S.I. 1945. On the petrology of the ultrabasic and basic rocks of the Isle of Rhum. Min. Mag., 27, 127-136.
- Turnbull, D. 1948. Transient nucleation. Trans. AIME, 175, 774-783.
- Tuttle, O.F. 1949. Two pressure vessels for silicate-water studies. Geol. Soc. Amer. Bull., 60, 1727-1729.
- Vance, J.A. 1969. On Synneusis. Contrib. Mineral. Petrol., 24, 7-29.
- Van Diver, B.B. and Maggetti, M. 1973. Comb layering and orbicular structure in the Reichenbach orbiculite, Odenwald, West Germany. Geol. Soc. Amer. Annual Meeting Abstracts with Programs, 7, 846-847.
- Vogt, J.H.L. 1884. Studier om Slagger. Bih. Svensk. Vetensk. Akad. Handl., 2, 3-10.
- Wadsworth, W.J. 1961. The layered ultrabasic rocks of south-west Rhum, Inner Hebrides. Phil. Trans. R. Soc., B, 244, 21-64.
- Wadsworth, W.J. 1973. Magmatic sediments. Minerals Sci. Engng., 5, 25-35.
- Wager, L.R. 1968. Rhythmic and cryptic layering in mafic and ultramafic plutons. In H. H. Hess and A. Poldervaart (eds.): Basalts, vol. 2, 573-622. New York.
- Wager, L.R. and Brown, G.M. 1951. A note on rhythmic layering in the ultrabasic rocks of Rhum. Geol. Mag., 88, 166-168.
- Wager, L.R. and Brown, G.M. 1968. Layered Igneous Rocks. Edinburgh.
- Wager, L.R., Brown, G.M. and Wadsworth, W.J. 1960. Types of igneous cumulates. J. Petrol., 1, 73-85.
- Wager, L.R. and Deer, W.A. 1939. Geological investigations in East Greenland. Part III. The petrology of the Skaergaard intrusion, Kangerdlugssuaq, East Greenland. Medd. om Grønland, 105, 352 pp.
- Walton, D. and Chalmers, B. 1959. The origin of preferred orientation in the columnar zone of ingots. Trans. Metall. Soc. AIME, 215, 447-456.
- Weedon, D.S. 1960. The Gars-Bheinn sill, Isle of Skye. Q. J. Geol. Soc., 116, 37-54.
- Wilkinson, J.F.G. 1968. The petrography of basaltic rocks. In H. H. Hess and A. Poldervaart: Basalts, vol. 1, 163-214.
- Williams, R.J. 1972. A solid ceramic electrolyte system for measuring redox conditions in high-temperature gas mixing studies. NASA Tech. Memorandum 58105.
- Winkler, H.G.F. 1947. Kristallgrosse und Abkühlung. Heidelberger Beiträge Mineral. Petrol., 1, 86-104.
- Wyllie, P.J. 1963. Effects of the changes of slope occurring on liquidus and solidus paths in the system diopside-anorthite-albite. Min. Soc. Amer. Special Paper 1, 204-212.
- Yoder, H.S. and Tilley, C.E. 1962. Origin of basalt magmas: An experimental study of natural and synthetic rock systems. J. Petrol., 1, 342-532.

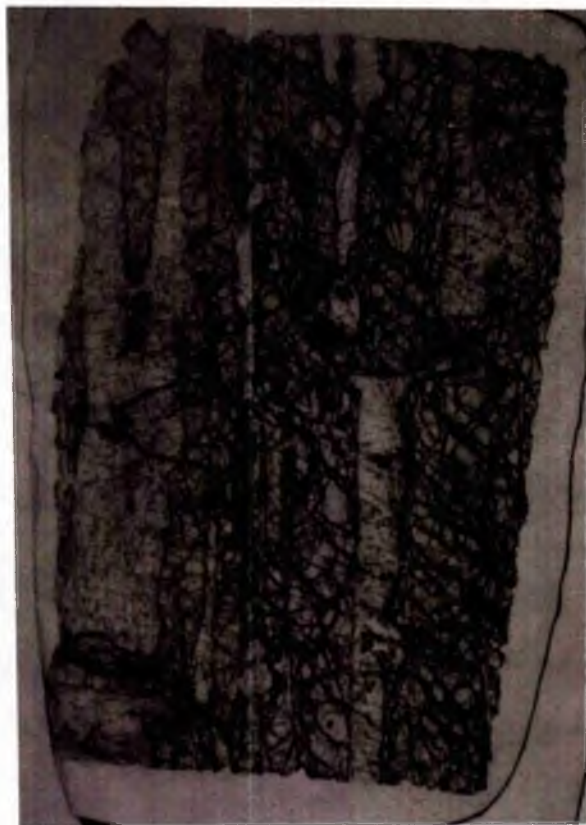


Fig. 51 Thin section of sample 74B showing the linked parallel-unit olivine with interstitial plagioclase (white) and augite (light grey). Plane polarized light. Length of section 3.2 cm.

Appendix I PETROGRAPHY OF ROCKS INVESTIGATED BY ELECTRON
MICROPROBE

Compositions of olivine, plagioclase and pyroxene, determined by electron microprobe analysis, are summarized for each rock in Table 2, together with the locations of samples. Brief petrographic descriptions of three other harrisite samples and their contiguous facies are presented in chapter V. Minerals in five thin sections through one of these layers (sample 211) were analyzed by electron microprobe.

Sample 74B, M and T

A large single linked parallel-unit olivine of indeterminable growth direction extends through the outcrop of comb-layered harrisite (Table 2). Individual units of the crystal are 1 - 0.1 cm thick, with similar-sized spaces between (fig. 51). The centre of the crystal is more magnesian than both the top and the bottom (Table 2). One olivine grain in the three thin sections studied is grossly out of crystallographic orientation with the elongate parallel-unit olivine. It is 0.5 x 0.2 cm in size, is subhedral in outline and is 1.5 mol. percent richer in Fo than the branching crystal. The vertically-oriented units of the branching crystal are elongate parallel to a.

Plagioclase forms euhedral tablets (0.1 x 0.3 cm), or anhedral plates (up to 1.5 cm across) either interstitial to, or subophitically enclosing, olivine. Compared to crystals at the top and middle of the layer, those at the base show less extensive peripheral zoning and the cores of crystals are more sodic (Table 2).

Anhedral grains of augite vary from 5.5 to 1 cm across. Some grains adopt highly elongate forms between the olivine fibres (fig. 51). Many crystals contain irregular trains of magnetite grains and nests of kaersutite, phlogopite and green hornblende. Both abrupt and continuous marginal zoning are visible.

In addition to being enclosed by pyroxene, olivine and plagioclase, anhedral chrome-magnetite crystals (0.2 - 0.05 cm across) also occupy indentations in olivines. Anhedral ilmenite grains (up to 0.2 cm across) are associated with hydrous phases.

Olivine or chrome magnetite may have nucleated first in this rock. The zoning pattern of the branching olivine could indicate nucleation of the crystal at the centre of the outcrop, followed by concomitant upward and downward growth. As discussed in chapter VIII, it is more likely that growth was consistently upward and the composition change reflects local temperature variation. Whatever the growth direction, the olivine fibres of the branching crystal engulfed chrome-magnetite grains which were present in a low concentration in the magma. Melt between the olivine fibres subsequently nucleated plagioclase, followed by pyroxene, and then by kaersutite, phlogopite and ilmenite. Olivine may have continued to grow through part, or all, of this period. Alteration of plagioclase to prehnite and zeolites



Fig. 52 Diffuse seam of spinel grains enclosed, or partially enclosed, in a single unit of linked parallel-unit olivine in sample 89A. Plane polarized light. Field of view 2 mm.

and of pyroxene to tremolite and hornblende was post magmatic. The chrome-magnetite crystals and the single subhedral olivine are interpreted as cumulus grains. Scarcity of subhedral olivine suggests a very low concentration of cumulus olivines during growth of branching crystals.

Sample 89A and B (two thin sections)

The linked parallel-unit olivines are deeply indented like that in sample 74, but they differ in lacking a preferred elongation direction; all units are elongate parallel to a, but that direction is randomly oriented for each crystal. Individual units terminate in dome faces. The crystals are up to 9 cm long by 1 cm wide and comprise up to six linked parallel-units. Both plagioclase and pyroxene occur as anhedral grains (up to 4 cm across) in subophitic or interstitial relation to the olivine. Euhedral chrome-magnetite grains (0.25 - 0.05 cm across) invariably are located along one side of an olivine, either wholly enclosed, or occupying an indentation in the olivine. The grains form trains parallel to the length of olivines (fig. 52), but not necessarily parallel to the horizontal plane.

The paragenetic sequence and mineral compositions of sample 89 are similar to sample 74, the nucleation rate of olivine was, however, greater. Only the chrome-magnetite crystals could be construed as settled grains. The random orientation of the linked parallel-unit olivines in the sample may be an indication of gentle current action, in contrast to stagnation promoting vertical growth in sample 74.

Sample 140

The thin section studied encompasses the peridotite underlying a harrisite layer and the base of the harrisite layer. On a scale of 1 cm or less, there is gradational upward change in both mineral proportions and texture. The modal analysis in Table 2 is for the complete thin section.

At the base of the section, olivine is subequant (up to 2 mm in size) and subhedral in shape. Crystals are poikilitically or subophitically enclosed by anhedral augite grains up to 4 mm across. Upwards, the olivines become highly elongate (5 x 0.4 mm) parallel to the plane of the layering, and the place of augite is totally taken over by interstitial plagioclase crystals, less than 1.5 mm across. Further upwards, the petrographic features return to those at the base of the section, which in turn give way to a further zone of elongate skeletal olivine and interstitial plagioclase. Plagioclase crystals in this zone are extensively altered to prehnite, grossular and clinozoisite. There is another upward change in olivine shape from elongate to subequant porphyritic crystals up to 1 cm across. Round chrome-magnetite crystals (0.05 mm or less in size) are preferentially located in the zones containing pyroxene and are very rare in zones containing plagioclase. Minerals are of uniform composition in all

zones.

Olivine continuously settled from the magma along with variable proportions of chrome magnetite. Below the harrisite zone (that containing skeletal olivine), these crystals were engulfed by the growth of either augite or plagioclase. The repetitious change in olivine morphology, chrome magnetite content and change from plagioclase to pyroxene crystallization (or vice versa) were concurrent events and the operation of some controlling cyclic physical-chemical factor(s) during formation of the rock seems likely. Plagioclase and pyroxene probably nucleated in situ, so that if the changes in texture and phase proportion did coincide, crystallization of olivine and chrome magnetite must have occurred close to the floor of the chamber.

Sample 189

The rock texture is dominated by bladed, linked parallel-unit olivine with dome terminations, and the elongation direction (a) of the units is inclined at 70° to the vertical. Crystals are as much as 0.8 m long and each parallel growth unit is 0.3 to 1 cm wide. A few crystals contain strain lamellae, transverse to the elongation direction. Channels between olivine units are filled by anhedral augite crystals (0.5 cm across) and by a mosaic of anhedral plagioclase grains (each approximately 0.3 cm across). Larger spaces are occupied by single plagioclase crystals (up to 1.5 cm across). One anhedral grain of orthopyroxene was found (1.5 x 2.5 cm) subophitically enclosing olivine. Large (0.2 - 0.6 mm diameter) anhedral magnetites are almost all located within olivine crystals.

The texture and paragenesis of this Harris Bay harrisite resembles that of Ard Mheall sample 74, except for the appearance of orthopyroxene. Upward growth of branching olivines and entrapment of settling magnetite grains are inferred, and some plagioclase may be cumulus. The transverse lamellae in some olivines and the mosaic plagioclase texture, are attributed to strain recrystallization during cooling of larger single crystals. All the minerals are of lower temperature varieties than those in sample 74 (Table 2).

Sample 17

Olivine crystals are elongate, anhedral, randomly oriented, porphyritic skeletons, up to 1 x 0.1 cm in size. Round indentations and lobes are prominent. Most crystals subophitically enclose euhedral plagioclase laths (up to 0.5 x 0.2 cm in size) which have unzoned cores and continuous normally-zoned mantles. Many small (0.1 mm or less), round or lath-shaped plagioclases are enclosed by olivine crystals. Anhedral augite and bronzite crystals up to 1.5 mm across ophitically or subophitically enclose plagioclase laths and olivine skeletons. Kaersutite and phlogopite are present as anhedral grains (0.2 - 0.3 mm in size) between plagioclase laths and in olivine embayments.

Subhedral and anhedral magnetite crystals (0.2 mm or less in size) abound within indentations in olivine grains. A few crystals are located within olivine and pyroxene grains, but are never enclosed by plagioclase.

Textural relations indicate that the paragenetic sequence was plagioclase followed by olivine and then augite and orthopyroxene. Magnetite apparently nucleated contemporaneously with olivine. Kaersutite and phlogopite postdate olivine crystallization.

Two petrogenetic interpretations seem possible. 1) Crystallization may have been wholly in situ, involving crystallization of plagioclase followed by magnetite, skeletal olivine and finally pyroxene. 2) Plagioclase ± olivine and magnetite settled from the magma while pyroxene crystallized in situ. The disparity in grain size of plagioclase crystals enclosed by olivine, and those occurring as large laths, does suggest that the olivine skeletons and the plagioclase laths have not crystallized in the same location. It is possible that the olivines nucleated on small plagioclase crystals in a unit of magma overlying or underlying that crystallizing the plagioclase laths, and subsequently, due to differing settling rates of the olivine crystals and the plagioclase laths, the two phases became associated. Magnetite apparently nucleated in the same location as the olivine. The rock is olivine rich (38 vol. percent, Table 2), effectively ruling out suggestion 1). The random orientation of the olivine is attributable, not to in situ crystallization, but to settling concurrent with abundant plagioclase crystals.

This rock indicates that olivine need not be the liquidus phase of a magma in order to form harrisite and that olivine is morphologically more sensitive than plagioclase as an index of crystallization under supersaturation conditions.

Samples 200(1) and (2)

Upwards through this layer, olivine crystals change in shape, size and degree of preferred orientation. At the base of the layer, crystals are elongate (3 x 0.4 mm in size) and porphyritic in shape. There is marked preferred orientation of crystals with the elongation direction parallel to the layering. Upwards, crystals become larger (up to 13 x 0.3 mm in size), are randomly oriented and change to chain-like shapes. There is a slight, but significant, increase in Fo content of the olivine with stratigraphic height (Table 2). Lath-shaped plagioclase crystals also become coarser upwards, changing in size from 2 x 1 mm to 8 x 2 mm, and grains totally enclosed by pyroxene are 1.5 x 1 mm in size. Zoning is absent or patchy, or of marginal normal type. Plagioclase crystals poikilitically or subophitically enclose olivine crystals and are themselves subophitically enclosed by augite. Anhedral, subequant augite crystals are up to 4 mm across. Schiller structure imparts a variegated light- and dark-brown colour to crystals. Phlogopite and kaersutite form equant, anhedral crystals up to 1.5 mm across in interstitial relation to olivine and plagioclase

and in irregular intergrowths with augite and ilmenite. Discrete subhedral crystals of magnetite (0.2 mm in size) are mostly confined to the interior or margins of olivine crystals.

It is inferred that olivine and magnetite nucleated above the floor, but close to it, and that both phases then settled on to the floor. The random orientation of olivines high in the layer may indicate cessation of settling, or intersection of the location of olivine nucleation with the crystal mush to magma interface. It is also inferred that each mineral nucleated at a particular level in the magma (cf. Jackson, 1961). Nucleation of magnetite above olivine, in turn above plagioclase would be consistent with textural relations observed in the rock. Initially abundant skeletal olivines settled with plagioclase; later the number of crystals of each of these phases decreased (Table 3). The absence of preferred orientation of plagioclase crystals suggests a lack of current action during deposition.

Sample 182

The sample contains white gabbroic pegmatite (I) in contact with eucritic harrisite containing porphyritic olivine (IIa), overlain by eucritic harrisite with parallel growth olivine (IIb).

I. Extensively-altered euhedral plagioclase laths (as much as 4.5 x 0.6 cm in size) are either poikilitically enclosed by anhedral pyroxene or are separated by interstitial pyroxene crystals up to 1 cm across. Some plagioclases have elongate, faceted 'channels' occupied by pyroxene and forming an intrafasciculate texture (Drever *et al.*, 1972). The plagioclase is not zoned adjacent to the channels. As in other rocks, apatite is preferentially located with hydrous minerals, suggesting that the last melt to crystallize was rich in P, Cl and F (Table 11). The pegmatite is devoid of magnetite, but contains large, elongate ilmenite crystals up to 2 x 0.5 mm.

IIa. The space in and around each subequant, porphyritic olivine (up to 1 cm across) is occupied by plagioclase laths (0.3 x 0.15 cm), ophitic pyroxene (1.0 x 0.6 cm) and small anhedral phlogopite, kaersutite and magnetite crystals.

IIb. Olivine crystals as large as 1.4 x 0.4 cm are preferentially oriented with the b axis vertical, but are otherwise in random orientation. Plagioclase forms euhedral laths (2.7 x 0.8 mm) or subequant crystals (1 mm across), some in glomerophytic groups, subophitically enclosing olivine and subophitically enclosed by anhedral augite (up to 5 mm across). The extent of normal continuous zoning varies among plagioclases. Hydrous phases are more abundant than in zone IIa.

The gradational change in both texture and grain size between zones indicates that the pegmatite is generated in situ, rather than being intrusive. The sequence of events may have commenced with crystallization and flowage of tabular, parallel-growth olivine and, from a pocket of trapped, water-enriched melt olivine grew as large, porphyritic crystals. Plagioclase and pyroxene subsequently nucleated in situ with decreasing

nucleation density from zone IIb → IIA → I. The intrafasciculate texture suggests rapid crystallization of the pegmatite due to intensified supersaturation (Drever *et al.*, 1972).

The change from abundant olivine crystals in zone IIb to few crystals in zone IIA resembles the upward change in olivine nucleation density and grain size in some harrisite layers. These similarities favour the possibility that harrisite also crystallizes due to an in situ change in physical-chemical conditions of the magma.

Samples 204, 171 and 163

These gabbroic pegmatites closely resemble one another in mineral content and texture. All contain large, euhedral plagioclase laths (up to 2 x 0.3 cm in size) subophitically enclosed by anhedral augite (up to 2 cm across). With progressive distance inside the pegmatite (*i.e.*, away from the enclosing ultrabasic rock), the pyroxene content diminishes and the alteration of plagioclase increases. Close to the ultrabasic rock, plagioclases are continuously normally zoned from bytownite to labradorite; away from the ultrabasic rock, a clouded rim of albite ($An_3 - 0.5$) mantles plagioclases. Space between laths is occupied by albite, phlogopite, skeletal ilmenite (up to 1 cm long), chlorite, green hornblende, prehnite, scolecite, clinozoisite, apatite and rare calcite crystals. Of these three samples, only sample 204 contained olivine (Fo_{54}). Plagioclase and pyroxene compositions are members of the solid solution series corresponding to a lower temperature than crystals in harrisite (Tables 2, 5 and 6). Plagioclase crystals are extensively zoned and have core compositions similar to those in adjacent harrisite. Crystallization was sufficiently fast to allow extensive normal zoning of plagioclase and also zoning of Al, Ti and Cr in the augite (Table 5).

The 'saussurite' assemblage of albite, prehnite, scolecite and calcite is attributed to post-magmatic metasomatism of plagioclase. The progressive increase in saussuritization away from the enclosing ultrabasic rock indicates that the water was not introduced to the rocks, but resided within each pegmatite. The pegmatites crystallized progressively inwards into a pool of trapped melt and are therefore interpreted as extreme fractional crystallization products of the parent melt of harrisite. The dyke of pegmatite (sample 171) indicates that the residual melt of harrisite crystallization was occasionally mobilized and intruded into the Layered Series.

Sample 22

This gabbro layer ("Glen Duain gabbro" of Wadsworth, 1961) intrudes a harrisite layer. It is banded: a central layer (6 cm thick) of dark, coarse-grained pegmatite (I) is overlain and underlain by 3 cm thick layers of white microgabbro (II).

I. The rock texture is porphyritic, with two generations of pyroxene. The earliest phase to crystallize was anhedral, unzoned, pale brown augite (crystals up to 0.2 cm across), now partially altered to green hornblende. The second generation of pyroxenes

(0.02 cm in diameter) has identical composition to the phenocrysts, except for higher Al and Ti content and less Si. These round crystals are either interstitial to, or are enclosed by, subhedral, continuously-zoned plagioclases (0.2 cm across, An₄₇ - ₄₁ in composition). Round granules of ilmenite (0.05 mm maximum size) and grains of clinozoisite and apatite are abundant.

II. Large euhedral augite crystals (up to 1.0 x 1.5 cm in size) and tabular euhedral plagioclases (up to 1.5 cm long) dominate the texture of this rock. Pyroxene, subophitically enclosing some plagioclase crystals, has a homogeneous core surrounded by a homogeneous mantle of different composition, in turn surrounded by a continuously-zoned margin. Some pyroxene crystals exhibit crude sector zoning and contain inclusions of phlogopite and kaersutite. Plagioclase also has a homogeneous core sharply separated from a continuously-zoned mantle. Alteration of plagioclase to sodic plagioclase, thomsonite, scolecite, prehnite and clinozoisite is extensive. Both plagioclase and augite may enclose, or be enclosed by, ilmenite.

The facies change from microgabbro to gabbroic pegmatite is abrupt. There is, however, no evidence for multiple intrusion or flow differentiation of magma. It is suggested that an intrusion of water-rich basic magma, containing small pyroxene phenocrysts of the size in zone I, cooled rapidly to form the microgabbro. Water was concentrated in the uncrystallized melt, lowering the nucleation density of both augite and plagioclase and promoting coarser grain size (zone II). The sector-zoning in the pyroxenes suggests accelerated crystal growth from a magma supersaturated in augite (Leung, 1974).

These rock types lack olivine and have an obscure relationship to the ultrabasic rocks (Wadsworth, 1961), but they share certain features with harrisite. These include the abundance of hydrous minerals, the evidence for accelerated growth rate under conditions of supersaturation and the contrast in nucleation density between the pegmatite and the microgabbro (cf. harrisite and cumulate). The pegmatite itself resembles the gabbroic pegmatite patches in harrisite (last page). It is not unreasonable that the Glen Duain gabbros represent intrusions of residual hydrous liquid from the differentiation of eucritic magma. This suggestion is favoured by the intrusive nature of pegmatite sample 171 (last page).

Appendix II EXPERIMENTAL TECHNIQUES AND EXPERIMENTAL PETROLOGY
 STUDY OF SIX RHUM ULTRABASIC ROCKS

A. Types of experiment

The following kinds of experiment were performed:

- i. Subjecting a powdered rock or glass to various pressure-temperature conditions to determine the phase relations of samples. This was done using the methods of Yoder and Tilley (1962).
- ii. Melting powdered rock or glass at $25 - 100^{\circ}$ above the liquidus temperature, then rapidly cooling to a predetermined temperature and re-equilibrating. This is distinguished as an "isothermal supercooling experiment".
- iii. Melting under similar conditions to ii, but cooling the melt at a controlled monotonic rate.

Isothermal runs are made by turning off power to the furnace and re-applying it gradually, as the crystallization temperature is approached. In an internally-heated pressure vessel cooling by 100° takes 20 s, by 200° takes 70 s. The same temperature drops in a gas-mixing furnace require 300 s and 650 s, respectively. Crystallization in isothermal runs was for 20 - 21 hours.

Cooling rate control is effected by means of a programmed controller (manufactured by DATATRACK SYSTEMS, DENVER) which progressively reduces input power to the furnace. The limit on cooling rate is set by the speed at which the furnace can respond to power removal at a given temperature. An internally-heated pressure vessel may be cooled as fast as $14,000^{\circ}/\text{hr}$, a gas-mixing furnace as fast as $2000^{\circ}/\text{hr}$. The slowest cooling rate investigated was $0.5^{\circ}/\text{hr}$.

Charges from isothermal and cooling rate crystallization runs are examined with binocular microscope or scanning electron microscope to study three-dimensional crystal morphology, where melt has decanted from around crystals. Thin sections of the charges are prepared and selected sections polished for electron microprobe study. The charges are photographed and the olivine morphology tabulated according to the classification scheme in chapter IV.

B. Hydrous versus anhydrous experiments

i. Hydrous systems

An internally-heated pressure vessel (Tuttle, 1949) is used to provide the experimental run conditions of $P = 2$ or 5 ± 0.1 kb water pressure and temperatures from $800 - 1250 \pm 3^{\circ}\text{C}$. High purity argon is the pressure medium. Samples (<100 mesh rock powders stored at 110°C under vacuum) are loaded with $1 - 45 \pm 0.5$ wt. percent of triply distilled water and sealed in platinum capsules. Phase relations are determined on 30 mg of material in 2 mm diameter capsules (310 mg). Crystallization experiments are performed with 50 mg of material in 3mm diameter capsules (420 mg). At 5 kb, the rocks are saturated with 3 - 4 wt. percent water. The capsule loading and opening techniques described by Holloway (1971) are used.

The hydrous experiments involve two uncontrolled chemical parameters, Fe loss from the melt to the capsule and unknown and changing $f\text{O}_2$. By using a large sample mass to sample container mass

and working at high f_{O_2} (10^{-2} - 10^{-4} atm.), the dramatic Fe losses reported by Merrill and Wyllie (1973) during high pressure piston-cylinder experiments are avoided.

ii. Anhydrous systems

Most experiments at 1 atm. were performed in a gas-mixing furnace (Williams, 1972) in which f_{O_2} is continuously monitored by an electrolyte cell (Sato, 1971). Samples are supported on a loop of platinum wire and run in the manner described by Donaldson et al. (1975).

Phase relations of the Rhum samples at 1 atm. were determined under different conditions. Relations below 1430° were investigated in platinum capsules placed in an externally-heated alumina muffle tube through which a gas mixture of $N_2/H_2 = 10/1$ is passed at 0.5 SCFH. Relations were also determined in air up to 1650° in a DELTECH furnace, using platinum capsules or graphite crucibles (Table 25). Oxygen fugacity in the N_2/H_2 mixture is calculated to be 10^{-15} atm. at 1100° , taking the water content of the gas as 0.2 wt. percent.

In both hydrous and anhydrous experiments, the f_{O_2} decreases during cooling; no attempt is made to prevent this. The experiments are therefore similar to the cooling of natural igneous rocks which are closed to access of an oxygen source (e.g., water). It should be noted that cooling an internally-heated pressure vessel lowers the gas pressure. Hence, experiments in the pressure vessel involve combined polythermal and polybaric crystallization.

C. Samples

The samples used and the experiments performed on each are listed in Table 21 in which the composition and phase relations of the lunar analogues studied are referenced. The compositions of the samples are given in Table 22.

D. Experimental petrology of six ultrabasic rocks from the Rhum pluton (Tables 23, 24 and 25)

The phase relations of Rhum rocks, obtained primarily for evaluation of the olivine shapes and textures in isothermal and cooling rate crystallization experiments, have some petrogenetic applications, as discussed below.

1. Textural relations of the natural rocks indicate that green hornblende apparently formed by reaction of pyroxene + plagioclase + fluid, after all the plagioclase had crystallized. Assuming the rocks were water-saturated at 900° , only at pressures less than 2.5 kb (fig. 53) can these conditions for reaction be fulfilled. Hence, harrisite crystallized at depths less than 9.5 km. (If the rocks were water-undersaturated, the stability limit of amphibole might shift to higher temperature and pressure.) The Layered Series has been estimated from field and petrographic evidence to have been uplifted between 1500 m (Brown, 1963) and 4000 m (Dunham, 1970), so that the rocks crystallized at pressures between 0.5 and 1.2 kb. The

Table 21. Summary of samples used in olivine crystallization experiments and types of experiment conducted on each.

Sample	Type	Reference to composition	Olivine liquidus temp. °C	Reference to phase relations	Experiments conducted	Oxygen fugacity range atm.	Source of sample
Apollo 12 olivine basalt 12009	Synthetic glass	Compston <u>et al.</u> (1971)	1230	Green <u>et al.</u> (1971)	Isothermal supercooling Cooling rate	10^{-12} - 10^{-14}	C. Simonds
Apollo 15 quartz-normative basalt	Synthetic glass	Lofgren <u>et al.</u> (1974)	1215	Lofgren <u>et al.</u> (1974)	Isothermal supercooling Cooling rate	10^{-12} - 10^{-15}	R. Williams
Apollo 11 high titanium basalt	Synthetic glass	Table 21	1170	O'Hara <u>et al.</u> (1970)	Isothermal supercooling Cooling rate	10^{-12} - 10^{-16}	T. Usselman
89 Eucritic harrisite (E)	Rock powder	Table 21	1360	This thesis Table 25	Phase relations Isothermal supercooling Cooling rate	10^{-6} - 10^{-8}	Self

Sample	Type	Reference to composition	Olivine liquidus temp. °C at $P_{H_2O} = P_{total} = 5kb$	Reference to phase relations	Experiments conducted	Oxygen fugacity range atm.	Source of sample
189 Euclitic harrisite (A)	Rock powder	Table 21	1225	Table 23, 24 and 25	Phase relations at 5kb and 2kb $P_{H_2O} = P_{total}$ and at 1atm. Isothermal supercooling and cooling rate at 5kb.	$10^{-0.2} - 10^{-15}$	Self
74 Peridotitic harrisite (B)	"	Same	1270	Same	Same	Same	Self
89 Peridotitic harrisite (E)	"	Same	1130	Same	Same	Same	Self
215 Euclitic harrisite (F)	"	Same	1130	Same	Same	Same	Self
28 Euclitic harrisite (C)	"	Same	1100	Same	Phase relations at 5kb and 2kb $P_{H_2O} = P_{total}$ and at 1atm.	Same	Self
132 Anorthosite vein (D)	"	Same	1090	Same	Same	Same	Self

Table 22. Compositions of Rhum rocks and synthetic lunar basalts in experimental petrology studies (see Tables 2 and 21 for sample descriptions).

Sample	189(A) ¹	74(B) ¹	28(C) ¹	132(D) ¹	89(E) ¹	215(F) ¹	Apollo 12 ²	Apollo 15 ²	Apollo 11 ²
SiO ₂	42.75	39.85	44.59	44.68	42.48	42.36	45.03	48.04	42.33
TiO ₂	0.62	0.32	1.11	0.23	0.25	1.03	2.85	1.76	10.64
Al ₂ O ₃	9.01	5.25	12.54	20.79	14.78	8.70	10.44	11.19	8.76
Fe ₂ O ₃	1.51	3.13	3.59	1.19	2.05	3.16	—	—	—
FeO	11.59	10.63	7.53	5.37	8.44	9.13	16.20	18.03	17.58
MnO	0.23	0.23	0.19	0.10	0.17	0.21	0.27	0.28	0.22
MgO	22.03	31.25	14.80	13.25	18.56	23.72	11.65	9.18	7.89
CaO	7.21	4.25	9.80	10.96	8.79	6.41	11.82	10.26	10.77
Na ₂ O	1.14	0.38	1.35	1.75	1.23	1.26	0.26	0.08	0.88
K ₂ O	0.19	0.10	0.53	0.09	0.08	0.16	n.d.	0.07	0.27
P ₂ O ₅	0.06	0.04	0.08	0.02	0.02	0.06	n.d.	n.d.	n.d.
SO ₂	0.04	0.02	0.02	0.01	0.01	0.01	n.d.	n.d.	n.d.
H ₂ O ⁺	1.81	2.78	1.77	1.04	1.64	1.97	n.d.	n.d.	n.d.
H ₂ O ⁻	0.40	0.45	0.53	0.39	0.34	0.45	n.d.	n.d.	n.d.
Total	98.59	98.68	98.43	99.87	98.84	98.63	99.69 Includes 0.37 Cr ₂ O ₃	98.89 Includes 0.44 Cr ₂ O ₃	99.52 Includes 0.18 Cr ₂ O ₃
CIPW Norms									
qz	—	—	—	—	—	—	—	2.17	1.93
or	1.12	0.59	3.13	0.53	0.47	0.95	—	0.41	1.60
ab	9.65	3.22	11.42	13.67	10.41	10.66	2.20	0.68	7.45
an	18.91	12.32	26.59	48.61	34.57	17.61	27.32	29.97	19.16
ne	—	—	—	0.62	—	—	—	—	—
di	13.25	6.77	17.18	4.50	7.13	10.99	25.80	17.49	28.11
hy	3.68	7.16	10.79	—	0.86	6.03	29.62	44.83	20.82
ol	46.24	60.14	19.51	28.29	39.92	43.29	8.96	—	—
mt	2.19	4.54	5.21	1.73	2.97	4.58	—	—	—
il	1.18	0.61	2.11	0.44	0.47	1.96	5.41	3.34	20.21
ap	0.13	0.09	0.17	0.04	0.04	0.13	—	—	—
Fo mol. percent	78.8	85.9	83.8	83.3	81.6	85.8	59.9	49.4	63.3
An mol. percent	64.9	78.3	68.7	77.0	75.8	60.9	92.1	97.7	70.8

1. Rock analysis. Si, Ti, Al, Fe (total), Mn, Mg, Ca, K, P and S determined by XRF analysis; Na determined by instrumental neutron activation analysis; FeO determined by titrimetry; H₂O⁺ and H₂O⁻ determined gravimetrically.

2. Microprobe analysis of glass melted for 2 hours at 20-30°C above liquidus temperature. All iron reported as FeO.

experiments in this study place a maximum value on this uplift.

2. From the positions of the water-saturated and water-absent liquid, rock C could have existed wholly as a liquid between 1250° and 1380° at 3 km depth and between 1135° and 1385° at 9.5 km depth. It has been argued from the presence of primary kaersutite and phlogopite (chapter VII) that the Rhum magma was hydrous. If rock C ever were a liquid in Rhum, the lower of these reported temperatures is probably closest to the liquidus temperature at 3 km and 9.5 km. A hydrous magma with 19.5 percent normative olivine, corresponding to rock C in composition, could, therefore, exist at geologically reasonable temperatures. [The effect of buffering the experiments at a lower, more geologically reasonable oxygen fugacity, would be to lower the above temperatures by approximately 30° (Nesbitt and Hamilton, 1969).]

3. The locations of the liquid of all six rocks differ. At a pressure equivalent to 3 km depth, the water-saturated liquid vary between 1250° (rock C) and 1575° (rock B). It is clear that the rocks cannot all have been liquids, melting temperatures for some of the samples being prohibitive. At least some of the rocks must be differentiates of a less olivine-rich liquid (cf. Wadsworth, 1961). The large differences in temperature between the entry of olivine and either plagioclase or pyroxene in any rock substantiate the conclusion that many harrisite rocks are differentiates of less olivine-rich magmas. Not all harrisite rocks can be considered as crystallized liquids, or fluids, as the hypotheses favouring a pegmatite origin suggest (Harker 1908b; Drever and Johnston, 1972). On the other hand, a differentiated pegmatite origin (melt plus olivine crystals plus vapour) cannot be excluded by the experimental data.

4. The phase relations of the anorthosite vein in which plagioclase apparently crystallized before pyroxene indicate that the liquid must have crystallized at a depth less than 7.6 km, assuming the vein was a water-saturated intrusion. (The olivine content of the vein is predominantly contaminant from the peridotite intruded by the vein, and not primary material from the vein itself.) At 3 km depth, the vein could have been a water-saturated bytownite-anorthosite liquid at 1165°. This value is 35° lower than the lowest estimate of the vein intrusion temperature made by Donaldson (1975).

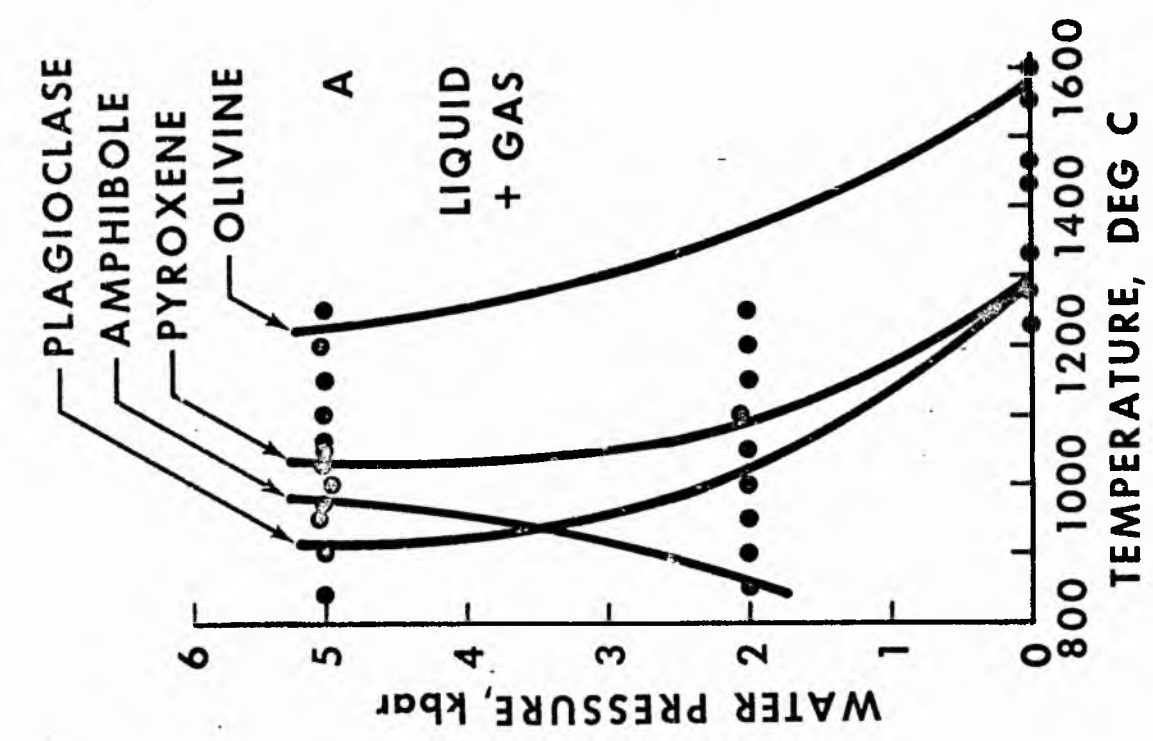
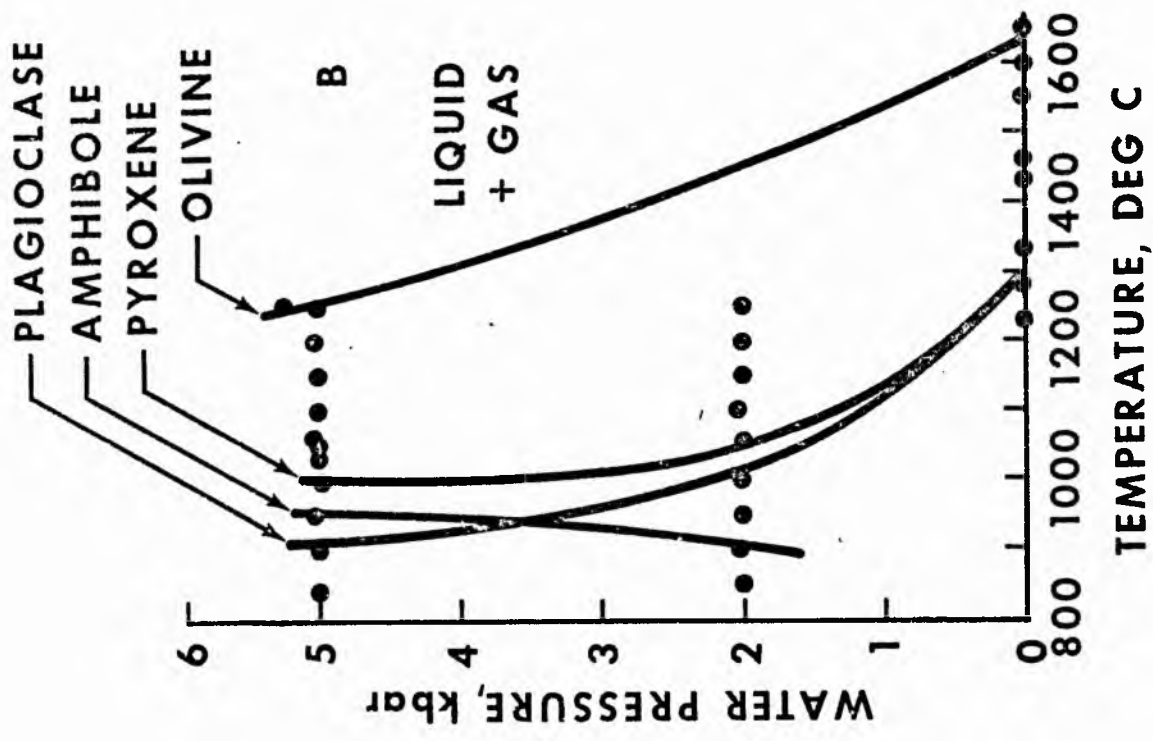
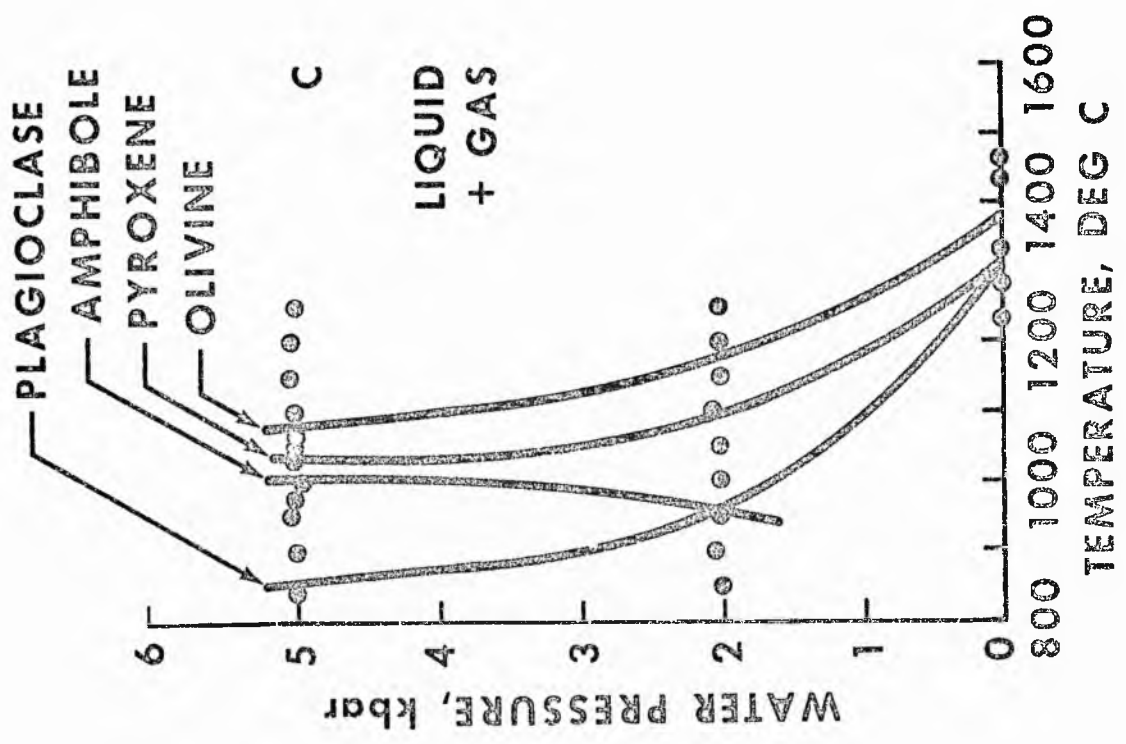
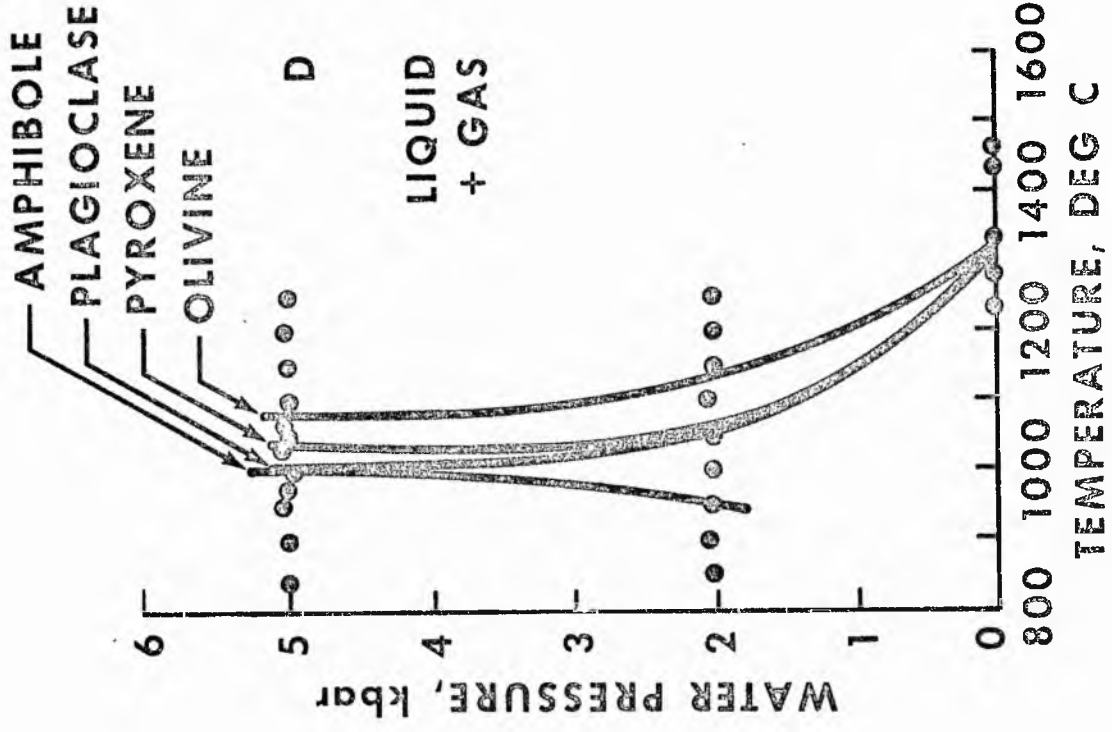


Fig. 53 Pressure-temperature projection of the natural peridotite, anorthositic and olivine eucrite systems (rocks A, B, C, D, E, F). Hydrothermal data is from Tables 23 and 24; 1 atm. data is from Table 25. Mineral is stable to the left of the curve along which it is shown.



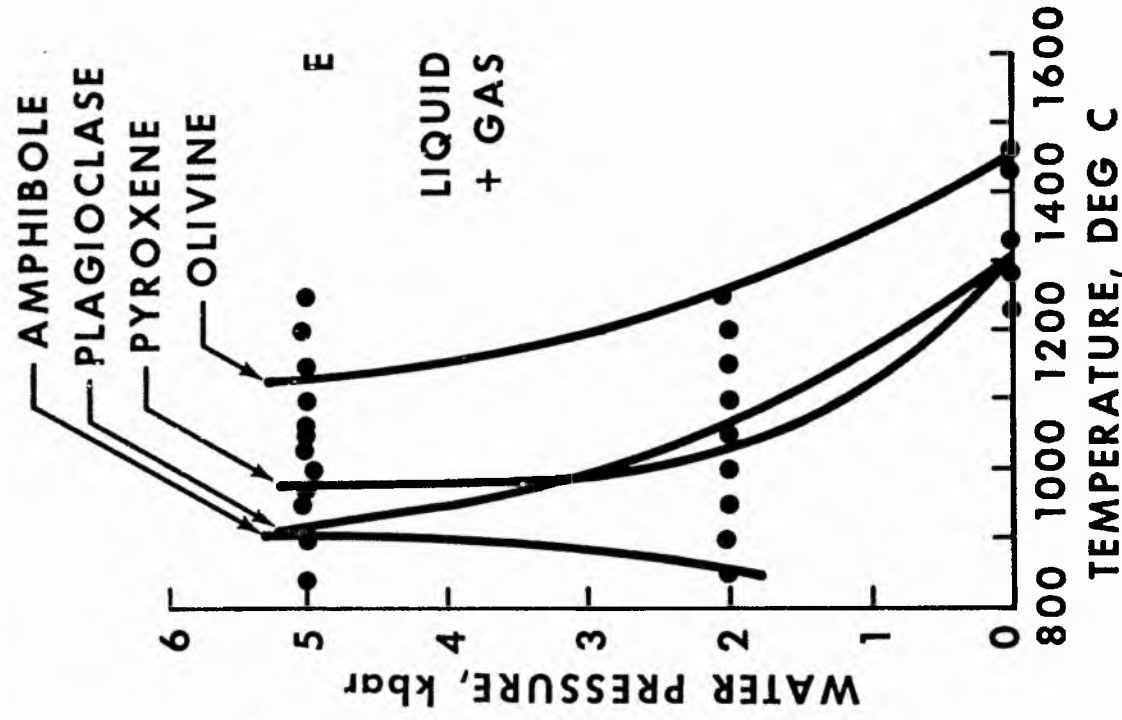
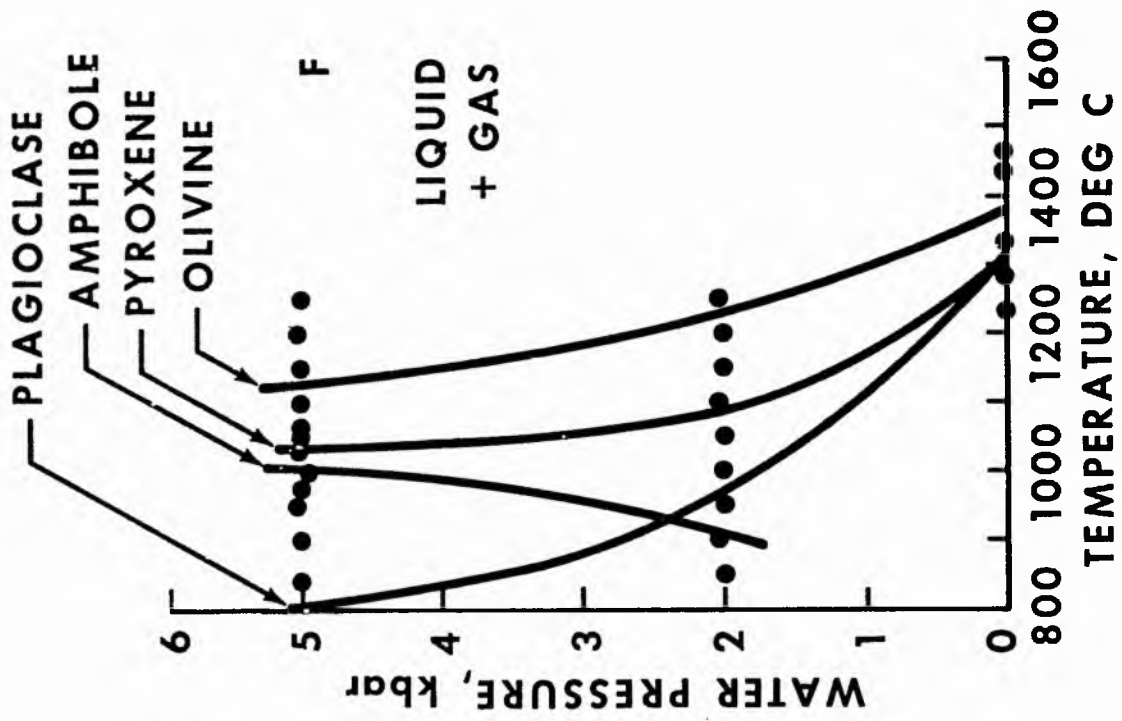


Table 24. Products obtained by holding Rhum peridotites and eucrites at various temperatures and approximately 2 kb water pressure in sealed platinum tubes.

Run Number	Rock	P _{fluid} kb	Temp. °C	Duration hours	H ₂ O wt. %	Condensed run products
1	A	2.1	1250	21	14.7	ol., q. am., q. ol.
	B				15.1	ol., q. am., q. ol.
	C				15.0	q. ol., g am.
	D				14.9	q. am.
	E				15.1	ol., q. ol., q. am.
	F				15.0	q. ol., q. am.
2	A	2.0	1200	7.0	14.6	ol., q. am., q. ol.
	B				15.0	ol., q. am., q. ol.
	C				15.1	q. ol., q. am.
	D				14.7	q. am.
	E				14.7	ol., q. ol., q. am.
	F				15.0	ol., q. ol., q. am.
3	A	2.0	1150	7.0	14.5	ol., q. am., q. ol.
	B				14.9	ol., q. am., q. ol.
	C				14.9	ol., q. am., q. ol.
	D				14.8	q. am.
	E				15.2	ol., q. ol., q. am.
	F				15.0	ol., q. am.
4	A	2.1	1100	16	14.8	ol., q. am., q. ol.
	B				15.0	ol., q. am., q. ol.
	C				15.9	ol., q. am., q. ol.
	D				15.3	ol., q. am.
	E				14.7	ol., q. ol., q. am.
	F				14.7	ol., q. am.
5	A	2.0	1050	18	15.6	ol., px., q. am.
	B				15.2	ol., q. am., q. ol.
	C				14.8	ol., px., q. am.
	D				15.7	ol., px., pl.
	E				15.1	ol., pl., q. am.
	F				15.4	ol., px., q. am.
6	A	2.0	1000	18	13.9	ol., px., pl.
	B				15.0	ol., px., pl., q. am.
	C				15.3	ol., px., q. am.
	D				15.7	ol., px., pl.
	E				14.6	ol., px., pl., q. am.
	F				15.6	ol., px., pl., q. am.
7	A	2.0	950	18	15.5	ol., px., pl.
	B				14.7	ol., px., pl., q. am.
	C				14.6	ol., px., pl., am. rim on px.
	D				14.8	ol., px., pl., am. rim on px.
	E				13.9	ol., px., pl.
	F				14.6	ol., px., pl.
8	A	2.1	900	18	15.2	ol., px., pl.
	B				15.1	ol., px., pl., am. rim on px.
	C				15.0	ol., px., pl., am. rim on px.
	D				14.7	ol., px., pl., am. rim on px.
	E				15.1	ol., px., pl.
	F				15.1	ol., px., pl., am. rim on px.
9	A	2.0	850	18	14.9	ol., px., pl., am. rim on px.
	B				14.9	ol., px., pl., am. rim on px.
	C				15.0	ol., px., pl., am. rim on px.
	D				15.0	ol., px., pl., am. rim on px.
	E				15.0	ol., px., pl., am. rim on px.
	F				14.7	ol., px., pl., am. rim on px.

q-quench ol- olivine pl- plagioclase px- pyroxene am- amphibole

Table 23. Products obtained by holding Rhum peridotites and eucrites at various temperatures and approximately 5 kb water pressure in sealed platinum tubes.

Run Number	Rock	P fluid kb	Temp. °C	Duration hours	H ₂ O wt. %	Condensed run products
1	A	5.0	1250	7	14.7	q. ol., q. am.
	B				14.7	ol., q. ol., q. am.
	C				15.1	q. ol., q. am.
	D				15.5	q. am.
	E				15.3	q. ol., q. am.
	F				15.3	q. ol., q. am.
2	A	5.1	1200	1	14.9	q. ol., q. am.
	B				14.9	ol., q. ol., q. am.
	C				14.7	q. ol., q. am.
	D				15.2	q. am.
	E				15.3	q. ol., q. am.
	F				14.7	q. ol., q. am.
3	A	5.0	1150	1	14.8	q. ol., q. am.
	B				15.2	ol., q. ol., q. am.
	C				14.9	q. ol., q. am.
	D				14.7	q. am.
	E				15.3	q. ol., q. am.
	F				15.0	q. ol., q. am.
4	A	5.0	1100	2.2	14.4	ol., q. ol., q. am.
	B				14.3	ol., q. ol., q. am.
	C				15.1	q. ol., q. am.
	D				15.5	q. am.
	E				15.0	ol., q. ol., q. am.
	F				14.9	ol., q. ol., q. am.
5	A	5.0	1050	1.5	14.8	ol., q. ol., q. am.
	B				14.7	ol., q. ol., q. am.
	C				14.9	ol., q. am.
	D				14.7	ol., q. am.
	E				15.3	ol., q. ol., q. am.
	F				15.5	ol., q. ol., q. am.
6	A	4.9	1000	1.5	14.7	ol., px., q. am.
	B				14.7	ol., px., q. am.
	C				15.0	ol., px., am. rim on px.
	D				15.0	ol., px., pl., am. rim on px.
	E				15.0	ol., q. am.
	F				15.2	ol., px., am. rim on px.
7	A	5.1	950	2.0	14.5	ol., px., q. am.
	B				14.7	ol., px., am. rim on px.
	C				14.9	ol., px., am. rim on px.
	D				15.3	ol., px., pl., am. rim on px.
	E				15.3	ol., px., q. am.
	F				14.9	ol., px., am. rim on px.
8	A	5.0	900	2.0	15.3	ol., px., pl., am. rim on px.
	B				13.7	ol., px., pl., am. rim on px.
	C				15.5	ol., px., am. rim on px.
	D				15.4	ol., px., pl., am. rim on px.
	E				15.6	ol., px., pl., am. rim on px.
	F				14.8	ol., px., am. rim on px.
9	A	5.0	840	24	14.3	ol., px., pl., am. rim on px.
	B				14.2	ol., px., pl., am. rim on px.
	C				14.8	ol., px., am. rim on px.
	D				14.9	ol., px., pl., am. rim on px.
	E				14.9	ol., px., pl., am. rim on px.
	F				14.9	ol., px., am. rim on px.
10	A	5.1	1060	2.0	14.2	ol., q. am.
	B				14.6	ol., q. ol., q. am.
	C				15.7	ol., q. am.
	D				15.0	ol., q. am.
	E				14.8	ol., q. ol., q. am.
	F				14.8	ol., q. am.
11	A	5.1	1030	2.0	15.3	ol., px., q. am.
	B				14.9	ol., q. ol., q. am.
	C				14.9	ol., px., q. am.
	D				15.3	ol., px., q. am.
	E				14.8	ol., q. ol., q. am.
	F				14.7	ol., px., q. am.
12	A	5.0	975	24	14.8	ol., px., q. am., am. rim on px.
	B				14.9	ol., px., q. am.
	C				15.1	ol., px., am. rim on px.
	D				15.2	ol., px., pl., am. rim on px.
	E				15.0	ol., px., q. am.
	F				15.0	ol., px., am. rim on px.

q- quartz; ol- olivine; px- pyroxene; pl- plagioclase; am- amphibole

Table 25. Results of quenching Rhum peridotites and eucrites held in platinum or carbon crucibles at various temperatures under 1 atm. air or 10:1 N₂/H₂.

Run Number	Rock	Temp. °C	Duration hours	Run atmosphere	Run products
1	A B C D E	1500	0.5	Air	gl. ol., gl. gl. gl. gl.
2	A B C D E	1400	0.5	Air	ol., px., gl. ol., px., gl. gl. gl. gl.
3	A B C D E	1300	0.5	Air	ol., px., gl. ol., px., gl. gl. gl. ol., px., gl.
4	A B C D E	1200	0.5	Air	ol., px., gl. ol., px., gl. ol., px., pl., gl. ol., px., pl., gl. ol., px., pl., gl.
5	A B C D E	1175	0.5	Air	ol., px., pl. (? gl.) ol., px., pl. (? gl.) ol., px., pl. ol., px., pl. (? gl.) ol., px., pl. (? gl.)
6	A B C D E	1250	0.5	Air	ol., px., gl. ol., px., gl. ol., px., pl., gl. ol., px., gl.
7	A B C D E	1375	0.5	Air	ol., px., gl. gl. gl. ol., px., gl.
8	A B C D E F	1230	1.0	N ₂ /H ₂	ol., px., pl. ol., px., pl. ol., px., pl. ol., px., pl. ol., px., pl. ol., px., pl.
9	A B C D E F	1280	1.0	N ₂ /H ₂	ol., px., pl. ol., px., pl. ol., px., pl. ol., px., pl. ol., px., pl. ol., px., pl.
10	A B C D E F	1330	1.0	N ₂ /H ₂	ol., gl., q. ol. ol., gl., q. ol. ol., gl., q. ol. gl. ol., gl., q. ol. ol., gl., q. ol.
11	A B C D E F	1430	1.0	N ₂ /H ₂	ol., gl., q. ol. ol., gl., q. ol. gl. gl. ol., gl., q. ol. gl.
12	A B C D E F	1460	1.0	C (run in graphite crucible)	ol., gl., q. ol. ol., gl., q. ol. gl. gl. gl. gl.
13	A B	1550	0.25	C (run in graphite crucible)	ol., gl., q. ol. ol., gl., q. ol.
14	A B	1600	0.25	C (run in graphite crucible)	gl., q. ol. ol., gl., q. ol.
15	B	1650	0.25	C (run in graphite crucible)	gl., q. ol.

gl - glass; ol - olivine; px - pyroxene; pl - plagioclase; q - quench phase.

Appendix III PUBLISHED AND IN PRESS PAPERS RESULTING FROM
THIS STUDY

Some of the references in the text are to published and in press papers resulting from this study. Copies of these are appended. The list below is a synopsis of the papers written during tenure of the Natural Environment Research Council Studentship.

Donaldson, C.H., Drever, H.I. and Johnston, R. 1973. Crystallization of poikilo-macrospherulitic feldspar in a Rhum peridotite. Nature Phys. Sci., 243, 69-70.

Donaldson, C.H., Reid, A.M., Ridley, W.I., Brown, R. and Dawson, J.B. 1973. The Igwisi Hills extrusive "kimberlites". Extended abstracts, International Kimberlite Conference, Cape Town, 93.

Reid, A.M., Ridley, W.I., Donaldson, C.H., Brown, R. and Dawson, J.B. 1973. Garnet and spinel peridotite xenoliths from the Lashaine volcano in northern Tanzania. Extended abstracts, International Kimberlite Conference, Cape Town, 273.

Ridley, W.I., Reid, A.M., Warner, J., Brown, R., Gooley, R. and Donaldson, C.H. 1973. Major element composition of glasses in two Apollo 16 soils and a comparison with Luna 20 glasses. Lunar Science IV, 625-627.

Reid, A.M., Ridley, W.I., Donaldson, C.H. and Brown, R. 1973. Glass compositions in the orange and gray soils from Shorty Crater, Apollo 17. EOS (Trans. Amer. Geophys. Union), 54, 607-608.

Lofgren, G.E. and Donaldson, C.H. 1973. Experimental evidence bearing on the origin of "Comb (Willow Lake) layering". Geol. Soc. Amer. Annual Meeting Abstracts with Programs, v. 5, 716.

Ridley, W.I., Reid, A.M., Warner, J.L., Brown, R., Gooley, R. and Donaldson, C.H. 1973. Glass compositions in Apollo 16 soils 60501 and 61221. Proc. Fourth Lunar Sci. Conf., Geochim. Cosmochim. Acta. (Suppl. 4), 1, 309-321.

Donaldson, C.H. 1974. Calculated diffusion coefficients and the growth rate of olivine. EOS (Trans. Amer. Geophys. Union), 55, 460-461.

Donaldson, C.H. 1974. Olivine crystal types in harrisitic rocks of the Rhum pluton and Archean spinifex rocks. Geol. Soc. Amer. Bull., 85, 1721-1726.

Donaldson, C.H. 1974. Experimental investigation of olivine morphology. Geol. Soc. Amer. Annual Meeting Abstracts with Programs, v. 6, 712.

- Lofgren, G.E., Donaldson, C.H., Williams, R.J. and Mullins, O. 1974. Experimentally reproduced textures and mineral chemistry of A-15 quartz basalts. Lunar Science V, 458-460.
- Reid, A.M., Donaldson, C.H., Jakeš, P. and Brown, R.W. 1974. Apollo 16 1-2 mm fines, sample 65702, chemical and petrographic correlations. Lunar Science V, 624-626.
- Lofgren, G.E., Donaldson, C.H., Williams, R.J., Mullins, O. and Usselman, T.M. 1974. Experimentally reproduced textures and mineral chemistry of Apollo 15 quartz normative basalts. Proc. Fifth Lunar Sci. Conf., Geochim. Cosmochim. Acta. (Suppl. 5), 1, 549-568.
- Lofgren, G.E., Usselman, T.M. and Donaldson, C.H. 1975. Cooling history of Apollo 15 quartz normative basalts determined from cooling rate experiments. Lunar Science VI, 515-517.
- Usselman, T.M., Lofgren, G.E., Donaldson, C.H. and Williams, R.J. 1975. Experimentally reproduced textures and mineral chemistries of high titanium mare basalts. Lunar Science VI, 835-837.
- In press:
- Donaldson, C.H. Ultrabasic breccias in layered intrusions- the Rhum complex. (J. Geol.)
- Donaldson, C.H. Calculated diffusion coefficients and the growth rate of olivine in a basalt magma. (Lithos)
- Donaldson, C.H., Williams, R.J. and Lofgren, G.E. A sample holding technique for study of crystal growth in silicate melts. (Amer. Min.)
- Donaldson, C.H., Brown, R.W. and Reid, A.M. Petrology and chemistry of basalts from the Nazca Plate: Part I- Petrography and mineral chemistry. (Initial Reports of the Deep Sea Drilling Project: Leg 34.)
- Lofgren, G.E. and Donaldson, C.H. Curved branching crystals and differentiation in comb-layered rocks. (Contrib. Mineral. Petrol.)
- Reid, A.M., Donaldson, C.H., Dawson, J.B., Brown, R., and Ridley, W.I. The Igwisi Hills extrusive "kimberlites". (Proc. Kimberlite Conf.)
- Reid, A.M., Donaldson, C.H., Brown, R., Ridley, W.I. and Dawson, J.B. Mineral chemistry of peridotite xenoliths from the Lashaine volcano, Tanzania. (Proc. Kimberlite Conf.)

Olivine Crystal Types in Harrisitic Rocks of the Rhum Pluton and in Archean Spinifex Rocks

COLIN H. DONALDSON *Lunar Science Institute, 3303 Nasa Road 1, Houston, Texas 77058 and Department of Geology, University of St. Andrews, St. Andrews, Fife, Scotland*

ABSTRACT

Skeletal and dendritic olivine crystals in the Archean volcanic ultramafic spinifex rocks and in harrisitic ultramafic layers of the Rhum pluton are classified as (1) plate, (2) randomly oriented, (3) porphyritic, or (4) branching type. Volcanic and plutonic examples are remarkably similar. Each type records the degree of pre-nucleation supersaturation with olivine that was attained by the parent melt. The rapid induction of supersaturation necessary to form skeletons and dendrites in a plutonic environment is attributed to changing water content or adiabatic expansion of the magma. The olivine crystals in harrisitic and spinifex rocks are not quench crystals; they grew rapidly from olivine-rich melts as the result of extreme supersaturation induced by slow cooling and slight supercooling below a liquidus with shallow slope in temperature-composition space. Skeletal and dendritic olivine crystals grow readily in magma and are poor indices of cooling rate and crystallization environment. *Key words:* igneous petrology; ultramafic family; plutonic, hypabyssal, volcanic rocks; Rhum harrisitic rocks; Archean spinifex rocks.

INTRODUCTION

An essential premise of petrography is that textures and crystal sizes of an igneous rock reflect the cooling rate of its parent magma and allow discrimination between an extrusive or intrusive origin. Skeletal and dendritic crystals are generally considered to indicate rapid cooling and supercooling, which produce rapid growth. These conditions have been postulated to explain the skeletal and dendritic olivine crystals in Archean hypabyssal and volcanic spinifex rocks (quench peridotite) in Australia, South Africa, and Canada (Lewis, 1971; Viljoen and Viljoen, 1969; Naldrett and Mason, 1968). "Spinifex" is a colloquial name used in Western Australia for ultramafic rocks that occur in greenstone belts and that show textures dominated by skeletal crystal forms (Nesbitt, 1971). Supercooling conditions have also been invoked (Wager and others, 1960; Wadsworth, 1961) to explain macrocrystalline

skeletal and dendritic olivine in the harrisitic eucrite and peridotite of the Tertiary Rhum pluton (Harker, 1908; Wager and Brown, 1951; Brown, 1956). That these two contrasting environments should produce textures so similar cannot be coincidental. A crystal-growth control that is dependent on more than cooling rate must be sought.

This study was undertaken to compare relative olivine growth rates in the olivine-rich harrisitic and spinifex rocks and to consider how very similar olivine crystal types may appear in rocks that have crystallized under very different physical conditions. Characterization of the complex nucleation and thermal histories of these unusual rocks is essential to understanding their origin and crystallization features. From this understanding, it is possible to examine harrisite as a potential basaltic differentiate (Wager and others, 1960), ultramafic pegmatite (Harker, 1908; Dreyer and Johnston, 1972), or crystallized

ultramafic magma (Donaldson and others, 1973).

TEXTURAL COMPARISON

Method

Nesbitt's (1971) classification scheme of olivine textures and crystal types in Archean spinifex rocks has been modified and applied to Rhum harrisite. The four prevalent olivine crystal types are designated plate, randomly oriented, porphyritic, and branching. More rigorous crystallographic comparison is not possible because olivine in spinifex rocks has generally undergone pseudomorphism (Williams, 1971).

Illustrations of spinifex rocks in the literature afford a basis for comparison with Rhum harrisite. In Table 1, I have classified and compared published illustrations of Archean spinifex olivine with olivine in Rhum harrisite and other rocks. Similar olivine crystal types occur in Cambrian layered igneous rocks (Robins, 1973).

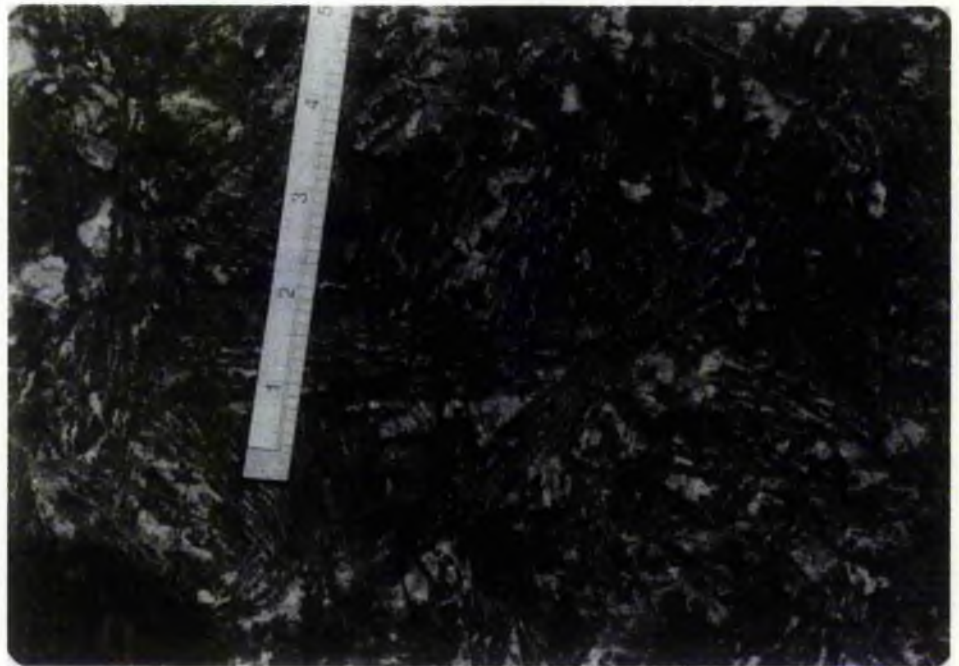






Figure 1. Bundles of intersecting plate olivine in harrisitic eucrite with coarsely crystalline plagioclase and diopside between plates. Scale = 5 in. (0.125 m); vertical surface. Locality: west Harris Bay, Rhum.

TABLE 1. CLASSIFICATION AND COMPARISON OF HARRISITIC AND SPINIFEX OLIVINES

Olivine type	Representative sketch (see text for possible scales)	Rhum harrisite illustrations	Skeletal and dendritic olivine illustrations from publication 2	Archean spinifex illustrations
Plate		1. P 1,2 3. F 11 14. F 2b inset	F 21a	4. F 10a, 12 5. P VIIb, VIIIb 6. P 12a, 13b 7. F 4b 8. P 24a, b 9. F 3, 5a 12. F 8, 11, 12, 13, 14, 15, 17
Randomly oriented		1. P 3 10. F 5a 11. F 2 17. F 142, 143	F 5 K, L, M: 9b, 11a	4. F 10b, c, 14 5. P VIIa, VIIIa 6. P 12b, 14c 8. P 24c 9. F 5b, c 12. F 12, 15 16. F 2, 3 (experimentally simulated)
Porphyritic		1. F 1 3. F 16 10. F 5b 17. F 145	F 1, 5, 6 7a-j, 8a, 21a	4. F 11, 13 6. P 12c 8. P 4e-g 12. F 19
Branching		1. P 4, F 2 13. F 14a 14. F 2b 15. *F 1a, b 17. F 144, 146 3. F 15, 14, 17, 13		

Note: P = Plate; F = Figure. Publication code: 1, This paper; 2, Drever and Johnston (1972); 3, Wadsworth (1961); 4, Naldrett and Mason (1968); 5, Viljoen and Viljoen (1969); 6, Nesbitt (1971); 7, Williams (1971); 8, Lewis (1971); 9, Naldrett (1971); 10, Drever and Johnston (1972); 11, Drever and others (1972); 12, Fyke and others (1973); 13, Wager (1968); 14, Harker (1908); 15, Robins (1973); 16, Dickey (1973); 17, Wager and Brown (1968).

* Crescumulate zone of the Rognsund gabbro, Norway.



Figure 2. Macrocrystalline olivine plates in harrisitic peridotite. Scale = 9 in. (0.27 m); horizontal surface. Locality: Ard Mheall ridge, Rhum (photograph by D. Meldrum).

Plate Olivine

Nesbitt noted that dendritic plate olivine appears to be cross-bedded in hand specimens because it consists of bundles of parallel plates that are crosscut randomly by other sets of plates, although without mutual interpenetration. Rhum harrisitic olivine with this appearance, as well as the wedge-shaped enclosures formed between adjacent bundles (Lewis, 1971) is shown in Figure 1. The large plate olivine crystals in Figure 2 closely resemble those in South African spinifex rocks illustrated by Viljoen and Viljoen (1969).

Lengths of plate olivine bundles vary from 0.3 to 0.9 m in spinifex rocks (Naldrett, 1971). In harrisite, many bundles have been found as much as 0.6 m long; the largest bundle observed was 2.1 m. Olivine in the two rock types is similar in texture and grain size, although Rhum olivine crystals are unusually large in some cases.

Randomly Oriented Olivine

The term "radiate" has been applied to some olivine-containing rocks in Australia by Nesbitt (1971), but because not all the crystals radiate from a common nucleus, "randomly oriented" is preferred.

In Archean spinifex rocks, the texture consists of randomly oriented, elongate, skeletal olivine ranging from 3 cm to 0.1 cm or less (Nesbitt, 1971). Crystal intersections form triangular- or polygonal-shaped interstitial patches. Figure 3 illustrates this type of olivine in harrisite; the skeletal crystal type is also shown in Figure 2 of Drever and others (1972).

Porphyritic Olivine

Naldrett and Mason (1968, p. 122) described the texture of porphyritic olivine as "small crystals, generally with well-developed euhedral exterior boundaries and hollow or skeletal cores." A number of examples that conform with this description in Rhum harrisite are illustrated in Figure 4.

Porphyritic olivine crystals in the Rhum pluton commonly have round, hollow cores, often with the irregularly embayed margins that Drever and Johnston (1972) termed "amoeboid." To this extent, olivine of this type in spinifex rocks differs from that in harrisite. Nonetheless, Rhum porphyritic olivine (Fig. 4) is dominantly euhedral with development of common olivine crystal forms (notably {010} and {021}) and hollow centers. The grain size of these olivine crystals, which usually are larger than associated plagioclase and pyroxene crystals, also justifies the term "porphyritic."

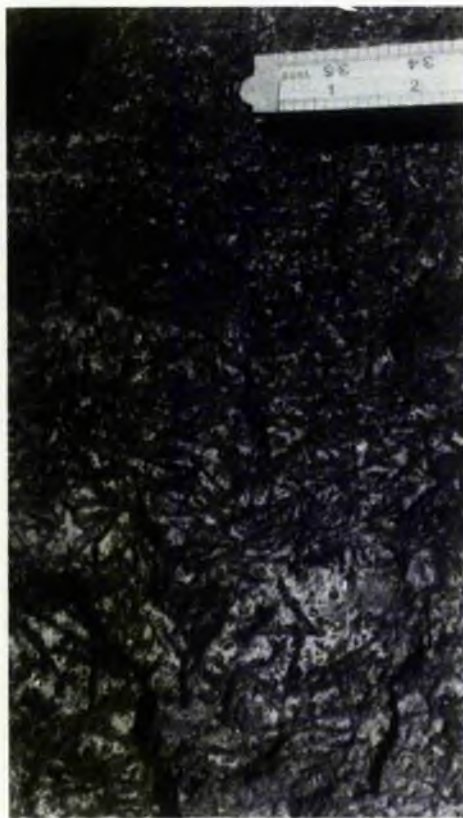


Figure 3. Elongate skeletal olivine of random orientation in harrisitic eucrite. Note upward decrease of olivine grain size as the rock grades into eucrite that has faint igneous lamination parallel to inch rule. Above photograph center, olivine is laminated but returns to random orientation farther upward; vertical surface. Locality: central Harris Bay, Rhum.

ten commun.). Plate olivine in harrisitic and spinifex rocks may have similar detailed form, with plates built of flattened parallel growth units. These complex olivine crystal types require further investigation.

OLIVINE GROWTH RATE

Nesbitt (1971) suggested that olivine in spinifex rocks crystallized rapidly about a few nascent nuclei in a crystal-free, supercooled ultramafic liquid. Olivine in Rhum harrisite is also thought to have grown from supercooled magma (Wadsworth, 1961; Wager and Brown, 1968), though without in situ nucleation. Rapid growth of olivine in spinifex rocks contrasts sharply with the necessarily slow mechanism that is diffusion rate dependent (crescumulus growth from a basaltic magma) postulated by Wager and others (1960) to explain crystallization of dendritic branching olivine in harrisite. Yet branching olivine is found in thin slag flows where rapid crystal growth is beyond doubt (Lewis, 1971; Naldrett, 1971); porphyritic olivine in Rhum harrisite is identical in shape to crystals that grew rapidly at the margins of Tertiary picritic sheets (Drever and Johnston, 1957). Most petrologists would consider the 0.13-m-long skeletal olivine in harrisite illustrated by Drever and others (1972, Fig. 2) to have grown rapidly, if the large size were not indicated. The similarity of olivine crystal types among all these rocks strongly suggests that the olivine in harrisite grew rapidly.

TEXTURE GENESIS

Relation of Crystal Type to Supersaturation, Supercooling, and Magma Composition

Emphasis is placed here on the nongenetic term "supersaturation" rather than "supercooling," because crystallization need not result solely from cooling. Other processes that can elevate liquidus temperature relative to magma temperature, thereby creating a supersaturated melt and leading to crystal precipitation, include changes in hydrostatic pressure or water content of a magma. Supersaturation and supercooling are not directly proportional if a silicate melt has a nonlinear liquidus in temperature-composition space. The amount of supercooling necessary to attain a given degree of supersaturation varies for different melt compositions as a function of their liquidus slopes (Fig. 7). If a fixed degree of supersaturation is a requirement to grow a particular crystal type in two chemically different magmas, then the formation of that type is a function not only of the supercooling of each melt but also of the

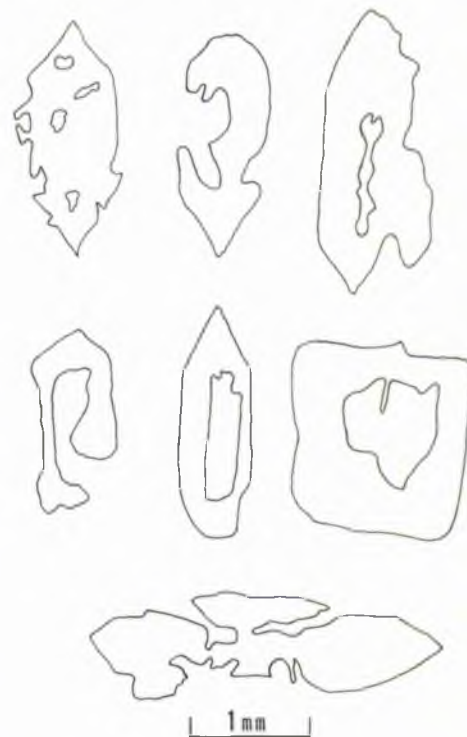


Figure 4. Skeletal, embayed, hollow, and euhedral to subhedral olivine displaying affinity with porphyritic spinifex rocks. Tracings from photographs of thin sections of Rhum harrisite.

melt compositions. The single term "supersaturation" covers both the compositional and the supercooling aspects of crystal-type control.

Saratovkin (1959) found that, depending on the degree of supersaturation in a melt before nucleation, postnucleation crystal types follow the scheme: polyhedral → sector-zoned → skeletal → dendritic → spherulitic (arrow points toward higher degree of supersaturation). The ratio of the magnitudes of crystal growth rate to the diffusion coefficient plus convection rate of melt impurities (material not required by the crystals) increases with degree of supersaturation (Keith and Padden, 1963; Tiller, 1964; Knight, 1967). Growth conditions for the skeletal and dendritic olivine discussed in this paper lie between those for polyhedral and spherulitic forms; that is, moderate to extreme supersaturation and growth rates considerably greater than the sum of the melt diffusion coefficient and convection rate.

Before any melt can crystallize, it must attain the minimum degree of supersaturation required to form stable crystal nuclei. Because nucleation is a chance event (Tammann, 1925), the more slowly the supersaturation is induced, the greater the chance of nucleation at low supersaturation. Growth of skeletal or dendritic crystals requires that rapid physical-chemical

Branching Olivine

Because branching of olivine is common in Rhum harrisite (Wadsworth, 1961), Nesbitt (1971) applied the term "harrisitic spinifex" to the branching dendritic olivine crystals in spinifex rocks. No illustration of branching growth in Archean spinifex has been published; therefore, no direct comparison with Rhum harrisite is possible. Nesbitt may have considered "branching" to mean inclined offshoots growing from a main stem, whereas "branching" was used by Wadsworth as a synonym for "budding" (two or more parallel growths being linked by right-angled buds in a dendritic growth system of primary and secondary units). Both types of branching occur in Rhum olivine (Figs. 5 and 6). Robins (1973) recognized both types in the Rognsund gabbro, Norway (Table 1).

In addition to these four crystal types, some Rhum olivine displays fanlike or bifurcating radiate texture (that is, with crystals sharing nuclei). This property is rare in spinifex rocks (Naldrett, 1972, writ-



Figure 5. Upward growing, branching harrisitic olivine in feldspathic peridotite; three inclined branches extend from main stem. Scale = 6 in. (0.15 m). Locality: Loch Dormabac, Rhum.

changes occur in the melt to prevent nucleation under low supersaturation conditions that would favor a polyhedral crystal type. Therefore, in addition to being referable to a specific degree of supersaturation, each of the olivine crystal types discussed in this paper is referable to a particular rate of physical-chemical change for a given magma composition. Thus, if crystallized from the same magma, skeletal porphyritic and randomly oriented olivine crystals will grow at a lower degree of supersaturation than dendritic plate and branching varieties, and the supersaturation will be more slowly induced.

Supersaturation in Harrisitic Parent Melt

The crescumulus hypothesis applied to harrisite assumes that olivine grew upward into supercooled basaltic magma from nuclei that were cumulus crystals lying on top of a crystal mush (Wager and others, 1960). This hypothesis does not, however, explain the origin of the porphyritic and randomly oriented olivine in harrisite. If, as the textures suggest, the olivine growth rate is large relative to the melt diffusional mobility and the convection rate, harrisite should have an olivine content similar to its parent melt. Also, material trapped between the olivine crystals must be olivine-depleted melt. Because harrisite is always olivine en-

riched (>30 volume percent) and often contains unzoned bytownite crystals, a basaltic parent magma is unacceptable. In situ crystallization of a magma that is more mafic and calcic than basalt is necessary. Olivine-enriched melts may have unusually shallow liquidus slopes in temperature-composition space (Wyllie, 1960). Hence, for a given degree of supercooling, supersaturation with olivine and olivine growth rate would both be greater in an olivine-rich melt than in the basalt postulated by Wager and others (1960).

Origin of Porphyritic Olivine

Two alternative mechanisms may explain the distinctive textures observed in the Rhum harrisite: (1) sudden decrease in the water content of a water-undersaturated feldspathic peridotitic liquid (Donaldson and others, 1973) and (2) transition of a water-saturated peridotitic magma to an unsaturated state by free-vapor loss. Supersaturation of magma with olivine components, which would result from either situation, would be reduced after nucleation by rapid crystal growth. Either mechanism could produce rapid crystallization in a pluton without significant cooling. If vapor loss is accompanied by adiabatic expansion of the magma, however, rapid (but slight) cooling would result as well.

These mechanisms are illustrated in Figure 8A. In case (1), a water-undersaturated magma (position 1), with X weight percent water, is slightly superheated. If Y weight percent water diffuses out of the magma in response to a pressure, temperature, or chemical gradient, the pressure-temperature coordinates of the magma are maintained, and olivine crystallizes rapidly under an induced supercooling, $\Delta T = T_3 - T_1$, where T_3 is the new liquidus temperature. If adiabatic expansion of the magma also occurs, there is additional supercooling, $\Delta T = T_3 - T_2$. In case (2), an initially water-saturated and superheated magma (position 2) loses both dissolved water (by diffusion) and water in the free gas-phase until it contains $X - Y$ weight percent dissolved water. Adiabatic expansion results in a total $\Delta T = T_3 - T_4$.

Zonation of olivine crystal types occurs in some spinifex rocks (Pyke and others, 1973), with a chilled margin overlying a plate olivine zone, which in turn overlies a porphyritic olivine zone. The vertically oriented plate olivine nucleated in situ after magmatic flow ceased. Lamination of porphyritic olivine indicates that the crystals were carried in suspension during flow and probably were oriented by it. The porphyritic olivine is an older crystal generation and necessarily reflects growth condi-

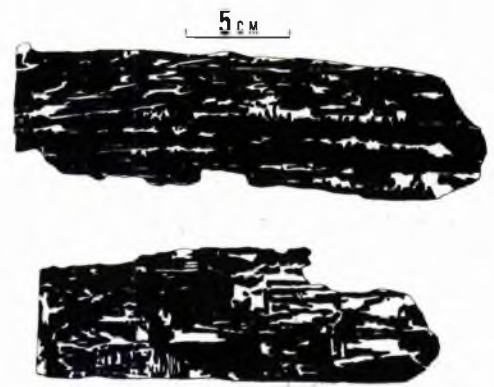


Figure 6. Tracings from sectioned rock surface of dendritic, budded, parallel growth features of highly elongate olivine. Lower section is parallel to (010), upper section is cut at 35° to (010). Olivine is black; plagioclase and diopside, white. Specimen is from feldspathic peridotite with >0.9-m-long olivine plates. Locality: Ard Mheall ridge, Rhum.

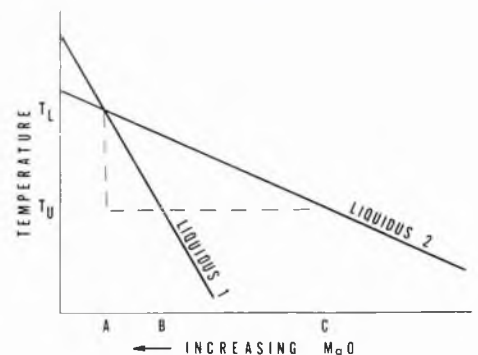


Figure 7. Effect of liquidus slope on relation of supercooling to supersaturation. For the same degree of supercooling ($T_L - T_U$, where T_L = liquidus temperature and T_U = undercooling temperature), melt A of steep liquidus (1) is mildly supersaturated (A - B), whereas if it has a shallow liquidus (2), the supersaturation is more extreme (A - C).

tions different from those responsible for the plate olivine. Possibly the porphyritic olivine results from a sudden change in the magma from a relatively hydrous to an anhydrous condition; this would cause mild olivine supersaturation and rapid crystallization. This scheme is shown in Figure 8B where positions 1, 2, and 3 are identical to those in Figure 8A (case 1). As the magma rises in the crust between stages 2 and 2', crystallization of porphyritic olivine continues as long as ascent is slower than the rate of loss of water by diffusion from the magma. Flow differentiation could concentrate olivine crystals locally within the liquid between stages 2 and 4. Between 2' and 4, the crystal-poor regions of the magma may fuse residual olivine crystals and emerge at the Earth's surface as superheated melt. It is from this liquid that plate olivine crystallized (Nesbitt, 1971).

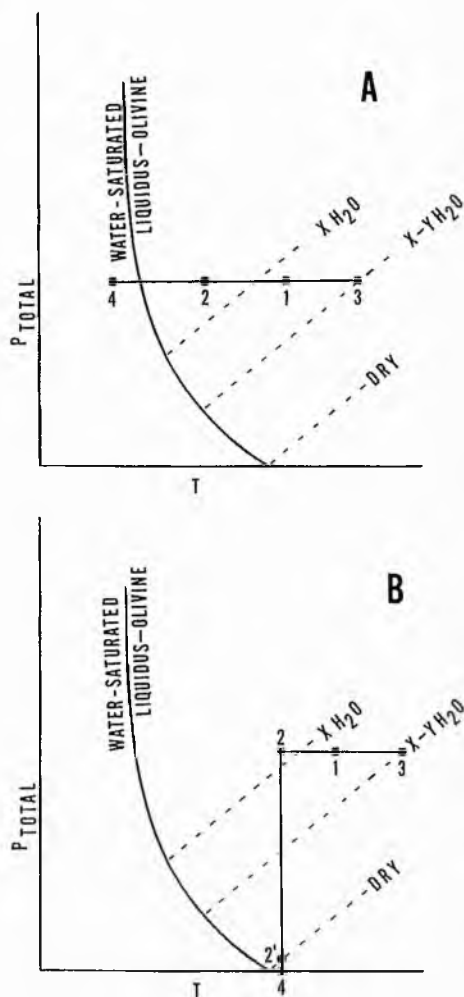


Figure 8. Schematic P - T relations for possible harrisitic origin (A) and for porphyritic and plate olivine in spinifex (B). Explanation in text.

Origin of Plate Olivine in Spinifex Rocks

Resemblance of plate olivine to olivine in experimentally quenched ultramafic liquids (for example, Dickey, 1973) led Viljoen and Viljoen (1969) to suggest a thermal history for spinifex rocks involving instant quenching in sea water. A 21-m-thick zone in a flow of peridotitic magma crystallizing as plate olivine (Lewis and Williams, 1973) will cool through the crystallization interval at an average rate of $0.20^{\circ}\text{C}/\text{hr}$; a 1-m-thick unit cools at $30^{\circ}\text{C}/\text{hr}$ (calculated from Jaeger, 1968). Neither of these cooling rates is sufficiently rapid to be termed quench.

In sheets of magma that are >1 m thick and crystallizing as plate olivine spinifex, a slow cooling rate implies that nucleation of olivine occurs at a low degree of supercooling, and the dendritic plate crystal type in-

dicates that growth occurs under conditions of extreme supersaturation. This may be achieved if the slope of the melt liquidus in temperature-composition space is shallow (Fig. 7; Wyllie, 1963; Nesbitt, 1971). Therefore, plate olivine in spinifex rocks need not be a quench (very rapid cooling) crystal type; this is a rapid growth type, but most examples are formed under slow cooling conditions. The apparent incompatibility in the cooling rate of harrisitic and spinifex rocks is therefore diminished, for once a supersaturated state has been attained, the parent melts of both rocks may cool slowly.

The textures and crystal sizes of plate olivine in harrisitic and spinifex rocks cannot be used as indices of extrusive or intrusive origin. Both texture and grain size in these rocks probably result from the easily induced extreme supersaturation in the parent melts, rather than from fast cooling rate.

Crystallization experiments by Lofgren (1973, 1974) show how plagioclase crystal type varies as a function of cooling rate and growth at isothermal, supercooling conditions. By analogy, the olivine crystal types in spinifex rocks may reflect different cooling rates and nucleation temperatures in an originally wholly molten magma sheet. Thus, dendritic plate olivine crystallizes at the top of sheets, and skeletal porphyritic olivine grows nearer the middle, where the cooling rate is slower and the nucleation temperature higher. This suggestion for complete *in situ* crystallization of an ultramafic melt is compatible with the field observations of Lewis and Williams (1973) but not of Pyke and others (1973). Multiple origins for the zonation of olivine crystal types in spinifex units are necessary.

SUMMARY

In olivine-enriched melts, extreme supersaturation in olivine can readily be achieved at slow cooling rates. Neither the size of the crystals nor the skeletal and dendritic shapes characteristic of rapid growth can be used as an index of cooling rate and crystallization environment. Similarities in the shapes and sizes of olivine in plutonic harrisitic and volcanic spinifex rocks highlight this conclusion. Supersaturation in the plutonic environment may be more readily achieved by changing water content or by adiabatic expansion of the magma than by conduction and convection cooling.

ACKNOWLEDGMENTS

I thank H. I. Drever, R. Johnston, and R. B. Merrill for improvements to the manuscript. In support of this study, the Natural Environment Research Council (United

Kingdom) provided me with a NATO studentship. The work was also supported by the Lunar Science Institute, which is operated by the Universities Space Research Association under Contract No. NSR 09-051-001 with the National Aeronautics and Space Administration.

REFERENCES CITED

- Brown, G. M., 1956, The layered ultrabasic rocks of Rhum, Inner Hebrides: Royal Soc. London Philos. Trans., ser. B, v. 240, p. 1-53.
- Dickey, J. S., 1973, A primary peridotite magma—Revisited: Olivine quench crystals in a peridotite lava, *in* Shagam, R., and others, eds., Studies in earth and space sciences (Hess volume): Geol. Soc. America Mem. 132, p. 289-297.
- Donaldson, C. H., Drever, H. I., and Johnston, R., 1973, Crystallization of poikilomacrospherulitic feldspar in a Rhum peridotite: Nature Phys. Sci., v. 243, p. 69-70.
- Drever, H. I., and Johnston, R., 1957, Crystal growth of forsteritic olivine in magmas and melts: Royal Soc. Edinburgh Trans., v. 63, pt. II, p. 289-317.
- 1972, Metastable growth patterns in some terrestrial and lunar rocks: Meteoritics, v. 7, p. 327-340.
- Drever, H. I., Johnston, R., Butler, P., Jr., and Gibb, F.G.F., 1972, Some textures in Apollo 12 lunar igneous rocks and terrestrial analogs: Lunar Sci. Conf., 3d, Houston 1972, Proc., v. 1, Massachusetts Inst. Technology Press, p. 171-184.
- Harker, A., 1908, The geology of the Small Isles of Inverness-Shire: Scotland Geol. Survey Mem., p. 1-210.
- Jaeger, J. C., 1968, Cooling and solidification of igneous rocks, *in* Hess, H. H., and Poldervaart, A., eds., Basalts, Vol. 2: New York, John Wiley & Sons, Inc., p. 503-536.
- Keith, H. D., and Padden, F. J., Jr., 1963, A phenomenological theory of spherulitic crystallization: Jour. Appl. Physics, v. 34, p. 2409-2421.
- Knight, C. A., 1967, The freezing of supercooled liquids: New York, Van Nostrand, 145 p.
- Lewis, J. D., 1971, "Spinifex texture" in a slag, as evidence for its origin in rocks: Western Australia Geol. Survey Ann. Rept., p. 45-49.
- Lewis, J. D., and Williams, I. R., 1973, The petrology of an ultramafic lava near Murphy Well, Eastern Goldfields, Western Australia: Western Australia Geol. Survey Ann. Rept., p. 60-68.
- Lofgren, G., 1973, Experimental crystallization of synthetic plagioclase at prescribed cooling rates [abs.]: EOS (Am. Geophys. Union Trans.), v. 54, p. 482.
- 1974, An experimental study of plagioclase crystal morphology: Am. Jour. Sci., v. 274, p. 243-273.
- Naldrett, A. J., 1971, Archean ultramafic rocks: Canada Dept. Energy, Mines and Resources Earth Physics Br. Pub., v. 44, p. 141-151.
- Naldrett, A. J., and Mason, G. D., 1968, Con-

- trasting Archean ultramafic igneous bodies in Dundonald and Clergue Townships, Ontario: Canadian Jour. Earth Sci., v. 5, p. 111-143.
- Nesbitt, R. W., 1971, Skeletal crystal forms in the ultramafic rocks of the Yilgarn Block, Western Australia: Evidence for an Archean ultramafic liquid: Geol. Soc. Australia Spec. Pub., v. 3, p. 331-347.
- Pyke, D. R., Naldrett, A. J., and Eckstrand, O. R., 1973, Archean ultramafic flows in Munro Township, Ontario: Geol. Soc. America Bull., v. 84, p. 955-978.
- Robins, B., 1973, Crescumulate layering in a gabbroic body on Seiland, northern Norway: Geol. Mag., v. 109, p. 533-542.
- Saratovkin, D. D., 1959, Dendritic crystallization: New York, Consultants Bureau, Plenum Pub. Corp., 126 p.
- Tammann, G., 1925, The states of aggregation: New York, Van Nostrand, 297 p.
- Tiller, W. A., 1964, Dendrites: Science, v. 146, p. 871-879.
- Viljoen, M. J., and Viljoen, R. P., 1969, Evidence for the existence of a mobile extrusive peridotitic magma from the Komati Formation of the Onverwacht Group: Geol. Soc. South Africa Spec. Pub. 2, Upper Mantle Project, p. 87-112.
- Wadsworth, W. J., 1961, The layered ultrabasic rocks of southwest Rhum, Inner Hebrides: Royal Soc. London Philos. Trans., ser. B, v. 244, p. 21-64.
- Wager, L. R., 1968, Rhythmic and cryptic layering in mafic and ultramafic plutons, in Hess, H. H., and Poldervaart, A., eds., Basalts, Vol. 2: New York, John Wiley & Sons, Inc., p. 573-622.
- Wager, L. R., and Brown, G. M., 1951, A note on rhythmic layering in the ultrabasic rocks of Rhum: Geol. Mag., v. 88, p. 166-168.
- 1968, Layered igneous rocks: Edinburgh, Oliver & Boyd, 588 p.
- Wager, L. R., Brown, G. M., and Wadsworth, W. J., 1960, Types of igneous cumulates: Jour. Petrology, v. 1, p. 73-85.
- Williams, D.A.C., 1971, Determination of primary mineralogy and textures in ultramafic rocks from Mount Monger, Western Australia: Geol. Soc. Australia Spec. Pub., v. 3, p. 259-268.
- Wyllie, P. J., 1960, The system CaO-MgO-FeO-SiO₂ and its bearing on the origin of ultrabasic and basic rocks: Mineralog. Mag., v. 32, p. 459-470.
- 1963, Effects of the changes of slope occurring on liquidus and solidus paths in the system diopside-anorthite-albite: Mineralog. Soc. America Spec. Paper, v. 1, p. 204-212.

MANUSCRIPT RECEIVED BY THE SOCIETY
SEPTEMBER 17, 1973

REVISED MANUSCRIPT RECEIVED FEBRUARY 19,
1974

CONTRIBUTION NO. 177, LUNAR SCIENCE
INSTITUTE, HOUSTON, TEXAS

14 1.6c. 2 1/2

FORFATTER

Calculated diffusion coefficients and the growth rate of olivine in a basalt magma*

COLIN H. DONALDSON

LITHOS



Donaldson, C. H. 1975: Calculated diffusion coefficients and the growth rate of olivine in a basalt magma. *Lithos* 8, ■—■.

Concentration gradients in glass adjacent to skeletal olivines in a DSDP basalt have been examined by electron probe. The glass is depleted in Mg, Fe, and Cr and enriched in Si, Al, Na, and Ca relative to that far from olivine. Ionic diffusion coefficients for the glass compositions are calculated from temperature, ionic radius and melt viscosity, using the Stokes-Einstein relation. At 1170°C, the diffusion coefficient of Mg²⁺ ions in the basalt is $4 \cdot 5 \cdot 10^{-9}$ cm²/s. Comparison with measured diffusion coefficients in a mugearite suggests this value may be 16 times too small. The concentration gradient data and the diffusion coefficients are used to calculate instantaneous olivine growth rates of $2-6 \cdot 10^{-7}$ cm/s. This is too slow for olivine to have grown in situ during quenching. Growth necessarily preceded emplacement such that the composition of the crystals plus the enclosing glass need not be that of a melt. The computed olivine growth rates are compatible with the rate of crystallization deduced for the Skaegaard intrusion.

Colin H. Donaldson, Lunar Science Institute, 3303 Nasa Road 1, Houston, Texas 77058, U.S.A. and University of St. Andrews, Scotland.

Two kinetic problems of particular petrologic importance are the rate of crystal growth and the diffusion rates in silicate melts. Without these parameters, the time necessary for solidification and crystal fractionation of magmas cannot be computed, and thermal models of magmatic crystallization may fail to agree with petrologic evidence (Hess 1973).

In this paper a method of calculating ionic diffusion coefficients is applied to magmas and used to estimate the instantaneous growth rate of olivine crystals in a chilled basalt. From this information a more detailed crystallization history can be assigned to the basalt, than that deducible from the petrography alone. The results also aid in understanding the mechanisms of postcumulus crystal growth (Jackson 1967) and chemical zoning of crystals in cumulates.

Before proceeding with a discussion of the methods of calculating diffusion coefficients and crystal growth rates, the results of an investigation of glass composition adjacent to olivine crystals in the basalt are presented. These data are essential to the subsequent calculations.

Basalt petrography and composition

Bottinga, Kudo & Weill (1966) demonstrated that compositional concentration gradients predicted by crystal growth theory to exist in liquid adjacent to a growing crystal can be found in chilled basalts containing plagioclase crystals. Concentration gradients are also reported close to olivine in basaltic glass (Anderson 1967). In this study, the compositions of olivine and glass at both the olivine-glass (chilled liquid) interface and far from the interface, have been determined for a basalt.

The basalt (77B-54), drilled to a depth of 0.3 m, is from Leg 9 of the Deep Sea Drilling Project. It is chilled against baked sediment and interpreted as the top of a sill (Hays et al. 1972).

A polished thin section with the following stratigraphy was studied: the upper 4 mm is palagonite, followed by 8 mm of yellow glass containing skeletal crystals of subequant to elongate olivine (Fig. 1) from 50-2000 μ long (average 700-1000 μ) and smaller plagioclase laths. The zone contains 10% plagioclase, 20%

* Lunar Science Institute Contribution No. 205

Berlingska Boktryckeriet, Lund	
1:a korr. 19 feb. 1975	Nytt korr. önskas i ex.
Godkännes till tryckning	/ 1975
För korrekturläsning	Ej prov å tryck och papper

Br.936

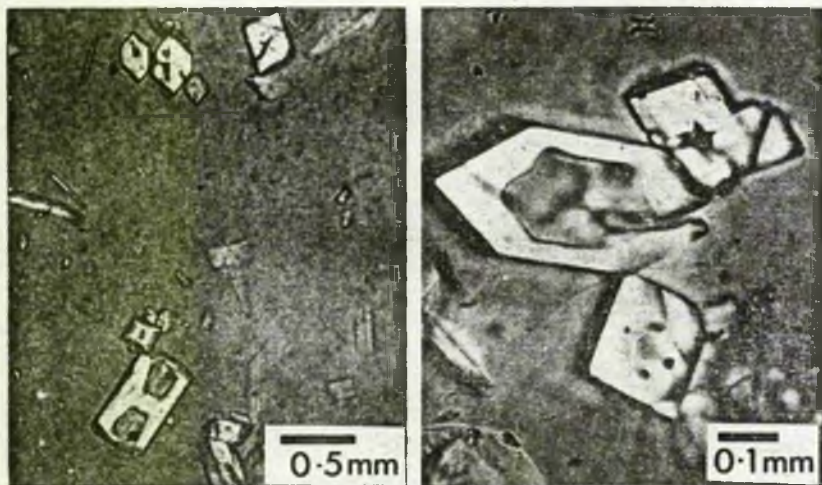


Fig. 1. Skeletal olivine crystals in glass 77B-54.

olivine and 70% glass. Distribution of crystals is heterogeneous and the plagioclase laths show weak preferred orientation. Below this is a dark-colored zone containing identical crystal morphologies set in finely crystallized matrix. Only the middle zone was studied.

Chemical analyses were made on an ARL-EMX-SM electron microprobe using analyzed mineral standards. Glasses were analyzed for K, Ti, Na; Si, Fe, Mg; and Ca, Cr, Al in these groups and in this order. Traverses at right angles to the crystal-glass interface were made at 16 μ /min and X-ray intensities continuously monitored on a strip chart. Close to each olivine studied, the glass was spot analyzed in two places: 'far' from the interface and adjacent to the interface. These positions will be referred to as glass A and glass B respectively. The latter position was identified as a maximum or mini-

mum X-ray intensity for one or more of the three elements being analyzed; the former position was taken 10 μ beyond the point where the X-ray intensities of all three elements first became constant. 80 second counting periods were used. X-ray intensities were corrected for dead-time and drift, using a program EMX (Frazer et al. 1966), and for matrix effects by the method of Bence & Albee (1968).

Na migration in glasses analyzed by microprobe necessitates a special technique for analyzing the K, Ti, Na group at the interface. Traverses from the crystal into the glass were made in 2 μ steps and the counts in a 1s counting period on each spot recorded. The interface position was assumed to be that with the maximum number of Na counts. Because the counting time is very short, results for K, Ti and Na at the interface may be in error by as much as 20% of the amount reported. Cr, Ca, Mg and Fe values are considered to be in error by $\pm 2\%$ and Si and Al values by $\pm 5\%$.

All the olivine in the rock is homogeneous (Fa₁₇₋₁₈, Table 1).

Compositional relationship of A and B glasses

Compositions of four pairs of glasses are shown in Table 2. Within each glass type, similar oxide values are found, but the spread of MgO and FeO values in B glasses is signifi-

cantly larger than the position, the A glass or transitional thole

B glasses exhibit enrichment relative to from an olivine illustrating the co depletions in glass of the scans, the Fe. The remaining Fe unknown origin, like

Relative to glass Si, Al, Ca and Na depleted, while Ti consistent enrichment shows the greatest interface, followed most enriched com and Ca.

Table 4 lists the tive components of The maximum depl (13 wt%) is subst compositional variat variations in the th concentration gradi analysis positions A not necessarily the s usually increases in Fe, Mg (Table 5). chemistry of B glass the range in δ values in crystal growth crystal vectors and a crystal with the pl situations are possi Situations (a) and (b and Fe contents an determined at the int a group of olivines to growth rate, a comb lowest Mg and Fe glass B. A crystal ad ditions apply should to Fig. 3c. This is tru

Diffusion coefficient

From Stokes' law, the of a spherical particle medium of viscosity η

$$f = 6\pi\eta r$$

Table 1. Representative olivine analysis.

SiO ₂	39.13
FeO	16.92
MgO	42.90
MnO	0.27
CaO	0.36
Total	99.57
Structure	0=4
Si	0.996
Fe	0.360
Mg	1.627
Mn	0.006
Ca	0.010
Fo ₁₈	

cantly larger than that in the A glasses. In composition, the A glasses resemble oceanic island or transitional tholeiite types (Rhodes 1973).

B glasses exhibit component depletion or enrichment relative to A glasses. Fig. 2 is a scan from an olivine into the surrounding glass, illustrating the component enrichments and depletions in glass close to the crystal. In 60% of the scans, the Fe trace is a smooth parabola. The remaining Fe traces have a maximum, of unknown origin, like that in Fig. 2.

Relative to glass A, B glasses are typically Si, Al, Ca and Na enriched and Cr, Fe and Mg depleted, while Ti and K show neither consistent enrichment nor depletion (Table 3). Cr shows the greatest percentage depletion at the interface, followed by Mg and Fe. Na is the most enriched component followed by Al, Si and Ca.

Table 4 lists the changes in certain normative components of glass B relative to glass A. The maximum depletion in normative olivine (13 wt%) is substantial. Accompanying the compositional variations in B glasses are large variations in the thickness (δ , Fig. 2) of the concentration gradients in the glass between analysis positions A and B. The value of δ is not necessarily the same for each element and usually increases in the order Si, Al, Ca, Na, Fe, Mg (Table 5). The wider variation in the chemistry of B glasses relative to A glasses and the range in δ values reflect both the difference in crystal growth rates parallel to different crystal vectors and the random orientation of a crystal with the plane of the section. Three situations are possible (Figs. 3a, b, and c). Situations (a) and (b) would increase the Mg and Fe contents and reduce the Si content determined at the interface. Hence, in studying a group of olivines to determine the maximum growth rate, a combination of highest Si and lowest Mg and Fe should be sought in the glass B. A crystal adjacent to which these conditions apply should have an orientation similar to Fig. 3c. This is true of the crystal in Fig. 2.

Diffusion coefficient calculation

From Stokes' law, the coefficient of friction, f , of a spherical particle of radius r moving in a medium of viscosity η is

$$f = 6 \pi \eta r \quad (1)$$

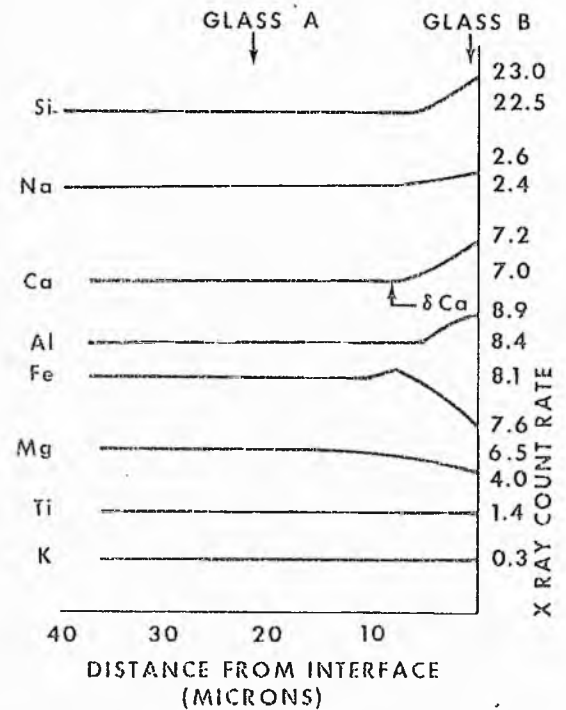


Fig. 2. Uncorrected X-ray intensities recorded on a strip chart during a traverse at 16 μ /min from olivine into glass. Values of the concentration (wt%) of each element in the glass adjacent to the olivine (glass B) and far from it (glass A) are shown. These values have been corrected for deadtime, drift and matrix effects.

The total friction (F) exerted on a mole of the particles is $N_A f$ (N_A is Avogadro's number) and the molar mobility per unit force, ω , is

$$\omega = \frac{1}{N_A f} \quad (2)$$

The diffusion coefficient, D , is calculated from the Stokes-Einstein relation

$$D = RT\omega \quad (3)$$

where R is the gas constant and T is the absolute temperature (Jost 1960).

Use of the Stokes-Einstein equation alone ignores five other factors controlling diffusion of ions, and hence requiring the following assumptions.

- (1) The diffusing particles are spherical and rigid.
- (2) The medium surrounding a diffusing particle is a continuum, rather than separate particles. Since the structure of a silicate melt is

Table 3. Statistics of glass A and B relationships.

B		SiO ₂	TiO ₂	Al ₂ O ₃	Cl ₂ O ₃	FeO	MgO	CaO	Na ₂ O	K ₂ O	Total
1.37	50.32										
1.29	2.49										
1.64	17.49										
1.04	0.02										
1.50	1.50										
1.92	8.44										
1.47	4.79										
1.74	9.72										
1.49	3.28										
1.56	0.49										
1.36	0.36										
7.57	99.09										
-	0.67										
3.31	2.93										
1.53	27.77										
5.36	31.55										
7.07	11.97										
2.74	16.47										
2.20	-										
2.17	2.17										
0.06	0.03										
4.35	4.74										
0.79	0.79										

Ratio of glass pairs showing oxide enrichment at interface to those showing depletion	12:1	7:6	13:0	3:10	1:12	0:13	12:1	10:3	5:8	10:3
Maximum oxide increase at interface	1.95	-	1.86	0.03	0.64	2.30	0.41	0.73	-	1.38
% difference*	4.0	-	11.9	59.5	6.2	36.3	4.0	21.5	-	1.4
Minimum oxide increase at interface	0.19	-	0.29	0.01	0.03	0.92	0.03	0.13	-	0.08
% difference*	0.5	-	1.7	8.1	0.3	14.5	0.3	4.1	-	0.1

* $\frac{wt\%_B - wt\%_A}{wt\%_A}$

must also be assumed < 10% for silicate melts.

(5) There is no chemical interaction between the diffusing species and the 'solvent'. This situation can only be approximated if the solution is dilute, a condition which does not hold for most components in a magma. These interactions could either increase or decrease the diffusion coefficient relative to the calculated value.

The importance of water in diffusion was stressed by Bottinga, Kudo & Weill (1966). The value used in this study is 0.25 wt%, given by Moore (1970) for oceanic tholeiites. Viscosities for the hydrous melts have been calculated by the method of Shaw (1972). Fig. 4 is a plot relating viscosity and temperature for A and B glasses (pair number 16, Table 1) with 0 and 0.5 wt% water. (Lines for 0.25 wt% water lie close to mid-way between the 0 and 0.5 wt% lines.) Addition of 0.25 wt% water to an anhydrous melt reduces η by 25% and hence increases D by the same percentage. For an equivalent water content, glass B is twice as viscous as glass A. However, a growing olivine rejects water at the crystal-liquid interface and the water will form a concentration gradient in the melt. This reduces η at the interface relative to that calculated for 0.25 wt% water and more similar D coefficients at the interface and far from the interface result. In subsequent calculations η and D will be assumed constant throughout the concentration gradient. (For A and B glass to have identical viscosities, B glass must contain 1.3 wt% water.)

The choice of radius for a diffusing species depends on the structure of the silicate melt. The elements Mg, Fe, Ca and Na are regarded

Table 4. Normative composition change in interface glass B relative to bulk glass A.

Analysis no.	Plagioclase increase wt%	Pyroxene increase wt%	Olivine increase wt%	Fe/Fe + Mg increase mol%
4	4.28	-1.00	-5.27	8.1
5	1.49	7.65	-9.41	2.0
6	3.26	0.65	-2.51	3.4
7	0.84	-1.20	0.08	4.6
8	4.06	-7.25	2.31	2.4
9	3.49	-3.00	-1.10	1.3
11	-0.40	12.05	-13.08	4.4
12	2.21	3.00	-5.50	4.6
13	0.73	0.38	-2.93	5.4
14	3.08	-0.30	-3.63	4.5
15	3.76	3.52	-7.74	4.7
16	4.05	8.63	-12.87	4.5
17	0.72	1.53	-0.30	4.6

as melt network modifiers while Si is a network former (Hutchins & Harrington 1966). Al is apparently capable of both types of behavior (Yoldas 1971). Diffusion coefficients for the network modifiers are calculated assuming existence of Mg²⁺, Fe²⁺, Ca²⁺, Na⁺ and Al³⁺ ions in a complex structured SiO₄ and AlO₄ 'solvent'. For the network formers, diffusion coefficients are calculated for SiO₄⁴⁻ and AlO₄⁵⁻ monomeric species and the possibility of polymerization (Hess 1970) neglected. The lengths of Si-O and Al-O bonds are taken as the radius of the SiO₄⁴⁻ and AlO₄⁵⁻ species. (Ionic radii are from Weast 1969.)

As an example of this calculation, the value of D for an AlO₄⁵⁻ species diffusing in anhydrous glass 16A is derived.

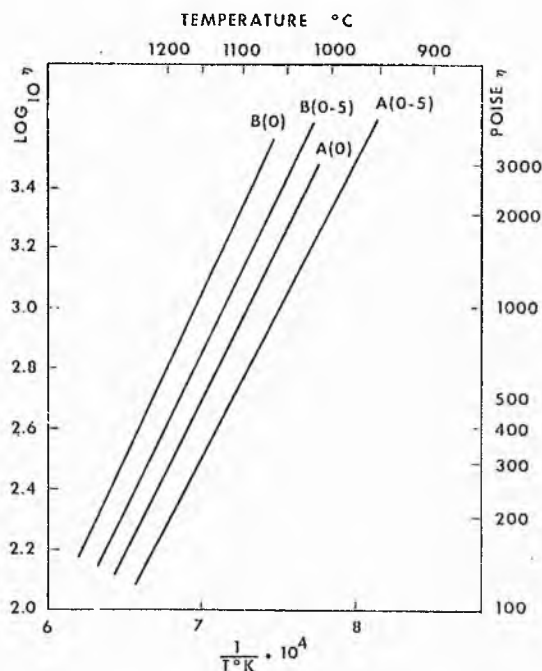


Fig. 4. Arrhenius plot of viscosity as a function of water content and bulk composition. (0) and (0.5) are wt% H_2O . A and B are glasses 16A and 16B.

r_{Al-O} $1.7 \cdot 10^{-8}$ cm
 T $1413^\circ K$
 η 920 poise
 $F = 2.9 \cdot 10^{-4}$ dyne s/cm
 $N_{Al} f = 1.77 \cdot 10^{20}$ dyne s/cm
 $\omega = 0.563 \cdot 10^{-20}$ cm/dyne s
 $D = RT\omega = 6.63 \cdot 10^{-10}$ cm²/s

At the liquidus temperatures of basalts (1100–1200 C), values of D for all species in glass 16A are around 10^{-9} (Fig. 5). At a given temperature, Mg diffuses 4.5 times faster than AlO_4^{5-} species. The parallelism of the lines in Fig. 5 implies that the activation energy of diffusion for each ion is identical. Furthermore, the method fails to predict the observations of Winchell & Norman (1969) that (1) diffusion in silicate melts is compensated, so that the activation energy (E) is correlated with $\log D_0$, where D_0 is a constant in the Arrhenius equation $D = D_0 \cdot \exp(-E/RT)$, and (2) single metal ions all diffuse at about the same rate (10^{-6} cm²/s) in silicate melts at 1500 K. These failings result from use of Stokes-Einstein equation which only allows for difference in size of

Table 5. Range of concentration gradient thicknesses δ (μ).

Si	1.6–5.6
Fe	4.5–16.0
Mg	6.0–20.0
Al	4.8–16.0
Ca	4.0–14.4
Na	4.8–25.6

ions, and for viscosity and temperature of the melt. The equation cannot allow for coupled diffusion, for the lack of rigidity of ions, for ionic charge or for charge density of ions.

Comparison between model and measured D

Diffusion coefficients are known for several ions all diffuse at about the same rate (10^{-6} cm²/s) in simple silicate systems (Table 6). Calculated values of $D_{Ca^{2+}}$ in Ca–Al–Si melts range from 0.7–0.1 of the measured values. With addition of Mg to the system, the discrepancy between calculated and measured $D_{Ca^{2+}}$ is reduced. Calculated $D_{SiO_4^{4-}}$ is low a factor of 1.3–1.7, while $D_{Al^{3-}}$ is low by a factor of 1.7–10. Agreement between calculated and measured D_{Fe} for the FeO–SiO₂ system is excellent. In summary, the calculated and measured diffusion coefficients for these simple systems agree within a factor of 13. In view of the empirical nature of the estimation of η for the model and errors in experimental determination of D , this agreement is good.

Data on Ca diffusion in a mugearite (Medford 1973) represents the only available information on diffusion in natural magmas. The calculated Ca diffusion coefficient ($8.3 \cdot 10^{-9}$ cm²/s at 1250 C) for this melt at 1250 C is 16 times smaller than the measured value. Shaw (in press) reports diffusion coefficients for water in obsidian glasses at 850 C. His measurements are up to 10^4 times larger than values calculated from the Stokes-Einstein equation.

Thus, the discrepancy between measured and calculated diffusion coefficients is greater for magmas than for simple silicate melts. It is also greater the lower the temperature and the more viscous the system. In simple silicate systems the measured diffusion coefficient is usually less than a factor of 100 times greater than the value calculated from the Stokes-

Fig. 5. Arrhenius plot

Table 6. Comparison of

Composition (wt.%)			
SiO ₂	Al ₂ O ₃	CaO	MgO
40.0	21.0	39.0	—
41.3	20.0	38.7	—
41.2	19.0	39.8	—
44.8	—	55.2	—
31.8	19.5	43.4	5.4
40.0	21.0	39.0	—
41.3	20.0	38.6	—
41.3	20.0	38.6	—
46.4	9.9	43.5	—
24.0	—	—	—
50.9	21.6	—	—
54.6	23.2	—	—

Einstein equation (W)
 Much more data is
 tematic effects of co
 temperature on the c

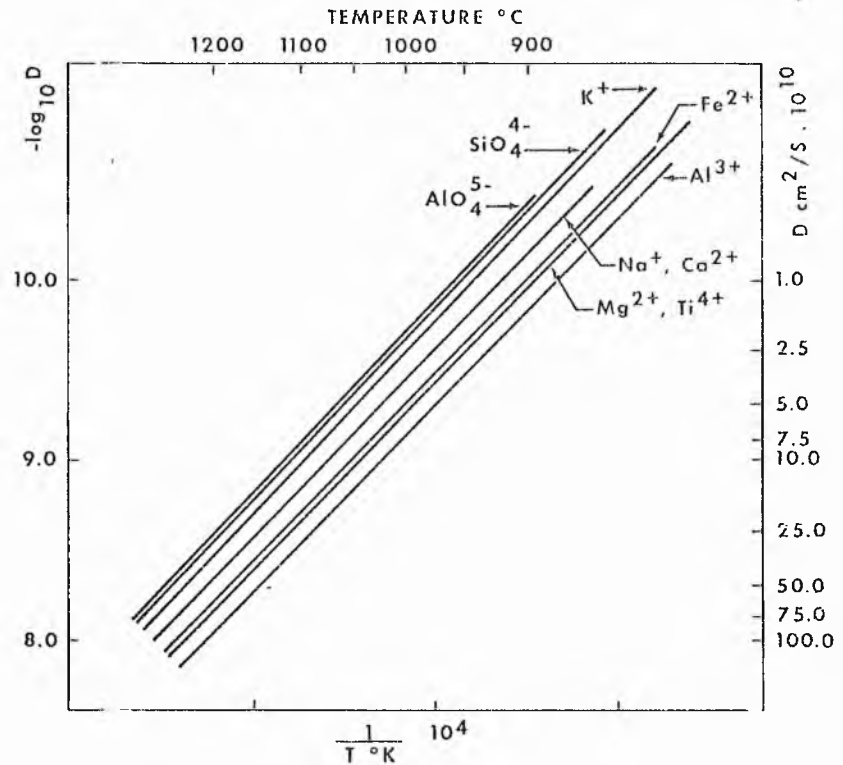


Fig. 5. Arrhenius plot of D for nine ions in glass 16A, with 0.25 wt% H₂O.

Table 6. Comparison of measured and calculated D in simple silicate systems.

Composition (wt%)								T°C	Diffusing ion	Diffusion coefficient .10 ⁷		Reference
SiO ₂	Al ₂ O ₃	CaO	MgO	FeO	K ₂ O	Na ₂ O	H ₂ O			Measured	Calculated	
40.0	21.0	39.0	-	-	-	-	-	1430	Ca ²⁺	10.0	1.3	Towers & Chipman (1957)
41.3	20.0	38.7	-	-	-	-	-	1450	Ca ²⁺	12.0	1.1	Henderson, Young & Derge (1961)
41.2	19.0	39.8	-	-	-	-	-	1350	Ca ²⁺	3.9	0.54	Saito & Maruya (1958)
44.8	-	55.2	-	-	-	-	-	1485	Ca ²⁺	7.1	2.3	Saito & Maruya (1958)
31.8	19.5	43.4	5.4	-	-	-	-	1530	Ca ²⁺	11.7	22.0	Saito & Maruya (1958)
40.0	21.0	39.0	-	-	-	-	-	1430	SiO ₄ ⁴⁻	1.0	0.75	Towers & Chipman (1957)
41.3	20.0	38.6	-	-	-	-	-	1450	SiO ₄ ⁴⁻	1.2	0.67	Henderson, Young & Derge (1961)
41.3	20.0	38.6	-	-	-	-	-	1400	Al ³⁺	2.4	1.4	Henderson, Young & Derge (1961)
46.4	9.9	43.5	-	-	-	-	-	1520	Al ³⁺	20.0	2.1	Henderson, Young & Derge (1961)
24.0	-	-	-	76.0	-	-	-	1275	Fe ²⁺	58.0	60.0	Matsumara (1969)
50.9	21.6	-	-	-	19.9	-	7.6	1300	K ⁺	14.0	0.82	Winchell (1969)
54.6	23.2	-	-	-	-	14.1	8.2	1300	Na ⁺	26.0	2.1	Winchell (1969)

Einstein equation (Winchell & Norman 1969). Much more data is needed before the systematic effects of composition, viscosity and temperature on the discrepancy can be eval-

uated. Comparison with the data of Medford (1973) suggests that the diffusion coefficients calculated for basalt 77B-54 may be too small by a factor of 16.

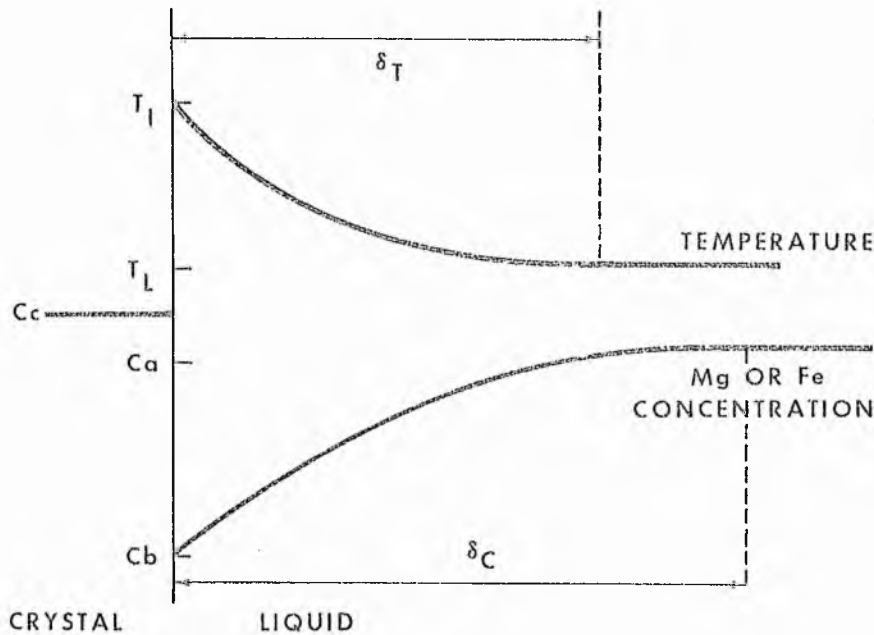


Fig. 6. Schematic temperature and composition profiles in melt adjacent to a growing olivine crystal. See text for discussion of symbols.

Olivine growth rate

The computed diffusion coefficients for Mg, Fe and SiO_4^{4-} in glass 16A with 0.25 wt% water are used in this section to calculate instantaneous growth rates for olivines in the glass portion of the basalt. Two methods of calculation may be used.

Method 1

The concentration gradients in the basaltic glass adjacent to crystals record preferred movement of Mg^{2+} and Fe^{2+} toward olivine crystals. From a knowledge of the diffusion rate of the ions, the linear rate of growth of a crystal can be calculated, assuming steady state growth and diffusion across a boundary layer from a large, well-mixed reservoir of melt.

The rate, J , at which species diffuse towards a crystal is given by

$$J = -D_1 \text{grad } c - D_2 \text{grad } T \cdot c_s \quad (4)$$

(Katchalsky & Curran 1967)

where D_1 is the chemical diffusion coefficient, D_2 is the thermal diffusion coefficient, $\text{grad } c$ is the difference in concentration of a species in the interfacial glass (B) minus that in the bulk

glass (A) divided by the concentration gradient thickness (δ_c) (i.e. $CB - CA/\delta_c$, Fig. 6), $\text{grad } T$ is the difference in temperature between the interface and the bulk liquid divided by the interfacial thickness (δ_T) (i.e. $T_1 - T_L/\delta_T$, Fig. 6) and c_s is the concentration of the species in the liquid.

For every mole of Mg or Fe ions reaching the olivine, 1/2 mole of olivine crystallizes. Hence, the product of the molar volume of olivine ($V_{ol.}$) and half the flow rate (J) gives the growth rate (G) of a crystal face on the olivine, i.e.

$$G = V_{ol.} J \cdot 1/2 \quad (5)$$

No value for D_2 is available for silicate melts and, since it is likely to be 10^2 – 10^3 times smaller than D_1 (Jost 1960), the second part of equation (4) can be neglected.

Method 2

An equation for steady state growth rate is given by Burton & Slichter (1958), based on an analysis of the partitioning of a chemical species between the bulk glass (A), the interface glass (B) and the crystal (C).

$$G = \frac{D_1}{\delta_c} \cdot \ln \frac{C_B - C_c}{C_A - C_c} \quad (9)$$

The symbols have the same significance as in method 1; C_c is the concentration of the species in the crystal (Fig. 6). This method has the advantage that G can also be estimated from the data for Si.

Both models require five assumptions: (1) The olivine grew continuously until the melt was quenched and diffusion became too slow to alter the concentration gradients. (2)

$$\frac{C_A - C_B}{\delta_c}$$

is a constant through the concentration gradient. (In reality this parameter decreases with increasing distance from the crystal.) (3) Transport of species in the melt is perpendicular to the growing crystal face, i.e. transport is uniaxial. (4) D_1 is constant in value through the concentration gradient. (5) The electrochemical mobility of ions is small compared to the diffusional mobility (Helfferich 1962) All these assumptions conspire to reduce the calculated growth rate.

Crystallization temperature

The ratio of Fe/Mg in olivine to Fe^{2+}/Mg in bulk glass A (0.28) is very close to the value of 0.3 predicted by Roeder & Emslie (1970) at equilibrium. This suggests that the olivines grew under only slight supercooling (non-equilibrium) conditions. Lack of zoning indicates that little, if any, growth can have occurred during cooling between the $T_{liquidus}$ and $T_{glass\ transition}$. The $T_{olivine\ liquidus}$ for this composition is 1170 C at 1 atm (Roeder & Emslie 1970; Fig. 8).

Table 7. Comparison of olivine 16 growth rates calculated using methods 1 and 2 (1170 C).

Diffusing ion	G method 1 cm/s .10 ⁷	G method 2 cm/s .10 ⁷
Mg ²⁺	2.2*	3.0
Fe ²⁺	-	2.8
SiO ₄ ⁴⁻	-	4.3

* Calculated from $J_{Mg^{2+}} + J_{Fe^{2+}}$

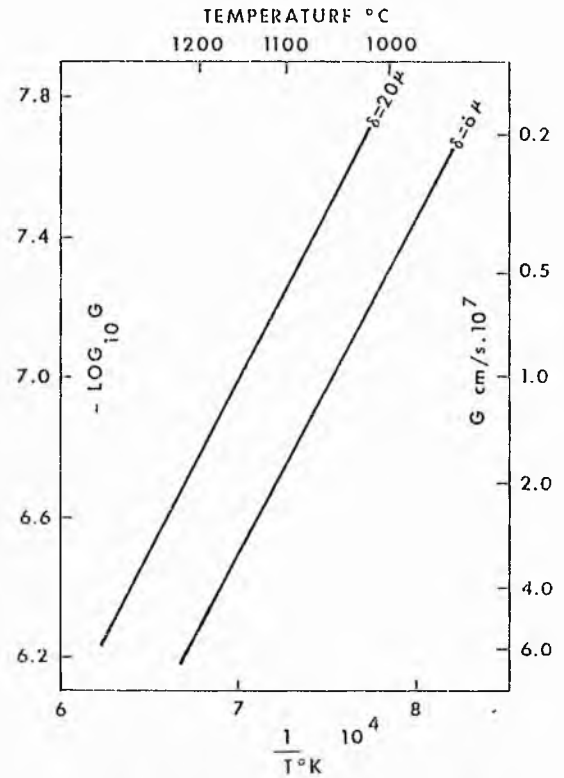


Fig. 7. Arrhenius plot of G for the widest and narrowest Mg concentration gradient encountered. (Method 2 values.)

Results

Table 7 summarizes the values of growth rate for olivine 16, determined by the two computational methods. All approaches suggest that G is between $2.2 - 4.3 \cdot 10^{-7}$ cm/s. These values are subject to the same errors as the diffusion coefficient. Agreement between the methods is excellent. The similarity in growth rates computed using diffusion coefficients for different ions suggests that the ionic diffusion model used here is self-consistent for Mg^{2+} , Fe^{2+} and SiO_4^{4-} . The lower growth rate computed using Fe^{2+} data, as compared to Mg^{2+} and SiO_4^{4-} data, are attributable to Fe^{3+} enrichment at the interface which cannot be distinguished by electron probe technique. Growth rates calculated from Mg^{2+} or SiO_4^{4-} data are therefore more reliable. For all the olivines studied, G varies by a factor of three, the lowest value being 2.10^{-7} and the highest 6.10^{-7} cm/s (Mg data).

Berlingska Boktryckeriet, Lund	
1:a korr. 19 feb. 1975	Nytt korr. önskas i ex.
Godkännes till tryckning	/ 1975
För korrekturläsning	Ej prov å tryck och papper

Br.937

mush, it is convection and/or turbulence and not diffusion which are necessary to connect interstitial and supernatant liquid (Jackson 1961) and maintain the interstitial liquid in the mush, 20μ from crystals, at a constant composition, C_A (Fig. 6).

4. Cumulus crystals are considered to have settled onto the floor of the Skaergaard intrusion to a thickness of 0.6 mm/day (Wager & Brown 1968). If crystal mushes at Skaergaard contained 70% cumulus crystals, a crystal growth rate of 0.45 mm/day would ensure complete solidification of mushes at a velocity compatible with the rate at which crystals settle. When this growth rate was achieved, cumulates lacking zoned crystals resulted. The fastest growth rates of olivines in basalt 77B-54 (0.5 mm/day) are compatible with the Skaergaard model.

5. Since a growing crystal has a sphere of influence on the liquid around it and, assuming it remains growing while mechanically separated (by flow or gravity differentiation) from the bulk of the liquid, not only will olivine components be removed from the bulk liquid, but so will those elements at the interface. For example, a spherical olivine 100μ in radius influencing the surrounding liquid within 20μ will remove with it 17% of its own volume of SiO_2 -enriched basalt. Petrochemical mass balance calculations which relate rock compositions by crystal-liquid fractionation may be neglecting a minor, but possibly significant, means of liquid-liquid fractionation.

6. The importance of the ratio G/D on the morphology of melt-grown crystals has been stressed by Keith & Padden (1963), Lofgren (1974) and Donaldson (1974). A low ratio favors growth of equant polyhedral crystals while higher ratios progressively favor skeletal, dendritic and spherulitic crystal morphologies. The methods described in this paper provide a means of quantifying the relation between crystal morphology and G/D ratio and interpreting rock textures. The skeletal olivines in sample 77B-54 grew at a G/D ratio of approximately $10^2/\text{cm}$.

7. The olivines in sample 77B-54 have partially entrapped melt inclusions (Fig. 1). This suggests that growth rates of 10^{-6} – 10^{-7} cm/s are adequate for formation of melt inclusions in olivine. On entrapment, the outer 10μ of a melt inclusion will differ from the bulk melt composition. In a 100μ spherical melt inclu-

sion this amounts to less than 25% by volume of the inclusion. Table 3 indicates the maximum possible difference between the composition of this 25% of the inclusion and the remaining 75%.

Conclusions

1. A model for calculating ionic diffusion coefficients has been applied to a basaltic melt. At liquidus temperatures, coefficients around 10^{-9} cm^2/s are obtained.

2. By applying $D_{\text{Mg}^{2+}}$, $D_{\text{Fe}^{2+}}$ and $D_{\text{SiO}_4^{4-}}$ to the concentration gradients adjacent to olivines in the basalt, instantaneous olivine crystal growth rates of approximately 10^{-7} cm/s are calculated.

3. Since these skeletal crystals cannot have grown in situ, the composition of the crystals plus enclosing glass need not represent a melt.

4. The crystal growth rate results are compatible with the Skaergaard intrusion crystallization model.

Acknowledgements. - I thank the Natural Environment Research Council and the Lunar Science Institute, which is operated by the Universities Space Research Association under Contract No. NSR 09-051-001 with the National Aeronautics and Space Administration, for financial support. The guidance of R. J. Williams and the comments of P. R. Brett, H. R. Shaw, H. I. Dreyer and A. T. Anderson on the manuscript are gratefully acknowledged.

References

- Anderson, A. T. 1967: Possible consequences of composition gradients in basalt glass adjacent to olivine phenocrysts. *Trans. Am. Geophys. Union* 48, 227-228.
- Bence, A. E. & Albee, A. L. 1968: Empirical correction factors for the electron microanalysis of silicates and oxides. *J. Geol.* 76, 382-403.
- Bottinga, Y., Kudo, A. & Weill, D. 1966: Some observations on oscillatory zoning and crystallization of magmatic plagioclase. *Am. Mineral.* 51, 792-806.
- Burton, J. A. & Slichter, W. P. 1958: The distribution of solute elements: steady-state growth. Pp. 71-106 in Bridgers, H. E. (ed.): *Transistor Technology*. Vol. 1. Van Nostrand, New York.
- Coombs, D. S. 1963: Affinities of basaltic magmas and pyroxenes as illustrated on the diopside-olivine-silica diagram. *Min. Soc. Am. Spec. Pap.* 1, 227-250.
- Dreyer, H. I. & Johnston, R. 1958: The petrology of picritic rocks in minor intrusions - a Hebridean group. *Trans. Roy. Soc. Edin.* 63, 459-499.

- Donaldson, C. H. 1974: Olivine morphology in the tertiary harristites of Rhum and in some Archaean spinifex rocks. *Geol. Soc. Am. Bull.* 85, 1721-1726.
- Frazer, J. Z., Fitzgerald, R. W. & Reid, A. M. 1966: Computer programs EMX and EMX2 for electron microprobe data processing. *Scripps Inst. of Oceanography, rept. 66-14*, unpublished.
- Hays, J. D., Cook, H., Jenkins, G., Orr, W., Goll, R., Cook, F., Milow, D. & Fuller, J. 1972: *Initial Report of the Deep Sea Drilling Project, Leg 9*. U.S. Government Printing Office.
- Helferich, F. 1962: *Ion Exchange*. McGraw-Hill, New York. 624 pp.
- Henderson, J., Yang, L. & Derge, G. 1961: Self diffusion of aluminum in $\text{CaO-SiO}_2\text{-Al}_2\text{O}_3$ melts. *Trans. Met. Soc. AIME* 221, 56-60.
- Hess, G. B. 1973: Heat and mass transport during crystallization of the Stillwater igneous complex. Pp. 503-520 in Shagam, R. (Ed.): *Studies in Earth and Space Sciences*. Geol. Soc. Amer. Mem. (Hess vol.)
- Hess, P. C. 1970: Polymer model of silicate melts. *Geochim. Cosmochim. Acta* 35, 289-306.
- Hutchins, J. R. & Harrington, R. V. 1966: Glass. Pp. 533-604 in Kirk, D. & Othmer, H. C. (Eds.): *Encyclopedia of Chemical Technology, III*. Wiley, New York.
- Jackson, E. D. 1961: Primary textures and mineral associations in the ultramafic zone of the Stillwater Complex, Montana. *U.S. Geol. Surv. Prof. Pap.* 358, 106 pp.
- Jackson, E. D. 1967: Ultramafic cumulates in the Stillwater, Great Dyke and Bushveld intrusions. Pp. 20-38 in Wyllie, P. J. (Ed.): *Ultramafic and Related Rocks*. Wiley, New York.
- Jost, W. 1960: *Diffusion in Solids, Liquids, Gases*. Academic Press, New York. 558 pp.
- Katchalsky, A. & Curran, P. F. 1967: *Nonequilibrium Thermodynamics in Biophysics*. Harvard University Press. 248 pp.
- Keith, H. D. & Padden, F. J. 1963: A phenomenological theory of spherulitic crystallization. *J. Appl. Phys.* 34, 2409-2421.
- Kushiro, I. 1974: Melting of hydrous upper mantle and possible generation of andesitic magma: an approach from synthetic systems. *Earth Planet. Sci. Lett.* 22, 294-299.
- Lofgren, G. E. 1974: An experimental study of plagioclase crystal morphology: isothermal crystallization. *Am. J. Sci.* 274, 243-273.
- Matsumara, G. 1969: Sintering of iron wires with a liquid phase. *Int. J. Powder Met.* 5 (2), 55-61.
- Medford, G. A. 1973: Calcium diffusion in a mugearite. *Can. J. Earth Sci.* 10, 394-402.
- Moore, J. G. 1970: Water content of basalt erupted on the ocean floor. *Contr. Mineral. Petrol.* 28, 272-279.
- Onsager, L. 1931: Reciprocal relations in irreversible processes II. *Phys. Review* 38, 2265-2279.
- Rhodes, J. M. 1973: Major and trace element chemistry of basalts from Leg 9 of the Deep Sea Drilling Project. *Trans. Am. Geophys. Union* 54, 1014-1015.
- Roeder, P. L. & Emslie, R. F. 1970: Olivine-liquid equilibrium. *Contr. Mineral. Petrol.* 29, 275-289.
- Saito, T. & Maruya, K. 1958: Diffusion of calcium in liquid slags. *Sci. Repts. Res. Inst. Tohoku Univ.* 10, 306-314.
- Shaw, H. R. 1972: Viscosities of magmatic silicate liquids: an empirical method of prediction. *Am. J. Sci.* 272, 870-893.
- Shaw, H. R.: Diffusion of H_2O in granitic liquids: Part I. Experimental data; Part II. Mass transfer in magma chambers. In Hoffman, A. (Ed.): *Geochemical Transport and Kinetics*. Carnegie Inst. Wash. Monograph. In press.
- Towers, H. & Chipman, J. 1957: Diffusion of calcium and silicon in a lime-alumina-silica slag. *Trans. Met. Soc. AIME* 209, 769-773.
- Wager, L. R. & Brown, G. M. 1968: *Layered Igneous Rocks*. Oliver & Boyd, Edinburgh.
- Weast, R. C. 1969: *Handbook of Chemistry and Physics*. Chemical Rubber Co.
- Winchell, P. 1969: The compensation law for diffusion in silicates. *High Temp. Sci.* 1, 200-215.
- Winchell, P. & Norman, J. H. 1969: A study of the diffusion of radioactive nuclides in molten silicates at high temperature. Pp. 419-492 in Heister, N. K. (Ed.): *Proc. Third Int. Symp. on High Temp. Technol.* Butterworths, London.
- Yoldas, B. E. 1971: The nature of the coexistence of four- and six co-ordinated Al^{3+} in glass. *Phys. Chem. Glasses* 12, 28-32.

Accepted for publication January 1975

Printed April 1975

ULTRABASIC BRECCIAS IN LAYERED INTRUSIONS—THE RHUM COMPLEX¹

COLIN H. DONALDSON

Lunar Science Institute, 3303 Nasa Road 1, Houston, Texas 77058; and Department of Geology, University of St. Andrews, Scotland

ABSTRACT

Two previously unmapped ultrabasic breccias—the Harris Bay and Ard Mheall breccias, in the Rhum layered complex—formed by upward intrusion of feldspathic peridotite magmas rather than by settling of cumulus crystals and fault-scar blocks into a faulted zone in the layers. The Harris Bay breccia was formed by forceful intrusion, the Ard Mheall breccia by comparatively gentle disruption. Olivine (Fo₈₂₋₈₃), plagioclase (An₄₇₋₅₀), diopside, chromite, magnesian phlogopite, and kaersutite are the dominant phases of the matrix. The intrusive magmas were hydrous and at least as hot as basaltic magma. Gabbroic anorthosite and anorthositic gabbro veins (plagioclase composition An₈₀₋₈₅) have been ejected as residual liquid from the breccias. The breccia matrices were intruded as suspensions of olivine and bytownite crystals in an ultrabasic, calcic liquid, both fractions having been derived from an olivine eucrite or picritic eucrite liquid. The study indicates that in addition to fractionating upon entry into the Rhum chamber, magma fractionated beforehand at a deeper level.

INTRODUCTION

The ultrabasic rocks of Rhum contain linear outcrops of unconformable ultrabasic breccias bearing blocks demonstrably derived from the layered series (Harker 1908). The blocks are enclosed in feldspathic peridotite matrices which are texturally similar to layered series rocks (Wadsworth 1961). Contacts of these breccias with the layered series are so poorly exposed, that Harker speculated that they were intrusive contacts while Wadsworth (1961, 1973) considered them as fault contacts. This paper presents field and petrographic evidence from two previously unmapped breccias which permits determination of the contact relations as intrusive.

The study has application to six features of the petrogenesis of the Rhum complex: (1) The mechanism of breccia formation, (2) the origin of the matrices of the breccias, (3) the importance of water in the genesis of the matrices, (4) the relationship of breccia matrices to the parent magma of the layered complex, (5) the mechanism of repetitive replenishment of magma to

the Rhum chamber (Brown 1956), and (6) whether the ultrabasic rocks originate from a basic magma (Brown 1956; Wager and Brown 1968) or an ultrabasic magma (Harker 1908; Wager 1968; Drever and Johnston 1972; Donaldson et al. 1973). Evidence suggests that Rhum may be a complex whose parent melt was more calcium rich than the basalts commonly postulated as parental to ultrabasic layered intrusions (Wager and Brown 1968).

GEOLOGICAL SETTING

Both breccias are in the southwest part of the ultrabasic complex. They will be referred to as the Harris Bay breccia and the Ard Mheall breccia (fig. 1). Three other breccias mapped by Harker (1908) and Wadsworth are also shown in figure 1. The five breccias converge to the northeast, the focus being $\frac{1}{2}$ mile north of the top of figure 1.

FIELD RELATIONS

Harris Bay breccia.—The breccia is 70 m wide and is exposed for 180 m in length. To the south, the sea covers the outcrop while to the north the breccia is covered by drift and is not exposed in the cliffs of country rock peridotite 20 m beyond. In contrast, contacts parallel to the northeast alignment of the mass are

¹ Manuscript received January 17, 1974; revised April 2, 1974.

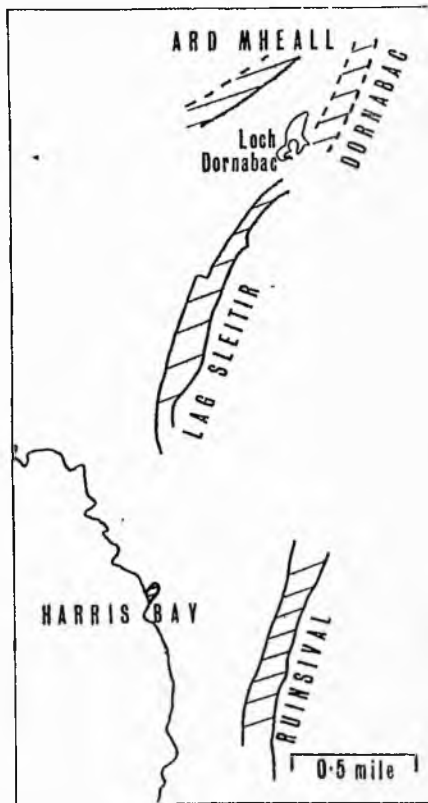


FIG. 1.—Map of the principal ultrabasic breccias intruding the western layered series of Rhum.

almost entirely exposed. These contacts are vertical. The country rock has neither slumped at the margins nor has it merged or mixed with the breccia matrix, facts which suggest that it remained rigid during breccia formation. Since there is neither evidence for matrix chilling, nor for hornfelsing of the country rock, the country rock must still have been hot, but solidified, during breccia emplacement. Vertical, upwardly closing masses (0.5 m maximum thickness) and a horizontal lens of matrix material transgress the western margin into the country rock.

Streaks and veins of gabbroic anorthosite and anorthositic gabbro (0.4–8 cm wide) are abundant at the contact. They are also common in the country rock up to 100 m from the contact. Pyroxene and

olivine tend to occur preferentially at the vein center, with plagioclase at the margin. The composition, determined optically, of the unzoned plagioclase in one vein is An_{82} .

Xenoliths include peridotite with textural varieties found in the layered series, allivalite, rocks gradational in modal mineralogy between these two, and hornfelsed eucrite. Some xenoliths are themselves breccia fragments, suggesting that polyphase or resurgent brecciation has occurred. Xenoliths range in size from 0.05–2.7 m in diameter, those 0.5 m in size being most common. Since preferred distribution of xenoliths according to size or density is not apparent, it is inferred that sorting processes had minimal effect in altering the random distribution produced during brecciation. The ratio of blocks to matrix is $\frac{1}{3}$ to $\frac{1}{2}$.

Closely spaced, wispy banding of plagioclase is developed in the matrix subparallel to the contacts, the banding being displaced by the included blocks. Some bands may be traced into allivalite xenoliths and clearly represent remobilized plagioclase from the blocks. Some of the matrix is therefore hybrid.

A few blocks are embayed or penetrated by the matrix (fig. 2). This feature is attributed to assimilation.

Ard Mheall breccia.—To the south the breccia merges into, and is covered by, layered country rock peridotite; to the north, and 75 m lower, outcrop tapers out. The well-exposed eastern side is in vertical contact with the country rock and is laterally transitional over 1–3 m, with abundant veins and stringers of anorthosite (plagioclase composition An_{84} , table 1). The poorly exposed western contact is vertical.

A bladed parallel olivine growth structure ("harrisite", Harker [1908]) up to 1.2 m long and with the blades commonly oriented in a vertical plane characterizes some layered country rock peridotite adjacent to this breccia. Within the breccia, some harrisite xenoliths retain

FIG. 2.—Peridotite matrix. Harris Bay.

the vertical orientation to gentle in matrix material broken into layers of peridotite layers horizontal to not sufficient suggest major eastern side of the typical breccia textures recorded in xenolith type graphically identified. This observation indicates incipient brecciation.

Some of the crystalline skin the "radiate" "bird's track" (Mason 1968) peridotites" a tramatific liquid

PETROGRAPHY

Textures of the Subhedral, subangular (3.3–0.15 (fig. 3a–d). embayed, other growths. Both

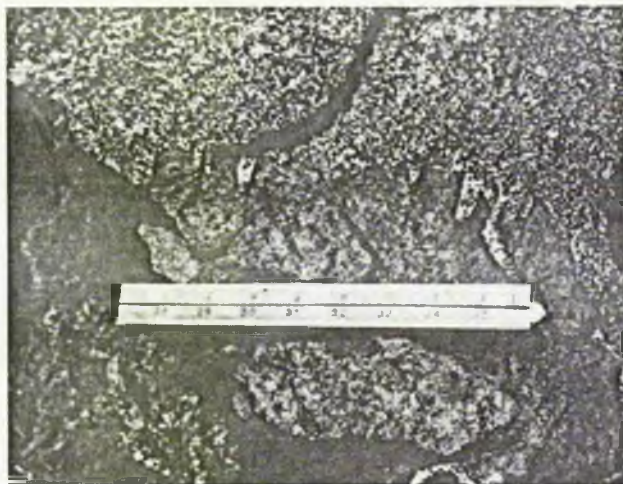


FIG. 2.—Peridotite xenolith embayed by tongues of coarser grained feldspathic peridotite breccia matrix. Harris Bay breccia. Scale in inches.

the vertical olivine orientation, testifying to gentle in situ envelopment by the matrix material. Elsewhere, harrisite is broken into 1–5 cm-sized fragments and peridotite layers are rotated from the horizontal to the vertical plane, though not sufficiently internally deformed to suggest major slumping. Only at the eastern side of the mass is a thin band of typical breccia developed. All these features record localized turbulence. The only xenolith type found is peridotite, petrographically identical to the country rocks. This observation favors an origin by incipient brecciation.

Some of the matrix contains macrocrystalline skeletal olivines, identical to the “radiate spinifex” (Nesbitt 1971) or “bird’s track” texture (Naldrett and Mason 1968) found in Archaean “quench peridotites” and laboratory-quenched ultramafic liquids (Dickey 1973).

PETROGRAPHY OF THE MATRIX

Textures and chemical mineralogy.—Subhedral, subequant, homogeneous olivines (3.3–0.15 mm in size) are abundant (fig. 3a–d). Some olivine crystals are embayed, others form elongate, parallel growths. Both morphologies are common

in harrisite (Donaldson 1974). The olivines are undeformed and so cannot be regarded as xenocrysts derived from the layered series. Both breccia masses have similar olivine compositions (Fo_{63-82} , table 1); low Ca-contents span the range found by Simkin and Smith (1970) for peridotites from the layered series. Simkin and Smith suggest that this feature indicates a slowly cooled, equilibrated crystallization environment.

Plagioclase most commonly forms anhedral plates (maximum size 3.6×2.5 mm) in subophitic relation to olivine (fig. 3a, b). Less common are tabular crystals (1.0×0.3 mm) enclosed in augite, and aggregates of up to 50 subequant plagioclases, with 120° intersections, occupying a volume similar to that of the anhedral plates. This last texture suggests plagioclase annealing. The broad unzoned cores are An_{83-87} at Ard Mheall and An_{70-82} at Harris Bay. A few plagioclases show sharp, narrow, marginal zoning to An_{60-70} (table 1). Moderate Fe content characterizes the plagioclase.

Clinopyroxene, faintly green in thin section, either poikilitically encloses both olivine and plagioclase or forms patches interstitial to these two minerals (fig. 3a,

TABLE 1

ELECTRON MICROPROBE ANALYSES OF MINERALS IN BRECCIAS*

	PLAGIOCLASE				PYROXENE	KAESUTITE	PHLOGOPITE
	Olivine	Core	Rim	Vein			
SiO ₂	39.08	46.51	53.90	50.94	50.35	42.23	37.97
Al ₂ O ₃	n.d.	32.59	28.78	30.62	4.38	11.60	15.53
TiO ₂	0.01	0.06	0.03	0.08	3.66	4.96	6.16
Cr ₂ O ₃	0	n.d.	n.d.	n.d.	1.14	0.52	0.46
FeO†.....	15.95	0.29	0.59	0.43	0.76	7.88	7.44
MgO.....	44.25	0.00	0.05	0.00	4.78	14.88	18.76
CaO.....	0.07	16.55	11.83	13.42	22.36	11.88	0
Na ₂ O.....	n.d.	2.71	5.25	4.62	0.43	2.53	1.16
K ₂ O.....	n.d.	0.05	0.09	0.15	0.00	1.05	8.45
Total.....	99.44	98.86	100.52	100.26	99.80	97.42	95.36

STRUCTURAL FORMULAE

	O = 4	O = 8	O = 6	O = 23	O = 22
Si.....	0.991	2.169	2.435	2.323	2.139
Al(4).....	0.002	1.797	1.532	1.645	1.838
Al(6).....	0	0.002	0.001	0.003	0.001
Ti.....	0	0	0	0	0
Cr.....	0	0	0	0	0
Mg.....	1.673	0	0.003	0	0
Fe.....	0.338	0.011	0.002	0.016	0.015
Ca.....	0.002	0.827	0.572	0.656	0.854
Na.....	0	0.245	0.460	0.408	0.184
K.....	0	0.003	0.005	0.009	0.001
Mg/Fe atoms.....	4.9	4.6	5.9	3.5	4.6

ATOMIC RATIOS

	Mol. %				
Mg.....	83.2	82.2	59.1	64.8	84.4
Fe.....	16.8	17.8	40.4	34.3	15.5
			0.3	0.9	0.1
			0.5	0.1	7.8
			0.3	0.1	8.7

NOTE.—Analyses in tables 1 and 2 were made on an ARL-EMX-SM microprobe, accelerating potential 15 kv, sample current 0.02 μA, 1-2 μ beam size and 80 sec total counting time on four spots.
 * First analysis of each pair from Harris Bay breccia, second from Ard Mheall breccia. Vein (8 cm wide gabbroic anorthosite).
 † All iron as FeO.



FIG. 3.—Photo
 b—crossed polar
 claso—white, low

Fe 16.8 17.8 40.4 16.9 34.3 16.3 49.8 48.2
 Mg 0.1 0.1 0.1 0.1 0.1 0.1 0.1 0.1
 Or 0.3 0.3 0.5 0.3 0.9 0.1 0.1 0.1
 Ab 20.1 20.1 40.4 16.9 34.3 16.3 49.8 48.2
 All iron as FeO.

NOTE.—Analyses in tables 1 and 2 were made on an ARL-EMX-8M microprobe, accelerating potential 15 kv, sample current 0.02 μ A, 1–2 μ beam size and 80 sec total counting time on four spots.
 * First analysis of each pair from Harris Bay breccia, second from Ard Mheall breccia. Vein (8 cm wide gabbroic anorthosite).
 † All iron as FeO.

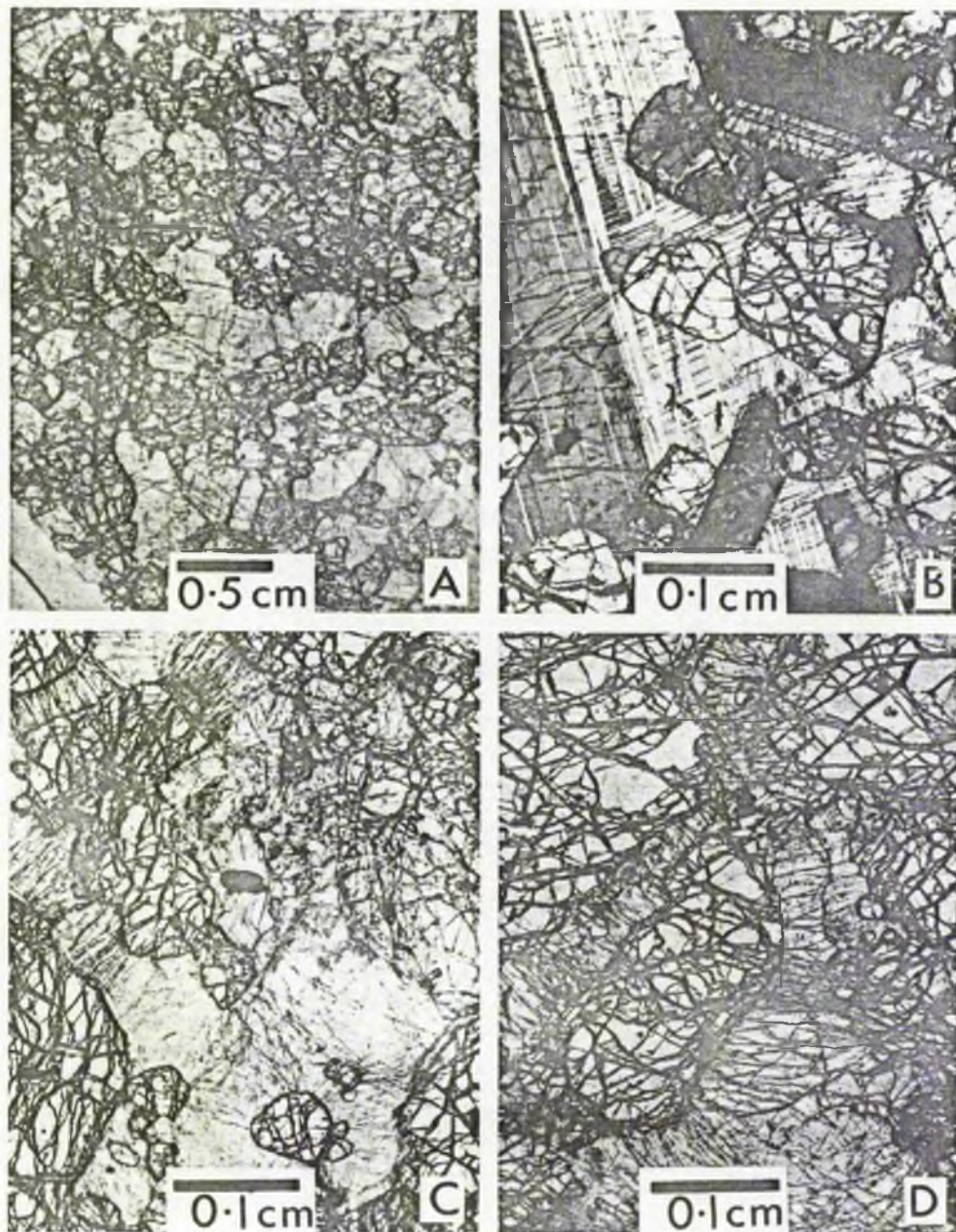


FIG. 3.—Photomicrographs of textures in the breccia matrices: *a*, *c*, and *d*—plane polarized light; *b*—crossed polars. Olivine—high relief and fractured; pyroxene—grey, intermediate relief; plagioclase—white, low relief. Mica and ilmenite, at center of *c*.

TABLE 2

ELECTRON MICROPROBE ANALYSES OF CHROMITES AND ILMENITE IN BRECCIAS

	A	B	C	Ilmenite
TiO ₂	2.08	2.31	3.12	52.27
Al ₂ O ₃	5.82	6.75	15.11	0
Cr ₂ O ₃	22.61	28.30	33.57	0.23
Fe ₂ O ₃ *	36.34	28.61	15.32	-
FeO	29.00	27.59	19.94	41.36†
MnO	0.40	0.37	0.22	0.55
MgO	3.07	4.03	10.57	5.44
Total	99.32	97.96	97.85	99.85
STRUCTURAL FORMULA				
	O = 4			O = 3
Fe ²⁺	0.88	0.83	0.55	0.85
Mn	0.01	0.01	0.01	0.01
Mg	0.17	0.22	0.52	0.20
Ti	0.06	0.06	0.08	0.97
Al	0.25	0.29	0.59	0.00
Cr	0.65	0.81	0.88	0.00
Fe ³⁺	0.99	0.78	0.38	-
R ²⁺	1.06	1.06	1.08	-
R ³⁺⁴	1.94	1.94	1.92	-
Fe ²⁺ /Fe ³⁺ atomic	0.88	1.06	1.44	-

NOTE.—A, grain between olivine and plagioclase; B, grain in olivine; C, grain in pyroxene.
 * Calculated assuming stoichiometry and perfect analysis.
 † All iron as FeO.

c, d). The compositions (table 1) are similar to those found in the layered series (Brown 1956). Peripheral zoning is rare.

Pale brown amphibole occurs (1) as inclusions in olivine, (2) as replacements after pyroxene, (3) as a primary interstitial growth, (4) in blebby intergrowth with pyroxene (possibly a primary intergrowth [Prinz and Nehru 1969]), and (5) in randomly distributed late-stage patches. This amphibole has sufficient Ti (table 1) to be called kaersutite (Leake 1968).

Chestnut-brown, magnesian, titanium-rich mica (table 1) shares the first and last of the kaersutite parageneses and also rims ilmenite grains (fig. 3c). Using the arbitrary 2:1 Mg:Fe ratio of Deer et al. (1963), this mica is classified as phlogopite.

Chlorite, zoisite, talc, tremolite, and epidote have developed in late-stage patches. These are attributed to metasomatic decomposition of plagioclase and pyroxene.

Extensive prehnitization of the plagioclase

occurs. Comparative lack of prehnite in plagioclase from the adjacent layered country rocks suggests that the source of water was the breccias themselves.

Cubic and less regular shaped chromespinels may occur within olivines, embaying their margins, or enclosed in plagioclase or pyroxene. These relations are reflected in the chemistry of the oxide mineral (table 2). Unexpectedly, the most Al- and Cr-rich spinels occur in the pyroxene and the most Fe-rich spinels in the olivine. Ilmenite occurs as exsolution lamellae in spinel and fills cracks in spinel grains. Some inhomogeneity is found within spinels, indicating a lack of internal equilibration, but no zoning pattern. The compositions closely resemble those of chromites in rocks from the eastern layered series of Rhum (Henderson and Suddaby 1971). The chemical variation within spinels (table 2), high Fe accompanied by low Mg, Al, Cr, corresponds to the trend of magnetite substitution for

Specimen

97	Centra
99	E. Ma
62	Centra
195	Matrix
		pho
		Har
9687	Lag Sl
9751	Ruinsi
9752	Ruinsi

NOTE.—All determinations are from electron microprobe analyses.
 * Includes rare ilmenite.
 † Includes tremolite.
 ‡ Wadsworth (1961).

spinel plus magnetite reported for Jackson (1963). more Fe-rich and liquidus chromite (Evans and Wright 1963).
 Picroilmenite
 6.7% MgO occurs invariably associated with ilmenite (fig. 3c).

In summary, the matrix phases in the breccia are similar to those in the layered series (cf. Wadsworth 1961). The textures of the breccia matrix are similar to those of the layered series and of optical pyroxene and hydrous minerals. The chemical compositions are similar to those of the layered series.

That the breccia silicate melt was mobilized at the time of the brecciation is indicated by the textures. This is the presence of ilmenite and relict olivine.

Composition.—The breccia is compared with the Ruinsival breccia. Three features are

TABLE 3
MODAL ANALYSES OF FOUR BRECCIA MATRICES

Ilmenite	Specimen	Setting	Olivine	Plagio- class	Pyrox- one	Chrom- ite*	Phlo- gopite	Kaersu- tite	Other Hydrous Minerals†
52.27	97	Central Ard Mheall	35.41	40.72	12.51	1.35	0.14	0.06	9.80
0	99	E. Margin Ard Mheall	42.89	45.95	3.18	0.82	0.08	tr.	7.08
0.23	62	Central Harris Bay	57.69	17.91	11.26	1.32	1.32	0.91	9.59
41.36†	9687	Matrix and rheomor- phosed plagioclase, Harris Bay	47.51	30.05	8.51	1.76	0.63	2.81	8.73
0.55	9751	Lag Sletir‡	68.5	29.2	0.6	1.7	-	-	-
5.44	9752	Ruinsival‡	35.2	62.0	2.1	0.7	-	-	-
99.85	9752	Ruinsival‡	70.0	29.3	0.2	0.5	-	-	-

NOTE.—All determinations made by point counting on sections a minimum of 16 cm².

* Includes rare ilmenite.

† Includes tremolite, talc, zoisite, prehnite, chlorite and epidote.

‡ Wadsworth (1961).

spinel plus magnesiochromite depletion reported for Stillwater chromites by Jackson (1963). All grains are considerably more Fe-rich and Mg, Al, Cr-poor than the liquidus chromites of Hawaiian tholeiites (Evans and Wright 1972).

Picroilmenite (table 2) with as much as 6.7% MgO occurs as anhedral grains, invariably associated with hydrous minerals (fig. 3c).

In summary, the compositions of the matrix phases in both breccias are closely similar. The anhydrous minerals in the breccia matrices have compositions and textures identical to those in the layered series (cf. Wager and Brown 1968, table 20). Compositions of hydrous phases in the layered series are unknown, but similarity of optical properties to those of the hydrous minerals in the breccias suggests chemical similarity.

That the breccia matrices did contain silicate melt and were not plastically mobilized at the time of brecciation is indicated by the lack of deformation textures. This conclusion is confirmed by the presence of feldspathic veins, assimilation and rheomorphic phenomena.

Composition.—Matrix modes of the Harris Bay and Ard Mheall breccias are compared with modes of the Lag Sletir and Ruinsival breccia matrices in table 3. Three features are noted:

1. The matrices do not have similar compositions (except 9687 and 9752). The major variation is an approximate antipathetic relation between plagioclase and olivine, whereas the pyroxene content remains low and shows inconsistent variation.

2. The matrices of each breccia lack homogeneity.

3. The breccias in this study have large contents of hydrous phases. This feature distinguishes the breccia matrices from layered series rocks, which generally contain less than 2 vol % hydrous minerals.

These features suggest that each matrix magma was significantly hydrous and was also inhomogeneous. The inhomogeneity is most simply explained by intrusion of a differentiated solid-liquid mixture. The matrices of different breccias are probably related by variable degrees of concentration of olivine, and possibly also plagioclase, from a common parent magma.

MECHANISM OF BRECCIATION

Wadsworth (1961) interpreted the textures of the breccia matrices as "typical cumulate" in which plagioclase was "considerably extended by adcumulus growth" (Wager et al. 1960). Unlike Harker (1908), Wadsworth did not consider the breccias to be intrusive in origin. He suggested that the blocks represented a "plutonic fault

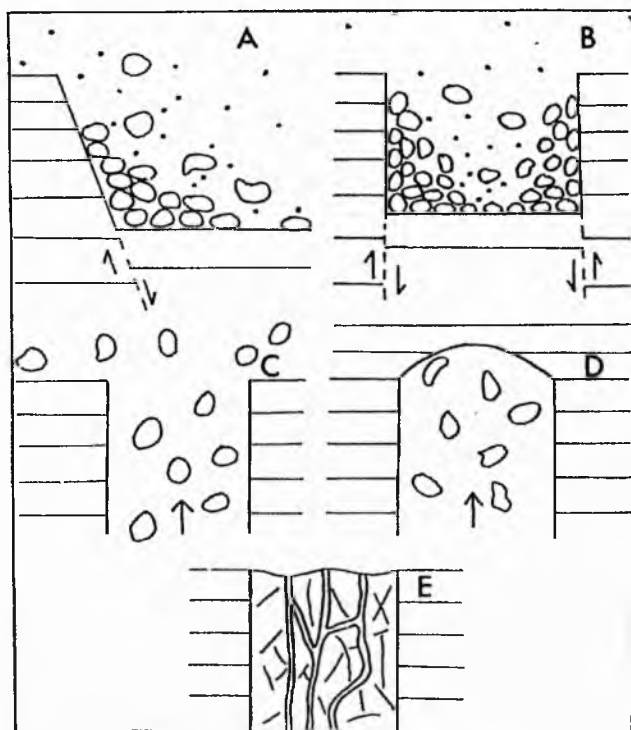


FIG. 4.—Hypotheses of origin of the ultrabasic breccias diagrammatically represented (not to scale): *A*, fault-scarpe (Wadsworth 1961); *B*, Wadsworth's suggestion applied to Harris Bay zone, breccia fills a graben; *C*, intrusive origin, intrusive magma penetrates layered series into the overlying magma chamber; *D*, intrusive origin, magma fails to penetrate the layered series (*C* and *D* are the Harris Bay breccia); *E*, in situ layered series dislocation and intrusion to yield Ard Mheall breccia.

scree" of layered ultrabasic rocks which accumulated contemporaneously with settling of magnesian olivine and calcic plagioclase crystals from a basaltic magma (fig. 4*A*, 4*B*).

Wadsworth's (1961, 1973) interpretation does not explain the following features.

1. All the breccia matrices lack the conspicuous mineral and textural layering which characterize the complex. If the matrix did form by crystal settling, it should have been subject to the same processes which caused the prominent banding of the layered series.

2. Calculations using Stokes's law and a modified form of the law to allow for differing Reynolds numbers between particles (Allen 1970), indicate that in a basalt magma ($\rho = 2.6 \text{ g/cm}^3$) a 0.5 m

diam peridotite block ($\rho = 3.3 \text{ g/cm}^3$) would sink 80,000–300,000 times faster than a 1 mm cumulus olivine ($\rho = 3.4 \text{ g/cm}^3$). Accordingly, a highly efficient sorting of blocks from cumulus grains and blocks from blocks according to size and density would have occurred. In the Harris Bay breccia where the faulting mechanism would require a graben to fit the field evidence, fault scarp debris would line the graben (fig. 4*B*). The proportion of blocks to matrix would be expected to decrease to a minimum in a traverse from the margin of the breccia to the center. No such regular variation is found. Since the xenoliths and matrices of the breccia are unsorted, the hypothesis of contemporaneous settling is not favored.

If the origin of the matrix material was

by slumping, cumulate layers could be reworked into slump features within breccias.

It is concluded that the breccias are of intrusive origin and faulting is not the cause of the breccias. Field contacts, and the breccias are not by feldspathic intrusions 75 m at the Ard Mheall intrusive origin. Only evidence of closure directed towards Harris Bay. Inferred from high to low level, ever, seems more

Both Brown (1961) concluded that the basics represent the possibility of a breccia mentioned by

Xenolithic intrusions studied in most of the Skye intrusion (Drever 1963). Soay with a euhedral peridotite and Cleat xenoliths attributed by segregation of peridotite whose origin is in the matrix of the breccias, the xenoliths are olivine-rich and resemble the inclusions here. The proportion of peridotite to plagioclase. The Sgurr Dubh (Weedon 1965), and narrow fault-like those described. It is suggested that the Sgurr Dubh rocks

The composition of the Ard Mheall breccia follows.

by slumping of a partially consolidated cumulate layer, both of these criticisms could be refuted. But there are neither slump features nor deformation structures within breccia matrix rocks.

It is concluded that the crystal settling and faulting hypothesis is inapplicable to the breccias. Field relations of the breccia contacts, and incipient in situ brecciation by feldspathic peridotite through at least 75 m at the Ard Mheall breccia indicate an intrusive origin (fig. 4C, 4D, 4E). The only evidence for upward intrusion is the closure direction of the minor intrusions at Harris Bay. Intrusive movement of magma from high to low confining pressure, however, seems more likely than the reverse.

MATRIX MAGMAS

Both Brown (1956) and Wadsworth (1961) concluded that the Rhum ultrabasics represented *basaltic* cumulates. The possibility of a eucritic parent magma is mentioned by Wager (1968).

Xenolithic intrusion breccias have been studied in more detail in the neighboring Skye intrusions (Harker 1904). Wyllie and Drever (1963) described a picrite sill from Soay with a eucritic margin which terminates abruptly in a xenolithic facies of peridotite and allivalite blocks. The Ben Cleat xenolithic ultrabasic dikes have been attributed by Gibb (1968, 1969) to disintegration of layered ultrabasic rocks whose origin is genetically related to the matrix of the dikes. In these Skye intrusions, the xenolith lithologies and the olivine-rich nature of the matrices resemble the intrusion breccias described here. The presence of largely unzoned bytownitic plagioclase is also comparable. The Sgurr Dubh layered series of Skye (Weedon 1965) contains ultrabasic breccias and narrow feldspathic veins (An_{83-75}) like those described here. Weedon suggested that the parent magma of the Sgurr Dubh rocks may have been picritic.

The composition of the Harris Bay and Ard Mheall breccias may be reviewed as follows.

1. The predominantly in situ envelopment of blocks in the Ard Mheall breccia implies that the magma can have undergone little differentiation after intrusion, and certainly no gravitational differentiation.

2. Since the breccia mush can mobilize plagioclase more calcic than An_{85} in the allivalite xenoliths, the liquid in the mush should be in equilibrium with plagioclase crystals at least as calcic as that of the xenoliths (Bowen 1928).

3. If the parent magma of the allivalite xenoliths was a basalt (Brown 1956), then the intrusive breccia matrices which caused rheomorphism either had temperatures in excess of the appearance of plagioclase from the basalt, or they had a similar temperature but a higher water content. Considering the abundance of hydrous minerals in the breccias, a high water content in the intrusive magmas is indicated.

4. It is impossible that the gabbroic anorthosite and anorthositic gabbro veins represent mobilization of a bytownite enriched crystal mush, when the breccia matrices themselves were olivine enriched crystal mushes. The veins must be filter-pressed residual liquid from the breccia matrices. The normative plagioclase composition of this liquid is at least 10% more anorthitic than that of a basalt.

If, as seems likely, this liquid was saturated with olivine, pyroxene, and plagioclase then, with reference to the system forsterite-anorthite-diopside (Osborn and Tait 1952), its maximum temperature was 1,270°C. The Rhum ultrabasics have probably been uplifted between 1,500 m (Wager and Brown 1968) and 4,000 m (Dunham 1970), so that the exposed matrix in the Harris Bay breccia crystallized at a pressure between 0.5 and 1.2 kb. By comparison with Yoder and Tilley (1962), the ternary cotectic point in Fo-An-Di would be lowered by at least 40°–70°C, if water saturated at these pressures. Addition of Na and Fe to the system would further lower the temper-

ature. The likely intrusion temperature of these calcic veins between 1,200° and 1,250°C is therefore petrologically reasonable, despite their unusual compositions.

5. The core composition of plagioclase crystals in breccia matrices is not unnecessarily calcic for the plagioclase to have been in equilibrium with basaltic magma upon intrusion, particularly as water promotes crystallization of more calcic plagioclase (Yoder et al. 1957). However, since intrusion of a crystal mush is deduced, there is no supernatant liquid (Jackson 1961) available to exchange with interstitial liquid in the mush during crystal growth; "accumulus" crystal growth (Wadsworth 1961) is not possible. If the intrusive mush consisted of olivine and bytownite crystals in a basaltic liquid, extensive plagioclase zoning should be found. Limited plagioclase zoning (table 1) and the absence of it in some thin sections indicates that the interstitial liquid was more anorthitic in normative plagioclase than basalt.

Since the intrusive magma is deduced to have been hydrous and water may cause steepening of the plagioclase solidus between An_{80} and An_{90} (Lofgren, personal communication), restricted zoning of plagioclase cores might be expected, even though the melt is trapped. This would weaken argument 5. However, if the liquid of the mush is basaltic (normative plagioclase approximately An_{70}), the bulk composition (cores and rims) of the plagioclase precipitated following intrusion should also be An_{70} . In the matrix rocks there is apparently insufficient plagioclase of composition less calcic than An_{80} to satisfy this criterion. Furthermore, if the feldspathic veins (argument 4) represent a calcic differentiate of hydrous basalt, a complementary differentiate enriched in plagioclase more sodic than An_{70} should exist. No such rock has been located.

This review, together with the textural and modal evidence, indicates that feldspathic peridotite magmas with much of the olivine suspended as crystals in a calcic liquid, were the intrusive phases.

Comparison with the Skye intrusions suggests that olivine eucrite or picritic eucrite with normative bytownite compositions are possible parent liquids of the intrusive magmas. Irrespective of the olivine content, this liquid more closely resembles a high-lime liquid (Drever and Johnston 1966) than a basalt. Hutchison (1966) suggested that a similar liquid was the parent of the brecciated allivalite dikes of north Skye (Anderson and Dunham 1966).

Those olivines in the breccia matrices which have skeletal morphologies may be attributed to rapid crystal growth under supersaturation conditions, possibly due to supercooling induced by adiabatic expansion of the intrusive magma (Donaldson 1974). This in situ crystallization indicates that not all the olivine had crystallized before intrusion.

CONCLUSIONS AND POSSIBLE IMPLICATIONS

The Harris Bay and Ard Mheall ultrabasic breccias formed by brecciation due to the intrusion of feldspathic peridotite magmas. A similar hypothesis seems applicable to the other Rhum ultrabasic breccias mapped by Harker (1908). The Ard Mheall breccia is unique in representing an arrested stage in the development of Rhum breccias. Convergence of the five breccias in figure 1 may reflect a common source within the complex.

The presence of abundant hydrous phases (table 3) suggests that the magmas contained much water, although not necessarily to the level of saturation. Textural and modal evidence indicates that the magmas were emplaced with a significant proportion of olivine in suspension but that the transporting liquid was more calcic than basalt. Water would be critical in suppressing the liquidus temperature of the melt in the mush and in reducing the mush viscosity.

The breccias are of local petrogenetic importance in three respects. Blocks should provide samples for investigating the relationship of the exposed layered

series to the basals believed by Quillin and Tuttle. The liquid more closely resembles the suggestion that the massifs of the Dornabac were crystallized in situ from a liquid. The similarity between the layered series and interstitial calcic liquid also existed in the layered series, rather than a series more calcic than the layered series.

Of more general interest is the petrogenesis of the layered series. The relationship of the layered series to the basals is relevant.

1. Brown (1951) divided the major units of Rhum (represented by the late) of a differentiated lava. The intermediate layer between a deep-seated magma and the earth's surface is a major ultrabasic magma. It seems possible that the breccias represent lines of differentiation in the deeper chamber (fig. 4c). The breccias and allivalite represent some of the products of the magma (Brown 1951) suggestion.

2. Alternatively, the breccias record explosive magma trapped (Dunham 1970) before minor intrusions. The breccias may be minor intrusions of stagnant magma before layered series.

3. Crystalliza

series to the 15 km of unexposed ultrabasics believed to underlie Rhum (McQuillin and Tuson 1963). Recognition of a liquid more calcic than basalt enforces the suggestion of Donaldson et al. (1973) that the massive bytownite spherulites in the Dornabac breccia (fig. 1) also crystallized in situ from a highly calcic liquid. The similarity in mineral composition between the breccia matrices and the layered series rocks suggests that the interstitial calcic liquid of the breccias also existed in crystal mushes in the layered series. Like the breccias, a eucritic rather than a basaltic parent magma seems more appropriate for the layered series.

Of more general importance to the petrogenesis of other layered plutons is the relationship of the breccias to the origin of the layered series. Four points are relevant.

1. Brown (1956) suggested that the major units of layered ultrabasic rock in Rhum represent the solid fraction (cumulate) of a differentiating magma, parts of which are periodically erupted as fractionated lava. The layered rocks form in an intermediate level magma chamber between a deeper magma source and the earth's surface. Brown considered each major ultrabasic unit (15–150 m thick) to record influx of additional unfractionated magma to the intermediate chamber. It seems possible, considering the abundance of breccias in Rhum, that breccias represent lines of access of magma from the deeper chamber to the intermediate one (fig. 4c). The presence of peridotite and allivalite xenoliths near the top of some of the major units (Wager and Brown 1951) is consistent with this suggestion.

2. Alternatively, the breccias could record explosive movement of pods of magma trapped within the layered series (Dunham 1970). These pods could either be minor intrusions into the layering or stagnant magma that failed to crystallize before layered rocks enclosed it.

3. Crystallization of the Rhum parent

magma is not as simple as the model developed by Brown (1956) and Wadsworth (1961). The breccia matrices indicate that considerable crystallization and differentiation could take place in magma underlying the layered series. If point 1 is correct, the magma flowing into the intermediate chamber may have had a considerable proportion of crystals already in suspension. Subsequent differentiation would not simply involve crystal nucleation at the cool top of the intermediate chamber followed by settling of crystals. Rather, crystal growth centers would be available throughout the chamber and varying degrees of crystal enlargement would be found when crystals settled onto the chamber floor.

4. Where, as in Rhum, direct evidence in the form of a chilled margin is lacking for the composition of the parental magma of a pluton, indirect methods of comparison and inference must be adopted. Certain field and textural relations of the Rhum ultrabasic rocks are apparently incompatible with the basaltic magma inferred by Brown (1956) to be parental to the intrusion (Drever and Johnston 1972; Donaldson 1974; this paper). It is suggested that other ultrabasic intrusions lacking direct evidence of parental magma might also be products of eucritic magma differentiation. A possible example is the Greenhills intrusion, New Zealand, which, by comparison with the chemical mineralogy of Rhum rocks, Mossman (1973) considered to be of tholeiitic basalt lineage.

ACKNOWLEDGMENTS.—I thank the Natural Environment Research Council and the Lunar Science Institute, which is operated by the Universities Space Research Association under Contract No. NSR 09-051-001 with the National Aeronautics and Space Administration, for financial support. H. I. Drever, R. Johnston, R. B. Merrill, A. M. Reid, and W. I. Ridley kindly improved the manuscript. This paper constitutes the Lunar Science Institute Contribution No. 181.

REFERENCES CITED

- ALLEN, J. R. L., 1970, Physical processes of sedimentation: London, Allen & Unwin.
- ANDERSON, F. W., and DUNHAM, K. C., 1966, The Geology of Northern Skye: Scotland, Geol. Survey Mem.
- BOWEN, N. L., 1928, The evolution of the igneous rocks: Princeton, N.J., Princeton Univ. Press.
- BROWN, G. M., 1956, The layered ultrabasic rocks of Rhum, Inner Hebrides: Royal Soc. (London) Philos. Trans., ser. B, v. 240, p. 1-53.
- DEER, W. A.; HOWIE, R. A.; and ZUSSMAN, J., 1966, An introduction to the rock forming minerals: London, Longmans.
- DROKE, J. S., 1973, A primary peridotite magma-revisited, in SHAGAN, R., ed., Studies in earth and space sciences: Geol. Soc. America Mem. 132 (Hess volume), p. 289-297.
- DONALDSON, C. H., 1974, Olivine morphology in the tertiary harrisite of Rhum and in some Archaean spinifex rocks: Geol. Soc. America Bull. (in press).
- ; DREVER, H. I.; and JOHNSTON, R., 1973, Crystallization of poikilo-macrospherulitic feldspar in a Rhum peridotite: Nature-Phys. Sci., v. 243, p. 69-70.
- DREVER, H. I., and JOHNSTON, R., 1966, A natural high-lime silicate liquid more basic than basalt: Jour. Petrology, v. 7, p. 414-420.
- , and —, 1972, Metastable growth patterns in some terrestrial and lunar rocks: Meteoritics, v. 7, p. 327-340.
- DUNHAM, A. C., 1970, The emplacement of the Tertiary igneous complex of Rhum, in NEWALL, G., and RAST, N., eds., Mechanism of igneous intrusion: Geol. Jour. Spec. Issue, v. 2, p. 23-32.
- EVANS, B. W., and WRIGHT, T. L., 1972, Composition of liquidus chromite from the 1959 (Kilauea Iki) and 1965 (Makaopuhi) eruptions of Kilauea volcano, Hawaii: Am. Mineralogist, v. 57, p. 217-230.
- GIBB, F. G. F., 1968, Flow differentiation in the xenolithic ultrabasic dykes of the Cuillins and the Strathaird peninsula, Isle of Skye, Scotland: Jour. Petrology, v. 9, p. 411-443.
- , 1969, Cognate xenoliths in the Tertiary ultrabasic dykes of southwest Skye: Mineralog. Mag., v. 37, p. 504-514.
- HARKER, A., 1904, The tertiary igneous rocks of Skye: Scotland, Geol. Survey, Mem.
- , 1908, The geology of the Small-Isles of Inverness-shire: Scotland, Geol. Survey Mem.
- HENDERSON, P., and SUDDABY, P., 1971, The nature and origin of the chrome-spinel of the Rhum layered intrusion: Contr. Mineralogy and Petrology, v. 33, p. 21-31.
- HUTCHISON, R., 1968, Origin of the White Allivalite, western Cuillin, Isle of Skye: Geol. Mag., v. 105, p. 338-347.
- JACKSON, E. D., 1961, Primary textures and mineral associations in the ultramafic zone of the Stillwater Complex, Montana: U.S. Geol. Survey Prof. Paper 358, 106 p.
- , 1963, Stratigraphic and lateral variation in chromite composition in the Stillwater Complex: Mineralog. Soc. America Spec. Paper 1, p. 46-54.
- LEAKE, B. E., 1968, A catalog of analyzed calciferous and subcalciferous amphiboles together with their nomenclature and associated minerals: Geol. Soc. America Spec. Paper 98, 210 p.
- MCQUILLIN, R., and TUSON, J., 1963, Gravity measurements over the Rhum tertiary plutonic complex: Nature, v. 199, p. 1276-1277.
- MOSSMAN, D. J., 1973, Geology of the Greenhills ultramafic complex, Bluff peninsula, Southland, New Zealand: Geol. Soc. America Bull., v. 84, p. 39-62.
- NALDRETT, A. J., and MASON, G. D., 1968, Contrasting Archaean ultramafic igneous bodies in Dundonald and Clergue Townships, Ontario: Canadian Jour. Earth Sci., v. 5, p. 111-143.
- NESBITT, R. W., 1971, Skeletal crystal forms in the ultramafic rocks of the Yilgarn Block, Western Australia: evidence for an Archaean ultramafic liquid: Geol. Soc. Australia Spec. Pubs., v. 3, p. 331-347.
- OSBORN, E. F., and TATE, D. B., 1952, The system diopside-forsterite-anorthite: Am. Jour. Sci. (Bowen volume), p. 413-433.
- PRINZ, M., and NEHRU, C. E., 1969, Comments on "Kaersutite from San Carlos, Arizona, with comments on the paragenesis of this mineral" by Brian Mason: Mineralog. Mag., v. 37, p. 333-337.
- SIMKIN, T., and SMITH, J. V., 1970, Minor element distribution in olivine: Jour. Geology, v. 78, p. 304-325.
- WADSWORTH, W. J., 1961, The ultrabasic rocks of southwest Rhum, Inner Hebrides: Royal Soc. (London) Philos. Trans., ser. B, v. 244, p. 21-64.
- , 1973, Magmatic sediments: Minerals Sci. Eng., v. 5, p. 25-35.
- WAGER, L. R., 1968, Rhythmic and cryptic layering in mafic and ultramafic plutons, in HESS, H. H., and POLDERVAART, A., eds., Basalts: New York, Wiley.
- , and BROWN, G. M., 1961, A note on rhythmic layering in the ultrabasic rocks of Rhum: Geol. Mag., v. 88, p. 166-168.
- , and —, 1968, Layered igneous rocks: Edinburgh, Oliver & Boyd.
- ; —; and WADSWORTH, W. J., 1960, Types of igneous cumulates: Jour. Petrology, v. 1, p. 73-85.

WEEDON, D. S.,
rocks of Sgurr
Jour. Geology,
WYLLIE, P. J.,
petrology of pl
— a picrite sill
Royal Soc. Edi

- WEEDON, D. S., 1965, The layered ultrabasic rocks of Sgurr Dubh, Isle of Skye: *Scottish Jour. Geology*, v. 1, p. 41-68.
- WYLLIE, P. J., and DREVER, H. I., 1963, The petrology of picritic rocks in minor intrusions—a picrite sill on the island of Soay (Hebrides): *Royal Soc. Edinburgh Trans*, v. 65, p. 155-177.
- YODER, H. S.; STEWART, D. B.; and SMITH, J. R., 1957, Ternary feldspars: *Carnegie Inst. Washington Yearbook 65*, p. 206-214.
- , and TILLEY, C. E., 1962, Origin of basalt magmas: an experimental study of natural and synthetic rock systems: *Jour. Petrology*, v. 3, p. 342-532.

Contrib. Mineral. Petrol. **55**, 000—000 (1975)
© by Springer-Verlag 1975

Curved Branching Crystals and Differentiation in Comb-Layered Rocks

Gary E. Lofgren

Geology Branch, TN6, NASA-Johnson Space Center, Houston, TX, USA

Colin H. Donaldson

Lunar Science Institute, Houston, TX, USA and
University of St. Andrews, Scotland

Received January 6, 1975

Abstract. Layering in which one or more of the component minerals has grown perpendicular to layer boundaries occurs, under a variety of names, in volcanic, hypabyssal and plutonic igneous rocks. The most recent and best name is comb layering. The oriented minerals are elongate, are commonly branching and may be curved. Experimental crystallization of plagioclase and ternary feldspar melts confirms that a substantial degree of supercooling or a significant cooling rate is necessary to produce the curved or branching crystal morphologies typical of comb layering. The more viscous the melt, the less the supercooling required. Changes in the water content or confining pressure are mechanisms for inducing supersaturation in deep-seated magmas, that are consistent with field and experimental evidence. The change from modal dominance by a single elongate crystal phase in one comb layer to dominance by another phase in a contiguous comb layer is explained by the presence of constitutional supercooling ahead of the growing crystals of a given layer.

Introduction

The discovery of more "comb layered", or "crescumulate" pyroxene and plagioclase rocks by the 1971 Skaergaard expedition (Goes, pers. comm.) and the recent paper on comb layering and orbicular rocks in the Sierra Nevada batholith (Moore and Lockwood, 1973a) has stimulated renewed research in the origin of comb layered rocks (Barriere *et al.*, 1971; Barriere, 1972; Van Diver and Magetti, 1973; Lofgren and Donaldson, 1973; Taubeneck, pers. com.). In this paper we examine two common features of comb layered rocks: the curvature of oriented, elongate, branching crystals and the tendency to form highly differentiated layers. Understanding the origin of both features is essential to interpreting the environment of formation of comb layering. Leveson (1973) interprets curved crystals as an index of shearing and crystallization under metamorphic conditions, whereas Moore and Lockwood (1973a, b) suggest that the curved crystals are bent by an upward moving, high velocity, low density, pegmatite fluid. These interpretations differ from the suggestion of Taubeneck and Poldervaart (1960) that comb layers form during supercooling of a silicate melt. We present experimental evidence that favors this last interpretation and give values of super-cooling and cooling rate that promote branching and curved crystal growth in simple silicate systems. An explanation of the sharp contrast in composition between layers in some comb-

layered sequences is sought in the change in composition of a melt at the interface between a crystal and its parent melt. This hypothesis precludes the need for multiple intrusions of contrasting composition for each layer or for gravity or flow differentiation.

Occurrence of Curved and Branching Crystals

Volcanic Environment

Bryan (1972) described randomly oriented olivine, pyroxene and plagioclase crystals with elongate branching morphologies in pillow lavas. Pyke and others (1973) described Archaean lavas containing crystals with a variety of skeletal and dendritic textures. Two of these textures, "plate spinifex" (Nesbitt, 1971) and "harrisitic" or "branching spinifex" (Donaldson, 1974), show branching, and occasionally curved, crystal shapes commonly perpendicular to the layer boundary. The origin of these textures typically is ascribed to rapid cooling of the silicate liquid.

Hypabyssal Environment

The Benfontein kimberlite sill contains elongate, dendritic and branching calcite crystals (Dawson and Hawthorne, 1970). Wyllie and Drever (1963) show vertically oriented, branching plagioclases at the margin of a picrite sill. Banding caused by rhythmic, perpendicular growth of curved branching crystals of olivine, plagioclase and pyroxene in dolerite dykes is discussed by Drever and Johnston (1972) (Fig. 1), Preston (1963), Platten and Watterson (1969), and Farquharson (1973). Magma supercooling is the only mechanism postulated for the origin of elongate branching crystals in these dikes and sills. Supercooling is usually ascribed to rapid cooling on intrusion. Although the branching crystals are preferentially located near intrusive margins, they are not located at the immediate contact. To preserve this crystal fringe, movement of the magma is generally considered to have been slight.

Plutonic Environment

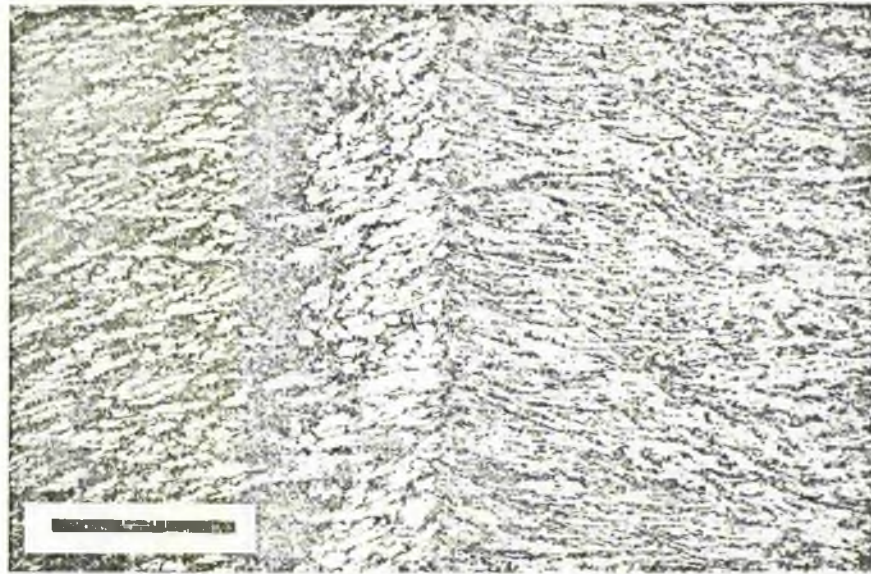
Layered plutonic rocks with perpendicularly oriented crystals have been reported by Taubeneck and Poldervaart (1960) as "Willow Lake layering", by Moore and Lockwood (1973a) as "comb layering" and by Wager *et al.* (1960) as "crescumulate layering." "Willowing Lake layering" is characterized by elongate, skeletal or branching, and often curved, crystals of plagioclase, hornblende, and orthopyroxene, which are generally less than 1 cm long (Fig. 2). Taubeneck and Poldervaart (1960) postulated crystal growth into a super-cooled magma near the margin of the intrusion. "Comb layering" has been proposed by Moore and Lockwood (1973a) as a more general term to include the type example from Willow Lake and similar layering common in the Sierra Nevada Batholith. They suggest that an upward-moving, supercritical fluid is the medium from which these elongate, perpendicular minerals grew. Movement of this fluid past the growing crystals is postulated to cause crystal curvature.



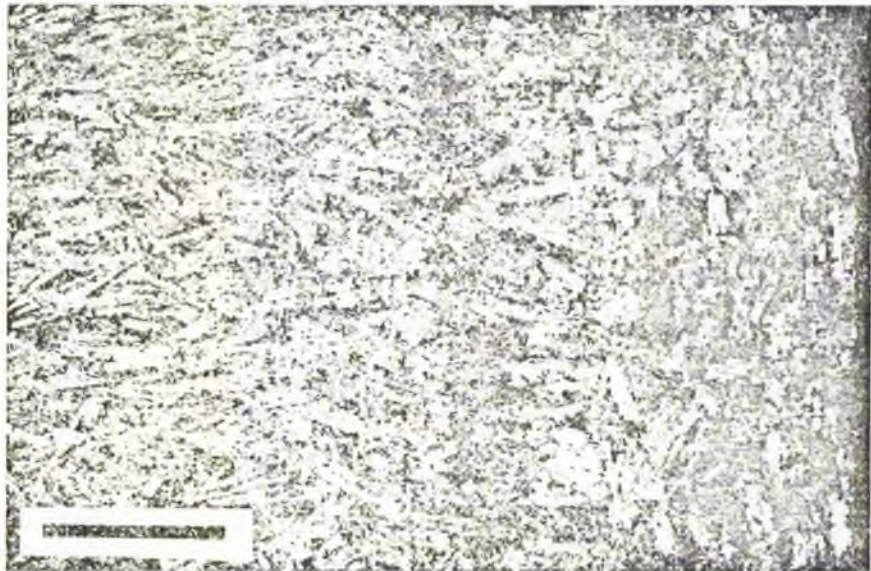
Fig. 1. Photo rich (lighter) and H. Drever

Fig. 2. Photo intrusion. Sa

Formation
Laboratory
Isothermal
elongate pl
200° C. The



1



2

Fig. 1. Photomicrograph of dolerite dike showing branching crystal morphologies in pyroxene-rich (lighter colored) and olivine and plagioclase-rich layers. Samples provided by S. Agrell and H. Drever. The bar is 5 mm

Fig. 2. Photomicrograph of branching plagioclase in comb-layered sample from the Willow Lake intrusion. Samples provided by J. Moore and J. Lockwood. The bar is 5 mm

Formation of Curved or Branching Plagioclase

Laboratory Crystallization

Isothermal crystallization in the plagioclase-H₂O system (Lofgren, 1974) produced elongate plagioclase crystals at supercooling (ΔT) values between 100° C and 200° C. The elongate crystals are skeletal or hollow and many have an irregular

extinction pattern revealing an infilled fibrous skeleton. A few skeletal crystals show small-angle side-branching at ΔT 's near 200° C. At larger ΔT 's the branching becomes more pronounced. The branching crystal forms radiate from a point in a fan shape, with branching occurring at small angles to the principal fibers. Individual fibers do not show extensive zoning and approximate the composition of the melt from which they grew.

In a series of monotonic cooling rate experiments with a water-undersaturated (≈ 5 wt. percent H_2O) plagioclase melt of An_{40} composition, tabular crystals grew at cooling rates less than 10° C/hr (Fig. 3a); elongate crystals, at 16° C/hr; curved, elongate, and incipiently branching crystals, at 32 and 66° C/hr (Fig. 3b, 3c); and complex, branching crystals, at 130° C/hr (Fig. 3d). In general, as the cooling rate decreased, or the supercooling diminished to near liquidus temperatures, the crystals became less elongate and more tabular. This sequence is described in detail elsewhere (Lofgren, 1973; in prep.). The curved, elongate, and branching crystals that grew in the rapidly cooled runs closely resemble those crystals that grew in isothermal runs at large ΔT 's.

A similar sequence of plagioclase crystal morphologies is observed in melts other than the An_{40} composition. However, the transitions between crystal morphologies do not occur at the same cooling rates for all compositions. In an An_{30} melt, the crystal branching is more intricate for the 66 and 130° C/hr cooling rates than in an An_{40} melt. The effect of composition on the crystal morphology is even more striking when crystals grown from plagioclase melts are compared with crystals grown from ternary feldspar melts. At 2° C/hr, tabular crystals grow in an An_{40} melt (Fig. 3a), while complexly branching crystals dominate the crystallization products of an $Ab_{45}An_{11}Or_{44}$ melt that approximates the feldspar ratio of a granite (Fig. 4). Similar comparisons can be made between the crystallization products of other ternary feldspar melts (Figs. 5, 6, and 7) and the crystals produced in plagioclase melts (Fig. 3b, 3c) at similar cooling rates. These results indicate that the crystals grown at the same cooling rate will progress from tabular to elongate to curved and then to branching forms as the melt compositions change from gabbro- to granite-like.

If crystallization is initiated while a melt is undersaturated with respect to water, the steadily increased water content in the melt during crystallization of anhydrous phases will act to reduce ΔT . This change in ΔT might be sufficiently large to change the morphology of growing crystals, to permit infilling of skeletal crystals and to promote conditions in which later-nucleating crystals assume a morphology different from that of earlier ones.

Conditions for Growth of Curved and Branching Crystals

The extrapolation of the experimental crystallization studies on melts as simple as the ternary feldspars to rock melts must be made with care. The experiments indicate how plagioclase morphology varies with composition, cooling rate, and degree of supercooling and provide limiting values for the cooling rates and degrees of supercooling necessary for comb-layer formation.

Relative cooling rates can be assigned to plagioclase crystals of differing morphologies grown from melts of the same composition. In general, an elongate,

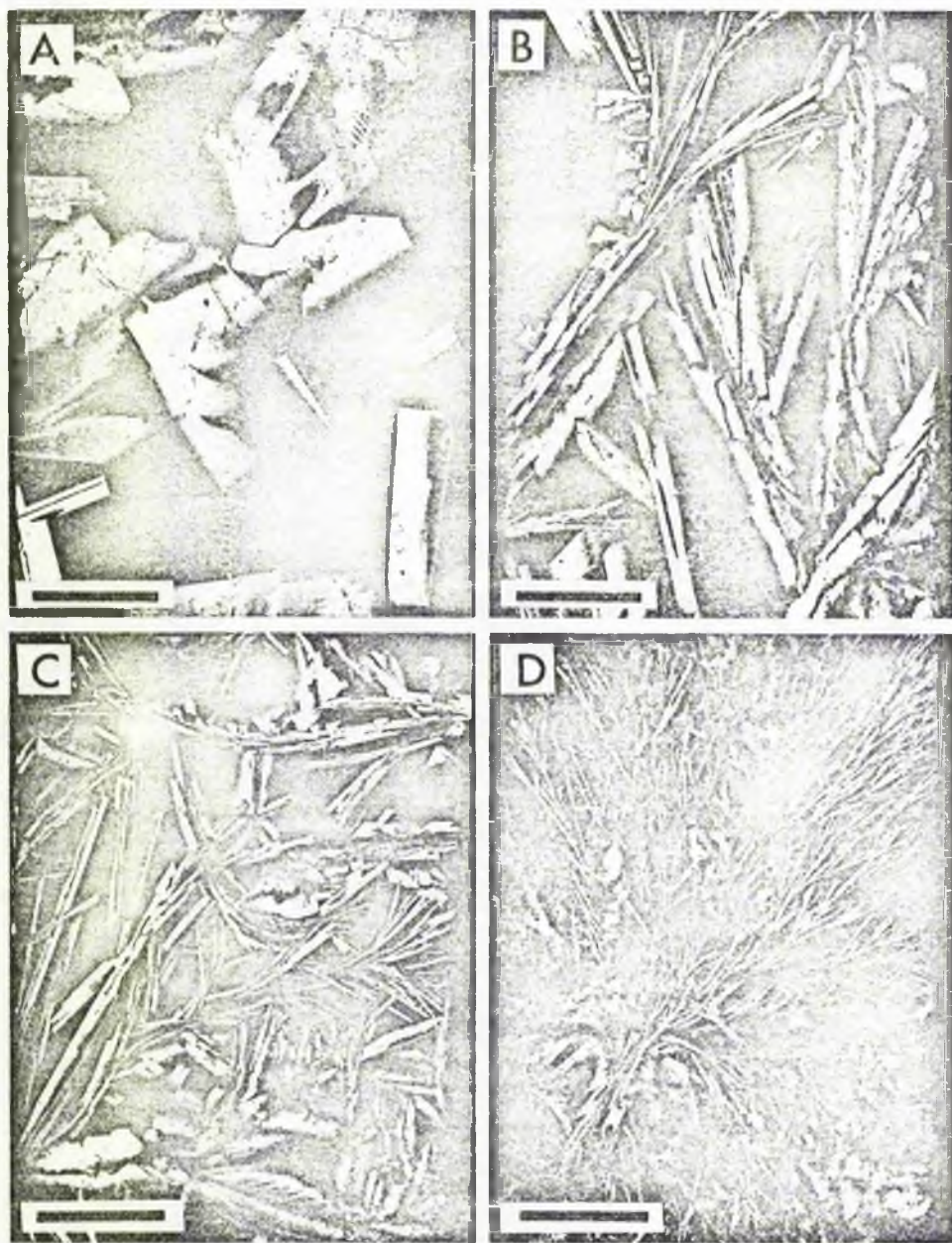


Fig. 3a—d. Photomicrographs of crystals grown from An₁₀ melt (5 wt. percent water) at four cooling rates, showing the progression from tabular crystals at low cooling rate to branching crystals (fan spherulites) at high cooling rate. Charges were melted at 1200° C, dropped rapidly to 1150° C and cooled to 860° C. Magnification $\times 20$. (a) Run 336, 2° C/hr; (b) run 324, 32° C/hr; (c) run 359, 66° C/hr; (d) run 391, 130° C/hr. The bar is 1 mm in each photograph

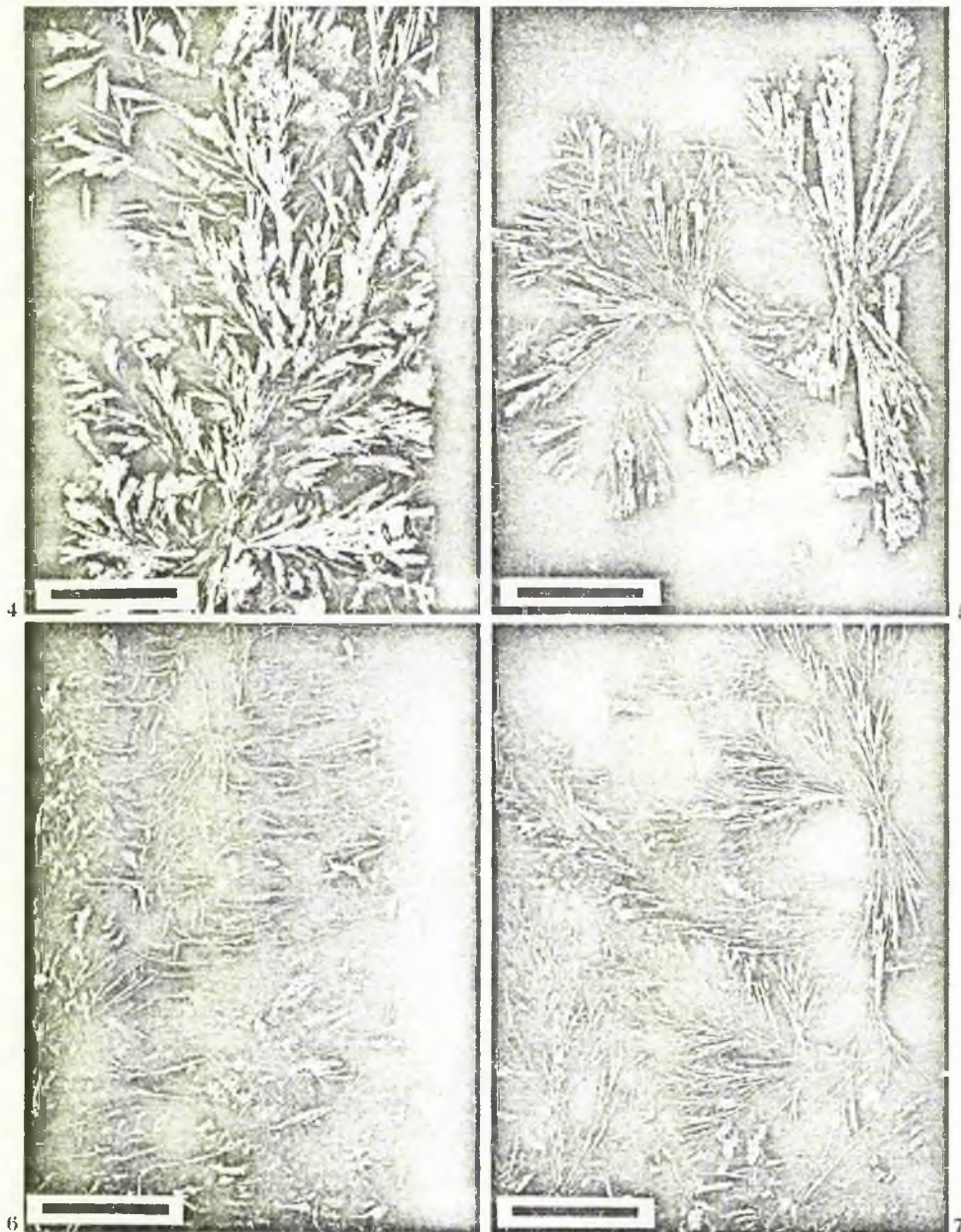


Fig. 4. Photomicrograph of crystals grown in $An_{11}Ab_{15}Or_{11}$ melt (2.0 wt. percent water) cooled at $2^{\circ}C/hr$, from $1050^{\circ}C$ to $765^{\circ}C$ after melting at $1100^{\circ}C$. Plumose, fan spherulites dominate; a few tabular crystals are present. The bar is 1 mm

Fig. 5. Photomicrograph of crystals grown from $An_{20}Ab_{60}Or_{20}$ melt (7.0 wt. percent water) cooled at $40^{\circ}C/hr$ from 995 to $670^{\circ}C$ after melting at $1100^{\circ}C$. Crystal aggregates are coarse, open, bow-tie spherulites with skeletal fibers. The bar is 1 mm

- Donaldson, C.H.: *Calcium magma* (in press)
- Drever, H.I., Johnston, Roy. Soc. Edinburgh
- Drever, H.I., Johnston Meteoritics 7, 327-3
- Elsdon, R.: *Crystallization Greenland. J. Petro*
- Farquharson, R.B.: *The British Columbia. C*
- Jahns, R.J., Burnham, derivation and crystal
- Jahns, R.J., Tuttle, O. 1, 78-92 (1963)
- Kadik, A.A., Khitarov, and the enclosing ro
- Knight, C.A.: *The freezing*
- Leveson, D.J.: *Origin California: Discussio*
- Lofgren, G.: *Experiment E.O.S. 54, 482 (197*
- Lofgren, G.: *An experim zation. Am. J. Sci. 1*
- Lofgren, G., Donaldson Lake) Layering." *Ge*
- Loomis, A.A.: *Noritic a Spec. Paper 1, 62-6*
- Moore, J.G., Lockwood batholith, California
- Moore, J.G., Lockwood Batholith, California
- Nesbitt, R.W.: *Skeletal Australia: Evidence 331-347 (1971)*
- Platten, I.M., Watterso 286-287 (1969)
- Preston, J.: *A columnar*
- Pyke, D.R., Naldrett, A Ontario. Geol. Soc.
- Tarshis, L.A., Tiller, W stability of a planar p. 709-719. Oxford:
- Taubeneck, W.H., Pold Part 2. Willow Lake
- Wager, L.R., Brown, C 73-85 (1960)
- Wyllie, P. J., Drever, F on the island of Soay
- Van Diver, B.B., Magg orbiculite, Odenwald (1973)

Dr. G.E. Lofgren
Geology Branch, TN6
NASA-Johnson Space C
Houston, Texas 77098,

tabular crystal grows at a slower cooling rate than an acicular or curved crystal. Faster cooling rates are necessary to produce branching crystals. The increased complexity and diminished diameter of the branches of the crystal reflect increasing cooling rates within this morphologic type. The specific ΔT or cooling rate required to produce a branching or a curved feldspar varies inversely with viscosity. Thus, a larger ΔT or cooling rate is needed to produce branching crystals with the normative feldspar composition of diorite than melts more typical of granite. The closest approximation to magmatic values of ΔT or cooling rate are afforded by the experiments on ternary feldspar melts with feldspar ratios similar to those of "diorites" and "granodiorites". To produce similar branching feldspar morphology, the "haplodiorite" melt requires a faster cooling rate than the "haplogranodiorite" melt; in either case, the rates are rapid and greater than 50°C/hr for branching crystals and greater than 10°C/hr for elongate, curved crystals. The addition of mafic mineral constituents to the melts would lower their viscosities and necessitate even greater cooling rates (or ΔT 's) for growth of curved or branching of feldspar crystals. In contrast, addition of quartz would increase the viscosity relative to the ternary feldspar composition necessitating slower cooling rates. Hence, the cooling rate and ΔT values reported here are only order-of-magnitude approximations to those required in natural magmas.

Chalmers (1964) presents experimental evidence that elongate crystals growing in a preferred direction will curve such that they are aligned parallel to the supersaturation gradient in the nourishing fluid. If the fluid is flowing, the crystals are concave toward the flow direction. This is opposite to the direction predicted by Moore and Lockwood (1973a, b) for curved crystals in comb layers. In our experiments, curved crystals grow in a hydrostatic environment. This obviates the conclusion of Moore and Lockwood (1973a, b) that curved crystals in comb layers need a fast moving, low viscosity fluid as a growth medium. Curvature seems to be a response to specific growth conditions which are, as yet, unknown (Knight, 1967). Hence, curved crystals in comb layers are not unequivocal indices of a pegmatite origin for comb layers, nor are they necessarily indices of crystallization from a moving fluid.

In only one experiment (Fig. 6) was there a suggestion of parallel growth of curved crystals. The general absence of parallel growth in the experimental charges is likely to be due to the lack of a thermal gradient and the absence of a planar crystallization front.

Origin of Supersaturation in the Plutonic Environment

Our experiments indicate that the growth of curved and branching crystals in magmas requires a certain degree of supersaturation. Where these crystals have

Fig. 6. Photomicrograph of crystals grown from $\text{An}_{30}\text{Ab}_{45}\text{Or}_{25}$ melt (5.0 wt. percent water) cooled at 32°C/hr from 1150 to 860°C after melting at 1200°C . Curved, skeletal, and dendritic plagioclase. The curved crystals display parallel orientation. The bar is 1 mm

Fig. 7. Photomicrograph of crystals grown from $\text{An}_{30}\text{Ab}_{45}\text{Or}_{25}$ melt (4.9 wt. percent water) cooled at 66°C/hr from 1150 to 855°C after melting at 1200°C . Crystal aggregates are plumose, fan and bow-tie spherulites that branch complexly along principle spherulite fibers. The bar is 1 mm

grown in the volcanic and hypabyssal environments, the supersaturation may generally be ascribed to supercooling due to the rapid cooling accompanying emplacement (Drever and Johnston, 1957). The difficulty of reaching a supercooled state by conduction in the plutonic environment has caused some investigators to discard magmas as the parents of comb layers (Moore and Lockwood, 1973a, b; Van Diver and Magetti, 1973) and favor a pegmatite origin. Comb layers occur preferentially near the margins of intrusive bodies, the regions most prone to supercooling. Yet, supercooling cannot always be ascribed simply to thermal cooling on intrusion, because comb layers in some instances first appear 100 m from pluton margins (Taubeneck, pers. comm. Furthermore, comb layers are sometimes separated by layers of crystals with polyhedral morphologies typical of slow growth conditions close to the liquids temperature (e.g., tabular plagioclase). The abrupt change from polyhedral to skeletal or dendritic morphologies, indicates that conditions of supersaturation were rapidly induced. Abrupt increases in supersaturation due to thermal conduction and convection processes at the margin of a pluton do not seem likely. Other mechanisms for rapidly supersaturating magmas in the plutonic environment are discussed by Jahns and Tuttle (1963); Jahns and Burnham (1969) and Donaldson (1974). These mechanisms involve little or no cooling and rely instead on raising the liquidus temperature relative to the actual temperature of a water bearing magma either by a change in confining pressure or by a change in dissolved water content. The loss of water from melts is diffusion controlled and rapid supersaturation induced by loss of volatiles is unlikely in a water undersaturated melt. There is evidence that the cool margins and top of a magma body will be enriched in water by diffusional loss from the interior of the body (Kadik and Khitarov, 1965; Elsdon, 1971). Thus, the parent melt of comb layers might be close to, or indeed be, water saturated (Loomis, 1973). Comb layers are commonly associated with orbicules that enclose fragments of comb layers. Violent and possibly explosive movement of magma is indicated by the presence of orbicules (Moore and Lockwood, 1973a). It seems that both sudden vapor loss due to deformational opening of fractures and pressure changes due to magma movement followed by quiescent growth of comb layers are compatible with the evidence.

The Origin of Alternating Layers

Successive comb layers are often highly differentiated because they are dominated volumetrically by the elongate, branching crystals. Any or all of the minerals plagioclase, pyroxene, olivine, or amphibole may be the elongate, curved or branching mineral in one layer and occur as more equant, interstitial grains in the next layer (Taubeneck and Poldervaart, 1960; Drever and Johnston, 1972). An excellent illustration of these features at the margins of an alkali olivine dolerite dike is given by Drever and Johnston (1972). Two types of layers develop (Fig. 1): one layer contains elongate, parallel, branching olivines, and elongate, and sometimes curved, plagioclases, while the other layer is dominated by branching pyroxenes. The first type of layer may have <5 percent pyroxene and is a feldspathic peridotite; the other is generally olivine poor and is a clinopyroxenite. Similarly abrupt modal variation occurs among comb layers of granitic rocks (Fig. 2; Taubeneck and Poldervaart, 1960; Moore and Lockwood, 1973a).

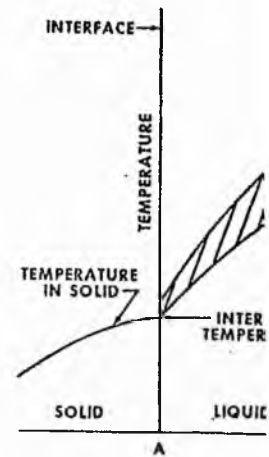


Fig. 8. Schematic liquid-strained crystal growth: modification of the liquid interface (after Tarshis a)

The origin of the boundary layer, and the growth of the boundary layer during steady state growth of a pluton resembles the growth of a crystal in a supercooled melt, and a positive temperature gradient exists (Fig. 8). If the crystal moving interface of the boundary layer enriches the melt in a lower liquidus temperature, a supercooled melt exists (Fig. 8). The maximum distance ahead of the interface is determined by the diffusion rates, cooling rate, and the temperature gradient.

Experiments on comb layers in binary systems with a positive temperature gradient. This component may be important where the proportion of the melt is such that it saturates the boundary layer. The common growth of a boundary layer perpendicular to the liquidus is determined by the nucleation of a crystal due to the temperature rise due to the melt between A and B.

ersaturation may
 ing accompanying
 ing a supercooled
 some investigators
 kwood, 1973 a, b;
 omb layers occur
 is most prone to
 mply to thermal
 st appear 100 m
 mm.). layers are
 hogies typical of
 ular plagioclase).
 ologies, indicates
 upt increases in
 sses at the margin
 supersaturating
 id Tuttle (1963);
 hanzisms involve
 perature relative
 a change in cons-
 ss of water from
 y loss of volatiles
 the cool margins
 al loss from the
 Thus, the parent
 l (Loomis, 1973).
 use fragments of
 is indicated by
 eems that both
 pressure changes
 layers are com-

y are dominated
 of the minerals
 curved or bran-
 al grains in the
 ston, 1972). An
 olivine dolerite
 levelop (Fig. 1):
 gate, and some-
 branching pyro-
 is a feldspathic
 enite. Similarly
 ks (Fig. 2; Tau-

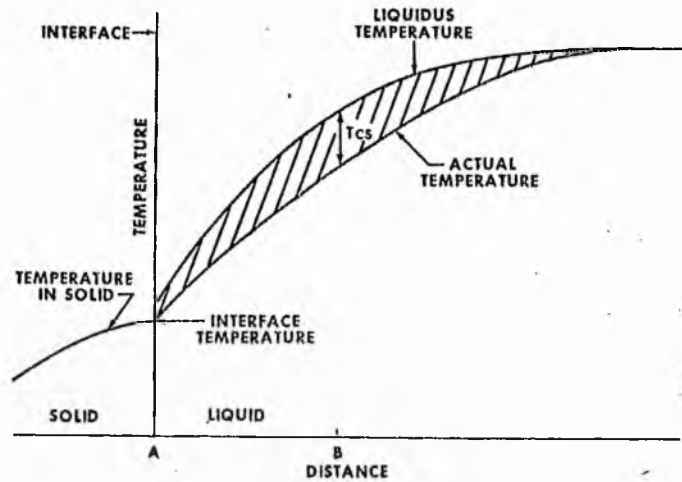


Fig. 8. Schematic liquidus and actual temperature profiles at solid-liquid interface for constrained crystal growth showing the constitutionally supercooled zone (hachured) caused by modification of the liquidus temperature by components rejected by the growing solid at the interface (after Tarshis and Tiller, 1967)

The origin of the alternating layers may be related to the development of a boundary layer, and thus constitutional supercooling, at the crystal-melt interface during steady state growth. Oriented inward growth from the margins of a dike or pluton resembles the constrained crystal growth condition described in the crystal growth literature Tarshis and Tiller (1967). Under this condition, latent heat is extracted through the growing crystals, rather than dissipated into the melt, and a positive temperature gradient exists in the melt adjacent to the crystal (Fig. 8). If the crystal growth rate is more rapid than the diffusion away from the moving interface of components rejected by the growing crystal, a gradational boundary layer enriched in these components forms. This boundary layer has a lower liquidus temperature than the bulk melt and thus a zone of constitutionally supercooled melt exists ahead of the interface, as shown by the hachured area (Fig. 8). The maximum supercooling is ΔT_{CS} and will generally occur at some small distance ahead of the interface, depending on such parameters as the growth rate, diffusion rates, cooling rate and the specific heats of the melt and crystal.

Experiments on constrained crystal growth invariably have been performed in binary systems with very small (<5 percent) amounts of one of the components. This component may be regarded as an impurity in a unary melt. In magmas, where the proportion of "impurity" is large, the buildup of "impurity" may supersaturate the boundary layer with a different phase, which nucleates in the constitutionally supercooled zone, and then becomes the directionally growing phase. The common growth direction is controlled by the temperature gradient which is perpendicular to the layer. The elongate minerals (2) of the previous layer are terminated by the nucleation and growth of the new phase aided possibly by the temperature rise due to latent heat evolved by the newly growing phase in the melt between A and B (Fig. 8). The thickness of a layer dominated by one or more

elongate minerals will vary with how rapidly the boundary layer builds up and how long nucleation of the new elongate crystal phase is delayed.

An example of a boundary layer adjacent to a plagioclase crystal in a basaltic melt is given by Bottinga and others (1966). Three microns from the crystal-glass interface, the glass is 7.5 wt percent deficient in the components of feldspar and 8.7 percent enriched in mafic components. Tholeiitic glass adjacent to skeletal olivines can be depleted by 13 wt percent normative olivine and enriched in 4wt percent normative feldspar and 9 wt percent normative pyroxene relative to the bulk glass (Donaldson, in press). These are examples for specific crystal growth parameters and for an unconstrained growth situation (latent heat evolved to melt). Similar compositional changes should occur for constrained growth. The magnitude of these changes in melt composition may be sufficient to cause nucleation of the new liquidus phases. Formation of comb layering in an igneous body will depend on the magnitude of the temperature gradient at its margin. In general, the larger the gradient the greater the possibility of comb layer development.

Conclusion

Crystallization studies of plagioclase have shown that some degree of supercooling is necessary to produce the skeletal, curved, and branching plagioclase crystal morphologies found in comb-layered rocks and that curved crystals can be grown without the presence of a directed stress. The experimental results support the supercooling hypothesis for the origin of comb layering. The development of a boundary layer ahead of a growing comb layer as a locus of nucleation for a new comb layer combined with the potentially periodic buildup and release of volatile pressure explain textural and differentiation features of comb layers.

Acknowledgements. We would like to thank S. Agrell, H. Drever, J. Moore, W. Taubeneck, and J. Lockwood for samples of comb-layered rocks. J. Gutmaun, A. Reid, and W. Taubeneck critically reviewed and improved the manuscript. Colin Donaldson thanks the Lunar Science Institute for a Visiting Graduate Fellowship and the Natural Environment Research Council (United Kingdom) for financial support. The Lunar Science Institute is operated by the Universities Space Research Association under Contract No. NSR-09-051-001 with the National Aeronautics and Space Administration. This paper constitutes the Lunar Science Institute Contribution number 202.

References

- Barriere, M.: Le gabbro orbiculaire des Alharesses (massif de Neouvielle, Pyrenees francaises). *Bull. Soc. Franc. Mineral. Crist.* 96, 495-506 (1972)
- Barriere, M., Chauris, L., Cotton, J.: Premieres donnees sur un facies orbiculaire dans le massif granitique de l'Aber-Ildut (Finistere, France). *Bull. Soc. Franc. Mineral. Crist.* 94, 402-410 (1971)
- Bottinga, Y., Kudo, A., Weill, D.: Some observations on oscillatory zoning and crystallization of magmatic plagioclase. *Am. Mineralogist* 51, 792-806 (1966)
- Bryan, W.B.: Morphology of quench crystals in submarine basalts. *J. Geophys. Res.* 77, 5812-5819 (1972)
- Chalmers, B.: Principles of solidification. New York: John Wiley 1964
- Dawson, J.B., Hawthorne, J.B.: Intrusion features of some hypabyssal South African Kimberlites. *Bull. Volcanol.* 34, 740-757 (1970)
- Donaldson, C.H.: Olivine crystal types in harrisitic rocks of the Rhum platon and Archaean spinifex rocks. *Geol. Soc. Am. Bull.* 85, 1721-1726 (1974)

tabular crystal grows at... Faster cooling rates are... complexity and diminis... creasing cooling rates w... rate required to produc... viscosity. Thus, a larg... with the normative fel... granite. The closest app... afforded by the experim... to those of "diorites" an... morphology, the "haploc... granodiorite" melt; in c... for branching crystals a... addition of mafic miner... and necessitate even gro... ching of feldspar crys... viscosity relative to th... rates. Hence, the cool... magnitude approximat...

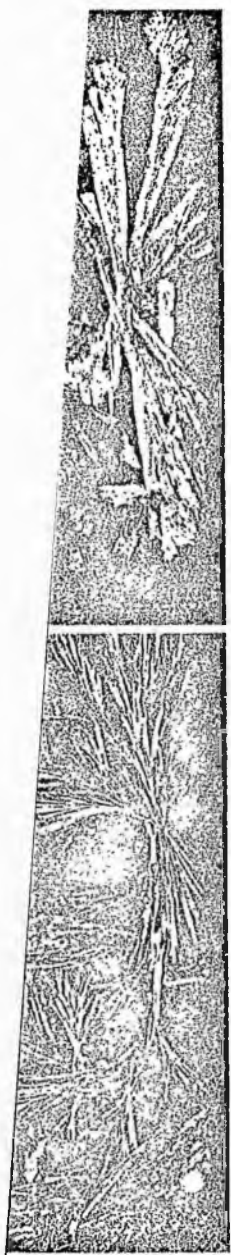
Chalmers (1964) pres... in a preferred direction... saturation gradient in... concave toward the fl... Moore and Lockwood... ments, curved crystal... elusion of Moore and... need a fast moving, lo... a response to specific... Hence, curved crysta... origin for comb laye... moving fluid.

In only one expe... curved crystals. The... is likely to be due t... crystallization from

Origin of Supersatu...
Our experiments in... magmas requires a

Fig. 6. Photomicrog... cooled at 32° C/hr fr... plagioclase. The cur...

Fig. 7. Photomicrog... cooled at 66° C/hr fr... fan and bow-tie spl... is 1 mm



(7.0 wt. percent water) cooled
spherulites dominate;

(7.0 wt. percent water)
aggregates are coarse,

Donaldson, C.H.: Calculated diffusion coefficients and the growth rate of olivine in basaltic magma (in press)

Drever, H.I., Johnston, R.: Crystal growth of forsteritic olivine in megmas and melts. *Trans. Roy. Soc. Edinburgh* **63**, 289-315 (1957)

Drever, H.I., Johnston, R.: Metastable growth patterns in some terrestrial and lunar rocks. *Meteoritics* **7**, 327-340 (1972)

Elsdon, R.: Crystallization history of the Upper Layered Series, Kap. Edvard Holm, East Greenland. *J. Petrol.* **12**, 499-521 (1971)

Farquharson, R.B.: The petrology of late tertiary dolerite plugs in the South Cariboo Region, British Columbia. *Can. J. Earth Sci.* **10**, 205-225 (1973)

Jahns, R.J., Burnham, C.W.: Experimental studies of pegmatite genesis: I. a model for the derivation and crystallization of granite pegmatites. *Econ. Geol.* **64**, 843-864 (1969)

Jahns, R.J., Tuttle, O.F.: Layered pegmatite-aplite intrusives. *Mining. Soc. Am. Spec. Paper* **1**, 78-92 (1963)

Kadik, A.A., Khitarov, N.I.: Effect of pressure on the exchange of water between magma and the enclosing rocks. *Geochemistry Int.* **2**, 397-406 (1965)

Knight, C.A.: *The freezing of supercooled liquids*. New York: Van Nostrand 1967

Leveson, D.J.: Origin of comb layering and orbicular structure, Sierra Nevada Batholith, California: Discussion. *Geol. Soc. Am. Bull.* **84**, 4005-4006 (1973)

Lofgren, G.: Experimental crystallization of synthetic plagioclase at prescribed cooling rates. *E.O.S.* **54**, 482 (1973)

Lofgren, G.: An experimental study of plagioclase crystal morphology: Isothermal crystallization. *Am. J. Sci.* **274**, 243-273 (1974)

Lofgren, G., Donaldson, C.H.: Experimental evidence bearing on the origin of "Comb (Willow Lake) Layering." *Geol. Soc. Am. Abst. with Programs* **5**, 716 (1973)

Loomis, A.A.: Noritic anorthositic bodies in the Sierra Nevada batholith. *Mining. Soc. Am. Spec. Paper* **1**, 62-68 (1963)

Moore, J.G., Lockwood, J.P.: Origin of comb layering and orbicular structure, Sierra Nevada batholith, California. *Bull. Geol. Soc. Am.* **84**, 1-20 (1973a)

Moore, J.G., Lockwood, J.P.: Origin of comb layering and orbicular structure, Sierra Nevada Batholith, California: Reply. *Geol. Soc. Am. Bull.* **84**, 4007-4010 (1973b)

Nesbitt, R.W.: Skeletal crystal forms in the ultramafic rocks of the Yilgarn Block, Western Australia: Evidence for an Archaean ultramafic liquid. *Spec. Publs. Geol. Soc. Austr.* **3**, 331-347 (1971)

Platten, I.M., Watterson, J.S.: Oriented crystal growth in some tertiary dykes. *Nature* **223**, 286-287 (1969)

Preston, J.: A columnar crystallization of olivine and plagioclase. *Geol. Mag.* **100**, 1-6 (1963)

Pyke, D.R., Naldrett, A.J., Eckstrand, O.R.: Archaean ultramafic flows in Munro Township, Ontario. *Geol. Soc. Am. Bull.* **84**, 955-978 (1973)

Tarshis, L.A., Tiller, W.A.: The effect of interface-attachment kinetics on the morphological stability of a planar interface during solidification. In: *Crystal growth*, H. S. Peiser, ed., p. 709-719. Oxford: Pergamon 1967

Taubeneck, W.H., Poldervaart, A.: Geology of the Elkhorn Mountains, Northeastern Oregon: Part 2. Willow Lake intrusion. *Geol. Soc. Am. Bull.* **71**, 1295-1322 (1960)

Wager, L.R., Brown, G.M., Wadsworth, W.J.: Types of igneous cumulates. *J. Petrol.* **1**, 73-85 (1960)

Wyllie, P. J., Drever, H.I.: The petrology of picritic rocks in minor intrusions - a picrite sill on the island of Soay (Hebrides). *Trans. Roy. Soc. Edinburgh* **65**, 155-177 (1963)

Van Diver, B.B., Maggetti, M.: Comb Layering and orbicular structure in the Reichenbach orbiculite, Odenwald, West Germany. *Geol. Soc. Am. Abst. with Programs* **7**, 846-847 (1973)

Dr. G.E. Lofgren
Geology Branch, TN6
NASA-Johnson Space Center
Houston, Texas 77098, USA

Crystallization of Poikilo-macro-spherulitic Feldspar in a Rhum Peridotite

HERE we define and describe a new macrocrystalline radiate texture in a major layered intrusion. This occurrence is inconsistent with the much applied adcumulus crystal growth hypothesis which dominates current thinking on the derivation of ultrabasic rocks from basaltic magmas. Some radical alternative mechanisms of origin are proposed.

During recent field work on the island of Rhum, a unique macrocrystalline facies, within the major layered ultrabasic complex, was discovered near Loch Dornabac. It is characterized by massive radial and braid-like growths of bytownite poikilitically enclosing orientated forsteritic olivines.

A hundred yards east of, and 50 foot above, Loch Dornabac is a broad ridge chiefly composed of igneous breccia containing peridotitic and allivalitic blocks set in a feldspathic peridotite matrix, which becomes progressively more feldspathic upwards and also develops slump and wispy banding on top of the ridge. The macrocrystalline facies occurs within this breccia as a near horizontal unit, co-extensive with the feldspathic peridotite matrix of the igneous breccia. Its maximum width is approximately twenty yards with an irregular attenuation toward the northeast and southwest, along the 300 yard of exposure.

The poikilitic plagioclase has grown in the form of branching rays radiating from a centre (Fig. 1a) or in less regular, diverging and bifurcating systems. The size of the radiate systems varies from a 6 inch to 36 inch diameter, and upwards of fifteen radiating and bifurcating rays from a single system can be observed on a planar surface. In most cases, the distribution of rays, as seen on outcrop surfaces, is asymmetrical, but approximate radial symmetry may be developed (Fig. 1a, b). This macrotexture has been observed on horizontal surfaces and on steeply inclined surfaces where the rays may extend downwards from a centre (Fig. 1b). If, as the evidence suggests, such rays extend in all directions the appropriate term for the texture is macrospherulitic. To ensure that this interpretation is accurate we will extract a large block from the outcrop and cut in critical directions.

Because the plagioclase poikilitically encloses many olivine crystals it must have grown around and between them. The composite term poikilo-macrospherulitic accurately conveys the principal textural characteristics of the rock as a whole.

Although a spherulitic development of plagioclase is the most distinctive form of this poikilitic macrotexture, the commoner forms are those illustrated in Fig. 1b (top right) in which rays of plagioclase are partially radiating but not clearly convergent to a centre. This type of macrotextural pattern is referred to as braid-like. Figure 1c illustrates another variant where offshoots from the macrotextural peridotite seem to "invade" the normal feldspathic peridotite.

The rays of poikilitic plagioclase weather in slight relief, due to the occurrence of most of the clinopyroxene between them, although a little of the clinopyroxene may occur in a plagioclase ray. With the olivine and clinopyroxene in the intervening hollows there is also some plagioclase, and the inferred order of crystallization is olivine-bytownite-clinopyroxene. The olivine appears to be uniformly distributed and comprises 60% of the rock by volume. Along a plagioclase ray there may be no more than 35% plagioclase, the differential weathering giving an exaggerated impression of its amount. In addition to the minor development of poikilitic clinopyroxene, moulded into elongated shapes by its later growth between the radiate feldspars, there are some brown amphibole, chestnut coloured biotite and opaque grains. These three constituents, in variable proportions, represent about 2% of the rock.



Fig. 1 a, Sections through a number of plagioclase poikilo-macrospherulites on an inclined surface. Pencil is 4 inch long. b, Radial and branching plagioclase growths in peridotite. The radiate macrotexture (lower left) is horizontal, whereas the braid-like form above it slopes downward from what appears to be a large "nucleus", horizontally transected by the outcrop surface. Rule is 16 inch long. c, Massive development, on a horizontal surface, of poikilitic feldspathic peridotite (upper half of photograph) with a development of feldspathic offshoots and patches in relatively plagioclase-deficient peridotite (bottom of photograph). Longer arm of the rule is 18 inch long.

The plagioclase seems to have nucleated at the centre of each radiating system. As a preliminary step toward testing this, a large thin section was cut along one of the rays. In this section, the plagioclase has nearly uniform albite-twin lamellae directions and twin extinction positions over a distance of 6 inch. A few small plagioclase crystals of different orientation may represent cross-sections of branches.

A more detailed textural analysis will be undertaken, but this preliminary evidence indicates that each ray of a macrospherulite consists of a single poikilitic plagioclase crystal. No difference in composition between nucleus and ray extremity has been detected, both being An_{80} (determined optically by both $2V$ (ref. 1) and Kohler angle² measurements). No zoning in any part of the ray has been detected. Olivine (For_{91} , determined by an XRD method³), predominantly orientated with (010) horizontal, also seems unzoned. It is usually euhedral with well developed pinacoidal and prism forms and rarely has some embayments.

The "honeycombed" texture and "lace structure" found in the eastern layered series^{4,5} bear some resemblance to the small scale features of the plagioclase textures considered here, but no large scale poikilospherulitic texture has been reported. The macrospherulitic plagioclase seems to have nucleated *in situ*, under conditions of very low nucleation density (in places one nucleus per 10 foot) and in some instances, plagioclase grew downwards over distances of 1 inch to 2 foot. If the model of crystal settling and adcumulus growth from a basaltic liquid, applied to the Rhum ultrabasic rocks⁵, is invoked to explain the origin of this rock, then 2 foot is an impossible distance for the necessary diffusion between liquid interstitial to the "settled" olivine and growing plagioclase crystals and an overlying basaltic liquid⁶. Indeed, Wager and Brown⁵ consider that a layer of cumulus crystals one crystal thick can prevent the necessary diffusion for adcumulus growth. Assuming cumulate development of contiguous facies, all the liquid below the plagioclase nucleus must be considered to have been trapped. Accordingly, if the parent magma were a basalt, the liquid interstitial to the olivines should have been basaltic at the time of plagioclase nucleation. But the minerals that crystallized late in these rocks do not correspond to a basaltic composition, the plagioclase in particular being too calcic.

Although the concept of crystal accumulation has for long been regarded as applicable to the layered ultrabasic complex in Rhum, including the harrisitic layers⁷, there now seems to be enough evidence to suggest that its applicability may have to be restricted. In any interpretative reassessment particular attention could most profitably be paid to the following. (1) The association in the same intrusion of two macrotextures, harristic and poikilo-spherulitic, the former being defined by massive skeletal olivine growth, the latter by massive radiate plagioclase growth. (2) The rocks in which both of these textures are developed can be classified as ultrabasic, with forsteritic olivine as the principal component. (3) The forsteritic olivine and bytownitic plagioclase are, characteristically, unzoned apart from some peripheral zoning in the plagioclase of harristic eucrite⁷. (4) In the macrotextural facies the large olivines and large plagioclases have crystallized *in situ*. (5) The

harrisitic texture is rhythmically repeated in layers interstratified with layers regarded as normal cumulate⁷, whereas the occurrence in Rhum of the poikilo-macrospherulitic texture seems to be much more restricted. (6) The feldspathic peridotites with macrotextures of both types can be observed to pass laterally into feldspathic peridotite of normal "cumulate" type. (7) Both macrotextures attain in Rhum a development of which there seems to be no near counterpart in any other major intrusive complex, although some useful comparisons can be made with a smaller scale development of plagioclase with poikilo-arborescent texture in an ultrabasic dyke in Skye⁸; the textures of "quench" peridotites ("spinifex" and "komatiite") comparable with those in harrisite; "willow-lake", "crescumulate" or thermotactic textures^{9,10}; and very coarse-grained hornblende pegmatite in the Duke island ultrabasic complex¹¹, and the Shiant Isles picrite and its veins⁸.

In the light of this it will now be necessary to discover the degree of validity of the following possibilities. (1) The existence in Rhum of a hydrous magma with the chemical composition of a feldspathic peridotite^{10,12}. (2) Post-depositional regeneration of plagioclase and olivine as radiate and harrisitic growths. (3) Changes in total pressure of H_2O causing shifts of the primary fields of olivine and plagioclase on the liquidus surface, or decrease in the ratio of olivine to plagioclase with fractional crystallization¹³. (4) Independent mobility of a liquid with the composition of bytownite-anorthosite saturated with H_2O ^{10,14}. (5) Nucleation and crystallization of plagioclase primocrysts at the bottom of the liquid column^{15,16}.

C. H. DONALDSON*
H. I. DREVER
R. JOHNSTON

*Department of Geology,
University of St Andrews*

Received March 5, 1973.

* Present address: Lunar Science Institute, Houston, Texas 77058.

- ¹ Smith, J. R., *Amer. Min.*, **43**, 1188 (1958).
- ² Van der Kaaden, G., thesis Univ. Utrecht (1951).
- ³ Yoder, H. S., and Sahama, T. G., *Amer. Min.*, **42**, 475 (1957).
- ⁴ Brown, G. M., *Phil. Trans. Roy. Soc.*, **240**, 3 (1957).
- ⁵ Wager, L. R., and Brown, G. M., *Layered Igneous Rocks* (Oliver and Boyd, Edinburgh and London, 1967).
- ⁶ Hess, G. B., in *Studies in Earth and Space Sciences, Geol. Soc. Amer. Mem. 132* (Hess volume) (edit. by Shagan, R., et al.), 503 (1973).
- ⁷ Wadsworth, W. J., *Phil. Trans. Roy. Soc.*, **244**, 21 (1961).
- ⁸ Drever, H. I., and Johnston, R., in *Ultramafic and Related Rocks* (edit. by Wyllie, P. J.) (Wiley, New York, 1967).
- ⁹ Loomis, A. A., *Min. Soc. Amer. Spec. Paper 1*, 62 (1963).
- ¹⁰ Drever, H. I., and Johnston, R., *Meteoritics*, **7**, 327 (1972).
- ¹¹ Irvine, T. N., *Min. Soc. Amer. Spec. Paper 1*, 36 (1963).
- ¹² Harker, A., *Mem. Geol. Surv. Scotland* (1908).
- ¹³ Emslie, R. F., *New York State Museum Sci. Service Mem. 18*, 163 (1968).
- ¹⁴ Hamilton, D. L., *Proc. Geol. Soc. London*, **1651**, 200 (1969).
- ¹⁵ Kennedy, G. C., *Geol. Soc. Amer. Spec. Paper 62*, 489 (1955).
- ¹⁶ Elsdon, R., *J. Petrol.*, 499 (1971).

A Sample Holding Technique for Study of Crystal Growth in
Silicate Melts

by

Colin H. Donaldson¹
Richard J. Williams²
Gary Lofgren²

1) Lunar Science Institute, Houston, TX 77058 and University of St.
Andrews, Scotland.

2) NASA Johnson Space Center, Houston, TX 77058.

Abstract

A thin platinum wire loop is an effective way to hold silicate melts during experimentation in a gas-mixing furnace. This method results in a minimum of physical and chemical interaction between the sample and container but maximum interaction between sample and gas mixture. However, volatilization of sodium occurs while the silicate is molten. By minimizing the chance of heterogeneous nucleation, the method is ideal for experimental investigation of the origin of rock textures.

Introduction

To study the textural features of rocks experimentally, it is desirable that physical interaction of the container and charge be minimized, so that the container is not a prominent nucleation site in the charge. Many containers are unsuitable for textural study of silicate melt crystallization because the melt adheres tenaciously to the container, spreads itself over the container walls, or because heterogeneous nucleation of silicate phases occurs on the container surfaces. The choice of a sample container is further complicated by the need to limit chemical interaction with the charge. All sample containers react chemically with silicate melts to some degree; for example, the commonly used metal containers, Pt and Pd alloys, extract iron from the silicate.

This paper describes and evaluates a variation of a sample holding arrangement first used by Ribould and Muan (1962) which minimizes these physical and chemical container-sample interactions. The technique has proved ideal for reproducing the textures and phase chemistry features of lunar basalts (Lofgren et al., in press). Variations of the arrangement have been used by McKay (pers. comm., 1973), but the technique differs substantially from that recently described by Presnall and Brenner (in press).

Technique Employed

Platinum is the sample container material most often used because it can be employed over the wide range of physical and chemical conditions required by experimental petrology. In Fe-containing systems, however,

the Fe rapidly alloys with the platinum and this changes the composition of the charge. In general, there is a problem with the use of crucibles or tubes for holding melted silicates because they have a high contact-area to sample-volume ratio. To minimize this ratio we have developed the technique of Ribould and Muan (1962) for suspending melted samples in a platinum wire loop. By reducing contact between melt and container to a minimum, Fe loss from the sample is minimized, as is the chance of heterogeneous nucleation of silicate phases at the melt-container boundary. The surface tension that holds the melted charge in the loop is sufficient, even in very fluid melts to maintain an ellipsoidal droplet 4-6 mm in diameter. The technique therefore has the added advantage that the interaction between sample and gas mixture is a maximum, since the surface area to volume of an ellipsoidal charge is large.

Run Procedure

A powdered starting material (80-100 mg) is pressed into a pellet 6-7 mm in diameter and 2-4 mm thick. The pellet is placed on a loop of 0.008" diameter platinum wire, attached to the electrodes of a strip heater (Fig. 1). The wire is heated electrically until slight sintering or melting tacks the pellet onto the wire. [In contrast, Ribould and Muan (1962) sintered pellets, enclosed by platinum foil, at 50°C below the solidus temperature for 5 minutes. The pellet was then placed in a platinum wire loop, but without tacking by electrical heating.] The loop and charge are then attached to a ceramic bead, itself suspended by a thin wire strung across two heavy duty platinum wires which are encased in a 30 cm long ceramic rod (Fig. 2). During the attachment

process a hemostat clamped across the ends of the loop prevents flexing of the wire which would dislodge the pellet. The ceramic rod and sample are then inserted into a gas-mixing furnace and a run made. Wire of 0.008" diameter is sufficiently strong to hold a 100 mg charge indefinitely at temperatures up to 1600°C. For smaller charges or lower temperatures, thinner wire may be used.

The resultant charge (Fig. 2) is ideally suited for examination of the surface shapes of crystals on the outside of the charge, for removal of single crystals, and for preparation of thin sections to study texture and phase chemistry. The wire acts as a nucleation site for very few crystals and has little effect on textures developed in the bulk of the charge (Fig. 3). However, some heterogeneous nucleation does occur at the melt-gas interface.

Chemical Changes During Runs

Analyses 1, 2 and 3 in Table 1 compare the compositions of a terrestrial basalt and of two aliquots of the basalt melted at 20-30°C above the liquidus for 1 and 24 hours respectively. The most significant change observed is that Na₂O content of samples decreases by about 1.3 weight percent in a 24 hour run. Analyses 4 and 5 respectively are the starting composition and run product of a synthetic lunar basalt (low initial Na₂O content). No Na₂O loss is apparent from this basalt after 3 hours melting at 1250°C (25°C above the liquidus). Hence, this technique does suffer significant loss of Na₂O from Na₂O-rich charges. The greater the initial Na₂O content of samples, the greater the loss of Na₂O during a given run duration. There is no significant change in K₂O content during runs.

The extent of iron loss from the melted basalts to the platinum wire may be gauged from analyses 1-5 in Table 1. For example, 0.9 weight percent FeO (4.8 percent of the total FeO initially present) is lost from the iron-rich lunar basalt during a three-hour melting experiment. The Fe content of the melt is uniform to within 5 μ of the wire. It must be stressed that the run conditions were highly reducing ($f_{O_2} = 10^{-12} - 10^{-13}$ atm. at 1250°C), thereby favoring removal of Fe from the melt. In runs under the more oxidizing conditions typical of terrestrial magmas, Fe loss would be less severe. This rate of Fe loss is tolerable and is considerably lower than was reported by Merrill and Wyllie (1973) for samples run completely enclosed in platinum capsules.

Electron microprobe analysis was made of the platinum wire in contact with the glass of composition 5 (Table 1). Less than 1 weight percent iron was found at the center of the wire and an alloy of 40 weight percent iron occurs at the rim. From the profile of the Fe content across the wire, the diffusion coefficient in platinum was calculated as 1.75×10^{-10} cm²/s (calculated using the method described by Medford, 1973).

Summary

The method of containing silicate liquids and charge preparation described in this paper should be of value to experimental petrologists and materials scientists. It is simple, cheap and provides minimum chemical and physical interaction between the sample and the container, but maximum interaction between sample and gas mixture. The technique is applicable to rock powders, glasses and solid samples. It is particularly suited to studies of highly reduced melts, such as Fe-rich lunar basalts.

Acknowledgments

The skill of Oscar Mullins has been invaluable to the success of the technique. C. H. Donaldson thanks the Lunar Science Institute for a Visiting Graduate Fellowship and the Natural Environment Research Council (United Kingdom) for financial support. The Lunar Science Institute is operated by the Universities Space Research Association under Contract No. NSR-09-051-001 with NASA. This paper constitutes Lunar Institute Contribution 000.

Note added in proof:

Basalt 1 (Table 1) run for 6 hours at 1250°C and $fO_2 = 10^{-8}$ atm lost 2.5% of the amount of Fe originally present and 3.1% of the Na. These losses are within the error of the microprobe determinations.

References

- Lofgren, G. E., C. H. Donaldson, R. J. Williams, O. Mullins and T. M. Usselman (1974) Experimentally reproduced textures and mineral chemistry of Apollo 15 quartz normative basalts. Proc. Fifth Lunar Sci. Conf., Geochim. Cosmochim. Acta Suppl. 5 (in press).
- Medford, G. A. (1973) Calcium diffusion in a mugearite melt. Can. J. Earth Sci. 10, 394-402.
- Merrill, R. B. and P. J. Wyllie (1973) Absorption of iron by platinum capsules in high pressure rock melting experiments. Amer. Mineral. 58, 16-20.
- Presnall, D. C. and N. L. Brenner (1974) A method for studying iron-silicate liquids under reducing conditions with negligible iron loss. Geochim. Cosmochim. Acta (in press).
- Ribould, P. V. and A. Muan (1962) Phase equilibria in a part of the system "FeO"-MnO-SiO₂. Trans. Metall. Soc. AIME 224, 27-33.

Fig. 1. Pellet in place on platinum loop and attached to strip heater. A transformer and variac comprise the electrical components of the heater.

Fig. 2. Melted sample on platinum loop, showing means of attachment to ceramic rod holder.

Fig. 3. Transmitted light photomicrograph of a charge of synthetic Apollo 15 basalt cooled from above the liquidus temperature at 2.5°C/hr . Large, subequant, euhedral phenocrysts of pyroxene are enclosed in a matrix of glass and fine-grained pyroxene and plagioclase. The two gray ellipsoids at the margin of the charge are remnants of the platinum loop. There is a slight tendency for increased nucleation of phases near the wire, but crystals at the center of the charge appear to have nucleated homogeneously.

Table 1. Comparison of compositions of starting material and melted (glass) run products.

	1	2	3	4	5
SiO ₂	50.19	50.63	51.00	48.70	48.04
TiO ₂	1.59	1.57	1.60	1.68	1.76
Al ₂ O ₃	15.39	15.31	15.63	10.70	11.19
FeO	9.72	9.83	9.25	18.90	18.03
MnO	0.19	0.17	0.17	0.26	0.28
MgO	8.53	9.09	9.13	8.94	9.18
CaO	10.81	11.04	11.18	10.41	10.26
Na ₂ O	3.34	2.70	2.09	0.05	0.08
K ₂ O	0.24	0.24	0.23	0.09	0.07
	100.00	100.58	100.28	99.73	98.89

1. Basalt recalculated free of H₂O, P₂O₅ and S.
2. 80 mg basalt pellet melted for 1 hour in platinum loop at 1250°C.
3. 80 mg basalt pellet run for 24 hours in platinum loop at 1250°C.
4. Synthetic Apollo 15 quartz normative basalt. (Lofgren *et al.*, in press.)
5. 80 mg pellet of synthetic quartz normative basalt run for 3 hours in platinum loop at 1250°C.

All experiments were performed at an oxygen fugacity of 10⁻¹² to 10⁻¹³ atm.

Analysis 1 is by X-ray fluorescence; J. M. Rhodes analyst.

Analyses 2-5 are by electron microprobe; C. H. Donaldson analyst.



Petrology and Chemistry of Basalts from the Nazca Plate:

Part 1 -- Petrography and Mineral Chemistry

Colin H. Donaldson

Lunar Science Institute
Houston, Texas 77058

and

University of St. Andrews
Scotland

Roy W. Brown

Lockheed Electronics Corp.
Houston, Texas 77058

and

Arch M. Reid

NASA Johnson Space Center
Houston, Texas 77058

We report on the petrography and mineral chemistry of 21 basalt samples drilled during Leg 34 of the Deep Sea Drilling Project from the Nazca Plate. The suite of samples comprises 13 from Site 319A, 3 from Site 320B, and 5 from Site 321. The same samples have also been analyzed for major, minor, and trace element contents (Rhodes et al., this volume). Results of petrographic observations and electron microprobe analyses are summarized in a series of Tables (1-6) and Figures (1-10).

Table 1 lists the catalog numbers of the samples and their locations in cooling units, and summarizes the rock types, textures, and the range of compositions for the three principal phases -- plagioclase, augite and olivine. Rock types are distinguished on the basis of the groundmass grain size [medium-grained (1-5 mm) versus fine-grained (<1 mm)] and phenocryst assemblage. Many of the rocks contain phenocrysts, the most abundant of which is plagioclase, followed by olivine. One sample, 319A-6-1, 84-89 cm contains pyroxene microphenocrysts. In the groundmass, elongate (in some cases, skeletal) plagioclase laths are set in a cryptocrystalline matrix, or form an ophitic or intergranular texture with pyroxene, or form an intersertal texture. All three of these textures coexist in some samples [e.g. 319A-4-1, 129-132 cm]. Groundmass olivine is present only in the finer grained rocks from Sites 319A and 320B and is totally absent in samples from Site 321. The groundmass olivines are subophitically enclosed by plagioclase laths (Fig. 4). They are particularly susceptible to alteration to dark brown smectite. Each olivine grain may be either completely replaced or mantled by smectite (Fig. 4). Those rocks in Table 1 for which the groundmass olivine column is labelled 'none' contain

neither groundmass crystals nor smectite crystals which could be inferred to be pseudomorphs after olivine. None of the samples contained glass. However, samples with intersertal texture contain abundant ~~chlorite~~^{smectite}, assumed to be the alteration product of glass and its associated devitrification products. Therefore, despite the low water contents and oxidation ratios of the Leg 34 basalts (Hart et al., 1974; Rhodes et al., this vol.), relative to most other basalts recovered by the Deep Sea Drilling Project, the rocks are not mineralogically fresh.

Plagioclase phenocrysts have two types of occurrence -- either isolated in the groundmass or, more commonly in glomerophyric units (Fig. 5), some of which also contain olivine. The cores of these crystals (An_{87-68}) are either unzoned or are oscillatory-zoned with adjacent zones differing by 1-4 mol. percent An. The margins of crystals in contact with the groundmass are continuously normal zoned. The periphery of each phenocryst has the same ^P composition as the margins of groundmass plagioclase laths, which are always normally zoned from core (An_{75-63}) to rim (An_{61-27}). Fe content of both phenocryst and groundmass plagioclase is substantial (i.e., 0.3-1.0 wt. percent) and increases with Ab content of the plagioclase (Table 3). Plagioclase zoning is much more extensive in medium-grained rocks than in fine-grained rocks (Table 1).

Olivine phenocrysts have limited ranges of core composition (Fo_{89-84} , Tables 1 and 2). An unzoned core is typically surrounded by a narrow normally zoned mantle. Groundmass olivines are slightly zoned (Table 2) and generally are 1-3 mol. percent less forsterite-rich than the core of the phenocrysts in the same rock. The CaO contents of both phenocrystic and groundmass

olivines exceed 1000 ppm (Table 2). The Ca content tends to increase with fayalite content of the olivine.

All the pyroxenes studied are augites. At Sites 319A and 321 pyroxenes have wide ranges of composition (Fig. 10 and Table 4). Pyroxene in the rocks from site 320B is very fine-grained and only 3 grains, all in one sample, were analyzed (Table 4). Augite compositions from individual rocks plotted in the pyroxene quadrilateral define either quench trends (cf. Evans and Moore, 1968) or trends subparallel to, and slightly less calcic than, the Skaergaard trend. Some single ophitic crystals in the coarse-grained rocks are extensively zoned with respect to Fe-Mg content (Table 4). The microphenocrysts in sample 319A-6-1, 84-89 cm, are similar in major element composition to the earliest augite to crystallize in the Skaergaard intrusion (Fig. 10).

The opaque phases are Fe-Ti oxides that occur in the groundmass, commonly as very small skeletal or dendritic crystallites. Titanomagnetite with around 25 wt. percent TiO_2 is present in virtually all of the basalts and is accompanied by ilmenite in more than half of the samples (Table 5). Only one sample [320B-3-1, 120-125 cm] has a small euhedral Mg-Al-Cr spinel grain (Table 6) which is enclosed by early plagioclase. All other samples lack a Cr-spinel phase, a deficiency which is atypical of most Mid-Ocean-Ridge basalts.

Conclusions

Basalts at Site 321 lack both phenocryst and groundmass olivine (Table 1; contrast Sites 319A and 320B); also, the plagioclase phenocrysts are much less calcic than those in basalts at Site 319A. Core compositions of groundmass plagioclases in Site 321 basalts are more sodic than those in samples from Site 319A, and they have larger orthoclase contents (Table 1). These petrographic differences are not attributable to differences in cooling history between the basalts at the two sites. Rather, Site 321 basalts are inferred to be more alkali-rich than those at Site 319A and to have had different crystallization histories. Although the core compositions of plagioclase phenocrysts in samples from Site 320B are not as calcic as those of the most anorthite-rich plagioclases at Site 319A, the rocks from both sites are similar in phase compositions (Table 1). The generally smaller range of phase zoning in rocks from Site 320B reflects faster cooling.

At each site, basalts from different cooling units and within individual cooling units have similar parageneses, except for crystallization of olivine. The absence of olivine phenocrysts from some of our samples from the thick cooling unit b (Table 1) may be due to crystal settling. Our companion paper (Rhodes et al., this volume) indicates that basalts at Site 319 are tholeiitic in composition rather than transitional to alkaline in affinity, as inferred in the preliminary report by the Shipboard Scientists from the occurrence of groundmass olivine. In the thick cooling unit (3, Table 1) groundmass olivine is absent from rocks at the center of the unit. As noted by Evans and Moore (1968), persistence of groundmass olivine in a tholeiite is favored

by rapid cooling and hence is an unsatisfactory index of magma type.

Our petrographic observations suggest that basalts at Sites 319 and 320 are plagioclase-(olivine) tholeiites, while those at Sites 321 are more fractionated tholeiites. We conclude that basalts from all three sites are oceanic tholeiites, and products of ocean ridge volcanism.

References

- Evans, B. W. and Moore, J. G., 1968. Mineralogy as a function of depth in the Prehistoric Makaopuhi tholeiitic lava lake, Hawaii: *Contr. Mineral. and Petrol.*, v. 17, p. 97.
- Muir, I. D., 1951, The clinopyroxenes of the Skaergaard intrusion, eastern Greenland: *Min. Mag.*, v. 29, p. 690.
- Rhodes, J. M., Blanchard, D. P., Rodgers, K. V., Jacobs, J. W. and Brannon, J. C., *Petrology and chemistry of basalts from the Nazca Plate: Part 2 - Major and trace element chemistry: this volume.*

C. H. Donaldson thanks the Natural Environment Research Council of the United Kingdom for financial support and the Lunar Science Institute for a Visiting Graduate Fellowship. Mike Rhodes kindly reviewed the manuscript. The Lunar Science Institute is operated by the Universities Space Research Association under contract no. NSR-09-051-001 with NASA. This paper is Lunar Science Institute Contribution No. 198.

Figure Captions

- Fig. 1. Skeletal olivine (top of photograph) and glomerocrysts of plagioclase laths and anhedral augite set in cryptocrystalline groundmass. [2 x 2.3 mm. Sample 319A-1-1, 138-142 cm.]
- Fig. 2. Poikilophitic and intersertal texture typical of those in medium-grained basalts at Site 319A. [1 x 1.3 cm. Sample 319A-3-3, 46-49 cm.]
- Fig. 3. Troctolite xenolith in olivine-feldspar phyric basalt. Large olivine crystal poikilitically encloses plagioclase crystals (bottom of photograph). Groundmass (at right of photograph) consists of plagioclase and augite. [5.2 x 5.5 mm. Polarized light. Sample 319A-3-5, 37-41 cm.]
- Fig. 4. Groundmass olivine crystals (top center and lower center) trapped between plagioclase laths (white) which are subophitically enclosed by augite (grey). Note the dark rim of smectite around the olivine. [2.1 x 2.3 mm. Sample 319A-4-1, 129-132 cm.]
- Fig. 5. Glomerocrysts of plagioclase set in cryptocrystalline groundmass. [4 x 4.3 mm. Polarized light. Sample 319A-6-1, 84-89 cm.]
- Fig. 6. Pyroxene microphenocryst and plagioclase lath set in a matrix of skeletal plagioclase laths and cryptocrystalline material. [1.5 x 1.7 mm. Sample 319A-6-1, 84-89 cm.]

Fig. 7. Skeletal plagioclase microphenocryst set in groundmass of felted plagioclase and cryptocrystalline material. [2 x 2.2 mm across. Sample 320B-4-1, 130-133 cm.]

Fig. 8. Intergranular texture of pyroxene and plagioclase in aphyric basalt. [1 x 1.2 mm. Polarized light. Sample 321-14-4, 61-64 cm.]

Fig. 9. Intergranular and intersertal textures in groundmass of fine-grained feldspar aphyric basalt. [5.2 x 5.5 mm. Sample 321-13-4, 119-124 cm.]

Fig. 10. Summary of pyroxene compositions in samples from Sites 319A, 320B and 321 plotted in the Di-He-En-Fs quadrilateral. Line on diagram for Site 320B shows the trend of early crystallizing augite in the Skaergaard intrusion (Muir, 1951).

Table 1. Summary of samples investigated, rock types present and their textures, and the range of phase composition in each rock

Sample No.	Cooling Unit ¹	Rock Type	Olivine phenocryst ² Fo mol percent	Olivine groundmass Plagioclase phenocryst (core) ³ Fo mol percent	An	Ab	Or	Plagioclase groundmass ⁴ An	Ab	Or	Ca	Augite ⁵ Mg	Fe	Comments
319A-1-1, 132-142	2	Fine-grained basalt	none	85										Skeletal olivine (0.1 mm across) and glomerophytic units of plagioclase (0.5x0.05 mm) subspatially enclosed by augite (0.1 mm across) set in crystalline matrix (fig. 1).
319A-2-2, 111-117	3	Medium-grained feldspar phytic	none	none	81.9-73.4	17.9-26.3	0.2-0.3	63.8-34.8	35.9-64.6	0.3-0.6	34.6-43.6	40.4-43.4	25.0-13.0	Plagioclase phenocrysts and glomerocrysts set in groundmass of intergranular and interstitial texture.
319A-3-2, 114-117	3	Medium-grained feldspar phytic	none	none	74.8-69.6	24.9-29.9	0.3-0.5	64.4-32.6	35.3-66.7	0.3-0.7	35.4-41.9	52 - 46.7	12.6-11.3	Plagioclase phenocrysts (up to 1.5 mm across) and glomerocrysts set in groundmass of polytypitic and interstitial textures (fig. 2).
319A-3-2, 127-130	3	Medium-grained feldspar phytic	none	none	78.8-67.5	21.0-32.1	0.2-0.4	66.0-36.0	33.6-63.3	0.4-0.7	40 - 36	50 - 37	10 - 27	Texture similar to sample 319A 3 2 (14-17).
319A-3-3, 146-149	3	Medium-grained feldspar phytic	none	none	85.1-76.9	14.6-22.9	0.3-0.2	73.2-31.7	26.4-67.6	0.4-0.7	41.3-36.5	43.6-50.8	15.1-12.8	Texture similar to sample 319A 3 2 (14-17).
319A-3-3, 106-109	3	Medium-grained feldspar phytic	none	none	77.8-72.6	22.0-27.4	0.2	65.7-37.0	34.0-62.6	0.3-0.4	41 - 31.3	46 - 44.1	13 - 24.6	Texture similar to sample 319A 3 2 (14-17).
319A-3-4, 100-103	4	Medium-grained feldspar phytic	none	none	77.9	21.9	0.2	75.4-33.2	25.3-66.2	0.3-0.6	43.2-34.2	43.9-48.7	12.9-17.1	Texture similar to sample 319A 3 2 (14-17).
319A-3-5, 37-41	5	Medium-grained olivine feldspar phytic basalt	88.8-79.5	none	80.5-75.1	19.3-24.7	0.2	65.4-30.6	34.2-68.8	0.3-0.6	41 - 37.3	47.2-45.2	11.7-17.6	Texture similar to sample 319A 3 2 (14-17).
319A-4-1, 129-132	5	Fine-grained olivine feldspar basalt	88-79	81.3	80.5-77.9	9.4-22.0	0.1-0.2	65.8-34.2	33.8-65.1	0.4-0.8	44.2-29.4	44.2-43	11.1-27.5	Olivine phenocrysts (up to 3 mm across), plagioclase phenocrysts (up to 1.3 mm across), plagioclase glomerocrysts and olivine-plagioclase glomerocrysts (trioctahedral fragments) set in groundmass of ophitic, intergranular and interstitial textures. Small grains of olivine scattered through matrix (fig. 4).
319A-5-1, 176-179	5	Fine-grained olivine feldspar	83.5-80.6	81.1	86.7-74.6	3.0-25.2	0.2-0.1	63.3-39.2	36.4-60.3	0.3-0.5	41.2-36.2	47.7-41.6	11.1-22.2	Texture similar to sample 319A 4 1 (129-132).

Xenoliths

Sample No.	Cooling Unit ¹	Rock Type	Olivine phenocryst ² Fo mol percent	Olivine groundmass Fo mol percent	Table 1. (continued)			Plagioclase groundmass ⁴			Augite ⁵			Comments
					Plagioclase phenocryst (core) ³	mol percent			atomic props.					
						An	Ab	Or	Ca	Mg	Fe			
319A-6-1, (64-89)	74	Fine-grained pyroxene-feldspar phyric basalt	none	none	82.1-70.6	17.7-29.1	0.2-0.3	63.3-60.0	36.3-39.6	0.4	41.5 (phenocrysts only analyzed; groundmass pyroxene too small for analysis)	49.7	8.7	Plagioclase phenocrysts (up to 3x1 mm) and glomerocrysts (fig. 5) and pyroxene glomerocrysts (up to 0.3 mm across, fig. 6) set in groundmass of felted plagioclase laths, cryptocrystalline material and altered glass.
319A-7-1, (119-122)	86	Fine-grained olivine-feldspar phyric basalt	84.0-81.5	83.0	78.8-73.2	21.0-26.6	0.2	69.1-39.6	30.7-59.9	0.2-0.5		48-43	10-15	Texture similar to sample 319A 5 1 (76-79).
3203-3-1, (120-125)		Fine-grained olivine-feldspar microphyric basalt	none	85.0-81.0	76.3	23.4	0.3	71.2-61.3	28.5-38.0	0.4-0.7		No pyroxene		Plagioclase microphenocrysts (up to 1 mm across), skeletal olivines (0.5 mm) and glomerophyric units of plagioclase laths (1x0.1 mm) subophitically enclosed by olivine (0.5 mm across) set in cryptocrystalline groundmass.
3203-4-1, (130-133)		Fine-grained feldspar microphyric basalt	none	none	69.7-67.2	29.9-32.5	0.4	68.4-46.9	31.2-52.4	0.4-0.8		46.5-54	16	Skeletal plagioclase microphenocrysts (up to 1x0.3 mm) set in groundmass of felted plagioclase laths (0.2x0.05 mm) and cryptocrystalline material (fig. 7)
3203-5-1, (117-123)		Fine-grained feldspar phyric basalt	none	none	69.4	30.1	0.2	70.7-49.1	29.1-50.0	0.3-0.9		No pyroxene		Texture similar to sample 3203 4 1 (130-133), but plagioclase phenocrysts are euhedral, some form glomerocrysts.
321-13-4, (119-124)		Fine-grained feldspar microphyric basalt	none	none	69.8-67.0	30.0-32.3	0.2-0.6	64.2-56.2	35.4-42.3	0.4-1.5		45-48	15.5-18	Small plagioclase phenocrysts (0.5 mm or less) set in groundmass of felted plagioclase laths forming intergranular (fig. 8) and intersertal textures. Vesicles and calcite-filled amygdules up to 0.6 mm.
321-14-1, (99-102)		Aphyric basalt		none				64.8-45.2	34.7-54.1	0.4-0.7		42.2-51.6	20.2-15.8	Texture identical to the groundmass of sample 321 13 4 (119-124) (fig. 9). Vesicles and amygdules up to 1.5 mm across.
321-14-2, (127-130)		Fine-grained feldspar phyric basalt	none	none	70.4	29.2	0.3	68.0-38.1	31.6-60.8	0.4-1.1		45.7-43.5	18.8-26.5	Texture similar to sample 321 13 4 (119-124). Vesicles and calcite-filled vesicles 1 mm across.
321-14-3, (93-96)		Fine-grained feldspar phyric basalt	none	none	68.7	31.0	0.3	67.9-46.1	31.7-53.2	0.4-0.7		50 - 47	20 - 21	Texture similar to sample 321 13 4 (119-124). Vesicles and amygdules 1 mm across.
321-14-4, (61-64)		Aphyric basalt		none				65.2-47.8	34.3-51.1	0.6-1.1		49.5 - 52	13.5 - 20	Texture similar to sample 321 14 1 (99-102). Vesicles less than 0.6 mm across.

- Notes: 1. Identified by shipboard party scientists. Numbering system that of Rhodes et al. (this volume).
 2. Core and rim compositions.
 3. Range of core compositions.
 4. Most calcic core and most sodic rim compositions.
 5. Most magnesian and least magnesian augite.

Table 2. Olivine compositions in selected Leg 34 samples.

	319A 1 1 (138-142)				319A 3 4 (18-21)					
	Skeletal grains		Phenocryst		Groundmass		Phenocryst			
	core	rim	core	rim	core	rim	core	rim		
SiO ₂	39.90	39.61	39.27	38.58	39.37	38.80	39.76	37.26	38.88	38.06
FeO	13.93	13.93	16.40	21.28	18.44	18.36	13.66	25.80	18.31	22.07
MnO	0.23	0.25	0.23	0.35	0.32	0.43	0.19	0.36	0.28	0.38
MgO	45.10	45.11	43.37	39.48	41.71	41.90	45.45	35.90	41.81	38.81
NiO	0.14	0.14	0.19	0.15	0.17	0.14	0.19	0.11	0.14	0.14
CaO	0.31	0.28	0.26	0.33	0.28	0.26	0.26	0.31	0.32	0.35
Total	99.61	99.32	99.72	100.17	100.29	99.89	99.51	99.74	99.74	99.81
Fo mol %	85	85	82	77	80	80	85.5	71	80	76

	319A 3 5 (37-41)				319A 4 1 (129-132)							
	Grains in troctolite fragment		Phenocryst		Phenocryst		Phenocryst					
	rim	core	core	rim	core	rim	core	rim				
SiO ₂	39.21	39.34	39.93	40.74	40.49	39.85	39.66	38.52	39.63	40.28	38.92	39.22
FeO	15.76	16.05	13.63	13.36	10.57	12.96	12.88	19.06	12.79	11.34	17.22	17.27
MnO	0.22	0.20	0.21	0.30	0.21	0.17	0.18	0.39	0.20	0.18	0.26	0.27
MgO	43.74	43.59	45.12	45.50	47.63	45.79	45.76	40.46	45.54	46.66	42.30	42.23
NiO	0.21	0.17	0.16	0.19	0.14	0.16	0.19	0.14	0.15	0.20	0.14	0.12
CaO	0.31	0.29	0.30	0.33	0.24	0.23	0.26	0.34	0.28	0.24	0.29	0.36
Total	99.45	99.64	99.35	100.42	99.28	99.16	98.93	98.91	98.59	98.90	99.13	99.47
Fo mol %	83	83	85.5	86	89	86	86	79	86	88	81	81

	319A 5 1 (76-79)				319A 7 1 (119-122)				3208 3 1 (120-125)			
	Phenocryst		Groundmass		Phenocryst		Groundmass		Groundmass		Groundmass	
	core	rim	core	rim	core	rim	core	rim	core	rim	core	rim
SiO ₂	39.23	39.14	39.18	38.80	39.25	39.20	39.06	39.06	39.30	39.56	39.65	
FeO	15.35	16.84	17.75	17.24	15.40	14.96	15.94	16.84	14.30	14.64	14.33	
MnO	0.26	0.30	0.27	0.28	0.25	0.20	0.25	0.27	0.22	0.26	0.21	
MgO	44.22	42.78	41.94	42.16	43.92	44.23	43.27	42.37	44.60	44.56	44.67	
NiO	0.14	0.15	0.17	0.14	0.15	0.18	0.12	0.12	0.21	0.22	0.16	
CaO	0.26	0.30	0.22	0.33	0.31	0.34	0.32	0.37	0.35	0.27	0.30	
Total	99.46	99.51	99.54	98.95	99.28	99.11	98.96	99.03	98.98	99.51	99.32	
Fo mol %	83.5	82	81	81	83.5	84	83	82	85	84	85	

Table 3. Plagioclase compositions in selected Leg 34 samples.

	319A 1 1 (138-142)		319A 2 2 (114-117)		319A 3 3 (46-49)		319A 3 5 (37-41)									
	core	rim	core	rim	core	rim	core	rim								
SiO ₂	50.73	50.91	51.78	51.20	52.52	56.45	48.68	60.55	47.47	60.41	52.57	59.69	52.13	50.49	59.39	48.20
Al ₂ O ₃	31.52	31.18	30.94	31.75	30.31	27.61	32.74	23.41	33.68	24.22	29.95	24.16	30.33	31.82	26.17	33.50
*FeO	0.63	0.71	0.60	0.63	0.63	1.04	0.48	0.66	0.42	1.24	0.69	0.60	0.64	0.54	0.74	0.39
CaO	14.39	14.31	13.96	13.03	12.69	8.53	16.14	6.15	16.70	6.16	14.45	6.17	12.91	14.71	6.17	15.94
Na ₂ O	3.01	3.07	3.17	3.88	4.05	6.22	2.03	7.73	1.65	7.33	2.99	7.53	3.85	2.76	7.72	2.20
K ₂ O	0.02	0.02	0.03	0.04	0.05	0.12	0.03	0.11	0.04	0.12	0.06	0.10	0.05	0.03	0.10	0.03
Total	100.30	100.20	100.48	100.53	100.25	99.97	100.10	98.61	99.96	99.48	100.71	98.25	99.91	100.35	100.29	100.26
An mol %	73	72.5	71	65	64	43	82	30.5	85	32	73	31	65	75	80	81

	319A 4 1 (129-132)		319A 6 1 (84-89)		319A 7 1 (119-122)		3208 5 1 (117-123)												
	core	rim	core	rim	core	rim	core	rim											
SiO ₂	53.92	58.36	52.50	48.85	57.68	48.59	51.70	53.26	53.86	50.58	57.19	49.21	55.16	51.79	54.91	52.08	53.88	52.33	54.93
Al ₂ O ₃	29.23	26.59	30.39	33.10	26.66	33.22	31.05	29.86	28.86	30.80	26.89	32.75	28.37	30.91	28.74	31.02	29.56	30.66	28.98
*FeO	0.83	1.04	0.69	0.41	0.92	0.40	0.66	0.96	1.12	0.96	1.14	0.42	1.24	0.54	0.97	0.58	0.91	0.62	0.99
CaO	11.19	6.91	12.40	15.35	8.11	16.12	11.81	12.10	12.02	14.27	9.52	15.46	9.12	13.90	9.29	10.51	10.51	13.29	11.08
Na ₂ O	4.57	7.35	3.63	2.13	6.31	2.00	4.42	4.24	4.28	2.97	5.81	2.37	6.00	3.41	5.85	5.10	5.13	3.66	5.07
K ₂ O	0.04	0.13	0.05	0.01	0.07	0.03	0.07	0.07	0.11	0.03	0.05	0.02	0.07	0.06	0.12	0.11	0.11	0.06	0.06
Total	99.78	100.38	99.67	99.85	99.75	100.36	99.71	100.49	100.25	99.61	100.60	100.23	99.96	100.61	99.88	99.40	100.10	100.62	101.11
An mol %	58	34	66	80.5	42	82	60	61.5	61	73	48	79	46	70	47	53	53	67	55

	3208 4 1 (130-133)			321 14 1 (99-102)			
	Groundmass core	Phenocryst core	rim	Groundmass core	rim	Groundmass core	rim
SiO ₂	51.44	51.76	53.46	54.01	59.26	54.06	56.16
Al ₂ O ₃	31.52	30.99	29.61	29.37	25.98	29.42	28.06
*FeO	0.59	0.57	0.87	0.92	0.88	0.94	1.11
CaO	13.94	13.56	9.79	12.55	8.91	11.69	9.86
Na ₂ O	3.28	3.45	5.61	3.84	5.99	4.37	5.42
K ₂ O	0.04	0.04	0.14	0.07	0.11	0.06	0.09
Total	100.81	100.37	99.48	100.76	101.13	100.54	100.70
An mol %	71	69	49	65	45	60	50.5

*All iron as FeO

321 14 2 (127-130)

Groundmass		Phenocryst	
core	rim	core	rim
53.29	56.76	51.10	58.81
29.31	27.59	30.96	26.32
0.85	0.94	0.71	0.84
12.65	9.31	13.95	7.54
4.13	5.40	3.38	6.74
0.06	0.12	0.06	0.18
100.23	100.62	100.16	100.43
63	47	70	38

Table 4. Pyroxene compositions in selected Leg 34 samples.

	319A 2 2 (114-117)			319A 3 2 (14-17)			319A 3 4 (100-103)				319A 3 5 (37-41)			319A 6 1 (84-89)		
							Core	rim				core	rim		core	rim
SiO ₂	49.77	49.94	48.72	51.21	51.05	50.93	50.71	49.66	50.99	51.50	51.96	50.50	50.41	52.03	53.02	51.39
TiO ₂	1.42	1.39	1.86	1.01	1.05	0.96	1.02	1.24	1.04	0.73	0.89	1.23	1.51	0.67	0.50	0.96
Al ₂ O ₃	3.48	3.08	4.86	3.48	3.74	3.49	3.44	2.52	3.03	1.29	2.42	3.88	3.83	2.93	2.46	4.17
Cr ₂ O ₃	0.24	0.07	0.22	0.30	0.32	0.35	0.39	0.02	0.19	0.10	0.06	0.18	0.13	0.59	0.57	0.43
FeO*	9.61	11.05	9.00	6.86	6.69	6.81	8.48	8.88	8.79	10.70	8.54	8.37 (10.63)	8.93	6.72	6.91	7.08
MnO	0.23	0.28	0.20	0.17	0.16	0.16	0.23	0.34	0.25	0.24	0.21	0.24	0.21	0.18	0.15	0.16
MgO	14.97	15.16	20.58	16.32	16.71	16.47	15.69	15.47	15.80	17.02	15.82	16.29 (15.50)	15.70	17.44	17.85	19.06
CaO	18.82	18.11	13.98	19.82	19.65	19.71	19.26	18.97	18.32	16.50	19.09	18.54 (17.77)	18.73	19.37	19.50	17.95
Na ₂ O	0.33	0.30	0.35	0.27	0.27	0.27	0.32	0.32	0.31	0.23	0.28	0.17	0.28	0.25	0.25	0.26
Total	98.87	99.38	99.77	99.44	99.64	99.15	99.54	97.42	98.72	98.31	99.27	99.40	99.73	100.19	101.20	101.48
Wo	39.9	37.9	28.2	41.4	40.8	41.1	40.4	40.0	38.8	34.0	40.0	38.8 (37.3)	39.4	39.6	39.2	35.9
En	44.2	44.1	57.7	47.4	48.3	47.8	45.8	45.4	46.6	48.8	46.1	47.5 (45.3)	45.9	49.6	49.9	53.0
Fs	15.9	18.0	14.2	11.2	10.9	11.1	13.9	14.6	14.5	17.2	14.0	13.7 (17.4)	14.7	10.7	10.8	11.1

	319A 7 1 (119-122)			320B 5 1 (117-123)				321 13 4 (119-124)				321 14 4 (61-64)		
SiO ₂	49.30	52.83	49.67	49.65	50.54	50.88	52.22	50.54	51.14	52.25	50.57	51.45	48.58	50.22
TiO ₂	1.66	0.67	1.50	1.46	1.31	0.98	0.96	1.11	0.94	0.53	1.08	0.86	1.67	1.18
Al ₂ O ₃	4.66	1.63	5.07	4.40	4.18	3.74	3.49	4.29	2.95	1.44	3.39	2.29	3.30	3.20
Cr ₂ O ₃	0.13	0.05	0.36	0.12	0.26	0.29	0.14	0.18	0.20	0.12	0.26	0.04	0.01	0.07
FeO	9.11	10.97	7.55	9.10	9.30	8.53	10.14	9.18	8.59	9.34	8.86	8.43	13.13	10.01
MnO	0.20	0.29	0.18	0.26	0.22	0.24	0.27	0.29	0.25	0.27	0.20	0.32	0.27	0.23
MgO	14.62	17.96	15.58	16.44	19.10	17.56	20.83	16.08	17.35	15.65	16.21	16.76	16.39	17.26
CaO	19.74	16.36	19.94	16.95	14.48	16.57	12.16	17.29	17.32	18.85	18.05	17.55	14.30	16.22
Na ₂ O	0.32	0.23	0.31	0.28	0.23	0.22	0.21	0.16	0.20	0.16	0.22	0.20	0.24	0.22
Total	99.74	101.00	100.15	98.66	99.62	99.01	100.42	99.12	98.94	98.61	98.84	97.70	97.89	98.61
Wo	41.8	32.8	42.0	36.1	30.0	34.8	24.8	36.9	36.0	39.3	38.0	37.0	30.2	33.8
En	43.1	50.1	45.6	48.7	55.0	51.3	59.1	47.8	50.1	45.4	47.5	49.1	48.2	50.0
Fs	15.1	17.2	12.4	15.1	15.0	14.0	16.1	15.3	13.9	15.2	14.6	13.9	21.6	16.3

*All iron as FeO

Table 5. Ilmenite and titanomagnetite compositions in selected Leg 34 samples.

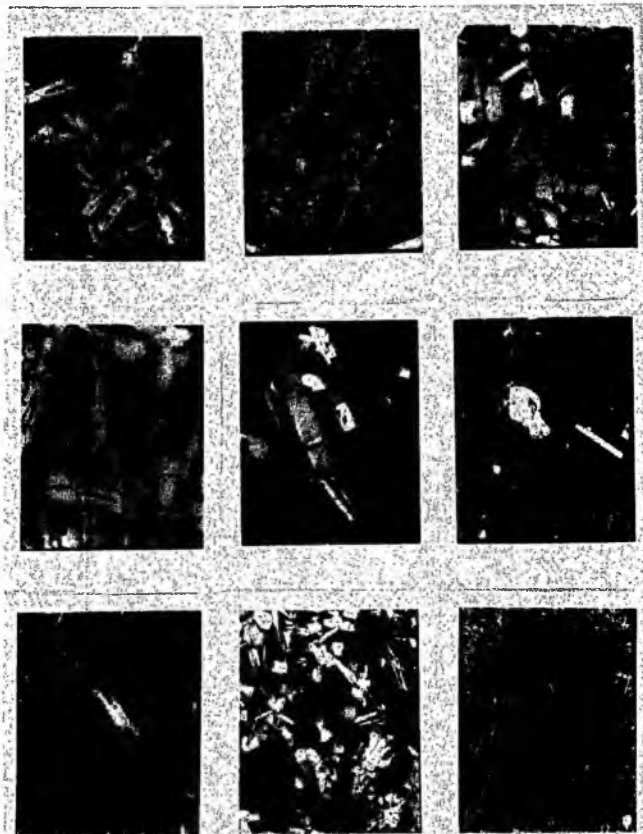
	319A 3 2 (127-130)				319A 3 3 (106-109)											
TiO ₂	29.42	25.12	26.00	25.94	50.34	50.55	48.92	16.79	50.46	25.69	24.72					
Al ₂ O ₃	1.89	2.00	1.55	1.41	0.11	0.00	0.06	1.69	0.10	2.08	2.03					
Cr ₂ O ₃	0.04	0.04	0.02	0.03	0.02	0.00	0.02	0.04	0.00	0.03	0.03					
FeO*	65.36	67.95	69.29	67.29	49.37	47.24	49.31	74.35	49.28	66.70	67.89					
MnO	0.60	0.62	0.78	0.80	0.98	2.84	0.74	0.58	0.61	0.65	0.76					
MgO	<u>0.36</u>	<u>0.65</u>	<u>0.30</u>	<u>0.27</u>	<u>0.62</u>	<u>0.26</u>	<u>0.53</u>	<u>0.24</u>	<u>0.84</u>	<u>1.01</u>	<u>0.48</u>					
Total	97.67	96.38	96.94	95.74	101.44	100.89	99.58	95.69	101.29	96.16	95.91					
	319A 2 2 (114-117)				319A 3 2 (14-17)				319A 3 3 (46-49)				319A 3 4 (18-21)			
TiO ₂	49.51	23.83	23.85	21.78	24.52	24.06	23.66	25.15	23.28	24.19	23.21	46.97	21.23	23.33		
FeO*	48.58	72.27	72.90	73.18	71.46	72.67	71.82	70.77	67.72	71.78	73.75	52.56	75.46	74.11		
MgO	<u>0.05</u>	<u>0.51</u>	<u>0.33</u>	<u>0.22</u>	<u>0.49</u>	<u>0.44</u>	<u>0.52</u>	<u>0.83</u>	<u>0.86</u>	<u>0.49</u>	<u>0.33</u>	<u>0.33</u>	<u>0.17</u>	<u>0.29</u>		
Total	98.94	96.61	97.08	95.18	96.47	97.17	96.00	96.75	91.86	96.46	97.29	99.86	96.86	97.73		
	319A 3 4 (100-103)				319A 3 5 (37-41)				319A 4 1 (129-132)				321 14 1 (99-102)			
TiO ₂	49.96	24.25	22.84	26.46	49.62	23.26	23.70	22.63	22.21	22.67	22.74	23.47	24.36			
FeO*	47.61	71.39	73.27	69.17	49.41	72.65	72.32	73.63	74.04	73.76	73.94	72.15	72.77			
MgO	<u>1.55</u>	<u>0.95</u>	<u>0.69</u>	<u>0.96</u>	<u>0.44</u>	<u>0.64</u>	<u>0.38</u>	<u>0.67</u>	<u>0.50</u>	<u>0.47</u>	<u>0.31</u>	<u>0.45</u>	<u>0.55</u>			
Total	99.13	96.59	96.80	96.59	99.47	96.55	96.40	96.93	96.75	96.90	96.99	96.07	97.68			
	321 14 2 (127-130)															
TiO ₂	23.64	23.47	23.13													
FeO*	71.10	71.64	72.22													
MgO	<u>0.46</u>	<u>0.62</u>	<u>0.34</u>													
Total	95.20	95.73	95.69													

* All iron as FeO.

Table 6. Spinel composition in sample 320B 3 1 (120-125)

TiO ₂	.1.08
Al ₂ O ₃	24.45
Cr ₂ O ₃	36.79
FeO*	23.73
MnO	0.22
MgO	<u>13.32</u>
Total	99.59

* All iron as FeO



Figs. 1-9

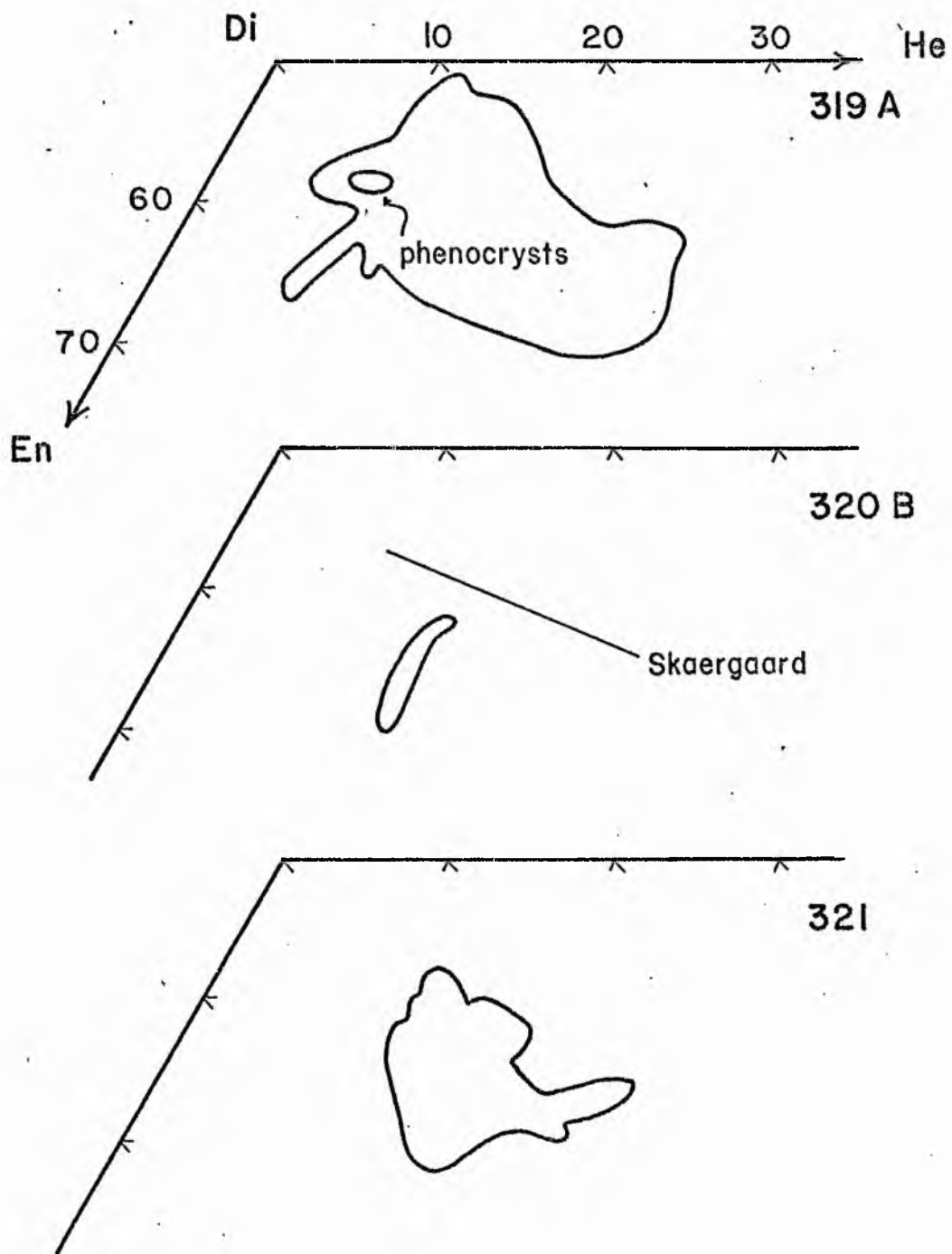


Fig. 10